DEVELOPMENT OF POLYMER LIPID PARTICLE TECHNOLOGY FOR DRUG DISCOVERY

by

BETHAN SIAN KELLY

A thesis submitted to the University of Birmingham for the degree of

DOCTOR OF PHILOSOPHY

School of Biosciences

College of Life and Environmental Sciences

University of Birmingham

September 2024

UNIVERSITY OF
BIRMINGHAM

University of Birmingham Research Archive

e-theses repository

This unpublished thesis/dissertation is copyright of the author and/or third parties. The intellectual property rights of the author or third parties in respect of this work are as defined by The Copyright Designs and Patents Act 1988 or as modified by any successor legislation.

Any use made of information contained in this thesis/dissertation must be in accordance with that legislation and must be properly acknowledged. Further distribution or reproduction in any format is prohibited without the permission of the copyright holder.

Abstract

G Protein-Coupled Receptors (GPCRs) represent 30-40% of all drug targets and have a massive therapeutic potential. Investigations into GPCR structure and function are often limited by their instability, flexible structure and location within the plasma membrane. Improved methodology to produce stable soluble GPCRs in an environment like the plasma membrane would be impactful for drug discovery. Amphipathic polymers, such as poly(styrene-co- maleic acid) (SMA), can be used as a solubilisation agent to produce polymer lipid particles (PoLiPa). These nanodiscs can encapsulate membrane proteins and surrounding lipids. PoLiPa have been shown to have a stabilising effect lending itself to GPCR investigations.

This project shows the expression, solubilisation and purification of GPCRs using PoLiPa technology, and preliminary data showing evidence that GPCRs are functional in an SMA lipid particle (SMALP). Firstly, the production of soluble human Neurotensin Receptor (hNTR1), expressed in *E. coli,* with a wild-type sequence was proven possible utilising SMA but low expression prevented its purification. Secondly, two MBP-fused GPCRs (rat NTR1 and Cannabinoid Receptor 2 (CB2)), expressed in *E. coli,* were solubilised and purified using SMA and were resistant to unfolding. Thirdly, mammalian cell expressed GPCRs (hNTR1 and CB2) were solubilised with different polymers and CB2 was successfully purified. Finally, SMALP-encapsulated GPCRs were proven suitable for functional analysis by fluorescent tryptophan spectroscopy (FTS), fluorescent correlation spectroscopy (FCS) and spectral shift assays. Key findings include the preferential solubilisation of GPCR oligomers or glycosylation forms dependent on the polymer type and hydrophobicity; the importance of resin types and excess polymer concentration on purification yield and allosteric modulation of Mini-G proteins for GPCR ligand binding.

It is anticipated that this project will be a starting point for other GPCR investigations to optimise the use of PoLiPa technology. This project presents key hurdles in the GPCR production process and a toolkit to overcome issues such as low expression, instability, and purification contamination.

Acknowledgements

This work was supported by the Biotechnology and Biological Sciences Research Council (BBSRC) and University of Birmingham funded Midlands Integrative Biosciences Training Partnership [grant number BB/T00746X/1].

Thank you to my sponsor company Domainex, particularly Kartika Shetty, Jim Reid, Satya Bhamidimarri, Trevor Askwith and Stefanie Reich. I was lucky enough to perform experiments in their lab and be hosted multiple times throughout the project. I especially appreciated all the teaching and advice. Working with them has made me a better scientist.

Thanks to the collaborators in this project: Joelle Goulding and Stephen Briddon at the University of Nottingham; Max Keller from the University of Regensburg and Marialessandro Contino from the University of Bari. Special thanks to the Klumpermann group at Stellenbosch University, who were kind enough to host me in their lab for 6 weeks and show me the sights.

I would like to thank Professor Tim Dafforn for his supervision, Naomi Pollock for her mentorship, the other members of the Dafforn group and all the other scientists of the 7th floor of the Bioscience Building over the last four years for their advice and kindness. A special thank you to Rachel Holyfield and Lauren Garbett for their friendship and support throughout the whole process.

I'd like to thank all the girls of 688 Pershore Road who have made my time in Birmingham full of fun and laughter: Sonja Bloch, Nina Dekker Doules, Elizabeth Starks and Babora Kostyrova. Thank you also to Rachel Austin and Jessica Neale for their friendship and long-distance support.

Thank you to my parents, Rose and Tom for their continued love and support and for always believing in me; I feel lucky every day to be part of our family.

Thanks to Benjamin Archer for being a kind and lovely housemate, boyfriend and best friend during a stressful time.

TABLE OF CONTENTS

CHAPTER 1: INTRODUCTION ***18***

1.1 G Protein Coupled Receptors (GPCRs) and Drug Discovery *18*

1.2 Structure and Function of GPCRs and G-proteins *19*

1.3 Membrane Proteins and Polymer Lipid Particle (PoLiPa) Technology *22*

1.4 Benefits of PoLiPa for GPCR Solubilisation *24*

1.5 Advantages and Disadvantages of Different Polymers *27*

1.6 Investigated GPCRs *30*

1.7 Choice of Expression System for GPCR Production *31*

1.8 Optimizing Purification Protocols for GCPRs in PoLiPa *33*

1.9 Biophysical Characterisation of PoLiPa *34*

1.9.1 DLS *34*

1.9.2 NanoDSF *35*

1.9.3 CD *35*

1.9.4 SEC *36*

1.9.5 SMA- or DIBMA-PAGE *36*

1.10 Ligand Binding Experiments *37*

1.11 Fluorescence Spectroscopy *38*

1.12 Mini-G proteins as a Function Assay Tool *40*

1.13 Previous Investigations of GPCRs Utilising PoLiPa Technology *40*

1.14 Thesis Aims *42*

1.15 Outline of the Thesis *42*

CHAPTER 2: MATERIALS AND METHODS ***44***

2.1 Materials *44*

2.2 Preparation of Polymers *44*

2.3 Strains *45*

2.4 Plasmids *46*

2.5 Bacterial Growth Media *46*

2.6 Transformation of E. coli for Recombinant Expression *47*

2.7 Plasmid extraction and Glycerol Stock Preparation *47*

2.8 GPCR Expression and Expression Optimisation *48*

2.8.1 Large-Scale GPCR Expression in E. coli *48*

2.8.2 Expression Trials for Optimal MBP-fused GPCR Expression in E. coli *48*

2.8.3 Lentiviral Overexpression of GPCRs in HEK293 Cells *49*

2.9 Buffers and Tubes for Cell, Membrane and Protein Handling *49*

2.10 GPCR Solubilisation and Purification *50*

2.10.1 E. coli and HEK293 Cell Membrane Preparation *50*

2.10.2 GPCR Solubilisation from Membranes *51*

2.10.3 Solubilisation Screens *51*

2.10.4 Immobilised Metal Affinity Chromatography (IMAC) Purification *51*

2.10.5 IMAC Purification Screens for Optimisation *52*

2.10.6 Post-IMAC Dialysis *53*

2.10.7 FLAG Purification *53*

2.10.8 FLAG Purification Optimisation 54
2.10.9 Post-FLAG Dialysis 54
2.11 Concentrating GPCRs 55
2.12 Storage Conditions Screens 55
2.13 Protein Concentration Estimation 55
2.14 SDS-PAGE 56
2.15 PAGE Analysis 56
2.16 Western blots 57
2.17 Biophysical Analysis of GPCRs in PoLiPas 58
2.17.1 SEC 58
2.17.2 DLS 58
2.17.3 CD 59
2.17.4 SMA-PAGE or DIBMA-PAGE 59
2.18 Production of Mini-G Proteins 59
2.19 Fluorescent Tryptophan Spectroscopy 60
2.20 Solution-based Fluorescent Correlation Spectroscopy 61
2.21 Spectral Shift Assays 63
CHAPTER 3: PRODUCTION AND SOLUBILISATION OF WILD-TYPE HUMAN NEUROTENSIN RECEPTOR EXPRESSED IN E. COLI 64
3.1 Testing Expression of hNTR1 in E. coli 65
3.2 Solubilisation Trials on E. coli Membranes 67
3.2.1 Comparison of SMA, SMI and DDM for the Extraction of hNTR1 68
3.2.2 Understanding Effect of Polymer Hydrophobicity on Solubilisation Efficiency of WT hNTR1 70
3.3 IMAC Purification of hNTR1 using PoLiPa Technology 72
3.3.1 IMAC Purification of SMA-hNTR1 Expressing E. coli Membranes 73
3.3.2. IMAC Purification of DIBMA-Solubilised hNTR1 Expressing E. coli Membranes 75
3.3.3. IMAC Purification of SMA-solubilised E. coli control membranes 75
3.4 Identification of hNTR1 in Elution Fractions Post-IMAC Purification 77
3.5 SEC of Protein Product Post-IMAC Purification 78
3.6 SMA-PAGE and DIBMA-PAGE Analysis of hNTR1 Oligomerisation 82
3.7 Excision of SMA-PAGE and DIBMA-PAGE Bands for SDS-PAGE 85
3.8 Conclusion 87
CHAPTER 4: MBP FUSED GPCR EXPRESSION IN E. COLI: PRODUCTION AND CHARACTERISATION OF MBP-FUSED rNTR1 USING POLIPA 88
4.1 Introduction to MBP Fusion Proteins 88
4.2 Comparison of MBP-fused GPCR Expression to hNTR1 Expression in E. coli 90
4.3 Introduction to Production of rNTR1 93
4.4 Optimisation of Expression of rNTR1 in E. coli 93
4.4.1 Comparison of E. coli Strains 94
4.4.2 Comparison of Growth Media 96
4.4.3 Comparison of IPTG Concentrations and Lengths of Expression Before Harvesting 97
4.4.4 Comparison of Temperature Concentrations 99
4.4.5 Expression of rNTR1 in E. coli Summary 101
4.5 Solubilisation Trials of rNTR1 in E. coli 101

4.5.1 Effect of Polymer Hydrophobicity on Solubilisation Efficiency of rNTR1 and Comparison of BzAM Series Polymers to SMA and DIBMA ... 101
4.5.2 Determining Optimal SMA Concentration ... 103
4.5.3 Determining Inclusion of Arginine in SMA Solubilisation Buffer ... 104

4.6 MBP Fusion Protein Purification of MBP-fused rNTR1 Expressed in E. coli ... 105

4.7 Optimisation of rNTR1 Purification by IMAC ... 106
4.7.1 Influence of Affinity Chromatography Resin Type ... 106
4.7.2 Confirmation of SMA-rNTR1 Purification Success by Western blot Analysis ... 109
4.7.3 IMAC Condition Screen ... 112
4.7.4 Salt Concentration ... 114
4.7.5 Reducing Agent ... 116

4.8 Biophysical Characterisation and Stability Analysis of rNTR1 Encapsulated in SMALP . 119
4.8.1 Biophysical Characterisation by SEC ... 119
4.8.2 SMA-PAGE Analysis Post-SEC ... 121
4.8.3 Biophysical Characterisation by DLS and Comparison of Buffer Systems ... 122
4.8.4 Determination of Optimal Storage ... 125
4.8.5 Biophysical Characterisation by CD Spectrometry ... 127
4.8.6 Overnight Changes in Secondary Structure of rNTR1 by Interval CD Spectrometry ... 129
4.8.7 Thermostability of rNTR1 Encapsulated in SMALP in Changes in Tryptophan Fluorescence by 350/330 Ratio ... 130

4.9 Summary of rNTR1 ... 132

CHAPTER 5: PRODUCTION AND CHARACTERISATION OF MBP-FUSED CB2 IN E. COLI USING POLIPA ... 133

5.1 Introduction ... 133

5.2 Expression Trials to Optimise CB2 Expression ... 133
5.2.1 Comparison of Cell Lines and Growth Media ... 134
5.2.2 Comparison of Three IPTG Concentrations ... 136
5.2.3 Comparison of Two Expression Temperatures ... 137

5.3 Assessment of Inclusion of Reducing Agent during Cell Lysis ... 138

5.4 Solubilisation Trials on CB2 Expressed in E. coli ... 141
5.4.1 Efficiency of Different Polymers ... 141
5.4.2 Effect of Polymer Hydrophobicity on CB2 Extraction from E. coli Membranes ... 143
5.4.3 Optimal SMA Concentration for CB2 Homogenisation ... 145

5.5 MBP Trap Purification of CB2 ... 146

5.6 FLAG Purifications Comparing CB2 Solubilised with Different Polymers or DDM ... 146

5.7 Optimising IMAC Purification of CB2 Expressed in E. coli using PoLiPa Technology ... 149
5.7.1 Solubilised with DDM ... 149
5.7.2 Resin Type, Salt Concentration and Addition of 20 mM Arginine as Variables ... 150
5.7.3 Addition of 200 mM Arginine ... 153
5.7.4 Effect of Reducing Agent addition to IMAC binding buffers: 25 mM DTT ... 155
5.7.5 Effect of Reducing Agent addition to IMAC binding buffer: 1 mM TCEP ... 157

5.8 FLAG Purification of CB2 Post-IMAC Purification ... 160
5.8.1 Addition of 25 mM DTT in Binding Buffers ... 160
5.8.2 Arginine and Salt Concentration ... 163

5.9 Optimal Storage of SMA-CB2 ... 166

5.10 Thermostability Analysis of SMA-CB2 of NanoDSF ... 168

5.11 Summary of CB2 Production and Characterisation using PoLiPa Technology ... 169

CHAPTER 6: EXPRESSION, SOLUBILISATION AND PURIFICATION OF GPCRS EXPRESSED IN MAMMALIAN CELLS USING POLIPA ... 170

6.1 Introduction ... 170

6.2 Solubilisation Screens to Understand how Efficiently Polymers Extract hNTR1 from HEK293 Cell Membranes *172*
6.2.1 Solubilisation screen of hNTR1 Expressed in HEK293 Cells *172*
6.2.2 SMA, DIBMA and Novel Polymer Series: AASTY *175*
6.3 Binding Trials of HEK293-expressed hNTR1 Purification *177*
6.4 IMAC Purification with Optimised Conditions for hNTR1 ..... *180*
6.5 HEK-Expressed hNTR1 Post-IMAC FLAG Purification *181*
6.6 Solubilisation screens of CB2 expressed from HEK293 cells *183*
6.6.1 Amphipathic Polymers and DDM *183*
6.6.2 Polymers with Different Hydrophobicities Compared to SMA and DIBMA *186*
6.6.3 SMA and DIBMA Concentration Compared to SMI and DDM *187*
6.7 Binding Trial of HEK293-expressed CB2 Purification *189*
6.8 IMAC Purification with Optimised Conditions for CB2 ..... *193*
6.9 Conclusions *195*
CHAPTER 7: FUNCTIONAL ASSESSMENT OF SMA-SOLUBILISED GPCRs BY LIGAND BINDING AND MINI-G PROTEIN BINDING* *196
7.1 Introduction *196*
7.2 Tryptophan Fluorescence Changes and Ligand Binding to SMA-hNTR1 ..... *198*
7.2.1 SMA-hNTR1 Protein Titrated Against Fluorescent NTR1 Ligands *199*
7.2.2 Fluorescent NTR1 Ligand Controls *201*
7.2.3 Anisotropy Changes of Tryptophan Fluorescence in SMA-Solubilised hNTR1 Protein Titrated Against NTR1 Agonists *203*
7.3 Tryptophan Fluorescence Changes and Ligand Binding to SMA-rNTR1 ..... *204*
..... *205*
7.3.3 SMA-rNTR1 Titrated Against Fluorescent MK337 Ligand and Effect of Gsq Incubation *205*
7.4 Tryptophan Fluorescence Changes and Ligand Binding to SMA-CB2 ..... *208*
7.4.4 FTS Analysis of SMA-CB2 Titrated Against SM15 ..... *208*
7.4.5 FTS Analysis of SMA-CB2 Titrated Against VM7 and Effect of Gs Incubation *210*
7.4.6 FTS Analysis of SMA-CB2 Expressed in E. coli Titrated Against 4Q3CF *212*
7.5 Fluorescence Correlation Spectroscopy (FCS) *213*
7.5.4 MK337 Series Binding Experiment Comparing SMA-rNTR1, SMA-CB2 and SMA-SAV With and Without SR 48692 ..... *215*
7.5.5 Specific MK337 binding to SMA-rNTR1 Incubated With Gs or Gsq *217*
7.5.6 Key findings of FCS Experiments *219*
7.6 Spectral Shift Assays *220*
7.6.1 MK350 Dose-Dependent Changes in Fluorescent Properties of Labelled SMA-NTR1 ..... *220*
7.6.2 SR 48692 Prevents MK350 Dose-dependent Changes in Fluorescent Properties of Labelled SMA-NTR1 222
..... *222*
7.6.3 Competitive Assay Shows SR 48692 Dose-Dependent Changes in Fluorescent Properties of Labelled SMA-NTR1 After Incubation with MK350 ..... *223*
7.7 SMA-PAGE to Assess Mini-G Protein Binding *225*
7.8 Conclusion *229*
CHAPTER 8: DISCUSSION* *230
8.1 Summary of Key Findings *230*
8.2 Interpretation of Results *230*
8.2.1 Expression of GPCRs in E. coli *230*
8.2.2 Expression of GPCRs in HEK293 Cells *233*

8.2.3 Polymer Solubilisation and Polymer Selection of GPCR Oligomerisation states or Glycosylation States 234
8.2.4 Purification Optimisation 236
8.2.5 Biophysical Analysis Techniques 239
8.2.6 Stabilising Effect of PoLiPa Compared to Other Methods 240
8.2.7 Functional Analysis 241
8.2.7.1 FTS 242
8.2.7.2 FCS 243
8.2.7.3 SMA-PAGE for GPCR: Mini-G protein complex detection 244

8.3 Implications of the findings and contribution to the field of drug discovery 245
8.3.1 PoLiPa Technology Implications 245
8.3.2 GPCR Implications 246

8.4 Limitations of the study 248
8.4.1 Low yield 248
8.4.2 GPCRs in this Project may not be Representative of GPCRs in a 'Native' Environment 248
8.4.3 GPCRs investigated are not representative of the whole class 249

8.5 Recommendations for Future Research 250
8.5.1 New Polymers 250
8.5.2 New GPCRs 251
8.5.3 Oligomerisation Studies 251
8.5.4 Solution-based Assessment of GPCR Interactions - Utilising Fluorescent Assays and Validation of Binding Experiments. 252

8.6 Final Remarks 254

APPENDIX 255

Appendix 1.1 – E. coli expressed hNTR1 extraction with different DIBMA concentrations. 255

Appendix 1.2 - Use of MBP fusion protein as a means of purification of MBP-fused rNTR1 Expressed in E. coli 256

Appendix 1.3 – Overnight binding to MBPTrap column to improve the use of MBP fusion protein as a means of purification of rNTR1 Expressed in E. coli, overnight binding to column 257

Appendix 1.4 –IMAC purification followed by MBPTrap purification to determine the possible benefit of MBPTrap Binding of SMA-rNTR1 expressed in E. coli 258

Appendix 1.5 – SMA-solubilised E. coli membranes expressing rNTR1 IMAC purification followed by MBPTrap purification 259

Appendix 1.6 – IMAC Purifications of E. coli Expressed Mini-G proteins 260

Appendix 1.7 – MK337 Characterisation for FCS: Testing the inclusion of BSA and glycerol in the buffer on the measured concentration of MK337 and the calculated diffusion rate 261

Appendix 1.8 – MK337 Characterisation for FCS: Testing the effect of laser power of MK337 measured concentration and brightness 262

Appendix 1.9 – MK337 Characterisation for FCS: MK337 series to determine the possible increase in bound MK337 to SMA-solubilised NTR1 with and without Bovine Gamma Globulin (BGG) 262

Appendix 1.10 – MK337 Characterisation for FCS: The effect of antagonist SR 48692. 263

REFERENCES 264

TABLE OF FIGURES

Figure 1.1: Flow chart of simplified Drug Development Pipeline and approximate timescales 18

Figure 1.2: Structures demonstrating the conserved conformational changes in the 'transduction site' of GPCRs 20

Figure 1.3: Schematic illustrating how GPCRs activates G proteins causing downstream signalling pathways. 21

Figure 1.4: Subclasses of the G-protein Alpha subunits 22

Figure 1.5: Cartoon representation of a PoLiPa containing a GPCR. 24

Figure 1.6: Chemical Structures of Amphipathic Co-polymers investigated in this project. 29

Figure 1.7: Example standard CD Spectra of proteins containing only one type of secondary structure. 36

Figure 3.1: Cartoon representation and features of WT hNTR1 expressed in E. coli in this Chapter.. 64

*Figure 3.2: Expression test for hNTR1 in E. coli ..... **Error! Bookmark not defined.***

Figure 3.3: Western blots showing of results of a solubilisation trial comparing two polymers and the detergent DDM. 69

Figure 3.4: Chemical structure of a BzAM series polymer. 70

Figure 3.5: Solubilisation trial comparing the BzAM polymer series to SMA and DIBMA. 71

Figure 3.6: SDS-PAGE analysis of an IMAC purification using Ni-NTA resin from hNTR1 expressing membranes solubilised with 2.5% (w/v) SMA. 73

Figure 3.7: SDS-PAGE analysis of an IMAC purification using Ni-NTA resin from hNTR1 expressing membranes solubilised with 2.5% (w/v) DIBMA. 75

Figure 3.8: SDS-PAGE analysis of an IMAC purification using Ni-NTA resin from E. coli membranes with no recombinant expression membranes solubilised with 2.5% (w/v) SMA. 76

Figure 3.9: Western blot of concentrated elution fractions from a IMAC purification of hNTR1 solubilised with SMA. 78

Figure 3.10: SEC of hNTR1 protein samples post-IMAC purification 80

Figure 3.11: SMA- or DIBMA-PAGE of Post-IMAC Post-SEC samples 83

Figure 3.12.: Silver stained SDS-PAGE gel of bands excised from SMA-PAGE (left) or DIBMA-PAGE (right). 86

Figure 4.1: Cartoon summarising of characteristics of MBP fused GPCRs in which expression was tested. 89

Figure 4.2 : Plasmid map showing the key characteristic of the pRG vector used to express MBP-fused GPCRs in E. coli 90

Figure 4.3: Expression Comparison of four GPCRs expressed in E. coli by Western blot analysis.....91

Figure 4.4: rNTR1 expression trial in two cell lines.....95

Figure 4.5: rNTR1 expression trial comparing three different broth types.....96

Figure 4.6: rNTR1 expression trial comparing three IPTG concentrations and harvesting time points. 98

Figure 4.7: rNTR1 expression trial comparing three expression temperatures and two harvesting time points. 100

Figure 4.8: Solubilisation trial showing comparison of BzAM polymer series to SMA and DIBMA..102

Figure 4.9: Solubilisation trial comparison SMA concentrations (0-2.5% (w/v)).....103

Figure 4.10: Solubilisation trial testing the inclusion of 20 mM arginine in the solubilisation buffer. 105

Figure 4.11: Four rNTR1 purifications using different IMAC resins.....108

Figure 4.12: Western blot analysis of SMA-rNTR1 IMAC purification fractions 110

Figure 4.13: Western blot analysis showing results of IMAC Condition Screen 113

Figure 4.14: Coomassie stained SDS-PAGE gel comparing two purifications with 150 mM or 500 mM NaCl in the binding buffer.....115

Figure 4.15: IMAC Condition Screen comparing the effect of reducing agents 117

Figure 4.16: The effect of DTT on the IMAC purification of SMA-rNTR1.....118

Figure 4.17 : SEC analysis of the SMA-rNTR1 using a Superose 6 increase 10/300 column.....120

Figure 4.18: SMA-PAGE analysis of SMA-rNTR1. 122

Figure 4.19: DLS analysis of purified SMA- rNTR1.....123

Figure 4.20: SMA-rNTR1 storage condition experiment.....126

Figure 4.21: CD Spectrometry Analysis of SMA-rNTR1. 128

Figure 4.22: Interval CD Spectrometry Data of SMA-rNTR1 over a 960-minute timeframe.....129

Figure 4.23: Thermostability assessment of SMA-rNTR1 by NanoDSF.....131

Figure 5.1: CB2 expression trial comparing four different growth media types and two different cell lines. 135

Figure 5.2: CB2 expression trial comparing three different IPTG concentrations for induction and two different cell lines.....136

Figure 5.3: CB2 expression trial comparing two expression temperatures and three harvesting times. 137

Figure 5.4: Comparing the effect of no reducing agent, 25 mM or 5 mM TCEP in the cell lysis buffer. 139

Figure 5.5: CB2 solubilisation trial comparing of four polymers and DDM. *142*

Figure 5.6: CB2 solubilisation trial comparing the BzAM polymer series to SMA, RAFT SMA 1:1 and DIBMA. *144*

Figure 5.7: CB2 solubilisation trial comparing three SMA concentration. *145*

Figure 5.8: SDS-PAGE analysis of five FLAG affinity purifications of CB2 solubilised with polymers or DDM. *147*

Figure 5.9: IMAC purification of DDM-CB2. ..... *150*

Figure 5.10: SMA-CB2-, 0.35 BzAM-CB2 and DIBMA-CB2 binding trial comparing the effect of resin-type, arginine and salt. *152*

Figure 5.11: Two comparative SMA-CB2 IMAC purifications with and without 200 mM arginine in the binding buffer. *154*

Figure 5.12: Two comparative SMA-CB2 IMAC purifications with and without 25 mM DTT in the binding buffer. *156*

Figure 5.13: SMA-CB2 IMAC purification with 1 mM TCEP in the binding buffer. *159*

Figure 5.14: Two comparative post-IMAC FLAG purifications with and without 25 mM DTT in the binding buffers. *161*

Figure 5.15: Four comparative post-IMAC FLAG purifications at low and high salt concentrations, with and without 20 mM arginine. *165*

Figure 5.16: SMA-CB2 optimal storage trial. *167*

Figure 5.17: Thermostability assessment of SMA-CB2 by NanoDSF. *168*

Figure 6.1: Cartoon representation of GPCRs expressed in HEK293 cells. *171*

Figure 6.2: Mammalian expressed hNTR1 solubilisation trial comparing BzAM series (0.05-0.4), SMA, DIBMA, DDM and SMI *173*

Figure 6.3: Mammalian expressed hNTR1 solubilisation trial comparing different SMA and DIBMA concentrations and the AASTY polymer series. *176*

Figure 6.4: IMAC binding screen of HEK293 expressed hNTR1 on different resins (IDA, Ni-NTA, TALON), different arginine concentrations (0 mM, 20 mM, 50 mM) and with a reducing agent (2 mM TCEP or 2 mM DTT). *178*

Figure 6.5: SDS-PAGE analysis of a IMAC purification of SMA-solubilised HEK293 membranes expressing hNTR1. ..... *181*

Figure 6.6: SDS-PAGE analysis of two FLAG purification of SMA-solubilised HEK293 membranes expressing NTR1. ..... *182*

Figure 6.7: Mammalian expressed CB2 solubilisation trial comparing different SMA, DIBMA, the AASTY polymer series and DDM. *185*

Figure 6.8: Mammalian expressed CB2 solubilisation trial comparing SMA, DIBMA and the BzAm polymer series *186*

Figure 6.9: Mammalian expressed CB2 solubilisation trial comparing different SMA and DIBMA concentrations to SMI and DDM. 188

Figure 6.10: IMAC binding screen of HEK293 expressed CB2 on different resins (IDA, Ni-NTA, TALON), different arginine concentrations (0mM, 20mM,50mM) and with 1mM TCEP. 191

Figure 6.11: SDS-PAGE analysis of an IMAC purification of SMA-solubilised HEK293 membranes expressing CB2. 194

Figure 7.1: Chemical Structure of Neurotensin Receptor 1 agonists used in this project and crystal Structure of agonist-bound hNTR1 with highlighted tryptophan residues in red. 199

Figure 7.2: Peak intensity from FTS analysis of SMA-hNTR1, expressed in E. coli, titrated with fluorescent agonists. 200

Figure 7.3: Intensity from FTS analysis of SMA-solubilised common IMAC contaminant proteins expressed in E. coli. 202

Figure 7.4: Fluorescence Anisotropy measurements taken from FTS analysis of SMA-hNTR1, expressed in E. coli after titration of NTR1 agonists (MK337, MK350 or Neurotensin 8-13). 203

Figure 7.5: Crystal Structures of agonist and antagonist bound rNTR1 variants 205

Figure 7.6: FTS analysis of SMA-rNTR1 expressed in E. coli with and without incubation with Gsq for 4 hours. 206

Figure 7.7: Chemical Structures of Fluorescent CB2 agonists used in this project and Crystal Structures of agonist and antagonist bound CB2 variants 208

Figure 7.8: FTS analysis of SMA-CB2 expressed in E. coli. SMA-CB2 concentration was 0.2 mg/mL 209

Figure 7.9: FTS analysis of SMA-CB2 expressed in E. coli. with and without incubation with Gs for 4 hours 211

Figure 7.10: FTS analysis of SMA-CB2 expressed in E. coli, titrated with CB2 agonist 4Q3CF. 213

Figure 7.11: Cartoon displaying the principle of how solution-based FCS can detect ligand binding. 215

Figure 7.12: FCS analysis of MK337 binding to SMA-rNTR1, SMA-CB2 or SMA-SAV 216

Figure 7.13: FCS analysis of MK337 binding to SMA-rNTR1 incubated with Mini-G proteins 218

Figure 7.14: Specific binding of MK337 to a neurotensin binding site calculated from FCS analysis. 219

Figure 7.15: Spectral shift assay investigating the effect of MK350 concentration on fluorescently labelled SMA-rNTR1 221

Figure 7.16: A spectral shift assay investigating the effect of MK350 concentration on fluorescently labelled SMA-rNTR1 with and without competitive inhibition with SR 48692. 222

Figure 7.17: A spectral shift assay investigating the effect of SR 48692 concentration on fluorescently labelled SMA-rNTR1 with and without 500 nM MK350. 224

Figure 7.18: SMA-PAGE and Western blot analysis of SMA-CB2, rNTR1 and SAV after incubation with and without Mini-G proteins. 226

Appendix 1.1: E. coli expressed hNTR1 solubilisation trial comparing 4 concentrations of DIBMA (3.5%, 4.5%, 5.5%, 6.5%) and 1.5% w/v SMA. 255

Appendix 1.2: Result of attempted MBPTRap Purification of SMA-rNTR1 expressing E. coli membranes. 256

Appendix 1.3: SDS-PAGE and Western blot analysis of the MBPTrap purification method when SMA-rNTR1 expressing membranes were continuously applied to the MBPTrap column overnight. 257

Appendix 1.4: Results of IMAC purification followed by MBP purification of MBP-fused rNTR1 expressed in E. coli..... 258

Appendix 1.5: Results of IMAC purification followed by MBP purification of MBP-fused CB2 - expressed in E. coli..... 259

Appendix 1.6: SDS-PAGE analysis of fractions from Mini-G protein IMAC Purifications. 260

Appendix 1.7: MK337 characterisation in four different buffer systems: with and without 5 mg/mL BSA and 10% (v/v) glycerol. 261

Appendix 1.8: MK337 characterisation using eight different laser power strengths (1- 40%). 262

Appendix 1.9: Concentration of bound MK337 calculated from a 2-component model after solution-based FCS analysis of seven different MK337 (7.8 nM – 500 nM) concentrations incubated with SMA-rNTR1, with and without bovine gamma globulin (BGG). 262

Appendix 1.9 MK337 characterisation with and without 170 nM SR 48692..... 263

TABLE OF TABLES

Table 1.1: Examples of non-fluorescence-based ligand binding techniques 38

Table 1.2: Fluorescence-based ligand binding assays 39

Table 1.3: Literature Summary of Previous GPCRs Investigated by PoLiPa Technology 41

Table 2.1: List of Polymers and Ligands used in this Project and their Supplier 44

Table 2.2: Bacterial Strains used in Study 45

Table 2.3: Plasmids 46

Table 2.4: Bacterial Growth Media Recipes 47

Table 2.5: Expression Conditions for each MBP-fused GPCR Expressed in E. coli 49

Table 2.6: Buffer Compositions for GPCR Production and Storage 50

Table 2.7: Recipe for 12% Polyacrylamide Laboratory-cast Gels 56

Table 2.8: Primary Antibodies and Dilution used for Western blot Analysis 58

Table 2.9: Models used to Plot Binding Curves 61

Table 3.1: MS Proteomics Analysis of Three Bands excised in the SDS-PAGE gel analysing the first Elution Fraction of an IMAC purification Attempting to purify SMA-hNTR1 74

Table 4.1: Summary of expression conditions previously used in the literature to express rNTR1 94

Table 4.2: Summary of Four Different Resin Types used for IMAC purification and their Key Characteristics 107

Table 6.1: Summary of AASTY Polymers in Solubilisation Trial 175

Table 7.1: List of Mini-G Proteins used in this Project 197

Table 7.2: List of GPCR Ligands used in this Project 197

Table 7.3: Values Derived from two-site Competitive Binding Curve fitted to MK337 SMA-rNTR1 FTS Intensity data 207

Table 8.1: Summary of Expression Conditions Optimised in this Project Compared to Literature 232

Table 8.2: Summary of Polymer Solubilisation Performance on Different GPCRs 235

Table 8.3: Summary of Optimised GPCR Production in this Project 237

Table 8.4: Non-exhaustive List of Known Lipids Capable of GPCR Allosteric Modulation 253

ABBREVIATIONS

2xYT	2x Yeast Extract Tryptone
5-HW	5-hydroxytryptohans
A2AR	Adenosine 2A receptor
AASTY	Poly (Acrylic Acid-alt-styrene)
APG	amphiphilic-gamma-glutamate
AcrB	acriflavine resistance B
APG	amphiphilic-gamma-glutamate
AI	autoinducing
ATP	adenosine triphosphate
AU	Arbitrary Units
b2AR	b2 adrenaline receptor
BGG	Bovine Gamma Globulin
BSA	Bovine Serum Albumin
BW	Buffer Wash
cAMP	cyclic adenosine monophosphate
CB2	Cannabinoid Receptor 2
CD	Circular Dichroism
CHAPS	3-[(3-cholamidopropyl)dimethylammonio]-1-propanesulfonate
CHESS	cellular high-throughput encapsulation, solubilisation and screening
CHS	cholesteryl hemisuccinate
CMA	carboxylmethylaspartate
CMC	critical micelle concentration
CSTR	continual stirred tank reactor method
CV	column volume
Cy5	Cyanine 5
D2R	Dopamine Receptor 2
DAG	diacylglycerol
DDM	n-dodecyl-b-maltoside
DIBMA	poly(Diisobutylene-co-Maleic acid
DIBMALP	DIBMA Lipid Particle
DLS	Dynamic Light Scattering
DMAP	4-Dimethylaminopyridine
DNA	Deoxyribonucleic acid
DTT	dithiothreitiol
E. coli	*Escherichia coli*
E1, E2, E3 etc	Elution 1, Elution 2, Elution 3 etc.
ECL	Enhanced Chemiluminescence
EDTA	Ethylenediaminetetraacetic acid
EM	Electron Microscopy
FACS	Fluorescence Activated Cell sorting
FCS	Fluorescent correlation spectroscopy

FLAG	octapeptide with following sequence: DYKDDDDK
FRET	Fluorescence resonance energy transfer
FT	Flow Through
FTS	Fluorescent tryptophan spectroscopy
GCI	Grated-coupled interferometry
GDP	guanine diphosphate
GFP	Green Fluorescent protein.
GHSR	Ghrelin Receptor
GPCR	G Protein Coupled Receptor
GTP	guanine triphosphate
HEK293	Human embryonic kidney 293 cells
HEPES	4-(2-hydroxyethyl)-1-piperazineethanesulfonic acid)
IC50	Half-maximal inhibitory concentration
hNTR1	human NTR1
IDA	iminodiacetic acid
IMAC	Immobilised Metal Affinity Chromatography
INSOL	Insoluble fraction
IP_3	Inositol triphosphate
IPTG	Isopropyl ß-D-1-thiogalactopyranoside
ITC	Isotherminal Calorimetry
IW20	20 mM Imidazole Wash
IW40	40 mM Imidazole Wash
K_D	Dissociation Constant
K_i	Inhibitor constant
LB	Luria Bertani
LDS	lithium dodecyl sulphate
MBP	Maltose Binding Protein
MS	Mass Spectrometry
MST	Microscale Thermophoresis
MST	Microscale Thermophoresis
MT1R	Melatonin Receptor
MW	Molecular weight
nano-DSF	nano-Differential Scanning Fluorimetry
NBD	Nitrobenzofurazan
NHS	N-hydroxysuccinimide
NMR	Nuclear magnetic resonance
NTA	Nitrilotriacetic acid
NTR1	Neurotensin Receptor 1
OD	Optical Density
P. Pastori	*Pichia Pastori*
PAGE	PolyAcrylamide Gel Electrophoresis
PBS-T	Phosphate Buffer Saline-0.1% Tween
PCR	polymerase chain reaction
PIP2	phosphatidylinositol 4,5 bisphosphate
PoLiPa	Polymer Lipid Particle

R	Arginine
RAFT	Reversible addition−fragmentation chain-transfer
rNTR1	rat NTR1
SAV	Sav1866 - control protein
SD	Standard Deviation
SDS	Sodium Dodecyl-Sulphate
SEC	Size Exclusion Chromatography
SMA	poly(styrene-co- maleic acid)
SMALP	SMA Lipid Particle
SMI	poly(styrene-co-maleimide)
SMILP	SMI Lipid Particle
SMO	Smoothened' Protein
SOL	Soluble Fraction
SPR	Surface Plasmon Resonance
TAMRA	Carboxytetramethylrhodamine
TB	Terrific Broth
TCEP	tris(2-carboxyethyl) phosphine
TEV	Tobacco Etch Virus
TFS	Tryptophan Fluorescent Spectroscopy
TM	Transmembrane domain
TrxA	Thioredoxin A
UV	Ultraviolet
WT	Wild Type

CHAPTER 1: INTRODUCTION

1.1 G Protein Coupled Receptors (GPCRs) and Drug Discovery

GPCRs represent approximately 35% of all drug targets (Sriram and Insel, 2018). There are 270 GPCR modulators approved by the National Health Service (NHS), important for the treatment of cardiovascular disease, allergies, pain, gastrointestinal issues, diabetes, obesity and central nervous system disorders (Pándy-Szekeres *et al*., 2022). These target 88 different GPCRs, 79 of which are Class A rhodopsin-like GPCRs, as reported by the GPCR database (Pándy-Szekeres *et al*., 2022). The development of new drugs is a billion-dollar industry and can take 12-15 years (Hughes *et al*., 2011). A key part of this process is 'Lead Discovery'; the hypothesis that activation or inhibition of a drug target will be therapeutic is validated and a 'candidate' is searched for.

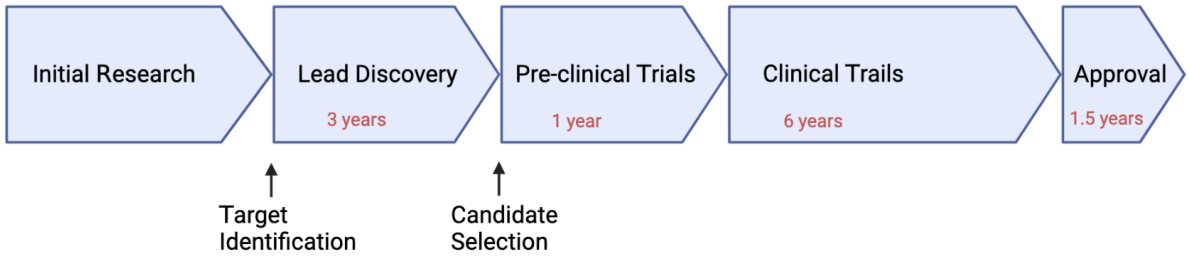


Figure 1.1: Flow chart of simplified Drug Development Pipeline and approximate timescales.

Several qualities make GPCRs a good pharmaceutical target. They are therapeutically relevant and dysregulated in many diseases. Their position in the plasma membrane improves the pharmacokinetics of possible new drugs. The complexity of GPCR interactions can produce a precise response to a ligand. Pharmaceuticals can mimic or block the effect of endogenous ligands to produce a desired effect in the cell. Approximately 350 non-sensory class A GPCRs are activated by diffusible ligands such as hormones and neurotransmitters and 56% have yet to be explored in clinical trials (Hauser *et al*., 2017).

GPCRs can have different conformational changes depending on the type of ligand that allow selective activation of G-proteins and β-arrestins (Carpenter and Tate, 2017). This structural plasticity and varied effect on intracellular signalling pathways allows them to mediate a wide range of responses in the cell (Kobilka, 2007). GPCRs can form specific activation states that activate some signalling pathways at the expense of others (Smith *et al*., 2018). This biased signalling allows 'fine-tuned' cell reactions to endogenous ligands and also pharmaceuticals (Kenakin, 2019). Designing pharmaceuticals that activate a GPCR in a specific fashion or only activate GPCRs in specific tissues can allow pharmaceuticals to have more targeted therapeutic effects with less toxic side effects.

Despite GPCRs having high therapeutic potential, their instability and amphipathic nature has restricted their investigation outside the plasma membrane. Excluding the olfactory, taste and visual, GPCRs, approximately 100 out of 360 endogenous GPCRs lack a known physiological agonist (Insel *et al*., 2019). The structural plasticity of GPCRs makes GPCRs notoriously unstable outside the cell (Wootten *et al*., 2018). Tools which improve the availability of GPCRs for biophysical techniques *in vitro* would be valuable in the drug discovery space.

1.2 Structure and Function of GPCRs and G-proteins

GPCRs have seven transmembrane α-helices, an extracellular region, consisting of the N-terminus and three extracellular loops, and an intracellular region, consisting of the C-terminus and three intracellular loops (Cavasotto and Palomba, 2015). The ligands typically interact with the extracellular region and within the centre of the transmembrane α-helices. G proteins and β-arrestins interact with intracellular regions. Binding of an agonist to a GPCR causes a conserved conformational change in the 'transduction site' or cytoplasmic interface: a large rotation and displacement of the 6th transmembrane domain (TM6) and smaller

rotations and movements of TM5 and TM7 (Figure 1.2). This change typically increases the affinity of GPCR-G protein coupling (Wingler and Lefkowitz, 2020).

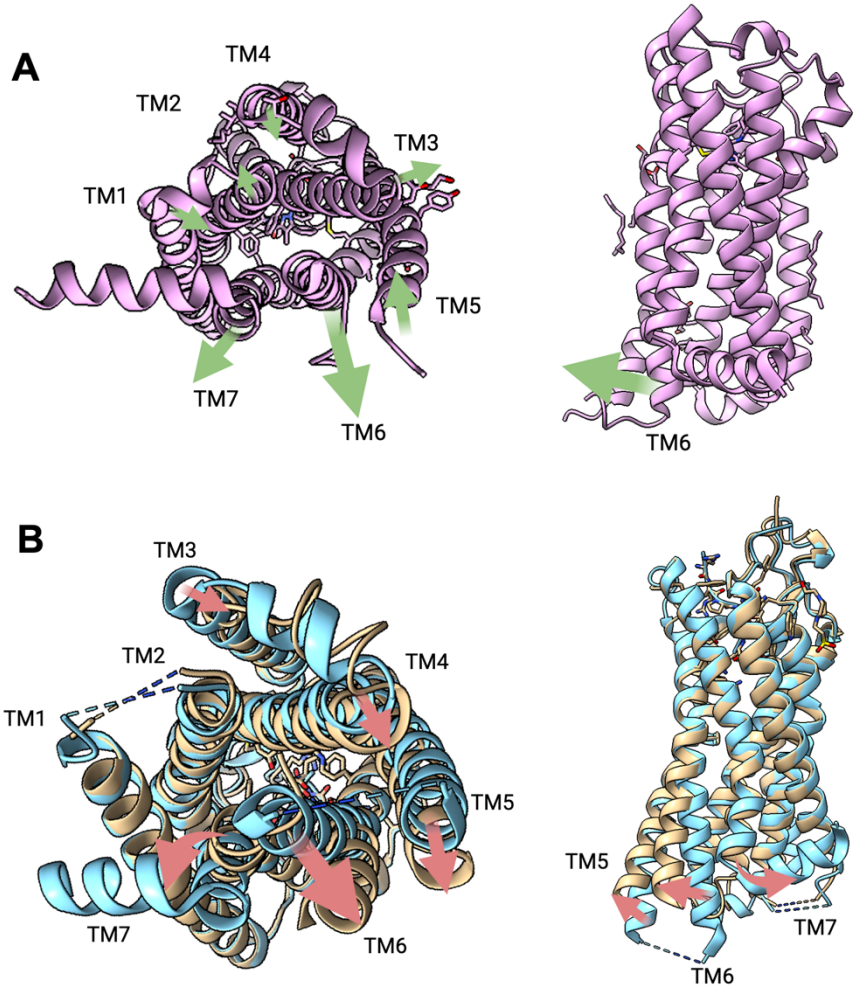


Figure 1.2: Structures demonstrating the conserved conformational changes in the 'transduction site' of GPCRs
(A) Inactive structure of Cannabinoid Receptor 2 (CB2) (PDB:5ZTY) (Li et al., 2019). Green arrows demonstrating the movement of the transmembrane domains in the transduction site, as demonstrated by homology modelling (Hu et al., 2016)
(B) Inactive (blue, PDB:4BUO) (Egloff et al., 2014) (Egloff et al., 2014) and active (Brown, PDB:4GRV) (White et al., 2012) structure of rat Neurotensin Receptor 1 (rNTR1) variants. Red arrows demonstrate the movement of the transmembrane domains in the transduction site. Figures made using ChimeraX (Pettersen et al., 2021).

In addition to G protein-independent mechanisms, GPCRs are capable of transducing signals through G protein coupling (Kristiansen, 2004). In the cell, the binding of an agonist causes conformational changes of the GPCR which can activate a bound G protein, releasing it. Heterotrimeric G proteins consist of three subunits: alpha, beta and gamma. Upon heterotrimeric G protein activation, the alpha subunit exchanges bound guanine diphosphate

(GDP) for guanine triphosphate (GTP) (Tuteja, 2009). The GTP-bound alpha subunit and beta-gamma subunit disassociate and interact with effector proteins such as ion channels and enzymes (Figure 1.2).

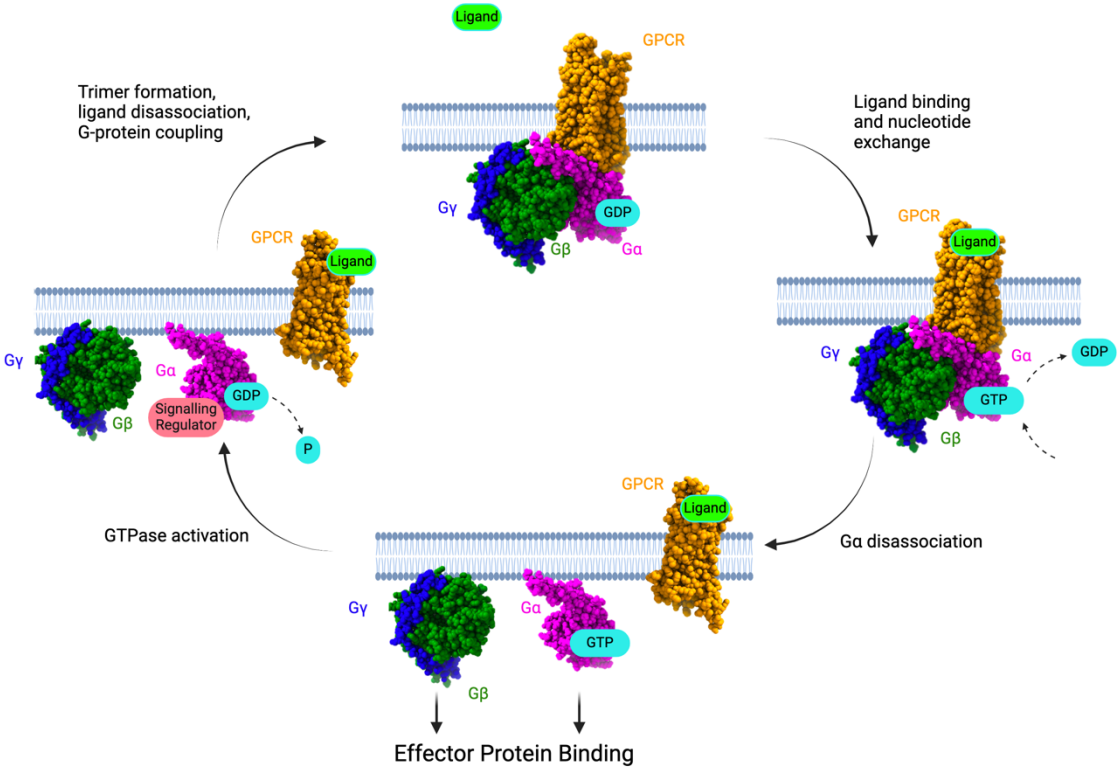


Figure 1.3: Schematic illustrating how GPCRs activates G proteins causing downstream signalling pathways. *Use of human neurotensin receptor 1 (hNTR1) - Gi1 complex structure (PDB: 6SO9) was used to represent a GPCR (orange) and a heterotrimeric G protein with G alpha (pink), G beta (green) and G gamma (blue) subunits (Kato et al., 2019). Conformational changes of the proteins not shown.*

The hydrolysis of GTP to GDP causes the re-association of the subunits; the conformational shape of the inactive G protein allows GPCR binding (Hamm, 1998). Different types of alpha subunits of G proteins cause different cell signalling pathways. Different GPCRs have different biases for the type of G protein they activate. The four classes of alpha subunit are Gs, Gi, Gq and G12/13 (Syrovatkina *et al*., 2016). Gs stimulates adenyl cyclase, increasing the production of the secondary messenger cyclic adenosine monophosphate (cAMP), as well as stimulating dihydropyridine-sensitive Ca^{2+} channels (Yatani *et al*., 1988). Gi inhibits adenyl cyclase, decreasing the production of cAMP (Wang *et al*., 2004). Gq activates

phospholipase C, generating inositol triphosphate (IP_3) and diacylglycerol (DAG) (Mizuno and Itoh, 2009). G12/13 regulates the actin cytoskeleton (Wang *et al*., 2006). Within these classes, several subclasses of G alpha subunits are categorised by sequence and expression (Figure 1.4). This begins to elucidate how signal transduction of a GPCR can cause a specific response in a cell.

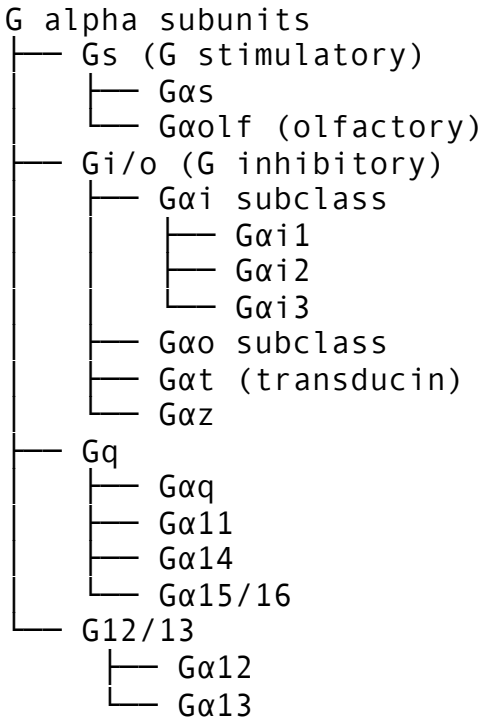


Figure 1.4: Subclasses of the G-protein Alpha subunits.

1.3 Membrane Proteins and Polymer Lipid Particle (PoLiPa) Technology

The fundamental structure of any membrane is a phospholipid bilayer. Two layers stack of phospholipids form a barrier between two aqueous compartments with the phosphorus head groups on the outside and the fatty acyl chains facing pointing inwards (Watson, 2015). The position of membrane proteins within this hydrophobic environment means research into the structure and function of membrane proteins is notoriously more difficult than soluble proteins.

In 2014, less than 2% of unique protein structures were membrane proteins (Egloff *et al*., 2014). The ability to produce, solubilise and purify membrane proteins has typically required detergents. However, the cell membrane stabilises and can be vital to the structure of the embedded protein. The production of membrane proteins through detergent solubilisation has typically led to small yields of active protein (Pandey *et al*., 2016). Many membrane proteins, such as GPCRs, have high therapeutic importance so improvements to solubilisation techniques have been impactful.

The discovery of poly(styrene-*co*-maleic acid) (SMA) as an alternative solubilisation agent to detergent has led to many advances in the structural and functional understanding of membrane proteins (Knowles *et al*., 2009). The hydrophobic styrene groups embed into the membrane and the hydrophilic maleic acid groups point outwards and interact with the solution. This causes the formation of nano-discs which contain sections of the native membrane wrapped in polymer (Figure 1.5) (Jamshad *et al*., 2015b). Nanodiscs encapsulating a protein of interest can then be purified to produce soluble protein surrounded by native lipids. These nanodiscs are referred to here as SMA lipid particles (SMALPs) or PoLiPa as there are now several amphipathic polymers that appear to have a similar solubilisation ability to SMA. PoLiPa is a trade name assigned to polymer lipid particle technology by the company Domainex. The most common alternative to SMA is Diisobutylene Maleic Acid (DIBMA) (Gulamhussein *et al*., 2020).

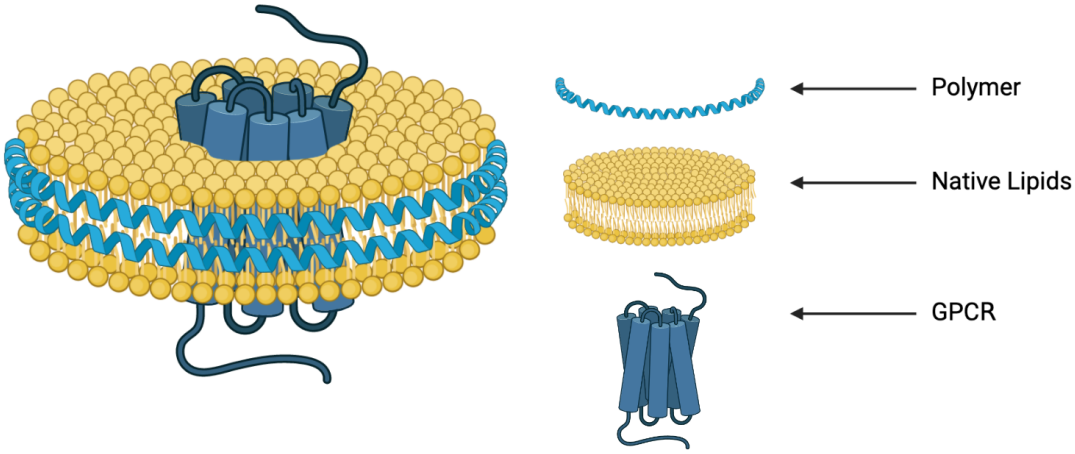


Figure 1.5: Cartoon representation of a PoLiPa containing a GPCR.
Polymer allows solubilisation of GPCR whilst maintaining surrounding native lipids.

Despite the usefulness of polymers for membrane protein solubilisation, the exact mechanism for PoLiPa formation is unknown. Kinetic experiments suggest two phases: burying of the hydrophobic groups such as styrene into the membrane followed by the formation of a disc (Scheidelaar *et al*., 2015). The phenyl group in styrene can intercalate into the bilayer and act like cholesterol does in the membrane, reducing fluidity. The intercalated phenyl groups could also interact with the encapsulated protein (Jamshad *et al*., 2015b). Another factor is the formation of polymer aggregates. Without sufficient lipids, SMA polymers can form a collapsed higher-order aggregate which often has to be removed after solubilisation in the purification process. It is thought that the polymer may have to disassociate from polymer aggregates before the formation of a PoLiPa. However, the number of polymer molecules that wrap around each PoLiPa and how the discs interact with each other, other membranes, lipids, and proteins are not fully understood.

1.4 Benefits of PoLiPa for GPCR Solubilisation

Efficient production of solubilised, purified GPCR is a common issue in biophysical characterisation and functional analysis, requiring the thorough optimisation of methods for obtaining a stable soluble GPCR. Detergent screens can be performed to determine which solubilisation agent produces the highest yield (Corin *et al*., 2011). Milder detergents like n-dodecyl-β-maltoside (DDM) are more commonly used (Lee *et al*., 2020). Mutagenesis to produce GPCR variants with increased stability is also common practice for the GPCR investigations (Grisshammer, 2009). Using amphipathic polymers could allow solubilisation without large detergent screens or mutagenesis investigations. Improving the stability of GPCRs via nanodiscs could prevent the need for mutations to tolerate detergents. This could make ligand binding experiments more representative of physiological interactions with drugs as fewer compromises need to be made regarding modifying GPCR structure.

Similar to many membrane proteins, the surrounding phospholipids regulate GPCR function (Dawaliby *et al*., 2016). A major advantage of using polymers as solubilisation agents is that they allow sampling of the membranes including the native lipids. The plasma membrane is organised to allow the functionalisation of receptors. Flexibility and mobility in the lipid membrane affect how receptors undergo conformational changes and binding events, whilst stabilising the receptor (Baccouch *et al*., 2022). The local membrane surrounding the protein also allows the formation of signalling platforms and protein complexes such as the G protein complex with a GPCR (Sejdiu and Tieleman, 2020). More rigid microdomains of the membrane called lipid rafts can contain clusters of receptors and the localisation of these rafts can affect receptor potency and efficiency (Allen *et al*., 2007). Finally, the exposure of receptors to a ligand is affected by the shape and movement of the lipid membrane (Besserer-Offroy *et al*., 2017). The sampling of nano-discs using polymers does not allow a large-scale analysis of the interplay between lipids and receptors. However, SMALPs have been used to show distinctive membrane environments for classes of protein (Teo *et al*., 2019).

Amphipathic polymers are a useful tool in understanding how the immediate lipid environment can affect the functionality of the protein.

Detergent-solubilised membrane proteins often require low temperatures to prevent aggregation and degradation (Kotov *et al*., 2019). Using PoLiPa can allow experiments to be performed at room temperature (RT) or higher, which more closely represents physiological conditions. A melting point (T_m) of DIBMA-solubilised β2 adrenaline receptor (β2AR) could not be calculated because the protein was seemingly stable up to 80°C (Harwood *et al*., 2021). This increased stability of proteins in PoLiPa not only allows more realistic experiments but creates flexibility around the production, purification, shipping and storage of membrane proteins.

The flexibility of GPCRs within the surrounding membrane could be an important factor in their function that is not being considered after detergent-based solubilisation. Other practical disadvantages of using detergent include the need to include detergent in all buffers post-solubilisation above the critical micelle concentration (CMC) (Stetsenko and Guskov, 2017). High concentrations of detergent cause de-lipidation of lipid-detergent-protein mixed micelles which can de-stabilize solubilised protein and cause aggregation. This can be an issue when concentrating protein as the detergent can also concentrate. Detergents can also be problematic during functional and structural analysis (Stetsenko and Guskov, 2017). Amphipathic polymers, on the other hand, only need to be used once to solubilise a protein and excess polymer can be diluted or removed by buffer exchange.

GPCRs in detergent often must be bound to an inverse agonist or antagonist to keep the receptor in the more stable non-signalling state (Grisshammer, 2009). However, assays which measure G protein activation require flexibility of the GPCR to move between active and non-

active conformations. Amphipathic polymers may be a solution to this problem. PoLiPa technology could also allow the discovery of new modulators of GPCRs as current ligand binding studies focus on maintaining the active site of the GPCR but compromise with the addition of tags and mutations to allow efficient expression, solubilisation and purification. PoLiPa could therefore allow the production of a more representative 'native' protein.

There has been some success in using amphipathic polymers to solubilize GPCRs (Wheatley *et al*., 2016). Fluorescence resonance energy transfer (FRET) assays showed a similar K_d of adrenaline in membranes, DDM-solubilised and DIBMA-solubilised β2AR (Harwood *et al*., 2021). At 4°C, the Adenosine 2A receptor (A2AR) in a SMALP had specific binding which did not drop below 75% until after 15 days, whereas DDM-solubilised A2AR had no specific binding after less than an hour at 37°C (Jamshad *et al*., 2015a).

1.5 Advantages and Disadvantages of Different Polymers

The most used polymer is SMA 2000, which is manufactured in a way that the styrene to maleic acid ratio is approximately 2:1, but the length and distribution of styrene and maleic acid across the chain is not regular. There are two main methods of producing polymer. The continual stirred tank reactor method (CSTR) produces consistent polymer composition but large variations in polymer lengths (Klumperman and Heuts, 2020). Reversible addition−fragmentation chain-transfer (RAFT) polymerisation can allow the production of polymers with a controlled length and more potential to have functional groups (Cunningham *et al*., 2020). Craig *et al* performed RAFT in a one-step reaction synthesis to create polymers consisting of two blocks (a block of styrene-MA alternated and a block of styrene only) with a variety of different ratios between these two blocks and molecular size. The best polymer by this method was still only 60% as effective as SMA 2000 made by CSTR (Craig *et al*., 2016).

However, consistency in the polymer is important for some modifications and the comparison between polymers.

The solubilisation efficiency of amphipathic polymers is dependent on hydrophobicity and length. When comparing SMA varieties, a styrene to maleic acid ratio greater than 1.5:1 meant better solubilisation but SMA 4:1 had solubilisation issues; for SMA 2:1 or 3:1, a molecular weight (MW) of 7.5-10 kDa was optimal (Craig *et al*., 2016). Testing different polymers may provide information about the best methodology for producing soluble GPCRs. The fragility of GPCRs makes optimal solubilisation and stabilisation an important investigation.

The drawbacks of SMA include the absorbance of light due to the aromatic structure of styrene which overlaps with 280 nm absorption readings, causing difficulty in estimating protein concentration. The sensitivity of SMALPs to divalent cations cause difficulties for assays that require Mg^{2+} concentrations greater than 5 mM, such as Adenosine triphosphate (ATP) enzymatic assays (Gulamhussein *et al*., 2019).

Confining a membrane protein to a disc is thought to reduce the fluidity of the surrounding lipids and can affect the ability of some membrane proteins to undergo conformational changes (Pollock *et al*., 2022). A major importance for investigating multiple polymers is that polymer architecture can determine the conformational state in which a GPCR is stabilised within the PoLiPa (Grime *et al*., 2021).

Research into novel polymers for solubilisation is continuous and provides an exciting toolkit of membrane protein investigations moving forward (Figure 1.6). DIBMA has allowed a larger disc size and no ultraviolet (UV) interference but with a typically smaller yield of

protein (Gulamhussein *et al*., 2020). Poly(styrene-co-maleimide) (SMI) was found to be an acid-compatible polymer that could solubilise lipids between the pH range of 5-7 (Hall *et al*., 2018). Poly(Acrylic Acid-alt-styrene) (AASTY) was recently shown to have an improved solubilisation efficiency of an ion channel expressed in mammalian cells (Smith *et al*., 2020).

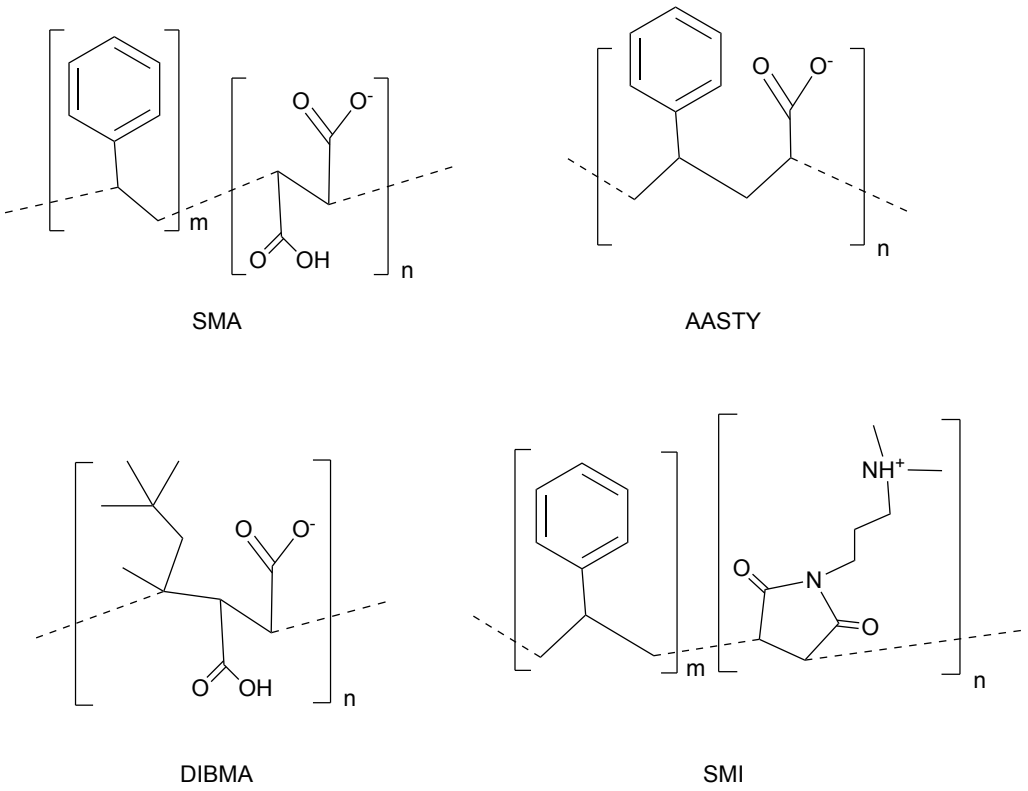


Figure 1.6: Chemical Structures of Amphipathic Co-polymers investigated in this project.
Poly (Styrene-co-maleic Acid (SMA), poly (Acrylic Acid-alt-styrene) (AASTY), poly (Diisobutylene-co-Maleic acid (DIBMA), poly (styrene-co-maleimide) (SMI).

Polymers with additional functionality are also in development. For example, polymers that include a Strep-tag or a biotinylated group could allow binding onto a surface, which would be useful for surface-based assays. Fluorescently-tagged SMA has been used to solubilise a membrane protein; for one polymer, there was energy transfer between the fluorescently-tagged polymer and the intrinsic fluorescence of tryptophan in the protein (Neville *et al*., 2022). More research is needed to understand the potential benefits of addition of

functionalised groups onto a polymer and the possible drawbacks on solubilisation efficiency and structure of the nanodisc.

1.6 Investigated GPCRs

Two GPCRs will be primarily investigated in this thesis: Neurotensin Receptor 1 (NTR1), and Cannabinoid Receptor 2 (CB2). These, like most non-sensory GPCRs, are of high therapeutic importance. Neurotensin has an important role in regulating the dopaminergic system; dysregulation of NTR1 signalling is important in cancer, schizophrenia, and methamphetamine abuse (Thomas *et al*., 2009). The CB2 receptor is a regulator of inflammation and has the potential to be a drug target for neuroinflammatory diseases (Turcotte *et al*., 2016).

Due to instability and large conformational changes, GPCR crystal structures tend to be obtained bound to agonists, antagonists, or other binding partners. Several structures of agonist bound human or rat NTR1 mutants have been solved (Deluigi *et al*., 2021; Egloff *et al*., 2014; Huang *et al*., 2020; Kato *et al*., 2019; White *et al*., 2012). Two structures of CB2 have been solved: antagonist bound CB2 with the addition of a T4-lysozyme in the sequence and agonist bound in complex with Gi was produced in insect cells and the structure solved bound to an antagonist (Li *et al*., 2019; Xing *et al*., 2020). Crystal structures are a helpful tool for identifying binding pockets and elucidating the structure of a protein but cannot illustrate the large multidimensional conformational changes of GPCRs. To find new binding partners, ligand binding experiments and compound screens are needed to complement structural analysis and computational studies.

1.7 Choice of Expression System for GPCR Production

Recombinant expression of GPCRs has been performed in several different cell systems. This has included the use of *E. coli*, mammalian, insect and yeast cells, specifically *Pichia Pastori* (Wiseman *et al*., 2020). GPCRs have also been expressed in the photoreceptor cells of *Drosophila melanogaster* (Eroglu *et al*., 2002). This project initially investigated the use of *E. coli* as an expression system. *E. coli* is a popular choice for recombinant protein expression because it is time- and cost-efficient (Rosano and Ceccarelli, 2014). Plasmid production, modification and transformation are efficient because there are *E. coli* strains that produce high copy numbers of plasmids. A disadvantage of *E. coli* expression for mammalian proteins is the high likelihood of low expression: misfolded and aggregated proteins are removed by *E. coli* by collecting into inclusion bodies (Palmer and Wingfield, 2004). To overcome this hurdle, addition of mutations and fusion proteins, such as Maltose-Binding Protein (MBP) can reduce misfolding (Bokhove *et al*., 2016). Other strategies include expression condition adjustments to temperature, cell line and induction method (Attrill *et al*., 2009).

This project also aimed to make a comparison between an *E. coli* expression system and a mammalian expression system. Human embryonic kidney 293 cells (HEK293) are a popular choice for small-scale protein expression due to their growth and transferability (Tan *et al*., 2021), however, mammalian cell culture is costly in terms of both time and financial expenditure (Gray, 2001). Luria Bertani (LB) media commonly used for *E. coli* growth is up to 40-fold less expensive than FreeStyle™ 293 Expression Medium used for HEK293 cell growth in this project. Despite the more labour-intensive and costly process of mammalian cell expression; this cell system is closer to the native environment of a GPCR. Unlike bacterial cells, mammalian cells have the machinery for post-translational modifications such as glycosylation (Verma *et al*., 1998). Glycosylation is not typically uniform and can cause heterogeneity in the purified protein sample. However, glycosylation may be important for

GPCR structure and function; the inclusion of specific glycosylation sites can improve solubility and reduce misfolding (Verma *et al*., 1998). A comparison of two cell systems is especially useful for PoLiPa investigations because the lipid nanodisc includes the native lipids of the cell from which the protein was expressed and GPCRs are modulated by their lipid environment.

1.7 Membrane Composition and its effect on GPCRs

In this project, GPCRs were investigated by recombinant expression in HEK293 cells or *E. coli*. However, the expression system and the expression protocol can have a large effect on the composition of the lipid membrane and therefore the environment of the GPCR. Use of PoLiPa technology enables a 'sampling' of the lipid environment, which can have a large effect on GPCR function. Therefore, it is important to note the types of lipids that may be co-extracted with a recombinantly expressed GPCR.

HEK293 cells will have a more 'native-like' lipid membrane composition than *E. coli.* However, the major component of the lipid membrane is the same in both expression systems: phosphatidylethanolamine (PE). Another significant component of HEK293 cell membranes is phosphatidylcholine (PC). Sphingomyelin is present in lower amounts but contributes to stability and some signalling pathways. Other lipids that are likely to be present in the HEK293 cell membrane, which have been associated with GPCR modulation include cholesterol, phosphatidylinositol 4,5 bisphosphate (PIP2) and glycosphingolipids (Damian *et al*., 2021). *E. coli* lipid membranes are primarily composed of PE (~75%), phosphatidylglycerol (PG) (~20%) and cardiolipin (~5%) (Raetz and Dowhan, 1990). Only trace amounts of cardiolipin are in the HEK293 cell membranes. The *E. coli* cell membrane

does not include lipids such as cholesterol, PIP2, glycosphingolipids or docosahexaenoic acid which have been shown to have a modulatory function on GPCRs.

There are several demonstrations of GPCR lipid modulation. Synthetic PG has been shown to stabilise the active conformation of β2AR whereas PE stabilised the inactive conformation (Dawaliby *et al*., 2016). Lipid nanodisc investigations of NTR1 have shown that synthetic lipid composition did not affect neurotensin affinity but did affect the G protein GDP/GTP exchange rate up to 2-fold (Inagaki *et al*., 2012). PoLiPa technology could provide a new toolkit for investigating lipid modulation of GPCRs.

1.8 Optimizing Purification Protocols for GCPRs in PoLiPa

Some possible challenges with purification include the size of the PoLiPa preventing access to porous resins, the possible obstruction of tags by the native lipids and surrounding polymer as well as the effects of excess polymer in solution. Ion exchange chromatography cannot be performed due to negatively charged SMA negating any differences in the isoelectric point of the GPCR and the contaminant proteins.

SMA-solubilised proteins are commonly purified by Immobilised Metal Affinity Chromatography (IMAC) using Ni-Nitrotriacetic (Ni-NTA) resin followed by size exclusion chromatography (SEC) (Lee *et al*., 2016). A GPCR, expressed in insect cells, was produced via this method to sufficient purity and yield for nuclear magnetic resonance (NMR) titrations to determine binding constants to other proteins (Zhu *et al*., 2022). The levels of contamination following IMAC purification are related to the expression of the protein of interest (Bartlow *et al*., 2011). Well-expressed proteins can out-compete proteins with lower affinity to the resin. Tedesco *et al* suggested a methodology for purifying SMA-solubilised

GPCRs from low-yielding cell lines by performing SEC followed by IMAC purification (Tedesco *et al*., 2021). The reasoning was that SEC removes large aggregates, chelating agents and excess SMA which interfere with the IMAC purification. However, there was only enough protein to confirm the presence of the GPCR by immunoblotting.

Multiple tags can be used to purify proteins, and many variables may improve yield and reduce contamination, for example, the use of different resin types, buffer components, binding times and temperatures (Ejima *et al*., 2005b; Boivin *et al*., 2013). This project will investigate how to best purify polymer-solubilised GPCRs. This will provide new insights into optimising a purification protocol when working with PoLiPa and challenging proteins.

1.9 Biophysical Characterisation of PoLiPa

This project intended to develop methods to generate pure GPCRs and then use them to understand the biophysical properties of GPCRs in PoLiPa. This includes whether the protein is folded, what oligomerisation state it inhabits and the stability of the protein. To test this, several biophysical techniques were utilised including Dynamic Light Scattering (DLS), nano-Differential Scanning Fluorimetry (nano-DSF), SEC, Circular Dichroism (CD) and SMA- or DIBMA-polyacrylamide gel electrophoresis (PAGE).

1.9.1 DLS

DLS has been used to assess the size of particles such as liposomes or nanodiscs (Fiori *et al*., 2017). The scattering of light through a solution is related to the Brownian motion of particles in the solution, which is related to the hydrodynamic size of a particle (Stetefeld *et al*., 2016). A size distribution profile can be obtained as a measure of the percentage of intensity of the scattered light. Heterogeneous samples are more difficult to dissect and analyse quantitatively but can provide key information about protein aggregation in a sample.

1.9.2 NanoDSF

The intrinsic tryptophan fluorescence of proteins can be utilised to calculate protein thermostability using nanoDSF (Kim *et al*., 2021b). This technique measures the ratio of fluorescence emitted at 330 and 350 nm. This increases upon protein unfolding as the tryptophan residues become more exposed to a hydrophilic environment. Thermostability can be calculated by performing a denaturing assay at different temperatures; the derived T_m describes the temperature when half of the proteins are unfolded. The T_m can be calculated from nanoDSF data by finding the inflexion point of the first derivative of the 350:330 ratio. PoLiPa typically have a stabilising effect on membrane proteins (Stroud *et al*., 2018). This technique provides a valuable tool for understanding the stabilising effect of PoLiPa on GPCRs.

1.9.3 CD

CD is a technique used to assess the secondary and tertiary structure of proteins by measuring the difference in absorption of circularly polarized light (Miles *et al*., 2021). Analysis of a CD spectrum can show characteristic peaks caused by α-helices and β-sheets (Figure 1.7). In this project, CD was used to confirm that a purified GPCR was correctly folded whilst encapsulated in a SMALP. Changes in CD spectra can be used to monitor protein unfolding and binding interactions (Greenfield, 2006).

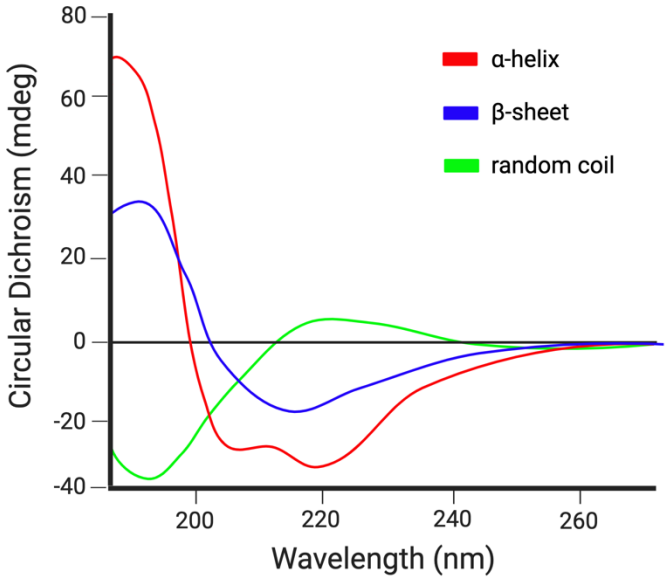


Figure 1.7: Example standard CD Spectra of proteins containing only one type of secondary structure.

1.9.4 SEC

SEC is commonly used as a purification step to separate proteins based on hydrodynamic radius (Hong *et al*., 2012). SEC is also a useful analytical tool. It can be used together with DLS measurements to give an understanding of the heterogeneity of a sample and the relative sizes of the particles compared to globular protein standards. Protein is detected from the column elution by UV absorbance. SEC has been used to show the SMA-solubilised protein elution by both the absorbance of the polymer and tyrosine residues at 254 nm and the intrinsic tryptophan residues at 280 nm (Lee *et al*., 2019). Understanding the benefits and drawbacks of SEC analysis for PoLiPa is an important reflection.

1.9.5 SMA- or DIBMA-PAGE

SMA- or DIBMA-PAGE is an adaptation of Native-PAGE which utilises the intrinsic negative charge of SMA or DIBMA to cause migration of SMALPs and DIBMALPs through an acrylamide gel towards an anode (Pollock *et al*., 2019). The amount of negatively charged

polymer around each SMALP is an unknown phenomenon. The size and charges of the protein and lipids inside the PoLiPa, protein aggregation and protein interactions will all affect the migration of the particles through an acrylamide gel. Despite this, the approximate molecular weight (MW) of proteins obtained from SMA-PAGE have been reflective of the expected MW of the SMA-solubilised proteins (Pollock *et al*., 2019). This technique offers a sensitive method of investigating PoLiPa size, protein oligomerisation states and protein-protein interactions.

1.10 Ligand Binding Experiments

Ligand binding experiments are important because they assess the functionality of the GPCR in a PoLiPa and the binding capacity of different ligands. Ligand screening or detection is important in the drug discovery pipeline (Hulme and Trevethick, 2010). Most ligand binding experiments aim to calculate K_d to define the affinity of a receptor for a particular ligand. K_d can be calculated by measuring the 'on rate' and 'off rate', which can be achieved by techniques that measure real-time binding such as surface plasmon resonance. More commonly, K_d is calculated by measuring the relationship between concentration of ligand and concentration of bound ligand. K_d equals the concentration of ligand when 50% of the receptors are occupied (Sykes *et al*., 2019). Traditionally, ligand binding assays of GPCRs have used radioactive labelling of ligands. Other techniques are becoming more popular due to limiting radioactive hazards and obtaining more information about the kinetics or conformational changes involved in a receptor-ligand interaction (Table 1.1). Several ligand binding techniques utilise fluorescence spectroscopy as a tool.

Table 1.1: Examples of non-fluorescence-based ligand binding techniques

Ligand binding technique	Description	Advantages	Disadvantages	Example
Radioligand binding assays	Radioligand disassociation can be measured upon addition of unlabelled ligand	Well-established	Radioactive hazard	(Hulme and Trevethick, 2010)
Isothermal calorimetry (ITC)	Measures exchanged heat in a binding reaction by titrating in ligand at a controlled temperature	No tags or labels required	More complex data analysis	(Saboury, 2006)
Surface plasmon resonance (SPR)	Measures changes in oscillation of free electrons at interface with immobilised ligand or receptor. Binding events increase resonance causing a peak.	Real-time binding event analysis	Immobilisation onto chip	(Navratilova *et al*., 2011)

1.11 Fluorescence Spectroscopy

Fluorescence spectroscopy is a sensitive tool that can provide structural and functional information about a protein. Fluorophores contain excitable electrons which absorb light at a certain wavelength and emit light at a longer wavelength (Lakowicz, 2006).

Fluorescent ligands are a useful tool for binding assays, however, receptors can also be tagged or mutated to contain a specific fluorophore. Fluorescence has been used in different ways to determine the affinity of a ligand (Table 1.2). One exciting technique, shown to be compatible with PoLiPa technology, is fluorescence correlation spectroscopy (FCS) (Grime *et al*., 2020). FCS can be used to determine whether the diffusion rate of a fluorescent ligand in a 'free' or 'bound' state and calculate the concentration of bound ligand in a solution (Stoddart *et al*., 2022).

Table 1.2: Fluorescence-based ligand binding assays

Ligand-Binding Technique	Description	Advantages	Reference
Separation	Receptor and fluorescent ligand incubated, bound ligand separated by filtration or centrifugation and quantified by fluorescence intensity	Simple and high throughput. Some tags can allow washing of the receptor ligand complex while bound to beads.	(Bumbak *et al*., 2020)
Fluorescent Tryptophan Spectroscopy	Measures changes in intensity and peak emission wavelength of tryptophan or tyrosine fluorescence upon ligand binding.	Gives insights into conformational changes.	(Sindrewicz *et al*., 2019)
Fluorescence Correlation Spectroscopy	Measures fluctuations in fluorescence to model how a fluorescent ligand moves through a solution. Modelling two-components can be used to calculate concentration of bound vs free ligand	Quantifies concentration and diffusion coefficient of fluorescent particles. Potential to model multiple fluorescent particles and characterise interactions.	(Yu *et al*., 2021)
Fluorescence Resonance Energy Transfer	Detects energy transfer over a small distance from a 'donor' fluorophore in its excited state to an 'acceptor' fluorophore which becomes excited and emits a specific wavelength.	Less background signal/ unspecific binding issues Can give information about distance between fluorophores	(Xie *et al*., 2011)
Microscale Thermophoresis (MST)	Measures the movement or change of fluorescence due to a temperature change. This should differ if a fluorescently labelled receptor is bound to a ligand.	Detects precipitation and aggregation real-time and doesn't require purification to obtain equilibrium constant	(Bartoschik *et al*., 2018)
Spectral Shift Assays	Measures the changes in emission spectra of a fluorescently labelled protein caused conformational changes.	Like MST but doesn't require a change in temperature. Isothermal measurement is more sensitive	(Langer *et al*., 2022)

As well as conjugated fluorophores, intrinsic fluorescence changes can be monitored by fluorescent tryptophan spectroscopy (FTS). Aromatic amino acids, such as tryptophan and tyrosine, have excitable electrons, which give proteins containing these amino acids intrinsic fluorescence. When measuring tryptophan fluorescence by excitation at 295 nm, proteins typically have a single maximum between 330-360 nm (Vladislav Victorovich *et al*., 2021). Changes to this intrinsic fluorescence can infer information about the environment of the tryptophan residues in a protein. This large amino acid usually forms hydrophobic interactions and is capable of pi-stacking. The binding of a ligand and conformational changes to the protein can change the interactions of the tryptophan residues with other amino acids, which can affect their fluorescent properties. Exposure of tryptophan residues to a more polar environment typically causes a decrease in fluorescence intensity and an increase in peak

wavelength (Ghisaidoobe and Chung, 2014). GPCRs can have different conformational changes depending on the type of ligand (Kobilka, 2007). Dose-dependent changes to intrinsic fluorescence properties upon the addition of a ligand could provide evidence of these conformational changes.

1.12 Mini-G proteins as a Function Assay Tool

The primary function of GPCRs is signal transduction across the plasma membrane, most notably by binding to an agonist and activating a coupled G protein. Mini-G proteins are engineered soluble proteins, expressed in *E. coli,* which simulate the alpha subunit of G proteins (Nehmé *et al*., 2017). Mini-G proteins were produced in this thesis to determine the 'coupling' capability of GPCRs encapsulated in a PoLiPa.

1.13 Previous Investigations of GPCRs Utilising PoLiPa Technology

Table 1.3 summarises previous solubilisation and purifications utilising PoLiPa technology for GPCR investigations. The first solubilisation of a GPCR by the SMALP method was A2AR (Jamshad *et al*., 2015a). Several other investigations have successfully produced pure GPCRs for various assays. Fluorescently labelled rNTR1 has been solubilised with SMA to investigate oligomerisation but the SMA-rNTR1 was not purified (Dathe *et al*., 2019). No other biophysical characterisation or ligand binding assays have been used to investigate polymer-solubilised NTR1. Polymer solubilisation of CB2 has never been reported. These were chosen as 'model' GPCRs for this investigation because their production using detergent is extensive, but the understanding of their behaviour in a lipid nanodisc is sparse.

Table 1.3: Literature Summary of Previous GPCRs Investigated by PoLiPa Technology

GPCR	Expression System	Polymer	Purification	Biophysical Assays	Functional Assays	Reference
rNTR1-mRuby3	HEK293T	SMA 2:1 (2% (w/v))	No Purification	homoFRET ABELtrap	Not applicable	(Dathe *et al*., 2019)
A2AR	P. Pastoris HEK293T	SMA 2:1 (2.5% (w/v))	IMAC: Ni-NTA	CD SEC	Radioligand Binding and Thermostability	(Jamshad *et al*., 2015a)
Melatonin Receptor (MT1R)	P. Pastoris	SMA 2:1 (2.5% (w/v)) (from proteo-liposomes)	IMAC: Ni-Sepharose	SEC	Radioligand binding, β-Arrestin and G protein recruitment	(Logez *et al*., 2016)
Ghrelin Receptor (GHS-R1a)	*E. coli*	SMA 2:1 (2.5% (w/v)) (from proteo-liposomes)	IMAC: Ni-Sepharose	SEC	FRET based ligand binding assay	(Logez *et al*., 2016)
Ghrelin Receptor Dopamine Receptor Heteromer (GHSR-D2R)	*E. coli* -GHSR *P. Pastoris* - D2R	SMA 2:1 (lipid to polymer ratio 0.1)	1. Anti-FLAG M1 affinity resin 2. S-protein agarose resin	FRET based oligomer-assay DLS SEC	FRET based G protein activation assay	(Damian *et al*., 2018)
Dopamine Receptor 1 (D1R)	HEK293F cells	SMA 3:1 (membrane: SMA weight ratio 1:1.15)	1. SEC 2. IMAC: Ni-Sepharose	SEC	Radioligand binding assay MST	(Bada Juarez *et al*., 2020)
Rhodopsin	Rod outer segments (native bovine cells)	SMA 3:1 (1-100 molar ratio SMA per rhodopsin)	No purification	Not applicable	Photobleaching Assay Retinal Release by FTS	(Pitch *et al*., 2021)
β2-adrenergic receptor	HEK293T cells	SMA 3:1 SMA 2.3:1 (0.5% (w/v))	1. SEC 2. IMAC: Ni-NTA	Not applicable	Not applicable	(Tedesco *et al*., 2021)
A2AR	P. Pastoris	SMA 2:1 (2.5%)	IMAC: Ni-NTA	Lipid Composition analysis	FTS, spectral shift ligand binding	(Routledge *et al*., 2020)
Melanocortin 4 receptor (MC4R)	Sf9 cells	Modified DIBMAs (mPEG-DIBMA) (0.5-4%)	No purification	Solubilisation Trials	No applicable	(Chu *et al*., 2024)
β2-adrenergic receptor	T-Rex-203 cells	DIBMA (3% (w/v))	Magnetic Strep Beads	Fluorescent-SEC	FRET ligand binding assay thermostability	(Harwood *et al*., 2021)
'Smoothened' Protein (SMO)	Sf9 cells	SMA 2:1 (3% (w/v))	1. IMAC: Ni-NTA 2. SEC	SEC DLS Transmission Election Microscopy imaging	NMR Spectroscopy for Ligand Binding	(Zhu *et al*., 2022)

1.14 Thesis Aims

The initial aim of the thesis was to utilise polymers as a tool for producing soluble GPCRs and to investigate a range of techniques to determine functionality. As the project progressed, it was revealed that the expression, solubilisation and purification of GPCRs were particularly challenging. This led to an important aim of the project: determining optimal expression, solubilisation and purification conditions for specific GPCRs, utilising PoLiPa technology. This process aimed to discover how NTR1 and CB2 could be produced but also to understand the appropriate steps required when encountering purification problems with polymer-solubilised GPCRs. A secondary aim was to compare the solubilisation and purification of GPCRs from two expression systems: *E. coli* and HEK293 cells. The final aim of this thesis was to determine if the polymer-solubilised GPCRs were capable of ligand and Mini-G protein binding. This involved preliminary studies with FTS, FCS and spectral shift assays.

1.15 Outline of the Thesis

This thesis investigated how different GPCRs can be encapsulated into PoLiPa to gain a better understanding of the benefits and pitfalls regarding solubilisation, purification, and ligand binding experiments.

The results in Chapter 3 describe the attempted production of the wild-type (WT) GPCR hNTR1 in *E. coli* without any fusion proteins or stabilising mutations. Following the low expression, purity and yield of this methodology, the use of a construct without any fusion proteins was deemed inappropriate for pure GPCR production.

Chapters 4 and 5 describe the expression, solubilisation and purification of MBP-fused rNTR1 and MBP-fused CB2 in *E. coli*. This included systematic investigations into optimal

expression, solubilisation and purification, as well as biophysical characterisation of the purified GPCRs encapsulated in PoLiPas.

Chapter 6 describes the solubilisation and attempted purification of two GPCRs (hNTR1 and CB2) in HEK293 cells.

Chapter 7 describes how FTS, FCS, spectral shift assays and SMA-PAGE provided some evidence that SMA-rNTR1 and SMA-CB2 demonstrated functionality. The described preliminary data suggested possible avenues for future research.

CHAPTER 2: MATERIALS AND METHODS

2.1 Materials

Unless specified otherwise, all reagents and chemicals were purchased from Sigma Aldrich. Polymers and ligands were purchased or kindly gifted from various collaborators (Table 2.1).

Table 2.1: List of Polymers and Ligands used in this Project and their Supplier

Resource	**Supplier/ Source**
SMA2000 and SMA2000I polymers	Purchased from Cray Valley
BzAM series polymers and RAFT SMA 1:1	Gifted by the Klumperman Group at the University of Stellenbosch
AASTY series polymers	Cube Biotech
Fluorescent NTR1 Ligands: MK337 and MK350	Gifted by Max Keller at the University of Regensburg (Keller *et al*., 2020)
NTR1 agonist Neurotensin (8-13) and NTR1 antagonist SR 48692	Purchased from SLS Ltd.
Fluorescent CB2 Ligands: SM15 and VM7	Gifted by Marialessandra Contino from the University of Bari (Intranuovo *et al*., 2024; Spinelli *et al*., 2020).
4-Quinolone-3-Carboxamide Furan (4Q3CF)	Purchased from Cayman Chemicals

2.2 Preparation of Polymers

SMA was prepared from styrene maleic anhydride (SMA2000) by autoclaving, following the protocol described by Kopf *et al* (2019). A 10% (w/v) suspension of SMA2000 in 0.6 M NaOH was autoclaved (21°C, 1.4 bar for 20 minutes) repeatedly until the solution was clarified. The polymer was precipitated with concentrated HCl and washed by centrifugation at 11000 x *g*, removal of the supernatant and re-suspension in deionised water, as described by Lee *et al* (2016). The wash steps were repeated twice before dissolving the polymer in 0.6 M NaOH. The precipitation and wash steps were repeated before the polymer was re-dissolved in a minimal volume of 0.6 M NaOH and pH was corrected to 8.0. The polymer was lyophilised, and the powder stored at RT.

SMA2000I resin was hydrolysed to produce SMI following the protocol described by Hall *et al* (2018). Concentrated HCl was added dropwise to a 10% (w/v) suspension of SMA2000I in deionised water to a final concentration of 1 M HCl. This solution was autoclaved (121°C, 1.4

bar for 20 minutes) repeatedly until the solution was clarified. The polymer was precipitated by the addition of 5 M NaOH, and pH corrected to 9.0. The precipitated polymer was washed by centrifugation at 11000 x g, removal of the supernatant and re-suspension in deionised water. These wash steps were repeated three times before the polymer was redissolved in 0.6 M HCl and pH corrected to 8.0. The polymer was lyophilised, and the powder stored at RT.

Sokalan® CP 9 (Chempoint) was the starting material to produce DIBMA. Small impurities and salt were removed by multiple dialysis steps through 1000 Da cut-off membranes. The polymer was lyophilised, and the powder stored at RT.

2.3 Strains

Table 2.2: Bacterial Strains used in Study

Strain (*E. coli*)	**Supplier or Source**	**Application**
BL21(DE3)	New England Biolabs	GPCR expression
C41(DE3)	Miroux and Walker (1996)	GPCR expression
C43(DE3)	Miroux and Walker (1996)	GPCR expression
One Shot™ BL21 Star™ (DE3)	Invitrogen™ ThermoFisher Scientific	Mini-G expression
NEB ® 5 alpha, DH5-α	New England Biolabs	Plasmid Amplification

2.4 Plasmids

Plasmid sequence analysis was outsourced to Source Biosciences.

Table 2.3: Plasmids

Plasmid Name	**Source**	**Description**	**Target Protein Expression**
pET21a(+)-hNTR1	Domainex Ltd, GenScript	Protein Expression Vector carrying C-terminal 6 x His tag. Ampicillin Resistance	WT hNTR1
pRG/III-hs-MBP-T43NTR1-TrxA-H10	Addgene: Tucker and Grisshammer (1996)	Protein expression vector carrying N-terminal MBP fused truncated rNTR1. C-terminal Thioredoxin A (TrxA) fusion protein and 10 x His tag Ampicillin Resistance	MBP fused rNTR1
pRG/III-hs-MBP-CB2-HF	Addgene: Calandra (1997)	Protein expression vector carrying N-terminal MBP fused CB2. C-terminal 6 x His Tag and FLAG tag. Ampicillin Resistance	MBP fused CB2
pET-15b -Gs	Nehma *et al* (2017) Gifted from Chris Tate's Group	Protein expression vector carrying Mini-G protein sequence and N-terminal His tag. Ampicillin Resistance	Mini-Gs,
pET-15b -Gs/q	Nehma *et al* (2017) Gifted from Chris Tate's Group	Protein expression vector carrying Mini-G protein sequence and N-terminal His tag. Ampicillin Resistance	Mini-Gs/q,
pET-15b -Gs-GFP	Nehma (2017) Gifted from Chris Tate's Group	Protein expression vector carrying Mini-G protein sequence and N-terminal His tag. Ampicillin Resistance	Mini-Gs-Green Fluorescent Protein (GFP)

2.5 Bacterial Growth Media

Luria broth (LB), Terrific Broth (TB), 2x Yeast Extract Tryptone (2xYT) broth and auto-inducing (AI) broth was prepared in deionised water following manufacturer instructions, following the compositions in Table 2.4. All growth media was sterilised by autoclaving at 121°C, 1.4 bar for 20 minutes. After cooling to RT, liquid growth media was supplemented with ampicillin to a working concentration of 100 μg/ml.

After sterilisation of LB agar, the solid growth media was allowed to cool to less than 50°C before supplementation with 100 μg/mL ampicillin. Plates were poured and set under aseptic conditions and used on the same day.

Table 2.4: Bacterial Growth Media Recipes

Growth Media	**Ingredients**
LB Broth (Lennox)	NaCl, 5 g/L Tryptone, 10 g/L Yeast Extract, 5 g/L
TB Broth	Tryptone 12 g/L Yeast Extract, 24 g/L Glycerol (0.4% v/v) 17mM KH2PO4, 2.31 g/L. 72 mM K2HPO4, 12.54 g/L.
2xYT Broth	NaCl, 5 g/L Tryptone, 16 g/L Yeast Extract, 10 g/L
AI Broth	Tryptone 10 g/L Yeast Extract, 5 g/L Na2HPO4 3.55 g/L KH2PO4, 3.4 g/L. K2HPO4, 2.675 g/L.
LB Agar	LB Broth, 15 g/L agar

2.6 Transformation of E. coli for Recombinant Expression

Competent *E. coli* cells were transformed for protein expression or plasmid amplification. A 50 µl aliquot of competent cells was inoculated with 100 µg/mLof plasmid and incubated on ice for 20 minutes. Cell membrane disruption was performed by heat shock at 42°C for 30-45 seconds and then inoculating on ice. 250 µL warmed sterile super optimal broth with catabolite repression (Thermo-Scientific™) was added to the cells for recovery at 37°C, shaking at 180 rpm for 30 minutes. Transformed cells were spread across an LB agar plate (100 µg/mL ampicillin).

2.7 Plasmid extraction and Glycerol Stock Preparation

For plasmid amplification, DH5-α cells were transformed. To extract plasmids from transformed DH5-α cells, 5 mL LB Broth was inoculated with a single colony and grown overnight (37°C, shaking at 180 rpm). QIAGEN® Spin MiniPrep Kit was used, following manufacturer instructions, to obtain plasmid DNA from the overnight culture.

Overnight cultures of transformed *E. coli* strains were used to produce glycerol stocks. Sterile 50% (v/v) glycerol (500 µl) and overnight culture (500 µl) was mixed in a 2 mL cryovial in aseptic conditions, before storage at -80°C.

2.8 GPCR Expression and Expression Optimisation

2.8.1 Large-Scale GPCR Expression in E. coli

Overnight cultures were made from singular colonies of transformed cells or glycerol stocks for inoculation of 1-2 L of LB broth in shaker flasks in a 1:1000 dilution. *E. coli* cultures were grown at 37°C, shaking at 180 rpm. Optical density at 600 nm (OD600) was measured every 30 minutes to 1 hour. Once the OD600 reached 0.6-0.8, the temperature was decreased to 18°C. Cells were induced with 1 mM Isopropyl ß-D-1-thiogalactopyranoside (IPTG) and left overnight (20-24 hours). Cells were harvested by centrifugation at 3982 x *g* for 30 minutes and pellets were stored at -80°C. This 'default' expression protocol was used to express hNTR1 using the pET-21a plasmid. Trials described in section 2.8.2 determined changes to expression protocol for expression of MBP-fused GPCRs.

2.8.2 Expression Trials for Optimal MBP-fused GPCR Expression in E. coli

Expression trials determined how cell lines (Table 2.1), broth type (Table 2.3), temperature (18°C, 25°C, 37°C), IPTG concentration (0.1 mM, 0.25 mM, 0.5 mM) and expression time (1hr, 3 hours, 4hours or overnight (20-24 hours)) affected growth and expression. Culture samples (1 mL or 10 mL) were taken at specific time points and centrifuged at 4000 x g for 10 minutes. Cell pellets from 1 mL samples were re-suspended in 15 µl of 4 X NuPAGE lithium dodecyl sulfate (LDS) sample buffer (Novex®, ThermoFisher). Cell pellets from 10 mL samples were re-suspended in lysis buffer (50 mM Tris-HCl pH 7.5, 2 mM

Ethylenediaminetetraacetic acid (EDTA), 10% (v/v) glycerol, EDTA-free protease inhibitor tablet, 40 mg/mL DNase, 2.5 mM $MgCl_2$) or Bugbuster® with 40 mg/mL DNase and 2.5 mM $MgCl_2$. Cells in the lysis buffer were lysed by sonication for 20 seconds on ice. A cell lysate sample was taken before centrifugation at 10000 x g for 30 minutes. Expression was tested comparing cell lysate and/or supernatant samples by Sodium Dodecyl-Sulfate (SDS)-PAGE gel and Western blot analysis (Sections 2.13 and 2.15). Large-scale GPCR expression conditions were modified depending on expression trial results (Table 2.5).

Table 2.5: Expression Conditions for each MBP-fused GPCR Expressed in E. coli

	Cell Line	**IPTG Concentration**	**Expression Temperature**	**Expression Time**	**Broth**
rNTR1	C43	0.25 mM	18ºC	O/N	LB
CB2	C41(DE3)	0.25 mM	18ºC	O/N	2xYT

2.8.3 Lentiviral Overexpression of GPCRs in HEK293 Cells

Lentiviral expression of hNTR1 and CB2 in HEK293 cells was performed in Michael Tomlinson's lab by two master's students: Alexia Taylor and Gabriele Cannucciari. Pellets were stored at -80°C before membrane preparations (Section 2.10).

2.9 Buffers and Tubes for Cell, Membrane and Protein Handling

The buffers described in Table 2.6 are 'starting points' to determine appropriate buffer compositions in the GPCR production process. These 'default' buffers were taken from Lee *et al* (2016). Tested buffer compositions included: addition of reducing agents (5 mM tris(2-carboxyethyl)phosphine (TCEP)) or 5-25 mM dithiothreitol (DTT)), use of a lower NaCl concentration (250 mM), addition of arginine (20-200 mM). Benefits of buffer changes to purity and yield of GPCR production was deciphered by solubilisation screens (section

2.10.3), purification screens (sections 2.10.5 and 2.10.8) and storage condition screens (section 2.12).

Table 2.6: Buffer Compositions for GPCR Production and Storage

Buffer Name	Purpose	Ingredients
Buffer A	Cell lysis and membrane harvesting	50 mM Tris-HCl pH 7.5 (r.t) 2 mM EDTA 5% (v/v) glycerol EDTA-free Protease inhibitor tablet (Thermo-ScientificTM)
Buffer B	Solubilisation IMAC Purification	50 mM Tris-HCl pH 8 (r.t) 500 mM NaCl 10% (v/v) glycerol
Buffer C	Post-IMAC Protein Storage FLAG Purification Protein Characterisation (except CD) Functional Assays	50 mM Tris-HCl pH 8 (r.t) 150 mM NaCl 10% (v/v) glycerol
Buffer D	Storage of Mini-G proteins	50 mM Tris-HCl pH 8 (r.t) 150 mM NaCl 10% (v/v) glycerol 50 μM GDP 1 mM Mg2Cl
Buffer E	CD measurements	10 mM Na Phosphate pH 8 50 mM Na F

For volumes less than 2 mL, membrane or protein sample handling was performed in low protein binding collection tubes (Pierce™). Larger volumes were handled in 15 mL or 50 mL Falcon tubes.

2.10 GPCR Solubilisation and Purification

2.10.1 E. coli and HEK293 Cell Membrane Preparation

Membranes were isolated to remove soluble proteins before solubilisation of membrane proteins (Fotiadis and Harder, 2012). During membrane preparation, material was kept on ice to reduce protease activity. Cells expressing a GPCR were re-suspended in 10 mL of Buffer A per 1 g of cells. Cells were lysed with a C3 Emulsifier using 20000 psi or 10000 psi of pressure for *E. coli* or HEK293 cells, respectively. The cell lysate was centrifuged at 12000 x *g* for 30 minutes to remove whole cells and inclusion bodies. The supernatant was centrifuged at 100000 x *g* for 45 minutes. The pellet consisting of isolated membranes was homogenised with a dounce homogeniser into Buffer B to a final concentration of 120 mg/ml.

2.10.2 GPCR Solubilisation from Membranes

Lee *et al* (2016) describes how SMA can be used to solubilise an *E. coli* protein; this methodology was translated to solubilise GPCRs with a variety of polymers. Polymer or DDM was dissolved in Buffer B; this solution was mixed in a 1:1 ratio with the prepared membranes to give a final polymer concentration of 2.5% (w/v) or detergent concentration of 1.5% (w/v) DDM and 60 mg/mL membranes. This mixture was left on a rotary wheel for 2 hours at RT or overnight at 4°C. The insoluble fraction of the membranes was removed by centrifugation at 100000 x *g* for 45 minutes, then re-suspended in the same volume as the soluble fraction for analysis for SDS-PAGE/Western blot. The supernatant was used for downstream purification steps.

2.10.3 Solubilisation Screens

Solubilisation screens were performed to test efficiency of different solubilisation agents, polymer concentrations and the addition of 20 mM arginine. Membranes, harvested as described in section 2.10.1, were added to an equal volume (20-1000 µL) of 5% (w/v) polymer or 3% (w/v) DDM and left for 2 hours at RT or overnight at 4°C. Polymers tested included SMA, DIBMA, SMI, RAFT SMA 1:1, the BzAM Polymer series and the AASTY series. Different concentrations of SMA (0.5-2.5% (w/v)) and DIBMA (2.5%-10% (w/v)) were also compared. Centrifugation was performed at 100000 x *g* for 45 mins to remove insoluble material. The amount of protein in the soluble fraction and re-suspended insoluble fraction was tested by SDS-PAGE/Western blot (section 2.14 and 2.16).

2.10.4 Immobilised Metal Affinity Chromatography (IMAC) Purification

The default IMAC resin used was Nickel-nitrilotriacetic acid (Ni-NTA) (Thermo-Scientific™). The IMAC resin was equilibrated into Buffer B by centrifugation at 1000 x *g* for 1 minute, removal of the supernatant and resuspension in Buffer B. This was done three times. The supernatant from section 2.9, from solubilised membranes containing His tagged GPCRs, was incubated with IMAC resin overnight at 4°C, on a rotary wheel. A volume of resin (column volume (CV)) 0.5-1 mL was used, depending on the volume of membranes solubilised. A gravity flow column was used to collect the flow through (FT) with material not bound to the resin. The resin was then washed with 20x CV of Buffer B, followed by low imidazole concentration washes (5x CV of 20 mM imidazole and 5x CV of 40 mM imidazole). Protein was eluted using a high concentration of imidazole (100-500 mM) and 6-10 elution fractions were collected. Flow-through samples, wash and elution fractions were analysed by SDS-PAGE (section 2.14) and Western blot (section 2.16). If DDM was used as a solubilisation agent, 0.03% (w/v) DDM was included in the binding, wash and elution buffers.

2.10.5 IMAC Purification Screens for Optimisation

Three other resins were also investigated: Ni-Sepharose (SLS), Ni-iminodiacetic acid (IDA) (Protino), and TALON (Takara) resin. Changes in the buffer composition by addition of arginine (20 mM, 50 mM, 200 mM), addition of a reducing agent (5 mM TCEP or (2-5 mM) DTT), dilution of NaCl (250 mM), were implemented during the resin equilibration step. The supernatant from section 2.9, from solubilised membranes containing His tagged GPCRs, was split evenly between the number of tested variables. Small-scale purification screens compared a maximum of four different conditions: complete IMAC purifications were performed (section 2.10.4).

Large-scale purification screens compared several different conditions at one time including resin type and buffer composition. 1 mL of solubilised material was incubated with 20 µl of

IMAC resin. The addition of buffer (up to 2 mL), arginine (20 mM or 50 mM) or reducing agents (5 mM TCEP or 2 mM DTT) were compared. After incubation with equilibrated IMAC resin overnight at 4°C, on a rotary wheel, the resin was collected by centrifugation at 1000 x *g* for 1 minute and removal of the supernatant. The resin was washed twice by re-suspension in Buffer B, re-centrifugation and supernatant removal. 20 µl of LDS sample buffer was added to the resin before boiling in a heat block at 100°C for 10 minutes. The resin/LDS samples were analysed by SDS-PAGE (section 2.13) and/or Western blot analysis. Samples of the 'flow through' which did not bind to the resin were also analysed.

2.10.6 Post-IMAC Dialysis

To remove high imidazole and salt concentrations from elution fractions post-IMAC purification, elution fractions containing the protein of interest were combined and dialysed into Buffer C using Spectra Pore dialysis tubing with a 3500 Dalton cut-off. The IMAC elution was enclosed in dialysis tubing and placed floating in a volume of Buffer C 100-fold greater than the volume of the IMAC elution. This was stirred overnight at 4°C. For complete removal of imidazole, the buffer was replenished and dialysed for another 6 hours at 4°C. This dialysis method was also used for buffer exchange before CD or DLS analysis.

2.10.7 FLAG Purification

Purification of solubilised GPCRs with a FLAG tag was performed with Anti-FLAG® M2 Magnetic Beads as per manufacturer instructions. Before purification, the resin (20–200 µL) was equilibrated in Buffer C. Resin was separated from the buffer using a Magnetic Rack, MagRack6™ (Cytiva). FLAG purifications were performed either immediately after solubilisation or post-IMAC, after dialysis. The protein sample and the anti-FLAG resin were added to a 15 mL falcon tube and the volume made up to 15 mL. The sample was mixed on a rotary wheel for 2 hours at RT, then the resin was separated from the flow through. The resin

was washed twice with Buffer C and transferred to a 2 mL low-bind Eppendorf tube (Pierce®). For elution, 200 µL of 0.1 mg/mL 3X ®FLAG peptide in Buffer C was incubated with the resin for 2 hours at RT or 4°C, mixing on a rotary wheel. The resin was separated, and the elution was collected. A 20 µL sample of the resin post-elution was mixed with 20 µL of LDS buffer and boiled in a heat block at 100°C for 10 minutes. Samples of the flow through, washes, elution and post-purification resin were analysed by SDS-PAGE (section 2.14) and Western blot (Section 2.16). Increased 3XFLAG peptide concentration up to 1 mg/ml, increased number of elution fractions up to three and increased agitation during elution were attempted to improve yield.

2.10.8 FLAG Purification Optimisation

Four FLAG purifications on the same post-IMAC SMA-CB2 sample were performed to compare the effect of arginine (0 mM or 20 mM) and NaCl concentration (150 mM or 500 mM) in the binding, wash and elution buffers. The elution of SMA-CB2 post-IMAC was split equally into four and dialysed into either Buffer B with or without 20 mM arginine or Buffer C with and without arginine. The dialysed samples were centrifuged at 100000 x *g* for 30 minutes to remove aggregates. Two 200 µL elution fractions were collected for each purification. Samples of the flow through, washes, elution and post-purification resin were analysed by SDS-PAGE (section 2.14) and Western blot (section 2.16).

2.10.9 Post-FLAG Dialysis

To remove FLAG peptide post-FLAG purification, a Pur-A-lyzer Mini-Dialysis Kit with a 25 kDa MW cut off, was used, as per manufacturer instructions. After wetting the dialysis membrane, the FLAG elution was transferred into a Pur-A-lyzer Mini-Dialysis tube and left to float in a volume of Buffer C 100-fold greater than the volume of the FLAG elution. This

was stirred overnight at 4°C. The buffer was replenished, and dialysis was continued for another 6 hours at 4°C.

2.11 Concentrating GPCRs

To minimise aggregation of GPCRs, Centrisart® reverse concentrators were used, with a 25 kDa MW cut off, as per manufacturer instructions. After dampening the centrifugal membrane with Buffer C, 2.5 mL of purified GPCR was placed in a concentrator and centrifuged at 1500 x *g* at 4°C. After concentration, samples were centrifuged at 130000 x *g* for 10 minutes and pipetted into a new tube to remove possible aggregates.

2.12 Storage Conditions Screens

To test storage conditions of SMA-solubilised GPCRs, 50 µL samples were left overnight at -80°C, -20°C, 4°C, and 25°C. When investigating the SMA-rNTR1, aliquots with and without 20 mM arginine in the storage buffer. When investigating SMA-CB2, the process of flash freezing by submersion of the tube in liquid nitrogen or in a mixture of ethanol and dry ice was tested before storage at -80°C overnight. After overnight storage, protein samples were analysed by SDS-PAGE (section 2.14), Western blot (section 2.16), and/or DLS analysis (section 2.17.2).

2.13 Protein Concentration Estimation

Protein concentration was estimated using a DeNovix DS-11 Series Spectrophotometer. 1 µL of sample was measured at absorbance at 280 nm to calculate the approximate protein concentration in mg/mL

2.14 SDS-PAGE

A vertical electrophoresis tank (Bio-rad) was assembled to submerge a 4-20% polyacrylamide gel (Bio-rad) or 12% polyacrylamide laboratory-cast gels in running buffer (25 mM Tris-HCl pH 8.8, 192 mM glycine, 3.4 mM SDS). Laboratory-cast gels were prepared following the recipe in Table 2.7.

Table 2.7: Recipe for 12% Polyacrylamide Laboratory-cast Gels

	Stacking Gel (4%)	**Resolving Gel (12%)**
30% Acrylamide/bis	1.33 mL	6 mL
0.5 M Tris-HCl, 0.4% SDS, pH 6.8	2.5 mL	-
1.5 M Tris-HCl, 0.4% SDS, pH 8.8	-	3.75 mL
Deionised water	6 mL	5 mL
Tetramethylethylenediamine	10 mL	15 mL
10% Ammonium persulfate	100 mL	150 mL
Total Volume	10 mL	15 mL

The sample (15 µL) was mixed with LDS sample buffer (5 µL) and 10 µl was loaded into wells alongside a protein standard, either peqGOLD pre-stained Protein marker VI (VWR®) or Precision Plus Protein Dual Colour Standards (Bio-Rad). Electrophoresis was performed using a 170 V charge for 50 minutes.

2.15 PAGE Analysis

Proteins which had migrated into the gel were visualised by Coomassie staining or silver staining. Quick Coomassie stain (Protein Ark) was used to submerge the SDS-PAGE gel for between 4 and 24 hours on a rocker at RT before de-staining with 15 mL of deionised water. For more sensitive silver staining of SDS-PAGE gels, a ProteoSilver silver staining kit was used as per manufacturer instructions. A GS-800 Calibrated Densitometer (Bio-Rad) was used to image gels.

Stained SDS-PAGE gels were thoroughly washed with deionised water for tandem mass spectrometry (MS) analysis of protein bands. The band of interest was removed with a clean scalpel and submitted to the University of Birmingham's Proteomics Facility. Unstained SDS-PAGE gels were also used for further analysis by Western blot (section 2.16)

2.16 Western blots

Gel-separated proteins were transferred onto a nitrocellulose membrane using the Trans-Blot Turbo transfer system and TransBlot® Turbo™ Mini Nitrocellulose Transfer packs, as per manufacturer instructions (Bio-Rad). The membrane was stored in a blocking buffer (5% (v/v) skim milk in Phosphate Buffer Saline-0.1% Tween (PBS-T)) for at least 30 minutes. Primary antibody was made up in 10 mL PBS-T at manufacturer recommendation (Table 2.8) and left on the membrane for at least 2 hours or overnight at 4°C. After removal of the primary antibody, the membrane was washed with PBS-T for 10 minutes on a rocker at RT. The washing step was performed three times before the addition of 10 nM Horse Radish Peroxidase-conjugated secondary antibody (Abcam). The membrane was washed again three times after secondary antibody removal. Enhanced Chemiluminescence (ECL) Western blotting detection reagent (Cytiva) was mixed and added to the membrane before visualisation on an Amersham Imager 680. Band intensity analysis was performed using ImageLab (Bio-Rad).

Table 2.8: Primary Antibodies and Dilution used for Western blot Analysis

Primary Antibody	Supplier	Dilution
Anti-His	Takara	1: 5000
Anti-MBP	New England Biolabs	1: 5000
Anti-NTR1	Merck	1:1000
Anti-CB2	Abcam	1:1000

2.17 Biophysical Analysis of GPCRs in PoLiPas

2.17.1 SEC

SEC of protein samples was performed on a Superdex® 200 Increase 10/300 GL or a Superose 6® 10/300 GL gel filtration column using an AKTAexplorer 10 chromatography system (Amersham) controlled by UNICORN 4.0 chromatography software. Columns were stored in 20% v/v ethanol. Before use, the column was equilibrated with 1 CV deionised water and 1 CV of Buffer C. All buffers were filtered through a 0.2 μm pore-sized membrane and de-gassed. The protein sample was concentrated to <1 mL, loaded into a 1 mL loop and injected onto the column. Elution was performed over 1 CV at 0.5 mL/minute in Buffer C. Absorbance at 280 nm was monitored as 0.5 mL fractions were collected.

2.17.2 DLS

Protein samples (40 μL**,** 0.1 mg/ml) were loaded into a 364-well glass bottom plate. Plates were loaded into a Dynapro™ Plate Reader (Wyatt technology). After equilibration to 25°C constant temperature, DLS measurements were taken using a HeNe gas laser at 824.9 nm; the detector was 150° from the incident beam. Five x 5 second scans were taken of each well. DLS data analysis was performed using DYNAMICS software; the cumulants algorithm and

Stokes-Einstein equation was used to report particle size and size distribution graphs calculated in terms of percentage intensity.

2.17.3 CD

Protein samples were dialysed into Buffer E, replenishing the buffer twice to ensure removal of chiral components in the buffer such as Tris-HCl or imidazole. Measurements were made on a JASCO J-1500 Circular Dichroism Spectrophotometer using Spectra Manager Software. Spectra were measured from 190-350 nm, taking measurements every 0.5 nm (321 data points). The scanning speed was 100 nm/min. A background CD reading was collected from 300 μL of Buffer E. This was loaded into a quartz cuvette with 1 mm pathlength. After a baseline spectrum was recorded, 300 μL of SMA-rNTR1 at a concentration of approximately 0.1 mg/mL was loaded into the quartz cuvette and spectra were measured. CD analysis of the same SMA-rNTR1 sample was performed every hour for 17 hours. Spectra Deconvulution was performed using DichroWeb (Whitmore and Wallace, 2004). The CDSSTR algorithm was used referencing the SMP180 dataset (Abdul-Gader *et al*., 2011).

2.17.4 SMA-PAGE or DIBMA-PAGE

Protein sample (15 μL) was mixed with loading dye (5 μL) (1 mg/mL bromophenol blue, 20 mM Tris-HCl pH 8, 50% (v/v) glycerol) and 10 μL was loaded into wells of a 4-20% polyacrylamide gel (Bio-rad). The casket was submerged in native running buffer (25 mM Tris-HCl pH 8.8, 192 mM glycine) and PAGE was run for 120 minutes at 150 V. Quick Coomassie stain (Protein Ark) was used to detect protein bands (section 2.14), or gel was used for Western blot analysis (section 2.16).

2.18 Production of Mini-G Proteins

Mini-G proteins were produced based on the protocol described by Carpenter and Tate (2017). *E. coli* BL21(DE3)star cells were transformed with plasmid for Mini-G protein expression (Table 1.2). LB broth (5 mL) was inoculated with singular colonies or glycerol stock stabbings and incubated overnight at 37°C, shaking at 180 rpm. Overnight culture was used to inoculate 500 mL of LB Broth. The culture was grown at until an OD 600 of 0.7 was reached. The temperature was reduced to 18°C and expression was induced with 0.1 mM IPTG. The culture was centrifuged at 3989 x *g* for 30 minutes and the cell pellet resuspended in 25 mM lysis buffer (50 mM Tris-HCl, 100 mM NaCl, 10 mM imidazole, 5 mM Mg_2Cl, 50 µM GDP, 1 mM phenylmethylsulfonyl fluoride, 1 µL DNase and EDTA-free protease inhibitor tablet). Re-suspended cells were sonicated for 20-second pulses at 70% power for 2 minutes. Lysate was centrifuged at 20000 x *g* for 45 minutes and supernatant collected. IMAC purification was performed using 3-4 mL of Ni-NTA resin. Elution was exchanged into Buffer D by dialysis or SEC.

2.19 Fluorescent Tryptophan Spectroscopy

FTS was performed in Hellma® fluorescent cuvettes with a chamber volume of 3500 µL or 1400 µL; an initial volume of 1000 µL or 300 µL was used, respectively. SMA-solubilised protein at a measured concentration over 0.1 mg/mL was added to a cuvette. Tryptophan fluorescence emission spectra were collected using an LS-50B Fluorescence Spectrometer by excitation with light at 295 nm wavelength. Emission Spectra were recorded from wavelength 300-550 nm, every 0.5 nm with a scan speed of 700 nm/min. The slit used for excitation and emission was adjusted between 5-10 dependent on the intensity. Anisotropy measurements were taken at 340 nm emission wavelength and with a slit of 10. A volume of 0.2-3 µL of ligand (0.1-10 mM) was added to the SMA-solubilised protein to produce the desired final concentration before incubation for 20 minutes. After the tryptophan fluorescence emission

spectra were re-collected, more ligand was titrated into the same SMA-solubilised protein sample. This was repeated to provide data for a series of ligand concentrations. Peak intensity and peak wavelength were calculated from the emission spectra. Apparent affinity (K_D) was calculated from the curves plotted from the peak intensity, peak wavelength or anisotropy against ligand concentration fitted to models in Table 2.9 (GraphPad).

Table 2.9: Models used to Plot Binding Curves

One-binding site model (Sigmoidal Curve)	Y= Bottom + (Top-Bottom)/1+10^((LogKd-X) +Slope)
Two-binding site model	Site 1= BmaxHi*X/(KdHi+X) Site 2= BmaxLo*X/(KdLo+X) Y= Site 1 +Site 2

2.20 Solution-based Fluorescent Correlation Spectroscopy

Solution-based FCS was performed as previously described (Briddon *et al*., 2011). FCS was performed on µ-Slide 18 Well Glass Bottom chambered coverslips (Ibidi). The confocal volume was placed 200 µm above the surface of the coverslip. ZEISS LSM510 Confocor3 was used for 633 nm excitation (0.5–1 kW cm^{-2}) and emission collection through an LP650 filter. Calibration readings were taken daily, using Cy5 as a standard dye at 10 nM and 500 nM concentrations. Cy5 N-hydroxysuccinimide ester (Amersham Pharmacia Bioscience) was diluted in high-performance liquid chromatography grade water. The diffusion coefficient of Cy5 is 3.16×10^{-10} m^2 s^{-1}(***D***). The equations below demonstrate how diffusion coefficient (***D***), dwell time (τ_{D1}), and structural parameter (*S*) were used to calculate confocal detection volume (V).

$$W_1 = (4 \cdot \mathbf{D} \cdot \tau_{D1})½$$

$$W_2 = W_1 \cdot S$$

$$V = \pi^{\frac{2}{3}} \cdot (W_1)^2 \cdot W_2$$

FCS measurements were performed in a volume of 50 µL. MK337 alone was measured in four different buffer systems: with and without 10% (v/v) glycerol and 10 mM Bovine Serum Albumin (BSA). SMA-solubilised protein (approximately 0.2 mg/mL) was incubated with varying concentrations of MK337 (4-500 nM) for 30 minutes with and without 10 mM Bovine Gamma Globulin (BGG). For competitive inhibition experiments, 170 nM of SR 48692 was pre-incubated for 30 minutes with SMA-solubilised proteins before MK337 incubation. SMA-SAV1866 (SAV) (provided by Pooja Sridhar) was used as a control. For Mini-G coupling experiments, a 4-hour incubation of SMA-rNTR1 with the Mini-G proteins (Gs or Gsq) before the addition of any ligands. Three 10-second reads were taken to record time-dependent fluctuations in fluorescence intensity. Fluorescence intensity data was analysed by autocorrelation functions using Zeiss AIM 4.4 software. The data was fitted to the equation below where N = particle number, f_i is the fraction of i^{th} component, τ_{Di} is the dwell time of i^{th} component and S is structural parameter.

$$G(\tau) = 1 + \frac{1}{N} \cdot \sum_{i=1}^{m} f_i \cdot \left(1 + \frac{\tau}{\tau_{Di}}\right) \cdot \left(1 + \frac{\tau}{S \cdot \tau_{Di}}\right)^{-\frac{1}{2}}$$

To incorporate a triplet state component, 1-component or 2-component 3-D diffusion models were fitted using a pre-exponential. Residuals to the fit were used to assess fit quality. The dwell time and diffusion rate of MK337 alone were calculated using a 1-component model. In two-component models, the first component (τ_{D1}), representing free MK337, was fixed to determine the properties of the second component, representing bound MK337. The free MK337 and bound MK337 concentrations were calculated from their relative contributions to the autocorrelation function amplitude. Bound ligand was calculated from the 2-component model for each 10-second read. Specific binding was calculated from the difference in bound MK337 concentration with and without pre-incubation with 170 nM SR 48692. Error bars

were used to represent standard deviation (SD) between the three measurements of the same well. Student's paired t-test determined significant differences in diffusion rates with and without Mini-G proteins (GraphPad).

2.21 Spectral Shift Assays

SMA-rNTR1 was labelled with RED-tris-NTA 2nd Generation dye (NanoTemper), following manufacturer instructions. Fluorescently labelled SMA-rNTR1 was incubated with a series of MK350 concentrations for 30 minutes in the dark. To test competitive inhibition, fluorescently labelled SMA-rNTR1 was incubated with 340 nM of SR 48692 for 30 minutes before incubation with MK350. 20 µl of each sample was examined in a Dianthus 384-well plate. A Dianthus plate reader measured spectral shifts in the fluorescent spectra of the labelled dye after excitation with 590 nm. Data was analysed by DI Screening Analysis software, which uses the ratio of fluorescence at 670 nm and 650 nm to determine ligand binding. Initial fluorescence at 650 nm was also measured as an indicator of a ligand-induced effect on fluorescence that may not be associated with ligand binding. Possible ligand interference caused by MK350 was tested for by taking spectral shift measurements of MK350 titrated against buffer and a control labelled peptide. Apparent affinity (K_D) or half maximal inhibition constant (IC50) was calculated from the curves plotted from the peak intensity or peak wavelength against ligand concentration (GraphPad). The Ki of SR 48692 was calculated using the equation below. Where the concentration of MK350 was 500 nM and the Kd of MK350 was calculated from the spectral shift experiments performed on the same day.

$$Ki = \frac{IC50}{(1 + \frac{[MK350]}{Kd})}$$

CHAPTER 3: PRODUCTION AND SOLUBILISATION OF WILD-TYPE HUMAN NEUROTENSIN RECEPTOR EXPRESSED IN *E. COLI*

This project initially investigated the production of wild-type (WT) human Neurotensin receptor 1 (hNTR1) with six histidine residues added to the C-terminus of the GPCR expressed in *E. coli* (Figure 3.1). Mutations and fusion proteins are regularly used to stabilise and improve the expression of GPCRs, which are notoriously unstable (Velloso *et al*., 2024). The chapter aimed to test the capabilities of polymers to solubilise and purify a GPCR with no stabilising mutations or fusion proteins. Lee *et al* (2016) described a methodology for producing membrane proteins with SMA, using the *E. coli* protein ZipA as an example. The purification methods used are IMAC purifications using Ni-NTA resin and SEC (Lee *et al*., 2016). The experiments in this chapter tested if the methodology for solubilising and purifying proteins by the SMALP method can be transferred to produce a more challenging protein. A second linked aim was to test the best solubilisation agent of multiple polymers including SMA, DIBMA and the BzAM series.

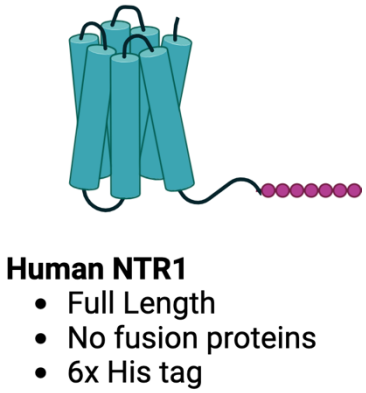


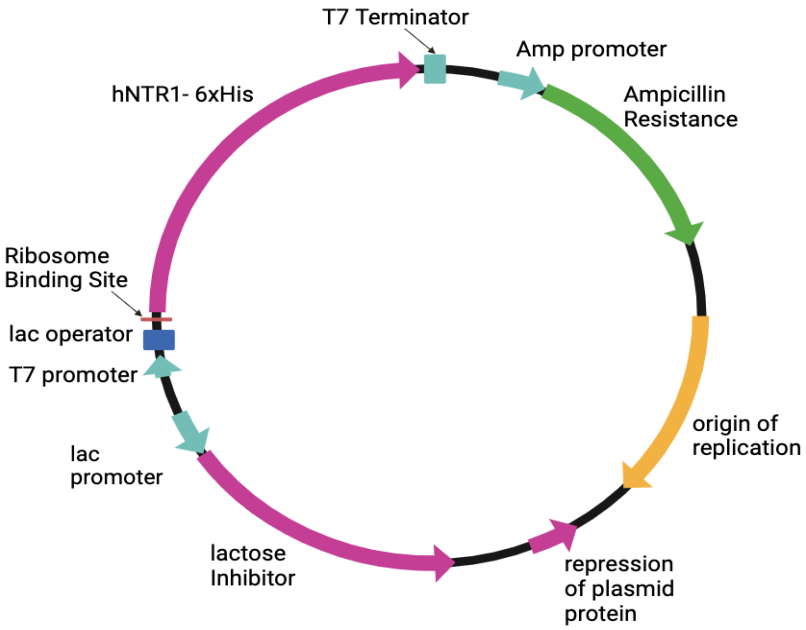
Figure 3.1: Cartoon representation and features of WT hNTR1 expressed in E. coli in this Chapter.

3.1 Testing Expression of hNTR1 in E. coli

It was hypothesised that WT hNTR1 could be expressed in *E. coli*, using the plasmid construct shown in Figure 3.2A. This plasmid was a pET-21a vector, which conferred ampicillin resistance and used a T7 promoter to control the expression of the hNTR1 gene inserted into the multiple cloning site.

To assess expression of the protein using this plasmid expression system, an *E. coli* culture containing the plasmid was grown and expression of hNTR1 was induced. Membranes were harvested from *E. coli* and analysed by Western blot (Figure 3.1B). The detection of a band on the Western blot using a His tag antibody would be indicative of the presence of the His tagged hNTR1. However, endogenous antigens can cross-react with Anti-His antibody (Mahmood and Xie, 2015). To confirm hNTR1 expression, a second Western blot was carried out with an NTR1-specific antibody. The anti-NTR1 antibody bound to the N-terminal sequence of hNTR1; when combined with the anti-His antibody bound to the C-terminal His tag provided confidence that the hNTR1 present in the sample represented the full-length protein

A



B

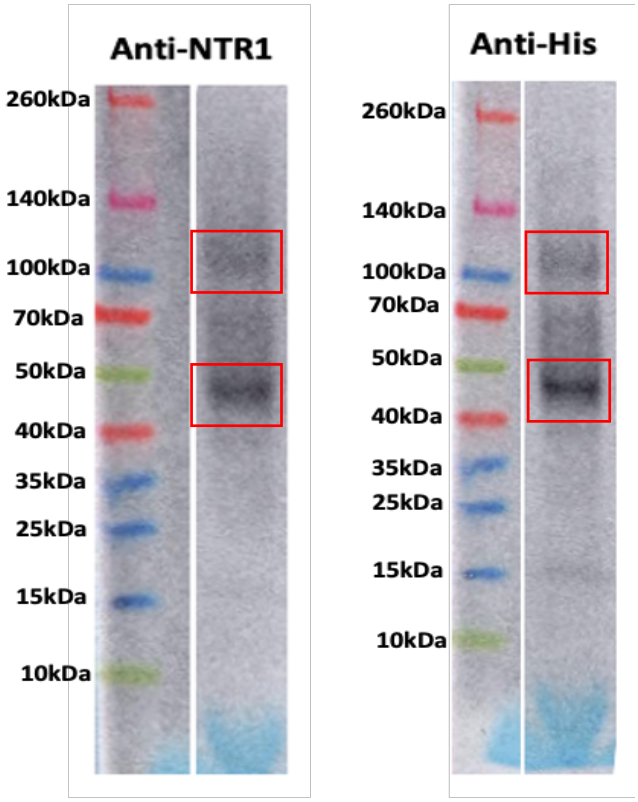


Figure 3.2: Expression test for hNTR1 in E. coli.
(A) Plasmid map (pET21a(+)) used for hNTR1 expression.
(B) Western blot showing homogenised membranes of E. coli expressing hNTR1 separated using a 4-20% polyacrylamide SDS gel. Two blots were probed with two different antibodies: 500 nM anti-His (left) and 1 µM anti-NTR1 (right). Red boxes show expected size of monomeric (46 kDa) and dimeric (92 kDa) hNTR1.

The expected mass of hNTR1 is 46 kDa, as calculated from its primary sequence. *E. coli* cannot glycosylate proteins, therefore, the observed weight for the protein on SDS-PAGE should be close to that of the peptide mass. Figure 3.1B showed a primary band between 40 kDa and 50 kDa when probed with both the anti-His and anti-NTR1 antibodies. This correlates well with the calculated mass of hNTR1. Additionally, a second higher MW band at approximately 110 kDa can be observed in both Western blots, which could indicate the presence of a dimeric hNTR1. Dimerization of rNTR1 has been reported physiologically by a FRET assay (Dijkman *et al*., 2018).

This expression test confirmed the presence of hNTR1 in *E. coli* membranes using standard expression conditions described previously (Lee *et al*., 2016). Despite the target protein being a WT mammalian protein, enough protein was expressed in *E. coli* to be detectable by Western blot analysis. Consequently, these membranes were used in solubilisation trials.

3.2 Solubilisation Trials on E. coli Membranes

Solubilisation trials are important for testing how well amphipathic polymers or detergents can extract membrane proteins and stabilise them in an aqueous environment. Polymers such as SMA work by inserting hydrophobic residues, such as styrene into a membrane and forming a disc that encapsulates a section of the membrane (Knowles *et al.*, 2009). Different polymers can have different hydrophobic and hydrophilic residues, and therefore different efficiencies in the insertion into a membrane. DIBMA is the second most used polymer; it produces a larger PoLiPa that does not absorb at 280 nm and is less sensitive to positive cations (Gulamhussein *et al*., 2020). SMI is a polymer that is acid compatible; able to produce SMI lipid particles (SMILPs) from pH 5-7.8 and insensitive to divalent cations up to at least

100 mM (Hall *et al*., 2018). Solubilisation trials were performed to understand the effect of polymer type and polymer hydrophobicity on hNTR1 extraction.

3.2.1 Comparison of SMA, SMI and DDM for the Extraction of hNTR1

The solubilisation of hNTR1 expressed in *E. coli* using SMA, SMI and the detergent DDM was tested and analysed by Western blot (Figure 3.3). Anti-His and anti-NTR1 antibodies were used to identify the hNTR1.

The red boxes on the Western blot images shown show where a protein the size of the hNTR1 monomer (46 kDa) or dimer (92 kDa) may appear. The strongest bands on the Western blots are at the expected sizes in the soluble fraction of SMA-solubilised membranes. These data suggest that SMA was the best solubilisation agent at the tested concentrations, as indicated by the intensity of the bands representing hNTR1 in the soluble fractions. Nearly 100% of hNTR1 was present in the soluble fraction compared to the insoluble fraction when solubilising with SMA. DDM was the second-best solubilisation agent followed by SMI. Nearly 100% of hNTR1 was present in the insoluble fraction compared to the soluble fraction when solubilising with SMI. This showed that SMI was incapable of solubilising hNTR1 in the tested conditions.

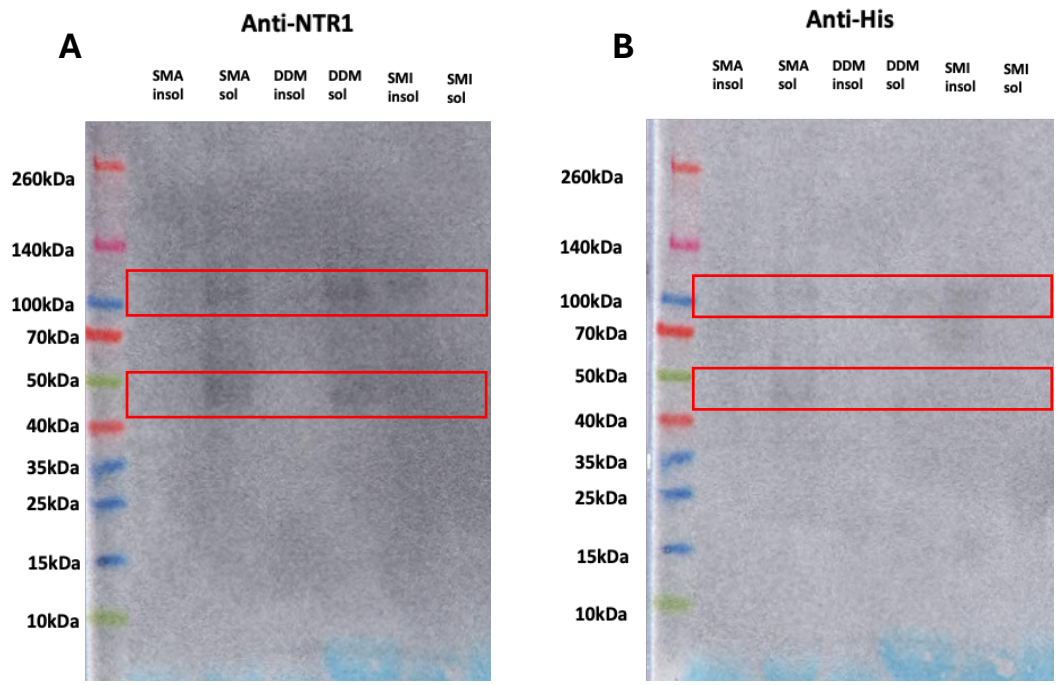


Figure 3.3: Western blots showing of results of a solubilisation trial comparing two polymers and the detergent DDM. *2.5% (w/v) SMA, 2.5% (w/v) SMI or 2% (w/v) DDM were incubated with hNTR1 expressing membranes for 2 hours at RT. Soluble (sol) and Insoluble (insol) fractions were, separated by centrifugation at 100 000 x g. Western blots were probed with two different antibodies: anti-NTR1 (A) and anti-His (B). The red boxes indicate the area where hNTR1 would run as a monomer or dimer. SDS-PAGE was performed on a 4-20% gradient acrylamide.*

Differences in the density of the bands between the anti-NTR1 probed Western blot and the anti-His probed Western blot are most likely due to different abilities of different antibodies to bind to and detect the chosen protein. The lack of bands at a MW lower than 46 kDa suggested that hNTR1, once encapsulated was resistant to proteolytic degradation. Taken together, these data show that hNTR1 can be successfully solubilised with SMA and DDM. However, the low intensity bands suggest the concentration of hNTR1 in the soluble fractions was low.

3.2.2 Understanding Effect of Polymer Hydrophobicity on Solubilisation Efficiency of WT hNTR1

Having established that SMA and DDM could successfully solubilise hNTR1, it was hypothesised that the relative hydrophobicity of SMA and SMA-like polymers could influence solubilisation efficiency. This hypothesis could be tested using a library of polymers with varied relative ratios of hydrophobic and hydrophilic monomers. Such polymers were made available in collaboration with the Klumperman Group. A series of polymers, called the BzAM series, has the same size distribution but different levels of substitution of a hydrophilic moiety to a hydrophobic moiety. The higher the degree of substitution, the more hydrophobic the polymer. The structure of a BzAM series polymer is shown in Figure 3.4. These polymers were produced by Dr Gestél Kuyler.

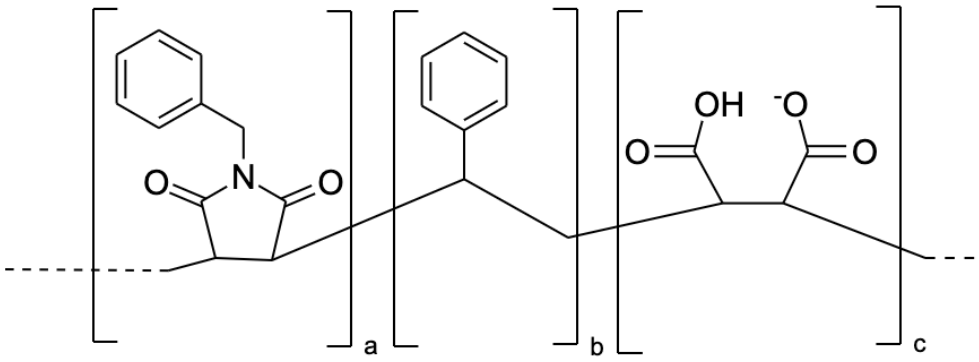


Figure 3.4: Chemical structure of a BzAM series polymer.
*The monomer in section **a** is N-benzyl maleimide, the monomer in section **b** is styrene and the monomer is section **c** is maleic acid.*

Production of BzAM polymers was carried out at the University of Stellenbosch using a two-step process. Firstly, RAFT polymerisation was used to produce a SMA polymer with a 1:1 ratio of styrene to maleic acid, where all polymers produced were the same length. Secondly, a percentage of the maleic acid monomers were chemically modified to a more hydrophobic moiety: N-benzyl maleimide. Modification of a maleic acid monomer by the addition of a

benzyl ring produced a monomer more comparable to styrene than maleic acid. The higher the percentage of maleic acids that were modified, the more hydrophobic the polymer.

Figure 3.5 shows the soluble fraction following a solubilisation trial comparing 8 polymers from the BzAM series to SMA and DIBMA. The number of each BzAM polymer represents the fraction of maleic acid monomers that have been chemically modified. The red boxes on the Western blot images show the position where a protein the size of the hNTR1 monomer (46 kDa) or dimer (92 kDa) may appear. The intensity of bands in the red boxes represents the concentration of hNTR1 in the soluble fraction and therefore solubilisation efficiency of each polymer.

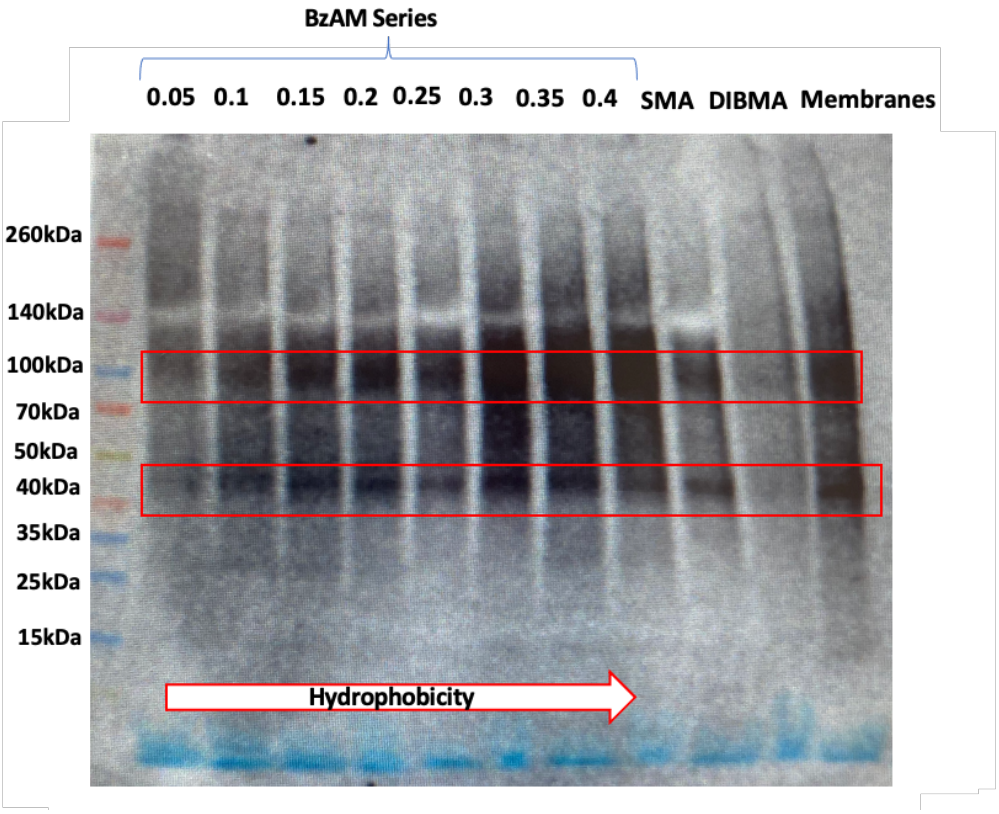


Figure 3.5: Solubilisation trial comparing the BzAM polymer series to SMA and DIBMA.
Western blot showing soluble fraction of hNTR1 expressing membranes solubilised with 2.5% polymer and the membranes diluted in 2-fold. SDS-PAGE was performed on a 4-20% gradient acrylamide gel. Arrow shows the increase in hydrophobicity of the BzAM series polymer. Red boxes indicate area where hNTR1 would run as a monomer or dimer. After transfer of protein to a nitrocellulose membrane, Western blot was probed with anti-NTR1 antibody.

Three of the polymers in the BzAM series had better solubilisation efficiency than SMA: 0.30, 0.35 and 0.4. These polymers had a similar percentage of hydrophobic residues to the SMA, which has two styrene residues for every maleic acid. DIBMA was the least effective solubilisation agent in this comparison.

The white band at approximately 140 kDa is likely due to overexposure in which the ECL reaction is completely exhausted (Mahmood and Yang, 2012). The higher-order oligomers could be due to disulphide bonds forming between the hNTR1, that were not able to be reduced by LDS sample buffer. The use of an anti-NTR1 specific antibody provided confidence that these bands were due to solubilised hNTR1 and not due to *E. coli* proteins.

Overall, the solubilisation trials showed PoLiPa are a good tool for the solubilisation of WT, full-length hNTR1. An improvement of the solubilisation efficiency of DIBMA was achieved by a higher concentration but even at the highest concentration tested (6.5% w/v), the concentration of extracted hNTR1 was lower than 1.5% w/v SMA (Appendix 1.1). Given that, SMA 2:1 performed well in the solubilisation trials and was an accessible and cost-effective method of solubilisation, purifications of hNTR1 in a SMALP were attempted.

3.3 IMAC Purification of hNTR1 using PoLiPa Technology

Purifications of SMA-solubilised hNTR1 were attempted using IMAC as previously described (Lee *et al*., 2019). IMAC resins contain immobilised metal ions which have an affinity for histidine residues. They can be used to selectively bind His tagged proteins. To improve the binding efficiency of proteins solubilised with the SMALP method, it is conventional to allow binding to occur overnight at 4°C (Lee *et al*., 2016). A His tag is a small, easily added tag which is unlikely to affect the function of the protein (Bornhorst and Falke, 2000). IMAC purification is relatively cheap and fast compared to other affinity purification methods (Magnusdottir *et al*., 2009). One major disadvantage of IMAC

purifications is the co-purification of proteins with cysteine- and histidine-rich regions (Bolanos-Garcia and Davies, 2006). This section aims to identify whether IMAC purification is a suitable method for purifying polymer-solubilised hNTR1. Three IMAC purifications of different starting material were compared: SMA-hNTR1 expressing *E. coli* membranes; DIBMA-hNTR1 expressing *E. coli* membranes and SMA-solubilised *E. coli* membranes with no recombinant expression.

3.3.1 IMAC Purification of SMA-hNTR1 Expressing E. coli Membranes

Samples were taken of the flow-through (FT) to show material that did not bind to the resin. However, the FT lanes appear heavily smeared due to the polymer in the sample. The resin was washed with buffer (BW), then 20 mM imidazole (IW20), then 40 mM imidazole (IW40). The imidazole washes allowed protein with a low affinity for the resin to be collected. The elution fractions (E1-E8) show protein products that had a high affinity for the resin that was eluted using a 500 mM imidazole concentration.

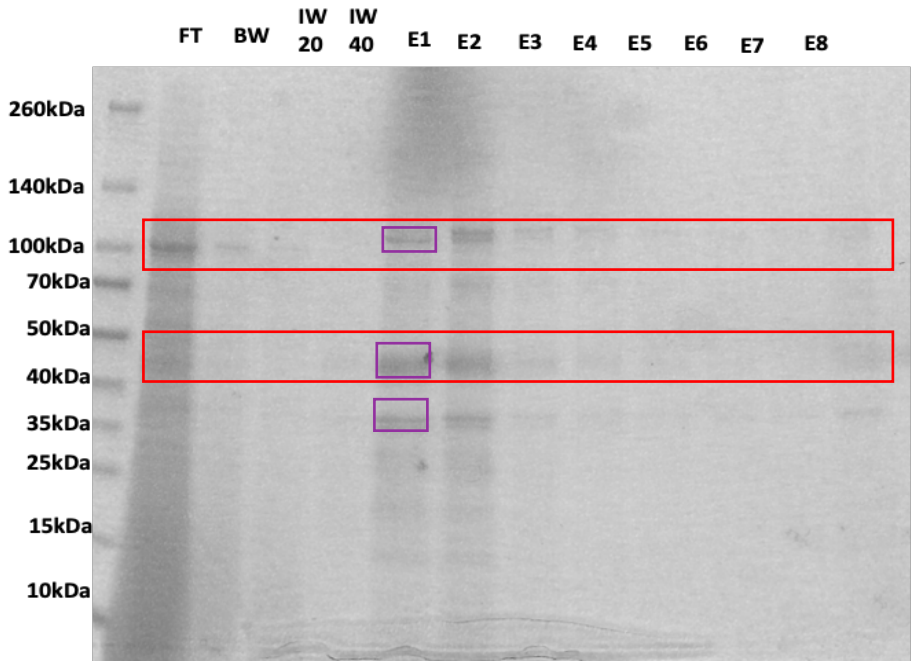


Figure 3.6: SDS-PAGE analysis of an IMAC purification using Ni-NTA resin from hNTR1 expressing membranes solubilised with 2.5% (w/v) SMA.
Purple Boxes indicate bands which were excised for MS analysis. Red Boxes indicate where bands of the hNTR1 dimer and monomer are expected to appear. Flow through (FT), Buffer wash (BW), 20 mM and 40 mM imidazole washes (IW20 and IW40) and 8 elution fractions (E1-E8) were analysed on a 4-20% gradient acrylamide gel and stained with Coomassie stain.

Figure 3.6 shows a purification of hNTR1 solubilised with SMA. The primary band in the elution fractions appeared between 40-50 kDa at the expected hNTR1 monomer size. A band also appeared at approximately 110 kDa close to where the hNTR1 dimer had appeared in previous Western blot analysis. At first, it was suggested that hNTR1 in its monomer and dimer form were successfully bound and eluted from the resin. However, MS Proteomics analysis of the band at 110 kDa, 45 kDa and 35 kDa did not identify hNTR1. When comparing identified peptides from the excised bands at 110 kDa, 45 kDa and 35 kDa to a protein database, a list of *E. coli* proteins identified them as likely contaminants, shown in Table 3.1. Acriflavine resistance B (AcrB) is a common contaminant in membrane protein purifications (Veesler *et al*., 2008). Unfortunately, this size of AcrB (110k Da) was close to the expected size of dimeric hNTR1. AcrB has been successfully investigated using SMALP technology previously (Postis *et al*., 2015).

Table 3.1: MS Proteomics Analysis of Three Bands excised in the SDS-PAGE gel analysing the first Elution Fraction of an IMAC purification Attempting to purify SMA-hNTR1.

Band excised from Gel (Figure 3.6A)	Identified Protein Hit (Accession number)	Coverage (%)	Unique Peptides	Peptide-spectrum match score	Amino Acids	MW (kDA)
110 kDa	Multidrug efflux pump subunit AcrB (P31224)	48	45	266	1049	113.5
110 kDa	2-oxoglutarate dehydrogenase E1 component (P0AFG3)	55	46	152	933	105
45 kDa	Cytochrome bo(3) ubiquinol oxidase subunit 1 (P0ABI8)	21	16	78	663	74.3
45 kDa	Glycogen synthase (P0A6U8)	40	16	33	477	52.8
45 kDa	ATP synthase subunit beta (P0ABB4)	54	18	27	460	50.3
45 kDa	Elongation factor Tu 1 (P0CE47)	48	13	19	394	43.3
45 kDa	ATP synthase subunit alpha (P0ABB0)	42	17	19	513	55.2
45 kDa	Glutamine synthetase (P0A9C5)	41	14	16	469	51.9
45 kDa	Zinc/cadmium/lead-transporting P-type ATPase (P37617)	26	15	54	732	76.8
45 kDa	Putative Lon protease homolog (P75867)	24	10	10	586	65.8
35 kDa	Cytochrome bo(3) ubiquinol oxidase subunit 2 (P0ABJ1)	62	12	93	315	34.9

3.3.2. IMAC Purification of DIBMA-Solubilised hNTR1 Expressing E. coli Membranes

IMAC purification of membranes expressing hNTR1 solubilised with DIBMA produced an impure elution with a large variety of bands, including bands at the size of the identified contaminants in Table 3.1 (110 kDa, 45 kDa and 35 kDa). Low-abundance protein targets are more likely to have contamination issues due to a larger relative concentration of *E. coli* proteins with histidine- and cysteine-rich regions (Bolanos-Garcia and Davies, 2006). Low MW *E. coli* proteins also interfere with the binding capacity of the IMAC resin (Magnusdottir *et al*., 2009).

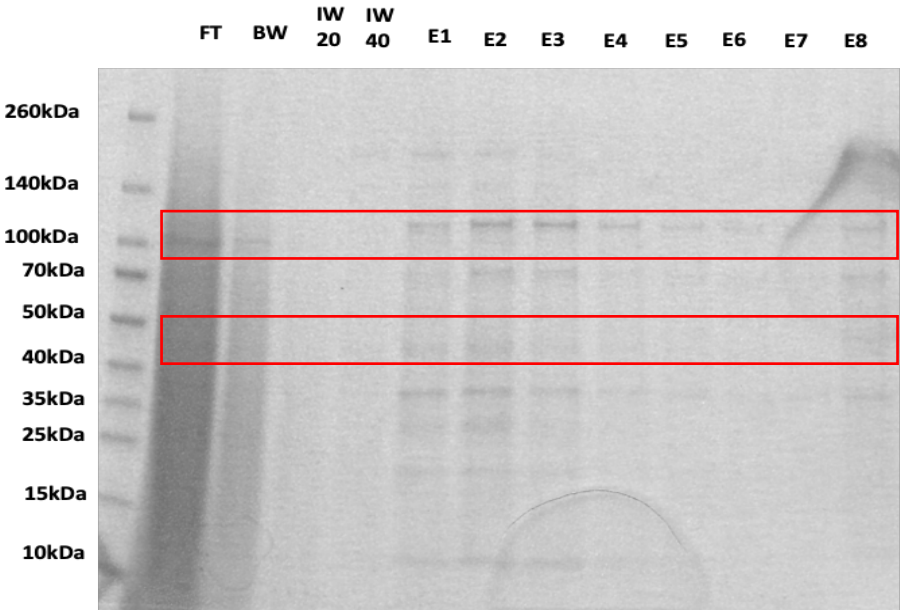


Figure 3.7: SDS-PAGE analysis of an IMAC purification using Ni-NTA resin from hNTR1 expressing membranes solubilised with 2.5% (w/v) DIBMA.
Red Boxes indicate where bands of the hNTR1 dimer and monomer are expected to appear. Flow through (FT), Buffer wash (BW), 20 mM and 40 mM imidazole washes (IW20 and IW40) and 8 elution fractions (E1-E8) were analysed on a 4-20% gradient acrylamide gel and stained with Coomassie stain.

3.3.3. IMAC Purification of SMA-solubilised E. coli control membranes

E. coli cultures that were not transformed with a plasmid were taken through the steps of SMA solubilisation and IMAC purification as a control. When no histidine-tagged protein is expressed, a variety of cysteine and histidine-rich proteins from the host bind to the Ni-NTA resin, as shown by the bands in the elution fractions of the SDS-PAGE gel in Figure 3.8. This

SDS-PAGE gel was useful for showing bands that are likely to be from the host rather than the protein being recombinantly expressed in the host. This included the common major bands at approximately 110 kDa, 45 kDa and 35 kDa. These are likely to be the same *E. coli* proteins identified by MS analysis. Unfortunately, the 110 kDa and 45 kDa contaminant bands are close to the expected size of monomeric and dimeric hNTR1 (shown in the red boxes).

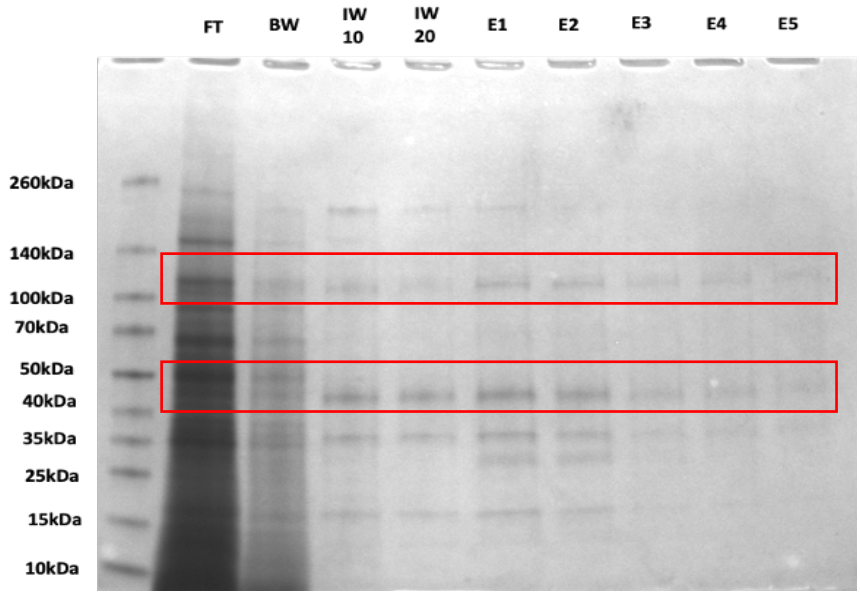


Figure 3.8: SDS-PAGE analysis of an IMAC purification using Ni-NTA resin from E. coli membranes with no recombinant expression membranes solubilised with 2.5% (w/v) SMA.
Red Boxes indicate where bands of the hNTR1 dimer and monomer are expected to appear. Flow through (FT), Buffer wash (BW), 20 mM and 40 mM imidazole washes (IW20 and IW40) and 5 elution fractions (E1-E5) were analysed on a 4-20% gradient acrylamide gel and stained with Coomassie stain.

Contamination is a common phenomenon associated with affinity purification. A repository of typical contaminants called 'the CRAPome' contains proteins identified post-affinity purification by mass spectroscopy (Mellacheruvu *et al.*, 2013). The database is focused on eukaryotic cell lines and is not specific to membrane proteins. The highly cited database shows the benefit of understanding the drawbacks of certain purification techniques. It is likely that due to low expression of hNTR1, there was not enough SMA-hNTR1 to out-compete the cysteine and histidine-rich *E. coli* proteins that have an affinity for the resin. Previously, research into common *E. coli* protein contaminants has focused on soluble proteins (Bolanos-Garcia and Davies, 2006). However, these gels and mass spectrometry

analysis (Table 3.1) give an insight into common SMA- or DIBMA-extracted membrane protein contaminants. The lipids and polymer may have the capability to block or reduce the affinity of a His tag to Ni-NTA resin. More information about how to improve IMAC purifications when polymers have been used for solubilisation could be useful for future membrane protein production. Müller *et al.* proposed a method for utilising a His tag twice by doing an anti-His immunoaffinity purification post-IMAC as a tool for reducing the contamination (Müller *et al*., 1998). Optimizing IMAC purification by making changes to the binding buffer, resin, washes and elution can also impure purity and yield (Bornhorst and Falke, 2000). It was decided that initial expression was too low to warrant extensive optimisation.

3.4 Identification of hNTR1 in Elution Fractions Post-IMAC Purification

E. coli protein contamination of IMAC elution fractions meant the presence of hNTR1 in the IMAC elution was not confirmed by SDS-PAGE or MS analysis. To test if any SMA-hNTR1 was purified by IMAC, the elution fractions were concentrated and analysed by Western blot (Figure 3.9). There was a band at approximately 100 kDa and 46 kDa reflecting the likely presence of the hNTR1 monomer and dimer. A band between 15-20 kDa was also visible. As the Western blot was probed by the anti-NTR1 specific antibody which has affinity of the N-terminus of NTR1, the band was likely representative of a fragment of hNTR1 that included the N-terminal region. This could indicate a loss of protein to fragmentation and instability during the IMAC purification or concentration process.

Despite a contamination issue, some SMA-hNTR1 was purified on IMAC. This justified further downstream processing of the impure hNTR1 sample. Downstream processing of the post-IMAC DIBMA solubilised protein product was also performed to give a comparison to SMA-solubilised material.

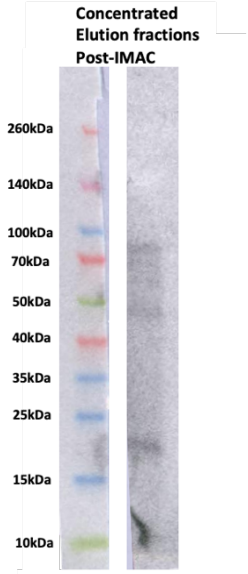


Figure 3.9: Western blot of concentrated elution fractions from a IMAC purification of hNTR1 solubilised with SMA.
SDS-PAGE performed on 4-20% acrylamide gel. anti-NTR1 antibody used to probe WB.

3.5 SEC of the Protein Product after IMAC Purification

Membrane proteins solubilised with the SMALP method have typically been purified by IMAC purification followed by SEC (Lee *et al*., 2016). SEC separates proteins by gel filtration: particles with a larger hydrodynamic radius flow through the column quicker than smaller particles (Hong *et al*., 2012). This section aims to investigate how the proteins solubilised with the SMA and DIBMA could be separated by SEC using a Superdex 200 Increase column and assess how SEC could aid SMA-hNTR1 purification.

Figure 3.10 shows how the protein samples post-IMAC purification were separated by SEC. The void volume for the column is 8 mL; this accounts for the volume of buffer that flows

through the column before any protein can be detected. Immediately after this volume, large aggregates of protein may elute. These may be too large to permeate into the acrylamide gel. Most of the protein in both samples was detected in the 8-12 mL elution volume, as shown by the peaks on the SEC absorbance traces (Figure 3.10A). The Superdex 200 Increase has the capacity for high-resolution analysis of globular proteins from 10-600 kDa (Cytiva, 2020). A standard protein, Ferritin, a 440 kDa soluble protein, should be detected after a 10 mL elution volume (Cytiva, 2020). The proteins encapsulated in a PoLiPa eluted similarly to large globular proteins, likely because of the increase in the hydrodynamic radius of the particle associated with a nanodisc.

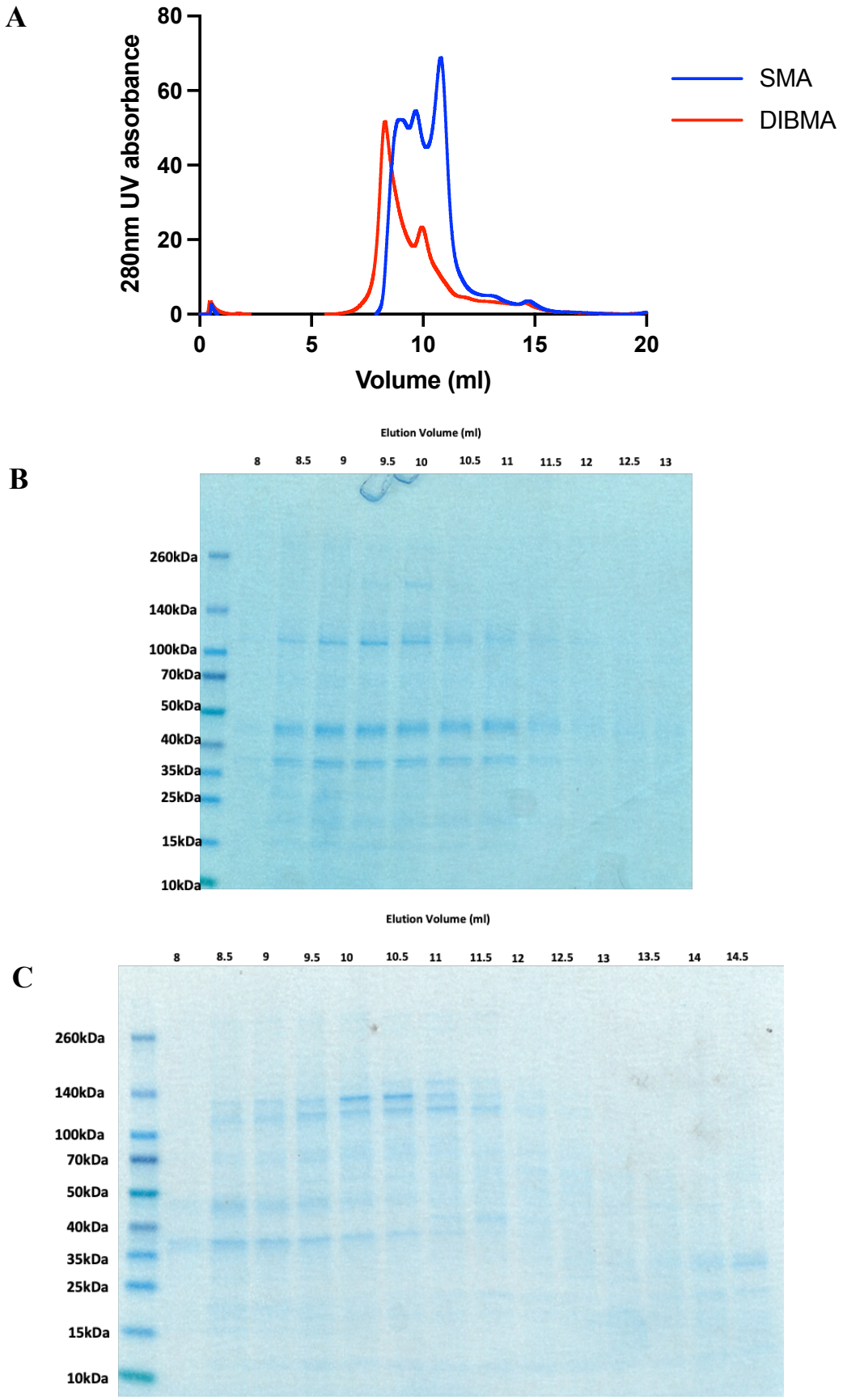


Figure 3.10: SEC of hNTR1 protein samples post-IMAC purification.
(A) Absorbance trace showing the absorbance reading as proteins eluted off Superdex 200 Increase column and comparison of the use of SMA and DIBMA as a solubilising agent.
(B) SDS-PAGE gel of elution fractions of the SMA-solubilised protein sample
(C) SDS-PAGE gel of elution fractions of the DIBMA solubilised protein sample. SDS-PAGE analysed on 4-20% acrylamide gel.

When the SMA-hNTR1 sample was analysed by SEC, the absorbance trace showed three poorly resolved peaks between elution volumes 8.5-12 mL. The SDS-PAGE analysis of elution fractions showed that the major bands that were present after IMAC purification, notably at approximate sizes 110 kDa, 45 kDa and 35 kDa, were present in all the 8.5-12 mL elution fractions (Figure 3.10B). The MWs of the bands on the SDS-PAGE gel do not correlate with the elution volume. This showed that SEC using a Superdex 200 Increase column cannot purify SMA-hNTR1 from a contaminated sample.

When the DIBMA-solubilised post-IMAC protein product was analysed by SEC, the absorbance trace showed two poorly resolved peaks between the elution volumes 8-11.5 mL. The slight shift to the left of the absorbance trace may be because DIBMA lipid particles (DIBMALPs) are reportedly larger than SMALPs (Gulamhussein *et al*., 2020). The SDS-PAGE gel in Figure 3.10C showed the proteins in each elution fraction. Bands were visible at approximately 45 kDa and 35 kDa in the elution fractions between 8-10 mL. The density of these bands decreases and there was an increase in intensity of protein bands between 100-140 kDa in the elution fractions between 10 mL and 12 mL. This indicates that the second peak of the SEC absorbance trace, between 9.5 mL and 11.5 mL, had a larger concentration of higher MW proteins compared to the first peak. This may seem counterintuitive as SEC should elute larger proteins first. This provides evidence that the size of a PoLiPa can be unrelated to the size of the proteins encapsulated. Some reasons for this could be that multiple proteins are being encapsulated into the same PoLiPa or particles could be sticking together. In the elution fractions between 14-14.5 mL, two protein bands between 25 and 15 kDa are visible on the SDS-PAGE gel. These could be protein fragments that are not encapsulated in a DIBMALP.

3.6 SMA-PAGE and DIBMA-PAGE Analysis of hNTR1 Oligomerisation

SMA-PAGE or DIBMA-PAGE is a type of native-PAGE that uses the charge of the SMA or the DIBMA to separate SMALPs or DIBMALPs through acrylamide gel without any denaturing agent (Pollock *et al*., 2019). To understand further the peaks on the SEC absorbance trace, fractions containing protein were separated using SMA-PAGE and DIBMA-PAGE to see if different-sized particles could be distinguished. When comparing SMA-PAGE bands to a native marker, SMA-solubilised proteins should appear at a similar size to the MWs of the encapsulated protein.

After SEC analysis of the SMA-solubilised protein product, the elution fractions between volumes 8-12 mL were analysed by SMA-PAGE. The SMA-PAGE gel (Figure 3.11A) shows three bands between 100 kDa and 720 kDa upon comparison to the native marker. These could represent three different particle sizes which would be reflective of the three peaks on the SEC absorbance trace. The particle sizes overlap across the elution fractions, which suggests that the peaks on the SEC absorbance trace are poorly resolved. The soluble fraction of SMA-hNTR1 expressing *E. coli* membranes was sampled before IMAC purification and was analysed by SMA-PAGE but showed no clear particle sizes. The sample of concentrated fractions post-IMAC and the sample of the concentrated elution fractions post-SEC look similar, indicating most of the protein was eluted within the elution volume 8-12 mL.

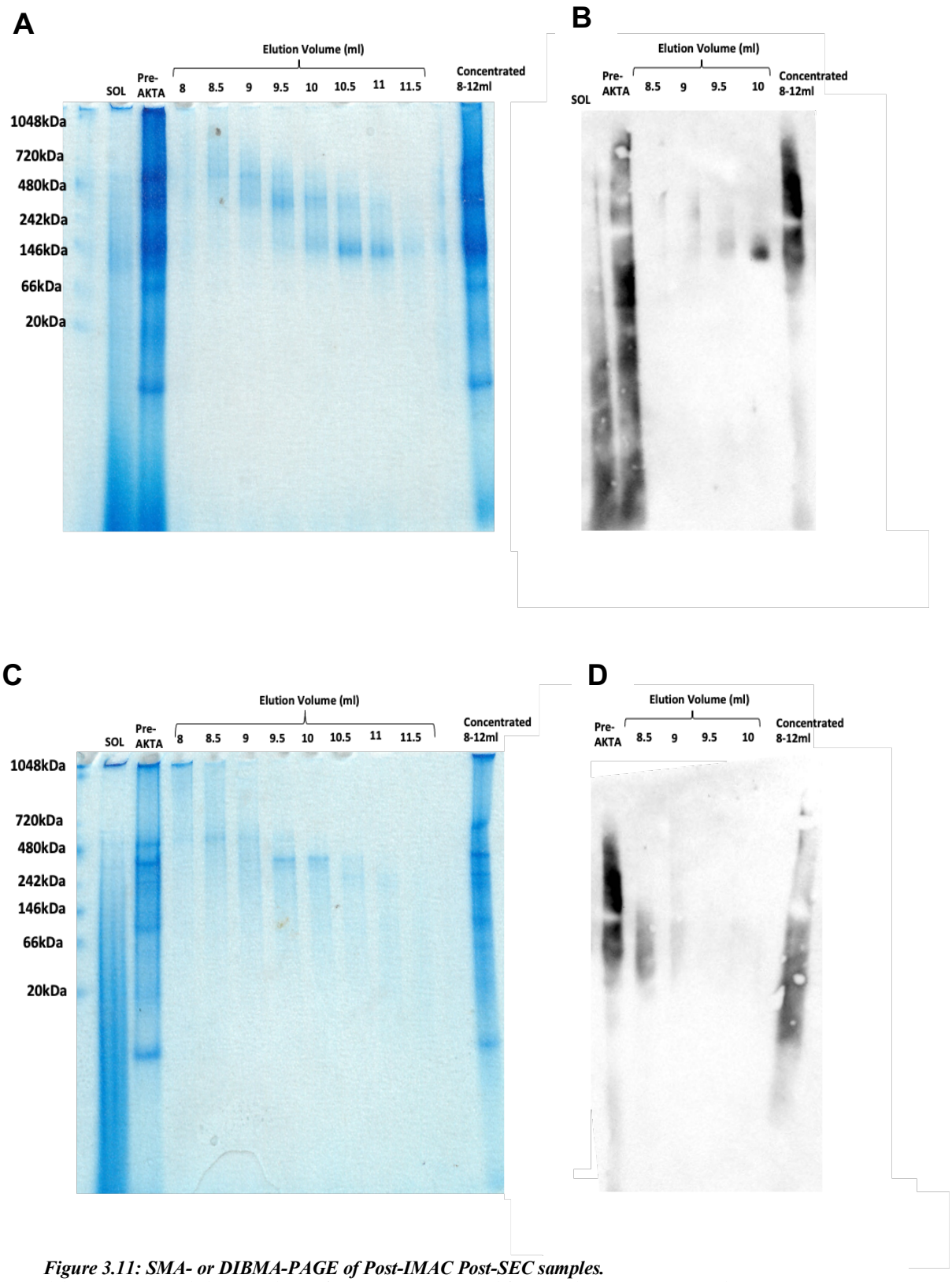


Figure 3.11: SMA- or DIBMA-PAGE of Post-IMAC Post-SEC samples.
(A) SMA-PAGE gel showing elution fractions post-SEC and for SMA-hNTR1 protein product.
(B) Western blot of SMA-PAGE gel using anti-his Antibody.
(C) DIBMA-PAGE gel showing elution fractions post-SEC and for SMA-hNTR1 protein product.
(D) Western blot of DIBMA-PAGE gel using anti-his Antibody. Other samples analysed by SMA- and DIBMA-PAGE shown are the soluble fraction pre-IMAC purification (SOL), the concentrated protein sample post-IMAC purification (pre-AKTA) and the concentrated elution fractions post-SEC (concentrated 8-12ml).

Elution fractions between volumes 8.5 mL to 10 mL were analysed by SMA-PAGE and Western blot (Figure 3.11B). The Western blot showed a similar pattern to the Coomassie-stained SMA-PAGE; however, the smallest particle size had the largest band intensity. This indicated that hNTR1 was encapsulated into a SMALP and was eluted at 10 mL volume. The hydrodynamic radius of this particle was equivalent to a globular protein of approximately 125 kDa (Cytiva, 2020). The less intense, smeared bands between 8.5 mL and 9.5 mL may be due to a lower concentration of hNTR1 or less availability of the His tag to bind the anti-His antibody for detection.

After SEC analysis of the DIBMA-solubilised protein product, the elution fractions between volumes 8 mL and 12 mL were analysed by DIBMA-PAGE. In elution fractions between 8 mL and 10.5 mL, the DIBMA-PAGE gel (Figure 3.11C) showed two bands between the 242 kDa and 480 kDa upon comparison to the native marker. These could represent two different particle sizes which would be reflective of the two peaks on the SEC absorbance trace. Between the elution volumes of 8 mL and 8.5 mL, a protein band showed material that was not able to migrate into the gel. This is likely aggregated material which eluted from the SEC column immediately after the void volume. This showed the largest DIBMALPs could not be separated from these aggregates with a Superdex 200 column.

The elution fraction between the volumes 8.5 mL to 10 mL was analysed by DIBMA-PAGE and Western blot (Figure 3.11B). The Western blot showed a possible band in the concentrated elution fractions post-IMAC (Pre-AKTA) sample. However, due to the smearing on the Western blot, the DIBMA-PAGE does not provide a clear confirmation of the presence of a His tagged protein.

Figure 3.11 showed the SMA-PAGE and DIBMA-PAGE gels have bands at much larger predicted MWs than the size of hNTR1 or the contaminants shown on an SDS-PAGE gel. Pollock *et al* suggested that SMA-PAGE could closely estimate the MW of the SMALP encapsulated protein (Pollock *et al*., 2019). This further suggested that multiple proteins are encapsulated within the same PoLiPa or that multiple particles are sticking together.

3.7 Excision of SMA-PAGE and DIBMA-PAGE Bands for SDS-PAGE

To test the theory that multiple proteins are being encapsulated within the particles of one size, the bands from the SMA-PAGE gels and DIBMA-PAGE gels were excised, vortexed and sonicated with LDS-sample buffer. The denatured sample was re-analysed on an SDS-PAGE gel and silver stained to detect proteins at a low concentration (Figure 3.11). The SEC fraction collected after a 10.5 mL elution volume generated two bands from SMA-PAGE analysis. These were excised and analysed by SDS-PAGE separately (labelled 10.5 Upper and 10.5 Lower). The DIBMA-PAGE excised samples were stained for longer to detect lower concentrations of proteins hence the darker colour of the gel.

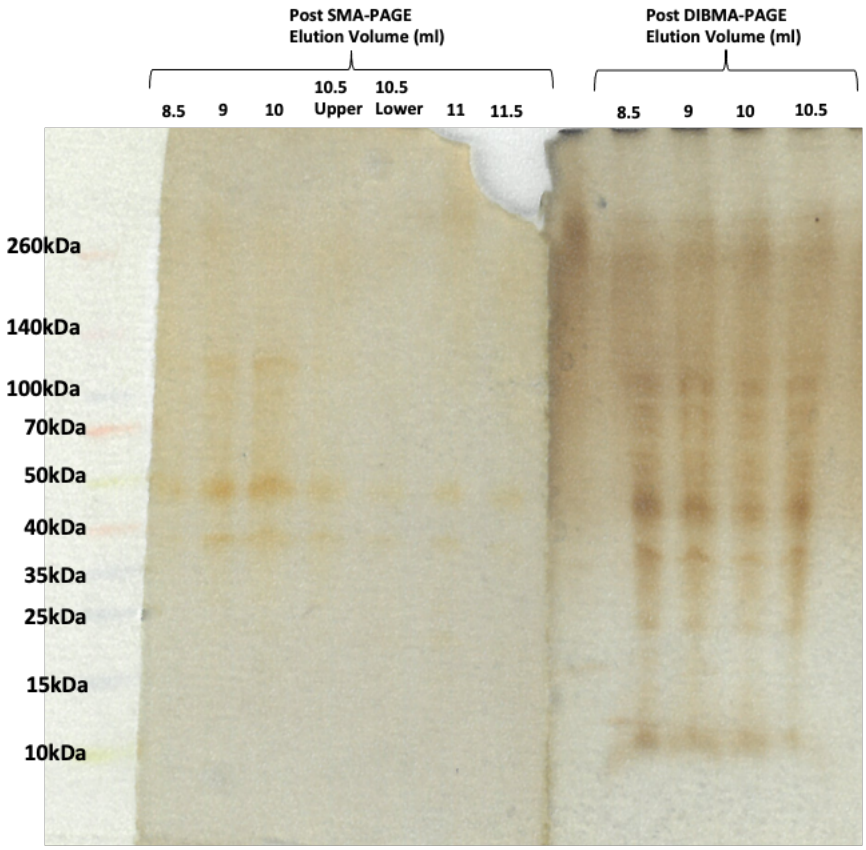


Figure 3.12.: Silver stained SDS-PAGE gel of bands excised from SMA-PAGE (left) or DIBMA-PAGE (right).
After the SMA-solubilised protein sample was eluted from SEC, the elution fraction at 10.5mL had two bands on visible on a gel analysed SMA-PAGE analysis. These were excised separately and labelled 10.5 Upper and 10.5 Lower. SDS-PAGE analysed on 4-20% gradient acrylamide gel.

Major contaminant bands at approximately 45 kDa and 35 kDa, which have been consistently appearing in post-IMAC samples were visible in all the SMA-PAGE and DIBMA-PAGE excised samples. A band at approximately 110 kDa, likely the *E. coli* protein AcrB as previously identified by MS analysis, was also visible. All the bands excised from the DIBMA-PAGE gel look similar, despite the two different sized bands excised.

Overall, the SDS-PAGE analysis showed a heterogeneous sample of proteins including the consistent contaminant bands. This gave more evidence that the particle sizes identified by SEC and SMA-/DIBMA-PAGE are representing clumps of SMALPs or DIBMALP or that multiple proteins are encapsulated within the same SMALP or DIBMALP. Use of a Superdex 200 Increase column was deemed an inappropriate method for removing contaminants from

PoLiPa samples. Despite the identification of different-sized particles, a variety of different-sized proteins appeared to co-elute at the same volume. This research questions the purity of a single fraction, as several SMA-solubilised proteins were eluted at the same volume, seemingly from the same sized particle.

3.8 Conclusion

This chapter has provided insights into how a GPCR with no stabilising mutations or fusion proteins could be expressed in *E. coli* and extracted by PoLiPa technology. Although SMA was shown to be a good solubilising agent, the complications of purifying a low-expressing membrane protein prevented the production of a pure sample. It was decided that this protein construct was too low yielding to warrant an extensive optimisation of the process. Despite the challenges of low expression and contaminated purification products, this construct was able to give valuable insights into solubilisation agents, purification methods and contamination problems. The impure hNTR1 product was still useful for sensitive ligand binding experiments such as FTS, discussed later in Chapter 8.

These experiments provided a good starting point to produce other GPCRs in *E. coli* and other purifications of GPCRs in a PoLiPa. This project continued to investigate GPCRs fused to MBP, as discussed in Chapter 4.

CHAPTER 4: MBP FUSED GPCR EXPRESSION IN *E. COLI:* PRODUCTION AND CHARACTERISATION OF MBP-FUSED rNTR1 USING POLIPA

4.1 Introduction to MBP Fusion Proteins

The results in Chapter 3 show that SMA can be used to solubilise a low-expressing, WT GPCR. However, it was recognised that to achieve a pure protein product after solubilisation with amphipathic polymers, a higher level of expression would be required. Literature review showed that successful expression of GPCRs in *E. coli* consistently required conjugation of the GPCR to other peptides (Kim *et al*., 2023). One such modification is maltose binding protein (MBP) fusion which is regularly used to aid recombinant expression in *E. coli* (Lebendiker and Danieli, 2011). MBP is a soluble *E. coli* protein which has been theorised to improve correct folding and solubility, prevent aggregation, and aid localisation of membrane proteins into the plasma membrane (Raran-Kurussi and Waugh, 2017). A mammalian version of MBP has even been used to improve protein expression in mammalian cell lines (Bokhove *et al*., 2016).

A concern with the addition of a fusion protein is the possibility of structural changes to the WT protein. 24 cases of proteins fused to MBP have had their structures compared to those of the unfused protein; these showed close agreement between the paired structures with only minor differences, most commonly occurring near the fusion point with little alteration of the overall structure (Waugh, 2016). Having attempted purification of a WT GPCR with no fusion protein, it was decided the MBP-fusion approach would have a higher probability of producing pure GPCR encapsulated in a PoLiPa.

Grisshammer and Henderson have previously developed plasmids for the expression of three MBP-fused GPCRs that use a pRG vector backbone (Tucker and Grisshammer, 1996). These plasmids were purchased from Addgene after deposition from the Richard Henderson Lab. These plasmids allowed the expression of rNTR1 (rat NTR1), human adenosine receptor 2 (A2AR), and human cannabinoid receptor 2 (CB2). Figure 4.1 summarises the truncations, fusion proteins and tags of these GPCRs, which have been previously expressed successfully in *E. coli*.

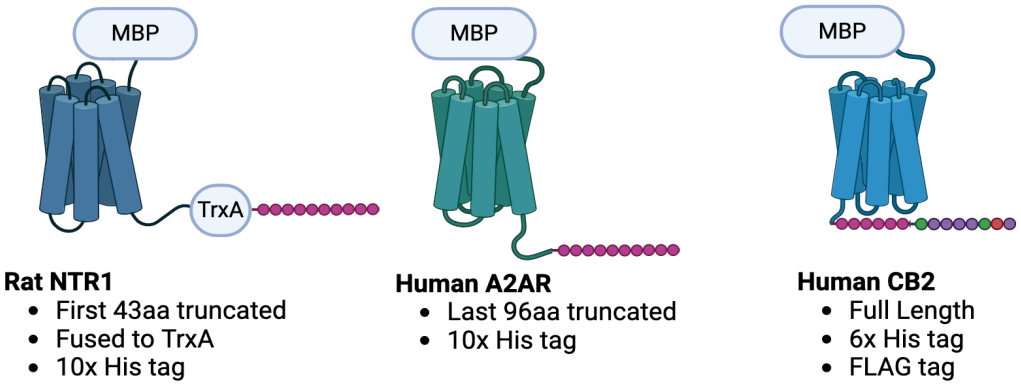


Figure 4.1: Cartoon summarising of characteristics of MBP fused GPCRs in which expression was tested. *Includes fusion proteins, truncations, and affinity tags.*

These constructs provided the opportunity to investigate multiple GPCRs and different purification methods. This project aimed to investigate how PoLiPa technology could aid the solubilisation and purification of three MBP-GPCR fusion proteins expressed in *E. coli.*

It was hypothesised that in the same expression conditions, the MBP-fused GPCRs would be expressed at a higher level than the hNTR1. This would provide validation for a more in-depth investigation into expression with the pRG constructs. The characteristics of the pRG construct are shown on the plasmid map in Figure 4.2. The MBP is fused via the N-terminus of the GPCR. The pRG vector used a lac operon system as a method of inducible protein expression, like the pET-21a(+) vector used to express hNTR1.

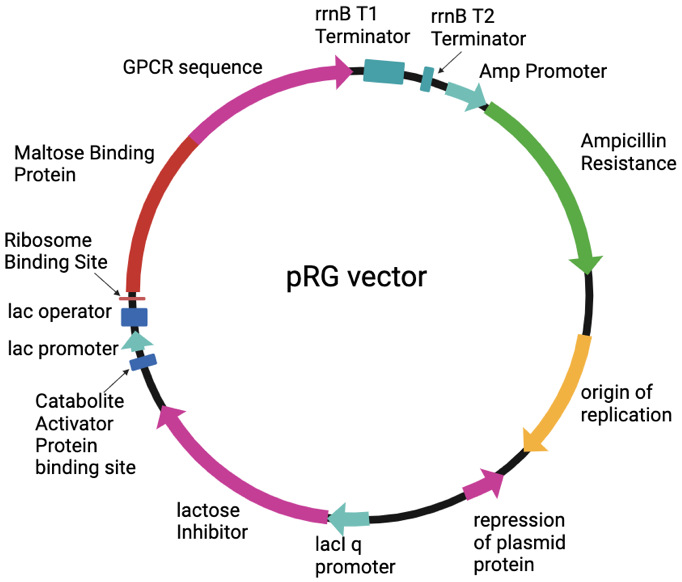


Figure 4.2 : Plasmid map showing the key characteristic of the pRG vector used to express MBP-fused GPCRs in E. coli.

4.2 Comparison of MBP-fused GPCR Expression to hNTR1 Expression in E. coli

Each protein was expressed under the same conditions as hNTR1. The intensity of the bands in Figure 4.3 represents the concentration of His tagged protein; in homogenized membranes of *E. coli* expressing each GPCR (Raw Membranes), solubilised with SMA (Soluble) and unable to be solubilised with SMA (Insoluble).

No band is present near the expected mass of hNTR1 (40-50 kDa), in the homogenised membranes of *E. coli* induced to express hNTR1 (Figure 4.3). The expression level was likely too low to be detected at the exposure level used. There is an unusual darkening effect on the background around 100 kDa that appears in all the lanes. This was likely an artefact caused by the transfer process (Mahmood and Yang, 2012). There was smearing in the lower half of the lanes in the soluble fraction of all four proteins likely to be caused by non-specific binding to residual SMA polymer.

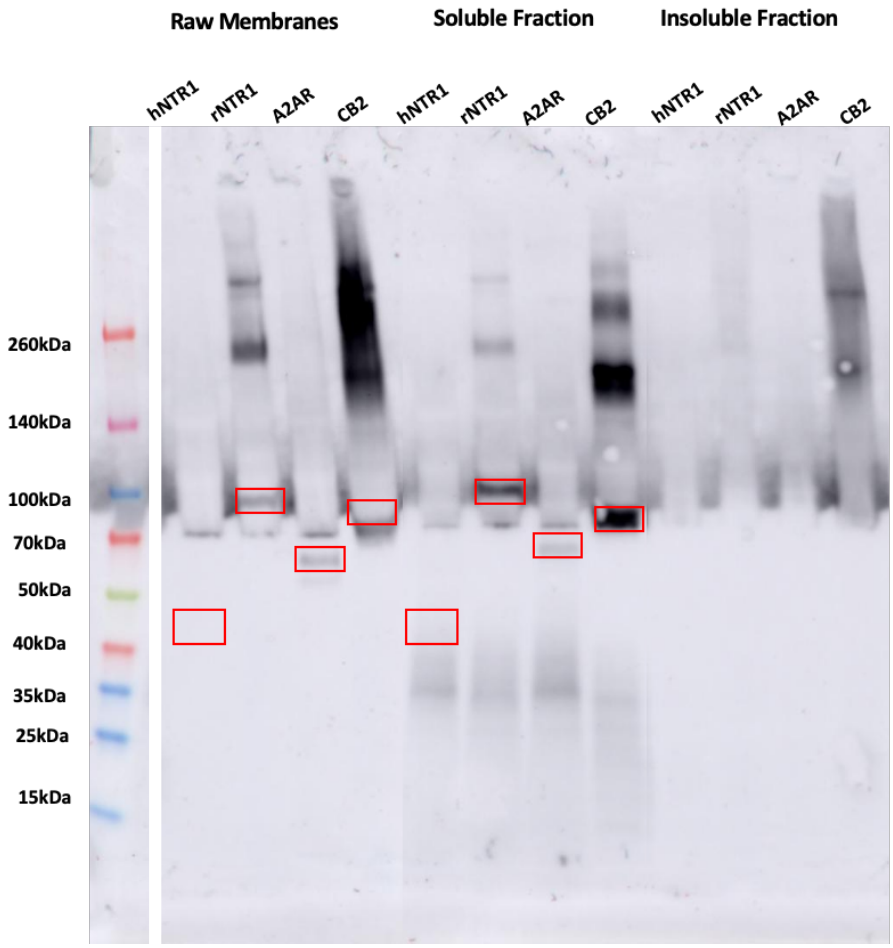


Figure 4.3: Expression Comparison of four GPCRs expressed in E. coli by Western blot analysis.
Homogenised membranes (left) of E.coli expressing a GPCR expressing one of four GPCRs: hNTR1, rNTR1, A2AR. CB2 were analysed, as well as the soluble fraction (middle) and insoluble fraction (right) of the homogenised membranes after 2.5% (w/v) SMA solubilisation. Red boxes show where a protein of the predicted MW of protein of interest would appear. Samples were separated using a 4-20% polyacrylamide SDS-PAGE gel and probed using an anti-His antibody.

The expected mass of MBP-fused rNTR1, hereby referred to as rNTR1, is 99 kDa, as calculated from its primary sequence. A band close to this expected mass was present in the homogenised membranes of *E. coli* induced to express rNTR1 (Figure 4.3). Two higher-order bands also appeared at a higher intensity which could represent dimers and higher-order oligomers of rNTR1 (a common artefact in SDS-PAGE separations of membrane proteins). All three of these bands were also visible in the soluble fraction. The monomer band was more intense after solubilisation whereas the intensity of the higher-order bands was lower after solubilisation. No bands were visible in the insoluble fraction indicating the concentration of rNTR1 that was not solubilised was too low for detection.

The expected mass of MBP fused A2AR, hereby referred to as A2AR, as calculated from its primary sequence, is 79.5 kDa (Figure 4.3). A band close to this expected mass was present in the homogenised membranes of *E. coli* induced to express A2AR. A second band was visible slightly below the band expected to be monomeric A2AR. This suggested some proteolytic digestion. No bands appeared in the insoluble fraction indicating the concentration of A2AR unable to be solubilised with SMA was too low for detection.

The expected mass of MBP fused CB2, hereby referred to as CB2, as calculated from its primary sequence is 85 kDa. In homogenised membranes of *E. coli* induced to express CB2, there is a large smear and a possible band at the expected size of CB2 (Figure 4.3). It is likely that the CB2 concentration was too high and caused overloading. The presence of bands that may represent a monomer, dimer, and higher-order oligomers of CB2 are distinguishable in the SMA-solubilised fraction. Two bands expected to represent CB2 oligomers were visible after analysis of the insoluble fraction. The bands representing the CB2 have a higher intensity than other GPCRs.

This Western blot showed that the MBP-fused GPCRs were expressed to a higher level in *E. coli* than the WT unlabelled hNTR1 construct. There was a large variation in protein concentration between the MBP-fused GPCRs. The order of best to worst expressed could be summarised as CB2 $\Rightarrow$ rNTR1 $\Rightarrow$ A2AR $\Rightarrow$ hNTR1. This small expression and solubilisation test gave evidence that MBP-fused GPCRs are a better investigative tool for the use of PoLiPa technology. This warranted an in-depth investigation into the production of rNTR1 and CB2. This chapter will now discuss the production and biophysical characterisation of rNTR1 only. Chapters 5 will describe how CB2 was expressed, solubilised, purified and characterised. Focus on rNTR1 and CB2 was due to the higher expression and less reported uses of PoLiPa solubilisation.

4.3 Introduction to Production of rNTR1

The rat version of NTR1 (rNTR1) was the first GPCR to be expressed in a prokaryote (Tucker and Grisshammer, 1996). As GPCRs are an important but difficult-to-investigate protein class and rNTR1 is one of the most successfully produced GPCRs, there has been significant research into the structure and function of rNTR1 (Abiko *et al*., 2021). The use of PoLiPa technology for rNTR1 characterisation was reported once when rNTR1 monomers or dimers were encapsulated in an SMALP but no purification was performed (Dathe *et al*., 2019). In this chapter, rNTR1 was used as a model GPCR for an in-depth investigation of the benefits and disadvantages of PoLiPa technology for GPCR production.

4.4 Optimisation of Expression of rNTR1 in E. coli

A series of small volume cultures under different conditions were performed to determine the best conditions for rNTR1 expression. The variables investigated included broth type, cell line, IPTG concentration and expression time. Since the initial expression of rNTR1 shown in Tucker and Grisshammer (1996), rNTR1 has been expressed in *E. coli* using the pRG vector or modified version (Table 4.1).

Table 4.1: Summary of expression conditions previously used in the literature to express rNTR1

Plasmid	Cell Line (*E. coli*)	IPTG Conc (mM)	Expression Temp (ºC)	Point of induction	Expression Time (hours)	Broth	Reference
pRG	DH5α	0.25 mM	22	OD 0.5	40	2xYT+0.2% (w/v) glucose + 67 µg/mL ampicillin	White *et al* (2004)
pRG	DH5α	0.5 mM	20	4-6 hours after inoculation	40	2xYT+0.2% (w/v) glucose + 100 µg/mL ampicillin	Tucker and Grisshammer (1996)
pRG	BL21(DE3)	1 mM	29	OD 0.5	Not specified	2xYT + 1% (w/v) glucose + 50 µg/mL ampicillin	Egloff PhD Thesis (2014)
pBR322	BL21(DE3)	1 mM	24 or 28	OD 0.5	20 or 16	2 x YT + 0.3% (w/v) glucose + 100 µg/mL ampicillin.	Egloff *et al* (2014)
pRG	BL21(DE3)	0.25 mM Or AI broth	20ºC	OD 0.5	30	2xYT + 0.2% glucose + 100 µg/mL ampicillin or AI broth	Attrill *et al* (2009)

4.4.1 Comparison of E. coli Strains

Identification of different serotypes of *E. coli* has led to the development of multiple strains. Grisshammer and Tucker (1996) used *E. coli* DH5-α cells to produce rNTR1, but better cell lines have been optimized for protein expression specifically. BL21(DE3) cells have been modified for protease deficiency and reduced plasmid loss (Rosano and Ceccarelli, 2014). *E. coli* strains have also been developed from the BL21(DE3) strain for toxic protein expression specifically, such as C43(DE3) (Dumon-Seignovert *et al*., 2004). To determine the cell line to use, a comparison of rNTR1 expression using BL21(DE3) or C43(DE3) cell lines was performed.

Figure 4.4 shows the Western blot analysis the of the cell lysate and cell lysate supernatant samples which were used to compare rNTR1 expression in BL21(DE3) and C43(DE3) cell lines. The intensity of the bands at the expected MW of rNTR1 (99 kDa) indicated that more rNTR1 was expressed in C43(DE3) cells than in the BL21(DE3) cells. The rNTR1 monomer band was visible in the supernatant sample expressing rNTR1 in C43(DE3) cells but not in BL21(DE3) cells.

This experiment showed that an improvement could be achieved by expressing rNTR1 in C43(DE3) cells. This suggested rNTR1 expression was toxic to the *E. coli* as modifications in the C43(DE3) strain may helped circumvent toxic effects of expression (Dumon-Seignovert *et al.*, 2004).

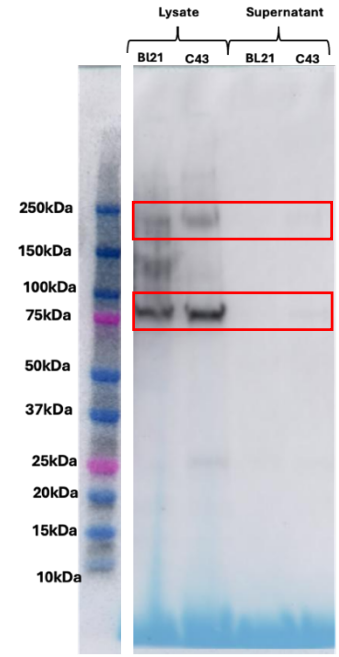


Figure 4.4: rNTR1 expression trial in two cell lines
10 mL samples of two cultures used to compare rNTR1 expression using BL21 and C43(DE3) cell lines were taken after overnight expression. Sample was lysed and centrifuged at 10000 x g. Western blot analysis of cell lysate and supernatant samples separated using a 4-20% polyacrylamide SDS gel and probed using an anti-His antibody. The red boxes indicate the expected MW of the rNTR1 monomer and dimer.

Production of a mammalian protein in a prokaryotic system is likely to be a large metabolic burden therefore use of an appropriate cell line is beneficial for GPCR production

(Pouresmaeil and Azizi-Dargahlou, 2023). The C43(DE3) cell line was used for further expression of rNTR1.

4.4.2 Comparison of Growth Media

All *E. coli* require vitamins and minerals, usually provided by yeast extract in growth media, and a source of nitrogen, usually provided by tryptone in growth media. LB growth media is the most used growth medium for *E. coli* but more nutrient-rich broths such as 2xYT or TB may improve growth and expression (Kram and Finkel, 2015). TB contains glycerol as an energy source, which results in a higher yield of bacterial biomass per volume. However, a larger biomass with lower expression may cause more difficult purification steps when moving forward. An expression trial was performed to understand which growth media was optimal for rNTR1 expression.

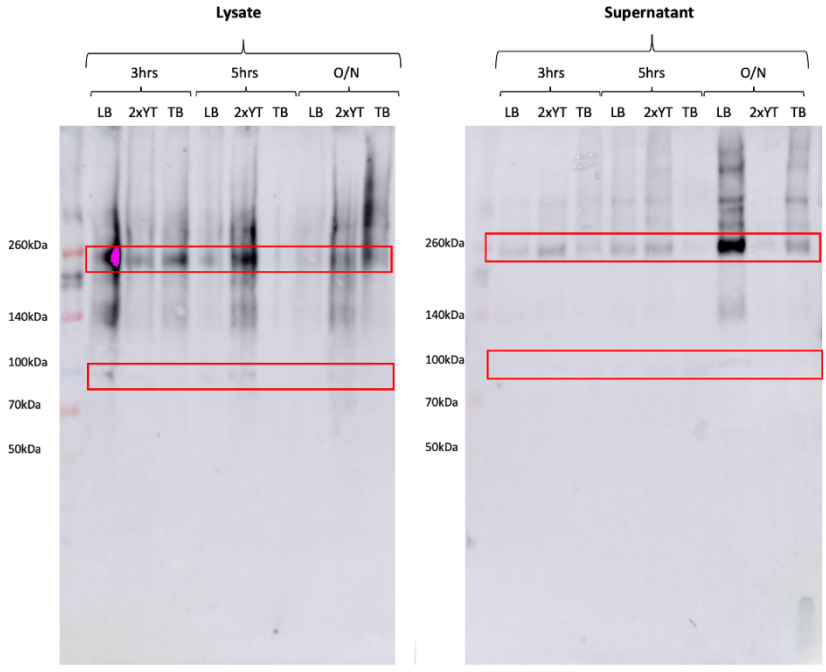


Figure 4.5: rNTR1 expression trial comparing three different broth types.
100 mL of LB, 2xYT or TB growth media was inoculated with 1 mL of overnight culture and grown at 37℃. At OD 0.6-0.8. Temperature was lowered to 18℃ and cells and induced with 0.5 mM IPTG. 10mL samples were taken 3 hours and 5 hours after induction and after overnight expression. Cells were centrifuged and resuspended in cell lysis buffer. A cell lysate sample was taken, and the lysate was centrifuged again. Samples of supernatant were taken. Western blot analysis of cell lysate (left) and supernatant (right) samples separated using a 4-20% polyacrylamide SDS gel and probed using an anti-His antibody. The red boxes indicate the expected MW of the rNTR1 monomer and dimer.

Western blot analysis indicated expression levels of rNTR1 in different growth media (Figure 4.5). The cell lysate samples lacked clarity because crude cellular extracts contain a range of compounds which could interfere with SDS-PAGE. Despite the inclusion of DNase in the lysis buffer, nucleic acids cause high viscosity of the cell lysate sample. Despite smearing, bands at the expected size of rNTR1 were visible and bands likely representing dimers of rNTR1 were visible at approximately 198 kDa. The supernatant samples gave a clearer image of which growth media supported the highest level of expression. The sample taken from cells grown in LB broth after overnight expression showed the most intense bands representing the rNTR1 monomer and dimer, indicating that rNTR1 expression was higher in LB broth than the two other growth media.

A higher concentration of rNTR1 in comparison to other possible contaminating proteins can aid purification downstream. LB broth has not been used to express rNTR1 in *E. coli* previously (Table 4.1). This demonstrates the benefit of performing expression trials to understand the optimal conditions for the protein of interest. The use of LB Broth was continued for the subsequent rNTR1 expression.

4.4.3 Comparison of IPTG Concentrations and Lengths of Expression Before Harvesting

IPTG is a molecular analogue of allolactose, which inactivates a repressor of the lac operon (William Studier *et al*., 1990). This initiates transcription of genes in the lac operon such as rNTR1 in the pRG plasmid. IPTG concentration can have a large effect on protein concentration: too high a concentration can cause a surge of expression that increases misfolding and formation of inclusion bodies, while too low a concentration can reduce transcription and protein yields. To optimise IPTG concentrations for expression of rNTR1, three IPTG concentrations were tested: 0.5 mM, 0.25 mM and 0.1 mM.

Western blot analysis showed a band close to the predicted mass of rNTR1 (99 kDa), indicating rNTR1 was present in all cell lysate and supernatant samples except the sample taken an hour post-induction (Figure 4.6). Higher-order bands that could represent oligomers were also present, most notably a band suspected to represent an rNTR1 dimer at approximately 198 kDa. After 3 hours the 0.1 mM IPTG concentration appeared to have higher expression of rNTR1, shown by the higher intensity of monomer and dimer bands in the cell lysate and supernatant samples. This is likely because the low IPTG concentration has minimally affected *E. coli* growth. IPTG can inhibit growth and cell viability; IPTG itself also has some toxicity but there was also an increase in metabolic burden due to increased protein expression (Gomes *et al*., 2020; Larentis *et al*., 2014).

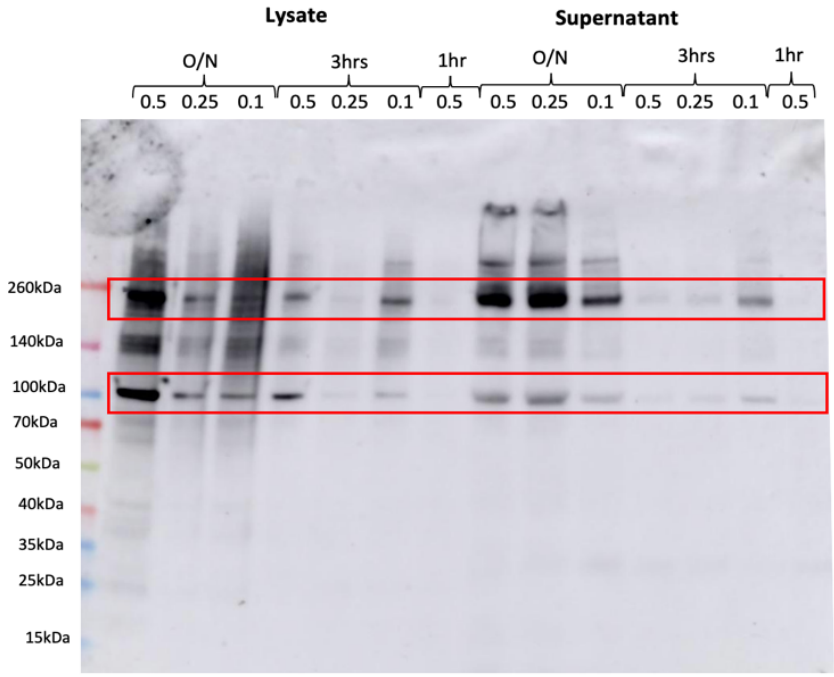


Figure 4.6: rNTR1 expression trial comparing three IPTG concentrations and harvesting time points. *100 mL of growth media was inoculated with 1mL of overnight culture and grown at 37 ℃. At OD600 of 0.8, the temperature of the incubator was lowered to 18 ℃ and cells and induced with 0.5 mM, 0.25 mM or 0.1 mM IPTG. 10 mL samples were taken 4 hours after induction and after overnight expression. Cells were centrifuged and resuspended in cell lysis buffer. Cell lysate sample was taken, and lysate was centrifuged again. Western blot analysis of supernatant and cell lysate were separated using a 4-20% polyacrylamide SDS gel and Western blot probed using an anti-His antibody. Red boves represent size of expected rNTR1 monomer and dimer.*

The bands with highest intensity appear in samples taken after overnight expression. In cell lysate samples, the most intense monomer bands appear after induction with 0.5 mM IPTG. However, after centrifugation, the intensity of the monomer band is depleted, in contrast to the band representing dimeric rNTR1. A proportion of the rNTR1 detected in the cell lysate could be inclusion bodies which would be removed by the centrifugation step.
The concentration of IPTG which was chosen for expression was 0.25 mM IPTG, given the higher intensity of the bands supernatant sample compared to the other two IPTG concentrations.

4.4.4 Comparison of Expression Temperatures

The temperature at which *E. coli* express protein and the time of expression before harvesting cells can have a large impact on final protein concentration and protein quality (Francis and Page, 2010). Some *E. coli* expression protocols require induction and expression at 37°C for 3-4 hours, whilst others require overnight expression at lower temperatures (Francis and Page, 2010). To compare expression time and temperature, before induction, four cultures were incubated at three different temperatures (18°C, 25°C, 37°C).

A band at approximately 99 kDa, representing rNTR1, was visible in cell lysate and supernatant samples after Western blot analysis (Figure 4.7). In the supernatant sample, bands representative of an rNTR1 dimer (198 kDa) appeared at a higher intensity than the monomer band. A band between 15 kDa and 25 kDa was also present which may represent a fragment of rNTR1 due to proteolytic digestion. The cell lysate samples do not give a clear indication of protein concentration due to smearing, likely caused by nucleic acids, aggregated protein and other compounds in crude cell extracts which can interfere with separation by SDS-PAGE. The supernatant samples provide clearer bands of the suspected rNTR1 monomer and

dimer. At the time-point, 4 hours post-induction the cells incubated at 37°C appear to have the best expression. However, after overnight expression, the cells incubated at 25°C or 18°C have the best expression. There was a small variation in the intensity of the bands in the two flasks which were incubated at 25°C after overnight expression. This shows the variability in the expression of two separate cultures.

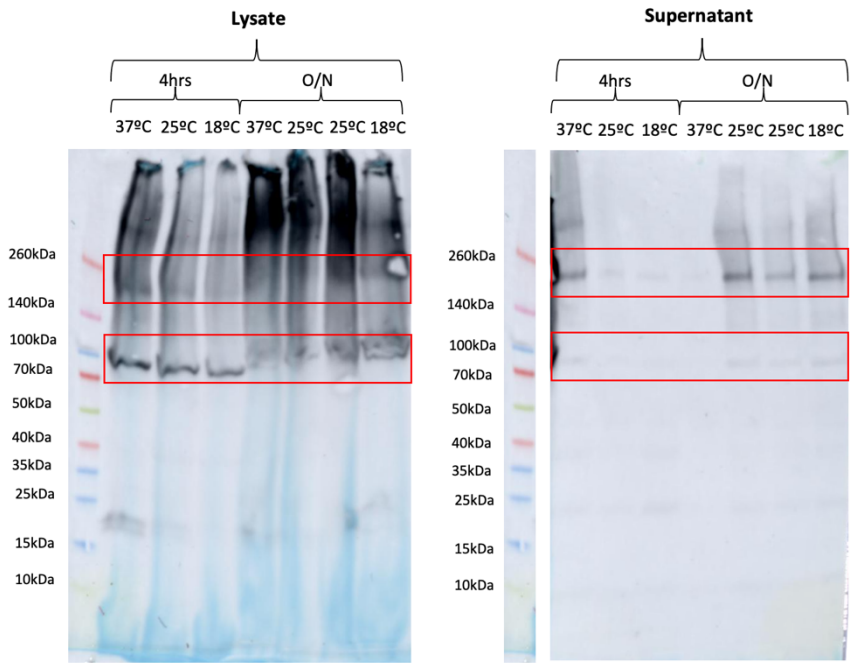


Figure 4.7: rNTR1 expression trial comparing three expression temperatures and two harvesting time points. *Four cultures (100 mL) were with 1 mL of overnight culture and grown at 37℃. At an OD600 of 0.6, flasks were moved to different incubation temperatures (18℃, 25℃, 37℃). 10 mL samples were taken 4 hours after induction and after overnight expression. Cells were centrifuged and resuspended in cell lysis buffer. Cell lysate sample was taken, and lysate was centrifuged again. Samples of cell lysate (left) and supernatant (right) were separated using a 4-20% polyacrylamide SDS gel and Western blot probed using an anti-His antibody.*

It was decided that 18°C was optimum for rNTR1 expression. Band intensity of the suspected monomer and dimer was comparable to cells incubated at 25°C, however cell density was lower at 18°C, suggesting there is higher expression per cell. It was decided that *E. coli* biomass per litre was less important than expression level. An increase in rNTR1 concentration and a decrease in endogenous bacterial protein concentration would be beneficial to purification efficiency. This supports previous eukaryotic protein expression in *E. coli,* which has been improved by low expression temperatures (San-Miguel *et al*., 2013).

4.4.5 Expression of rNTR1 in E. coli Summary

Expression optimisation led to the following chosen conditions for large-scale rNTR1 expression: the use of C43(DE3) cells, LB Broth, 0.25 mM IPTG induction and overnight expression at 18°C. Membrane preparations from rNTR1 expressing *E. coli* were performed to allow membranes to be ready for solubilisation.

4.5 Solubilisation Trials of rNTR1 in E. coli

Detergent screens have been an important step in solubilisation of GPCRs to produce the most efficient and stable extraction method (Rich *et al*., 2009). The use of polymers instead of detergents should produce a more stable protein product, however, biophysical characteristics of a polymer can affect its solubilisation efficiency in a protein-dependent way. Solubilisation trials were performed to provide a comparison of different amphipathic polymers and to understand which solubilisation agents have the most efficient extraction and stabilisation of rNTR1. Three solubilisation trials were performed: a BzAM polymer series comparison, a study of dependency of protein extraction on SMA concentration and a comparison of the influence of arginine as an additive during SMA solubilisation.

4.5.1 Effect of Polymer Hydrophobicity on Solubilisation Efficiency of rNTR1 and Comparison of BzAM Series Polymers to SMA and DIBMA

To understand how polymer hydrophobicity affected solubilisation efficiency, polymers in the BzAM series were included in the solubilisation trial. The stepwise increase in hydrophobicity across the polymers in the series, whilst maintaining a controlled polymer length, made the BzAM series a useful tool. It was hypothesised that rNTR1 would be extracted from the bulk

E. coli membrane efficiently by SMA and the more hydrophobic BzAM series polymers, given its similar structure to hNTR1.

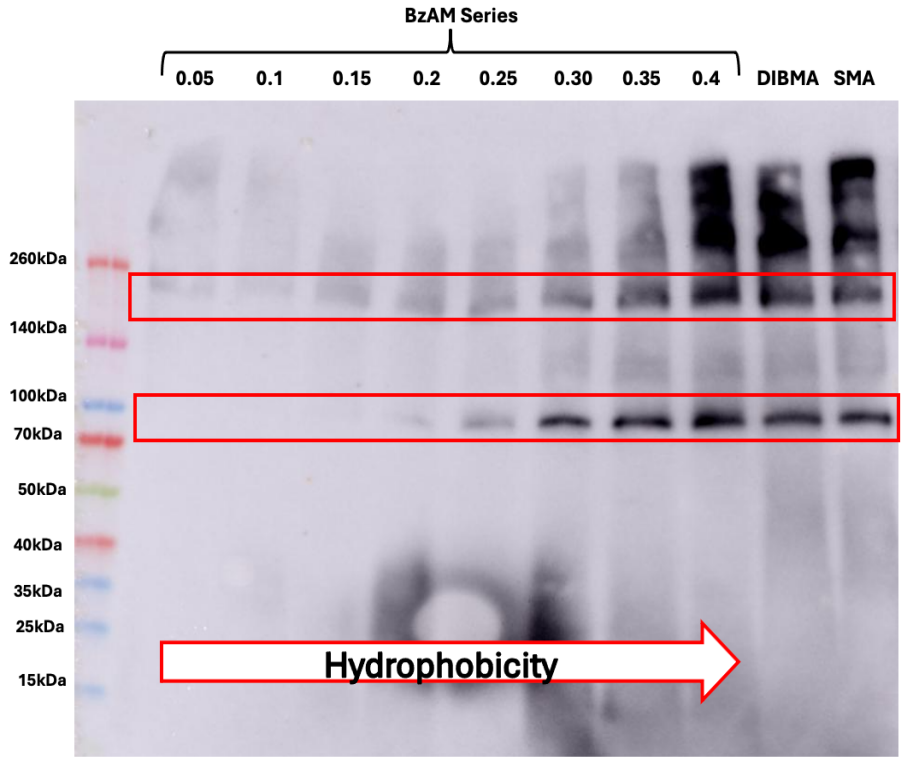


Figure 4.8: Solubilisation trial showing comparison of BzAM polymer series to SMA and DIBMA.
Western blot showing soluble fraction of rNTR1 expressing membranes solubilised with 2.5% (w/v) polymer. SDS-PAGE was performed on a 4-20% gradient acrylamide gel. WB probed with anti-His antibody. Arrow shows the increase in hydrophobicity of the BzAM series polymer. Red boxes indicate area where rNTR1 would run as a monomer or dimer.

Figure 4.8 shows the Western blot analysis of the soluble fractions following a solubilisation trial comparing the BzAM series polymers to SMA and DIBMA. Highest solubilisation efficiency occurred when using a BzAM 0.4 polymer. Lower solubilisation efficiency occurred when using less hydrophobic polymers. SMA and DIBMA extracted a comparable concentration of rNTR1 to the most hydrophobic BzAM polymers. The slight increase in solubilisation efficiency did not warrant the use of the BzAM series downstream due to the low availability and high cost of these polymers.

4.5.2 Determining Optimal SMA Concentration

Having determined that SMA was one of the best polymers for rNTR1 solubilisation, a solubilisation trial was performed to determine how SMA concentration affected solubilisation efficiency. Typically, 2.5% (w/v) SMA is used but it had been hypothesised that this was an excessive concentration.

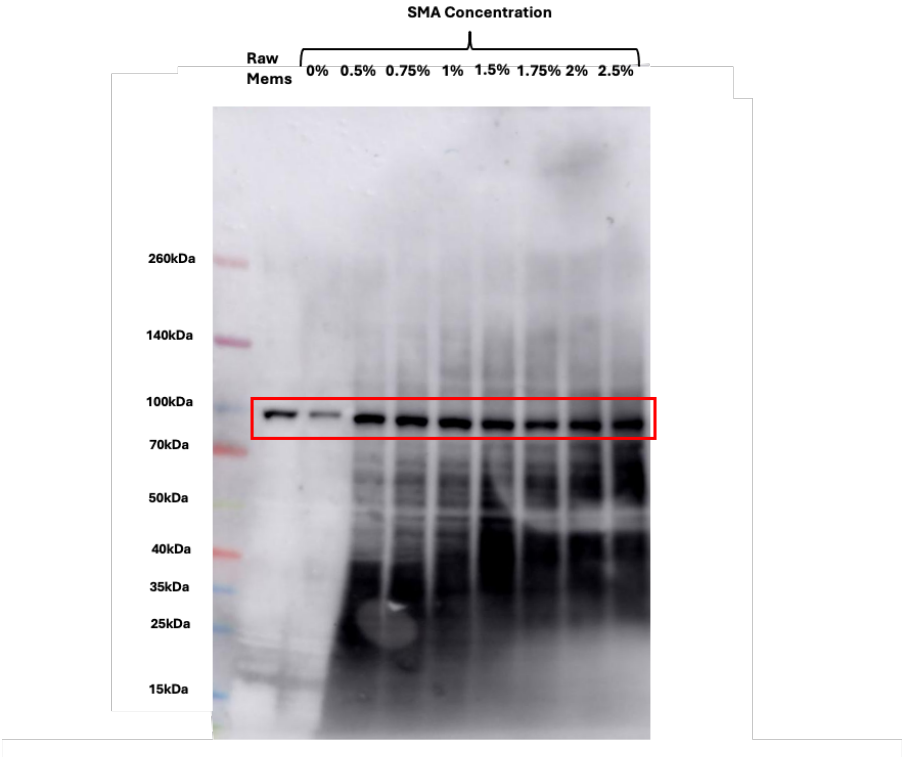


Figure 4.9: Solubilisation trial comparison SMA concentrations (0-2.5% (w/v)).
Western blot showing the soluble fraction of rNTR1 expressing membranes obtained by centrifugation (Raw Mems). SDS-PAGE was performed on a 4-20% gradient acrylamide gel. Western blot probed with anti-His antibody. Red boxes indicate the area where rNTR1 would run as a monomer.

Figure 4.9 shows a comparison of soluble fractions after rNTR1 expressing *E. coli* membranes were solubilised with eight different concentrations of SMA (0-2.5% (w/v)). The intensity of the band at approximately 99 kDa represents the concentration of rNTR1 monomer in the soluble fraction, highlighted by the red box. There was negligible difference in band intensity when SMA concentrations were between 0.5% (w/v) and 2.5% (w/v). The concentration of rNTR1 was saturated in the soluble fraction after SMA solubilisation compared to the membrane sample. When no solubilisation agent was used, the faint

monomer band showed most of the rNTR1 was insoluble and removed by centrifugation. The smearing on the Western blot was likely due to excess SMA being separated by SDS-PAGE, causing non-specific binding of the antibodies in the Western blot. The amount of smearing correlated with the SMA concentration in each sample.

The solubilisation trial suggests that 0.5% (w/v) SMA is an appropriate concentration for solubilisation of the rNTR1 expressing *E. coli* membranes and additional SMA is excessive. This was lower than the reported concentrations in the literature, where 2.5% (w/v) of the same SMA sample extracted 74±2% of their target membrane protein (Swainsbury *et al*., 2017). Due to low expression of GPCRs, smaller concentrations of SMA for solubilisation may be more appropriate. Using a smaller concentration of SMA may have helpful applications; excess SMA in solution after solubilisation may affect purification steps downstream.

4.5.3 Determining Inclusion of Arginine in SMA Solubilisation Buffer

The inclusion of arginine aids some purification methods and can improve protein stability (Abe *et al*., 2009). Arginine has both hydrophobic and hydrophilic functional groups. Arakura *et al* (2007) showed that arginine interacts with all amino acid side chains and peptide bonds causing a reduction in both electrostatic and hydrophobic interactions. This suppresses protein aggregation and protein-protein interaction (Arakawa *et al*., 2007). Limited research reports how arginine may interact with SMA. To test whether the addition of arginine would affect the solubilisation efficiency of SMA, a solubilisation trial comparing the inclusion of 20 mM arginine in the solubilisation buffer was performed.

Figure 4.10 compares the soluble fraction and insoluble fraction, when rNTR1 expressing *E. coli* membranes were solubilised with SMA, with and without 20 mM arginine in the solubilisation buffer. The intensity of the 99 kDa bands represent the concentration of rNTR1 monomer in the sample. No bands were visible in the insoluble fractions.

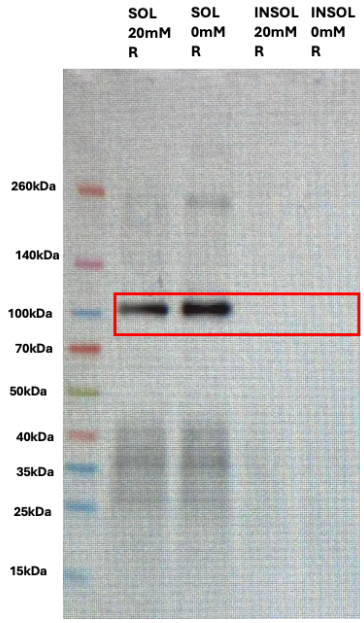


Figure 4.10: Solubilisation trial testing the inclusion of 20 mM arginine in the solubilisation buffer.
Western blot showing soluble and insoluble fractions of rNTR1 expressing membranes separated by centrifugation. SDS-PAGE was performed on a 4-20% gradient acrylamide gel. WB probed with anti-His antibody. Red boxes indicate area where rNTR1 would run as a monomer.

There was an increase in intensity of the monomer band and the addition of a possible dimer band in the soluble fraction with no arginine. This suggests that arginine decreased SMA solubilisation efficiency and if arginine was a beneficial addition to the buffer system for purification steps downstream, then it was most efficient to add after the solubilisation step.

4.6 MBP Fusion Protein Purification of MBP-fused rNTR1 Expressed in E. coli

It was hoped that the MBP-fusion protein would provide an efficient tool for purification, possibly yielding rNTR1 at a higher yield and purity than utilising the His tag. The MBP Trap affinity purification method utilises the natural affinity of MBP for α-(1–4) maltodextrin (Duong-Ly and Gabelli, 2015). It was hypothesised that the MBP fused to rNTR1 would be

minimally affected by the lipid nanodisc due to its soluble hydrophilic nature. However, nearly 100% of solubilised protein failed to bind the MBPTrap column and no protein was eluted after the application of 10 mM Maltose solution (Appendix 1.2). Attempts to improve the binding of the SMA-rNTR1 to the MBPTrap included overnight binding to the MBPTrap (Appendix 1.3) and performing the MBPTrap purification as a second step after an IMAC purification (Appendix 1.4). Unfortunately, neither method was successful at binding any material to the MBPTrap.

It was decided that the use of MBPTrap was an inappropriate purification method for SMA-rNTR1, as there was binding to Ni-NTA resin but not the MBPTrap. It was predicted IMAC would be a more successful purification method.

4.7 Optimisation of rNTR1 Purification by IMAC

The optimization of the IMAC purification of rNTR1 was performed, investigating variables such as: the type of IMAC resin used, the concentration of the solubilised material, the buffer system used, salt concentration and other additives to the buffer such as protease inhibitor tablets, arginine and reducing agents.

4.7.1 Influence of Affinity Chromatography Resin Type

Several types of commercially available resins have different biophysical properties and different chelating heavy metal ions. The optimal resin for IMAC purification can be protein-specific (Bornhorst and Falke, 2000). Different immobilized metal matrices bind divalent cations with different strengths: carboxymethyl aspartate (CMA) and NTA bind the divalent cations with four coordination points, whereas IDA weakly binds divalent cations with three coordination points (Bornhorst and Falke, 2000). The matrices are manufactured onto a cross-

linked agarose bead support which can have different pore sizes and bead sizes depending on the provider (Table 4.2).

Table 4.2: Summary of Four Different Resin Types used for IMAC purification and their Key Characteristics

Resin	**Heavy Metal Ion**	**Chelating Agent**	**Matrix**	**Binding Capacity (mg protein /mL absorbent)**	**Bead Size μm**
HisPurTM Ni-NTA Resin (Thermo-ScientificTM)	Ni^{2+}	NTA	6% beaded agarose	Static: 18 Dynamic: 60	45 -165
Ni-Sepharose High Performance (Sigma-Alrich)	Ni^{2+}	NTA	Highly cross-linked 6% agarose	Dynamic: 40	Average 34
TALON Resin (Takara)	Co^{2+}	CMA	6% Cross-linked agarose	5-15	45- 165
IDA Protino	Ni^{2+}	IDA	Information not available	10	Information not available

The polymer and lipids surrounding the protein may reduce the affinity of it's His tag by steric hindrance or interference with charge. The increased size of the PoLiPa may prevent movement into the beads in the resin which could prevent access to binding sites. Ni-NTA has been the standard resin used for IMAC purification of proteins solubilised with SMA (Lee *et al*., 2016) since the development of SMALPs, but screening other chromatography resins might offer advantages for different proteins. To test this, 4 different resins were compared to assess which was most appropriate for the purification of the SMA-rNTR1. A stepwise increase in imidazole concentration was used to elute the bound protein. This helped determine whether different resins could separate rNTR1 and contaminant proteins based on different levels of affinity, distinguishable by different imidazole concentrations. Data was analysed to determine the optimal resin in terms of rNTR1's highest yield and purity.

IMAC purification performed with the Ni-NTA resin had the most contaminated 100 mM imidazole elution fraction (Figure 4.11A left). There are visible bands at 110 kDa, 45 kDa, and 35 kDa, identified as common contaminants when using this resin in Chapter 3. The 500 mM imidazole elution showed a single band, however a majority of the rNTR1 eluted in the 100 mM and 250 mM imidazole elution fractions.

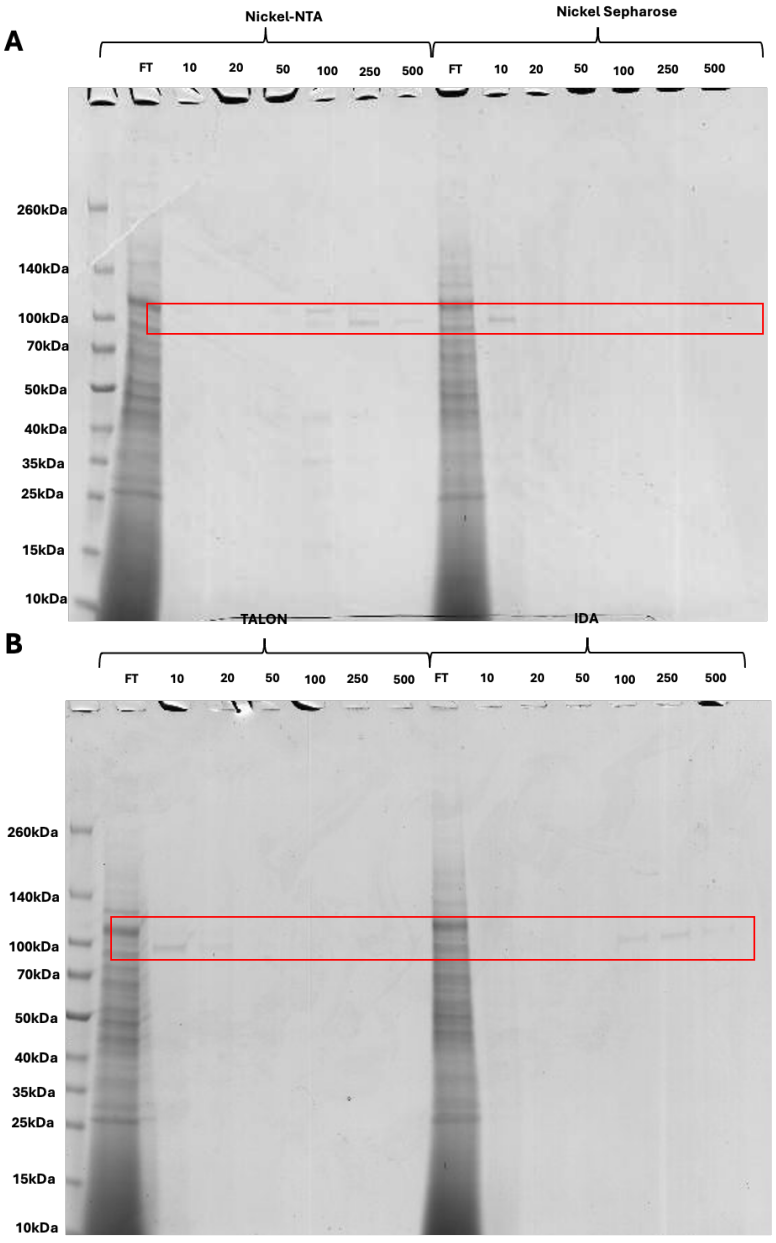


Figure 4.11: Four rNTR1 purifications using different IMAC resins.
rNTR1 expressing membranes were solubilised with 2% SMA diluted 2-fold after solubilisation before incubation with resin overnight. Protein was eluted using stepwise increases in imidazole concentration (10,20, 50, 100, 250,500). Samples are each elution fraction and the flow through (FT) was analysed by SDS-PAGE performed on a 4-20% gradient acrylamide gel. Red boxes show where the rNTR1 monomer would be expected to appear.
(A) Purifications using Ni-NTA or Ni-Sepharose Resin.
(B) Purifications using TALON or IDA.

SDS-PAGE analysis showed no protein was eluted from the Ni-Sepharose resin in the 50-500 mM imidazole elution fractions. (Figure 4.11A right). There is a band, likely to be rNTR1 in the 10 mM imidazole wash. This indicated that rNTR1 was weakly bound to the resin. Despite an improved purity compared to Ni-NTA resin, there are contaminants present including bands at approximately 110 kDa and 140 kDa.

TALON resin which utilised a different heavy metal ion (Cobalt), also bound to rNTR1 with a lower affinity than Ni-NTA; the band representing the rNTR1 monomer was mostly detected in the 10 mM elution compared to higher imidazole concentrations (Figure 4.11B left). This is consistent with the lower affinity of Cobalt ions for histidine residues compared to Nickel ions (Bornhorst and Falke, 2000). However, the 110 kDa band, likely the contaminant protein AcrB as identified in Chapter 3, was present in the 10 mM and 20 mM imidazole fractions.

The use of Ni-IDA resin generated the purest product when comparing the four resins. A single band was visible at the expected MW of rNTR1 in the 100 mM, 250 mM and 500 mM elution fractions (Figure 4.11B right). Near 100% purity of rNTR1 was achieved from a single purification step. Contamination appeared to be removed by a 10 mM imidazole wash. The band at 99 kDa was confirmed to represent rNTR1 by mass spectrometry analysis: 17 peptides unique to the rNTR1 sequence were identified.

4.7.2 Confirmation of SMA-rNTR1 Purification Success by Western blot Analysis

Given previous issues with contaminant proteins appearing at the expected size, the identity of rNTR1 was confirmed by Western blot analysis using an anti-MBP antibody. Identification of a 99 kDa protein with anti-MBP from a Western blot would be sufficient evidence that the full-length protein was able to be purified. The previous identification used an anti-His

antibody, which binds to the C-terminus of rNTR1, whereas the MBP is fused via the N-terminus. Samples of the soluble and insoluble fractions were taken before the IMAC resin screen.

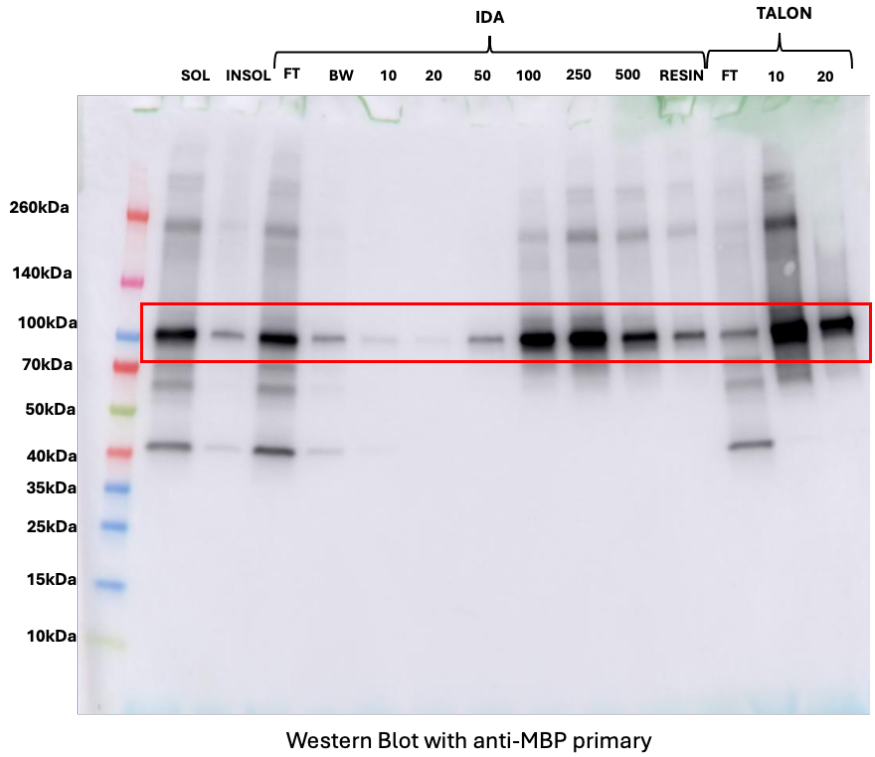


Figure 4.12: Western blot analysis of SMA-rNTR1 IMAC purification fractions
Soluble and insoluble fractions of rNTR1 expressing membranes solubilised with 2% SMA separated by centrifugation were analysed as well as fractions of IMAC purifications using IDA and TALON resin. SDS-PAGE was performed on a 4-20% gradient acrylamide gel. Western blot was probed with an anti-MBP antibody. The red box indicates the area where rNTR1 would run as a monomer.

Figure 4.12 shows the Western blot analysis of these samples and the fractions of the IMAC purifications using IDA or TALON resin. The bands represent protein in the sample fused with MBP or MBP itself. The analysis of the soluble fraction showed four bands including a primary band at the expected MW of rNTR1: 99 kDa. The band at approximately 198 kDa was suspected to be a dimer of the rNTR1. There were possibly higher-order oligomers represented as well. These bands were present in the previous solubilisation trials in which the Western blots were performed with an anti-His antibody. The MW of MBP is 42.5 kDa, a band at approximately this size was visible in the soluble fraction in the flow through (FT) of both IMAC purifications using IDA and TALON resin. This band is likely MBP which has

been fragmented from the rNTR1 fusion protein. There was a fourth band between 50-70 kDa present in soluble fraction which may be a C-terminally truncated version of the rNTR1.

The 42.5 kDa band representing MBP was not present in the 20-500 mM imidazole elution fractions, indicating there is no binding to IMAC resin. This confirms that non-His tagged proteins were successfully separated from rNTR1 and remained in the flow-through fraction.

The Western blot of the IMAC purification using the IDA resin was supportive of the Coomassie-stained SDS-PAGE gel: the highest intensity band representing monomeric rNTR1 was in the 250 mM imidazole elution fraction. The bands in the 250 mM elution and 500 mM elution fraction were larger than the band in the soluble fraction indicating that the IMAC purification concentrated and purified rNTR1.

Three fractions from the IMAC purification using TALON resin were also analysed by Western blot analysis for comparison to IDA (Figure 4.12). TALON appeared to have a higher binding capacity for the SMA-rNTR1 than IDA resin: less rNTR1 remained in the flow-through. The rNTR1 band of highest intensity was visible when analysing the 10 mM imidazole elution from TALON resin. This showed that despite the higher binding capacity, the affinity of the TALON resin is significantly weaker for SMA-rNTR1. This meant that TALON resin was not able to separate rNTR1 from contaminants.

This Western blot was able to elucidate a more in-depth comparison of the two most promising IMAC resins: IDA and TALON. It was decided the IDA resin would be chosen as the ideal resin for further optimisation.

4.7.3 IMAC Condition Screen

To improve efficiency of IMAC purification and obtain a higher concentration of rNTR1, a screen of different conditions was performed by binding the same volume of SMA-solubilised material to 20 μL of IDA resin with or without the addition of other components to the binding buffer. It was hypothesised that dilution of the soluble fraction would dilute excess SMA, which might interfere with the binding capacity of the resin. Inclusion of an EDTA-free protease inhibitor tablet in the binding buffer was also investigated. It was hypothesised that including protease inhibitors may reduce the fragmentation of rNTR1 by proteases. Reduced fragmentation would result in higher concentration of purified full-length protein. The third condition included arginine in the binding buffer; four concentrations were tested (0 mM, 20 mM, 100 mM, 200 mM). Arginine has been a beneficial additive to SEC (Ejima *et al*., 2005a), anion exchange (Arakawa *et al*., 2011) and immunoaffinity purifications (Tsumoto *et al*., 2004) . Abe *et al* (2009) showed arginine can interfere with Ni-columns but is compatible at concentrations below 200 mM. For each of the conditions, the protein bound to the resin was analysed by Western blot analysis (Figure 4.13).

The intensity of the band visible in the red boxes inferred the concentration of rNTR1 protein. The FT indicates what did not bind to the IDA resin after overnight incubation. The intensity of the bands indicated the undiluted soluble fraction sample (lane 1) and the soluble material with highest arginine concentration (lane 7) have the lowest binding to the IDA resin. The resin analysis gave a more distinguishable comparison of the 7 conditions. Lane 4 shows the protein bound to IDA resin with no protease inhibitor tablet and arginine (20 mM) had the highest band intensity and hence protein yield.

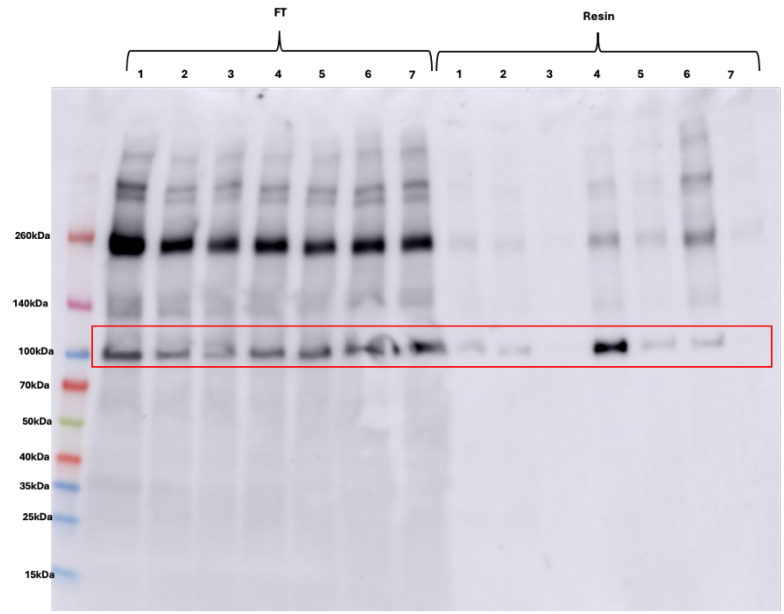


Figure 4.13: Western blot analysis showing results of IMAC Condition Screen
Seven conditions were tested for the effect on SMA-rNTR1 binding to IDA Resin. The number of each lane represents the condition listed below. SDS-PAGE was performed on a 4-20% gradient acrylamide gel. The red boxes indicate the area where rNTR1 would run as a monomer. Western blot was probed with an anti-His antibody.
1: Undiluted soluble fraction.
2. Diluted soluble fraction (2-fold).
3. Diluted soluble fraction plus protease inhibitor tablet (EDTA free).
4. Diluted soluble fraction + 20 mM arginine.
5. Diluted soluble fraction + 20 mM arginine plus protease inhibitor tablet.
6. Diluted soluble fraction + 100 mM arginine.
7. Diluted soluble fraction + 200 mM arginine.

Screening these conditions shows that diluting solubilised material and including 20 mM arginine improved the efficiency of the IMAC purification. Higher concentrations of arginine appeared to reduce the binding capacity of IMAC resin. The reduction in binding capacity with the inclusion of protease inhibitor tablets supported the requirement for membrane isolation. Membrane isolation allowed resuspension of the membranes in the most optimal buffer for solubilisation and purification and the removal of soluble proteins before solubilisation. This reduced the non-specific binding of soluble contaminants and fragmentation by soluble proteases, reducing the need for a protease inhibitor tablet in the binding buffer. These findings on the optimisation of SMA-rNTR1 have potential use for all membrane protein purification investigations.

4.7.4 Salt Concentration

Salt concentration can be an important variable in how proteins interact when encapsulated in a PoLiPa. SMA is negatively charged so it was hypothesised that a higher salt concentration would reduce the charge repulsion due to the attraction of positive sodium ions. Typical ionic strength is approximately 150 mM in the cell. However, the protocol for purifying an exemplar SMA-solubilised protein uses 500 mM NaCl (Lee *et al*., 2016). A comparison of 150 mM and 500 mM NaCl concentrations was performed to determine how purification of SMA-rNTR1 would be affected.

The SDS-PAGE gel shows two IMAC purifications performed on the same volume and concentration of rNTR1 expressing *E. coli* membranes (Figure 4.14). The intensity of the band representing rNTR1 at approximately 99 kDa is larger in the elution fractions when a higher NaCl concentration was used. Bands likely representative of dimeric rNTR1 were also visible in the elution fractions only when the higher salt concentration was used.

SMA was not easily solubilised in 1 M NaCl. Therefore, it was decided that 500 mM would be an appropriate concentration for IMAC purifications. After IMAC purification, dialysis into a buffer with 150 mM NaCl concentration was performed. This was more representative of physiological conditions and allowed the removal of imidazole used for elution.

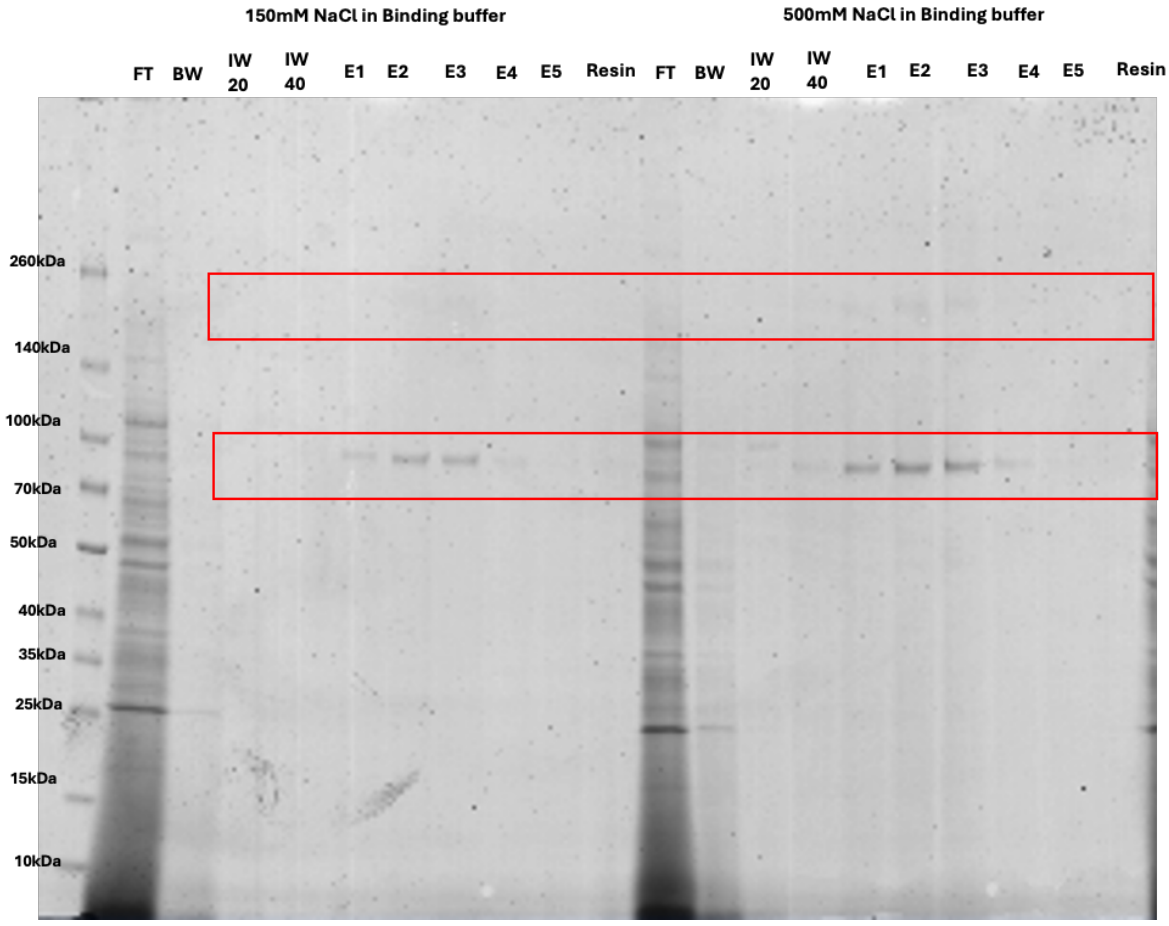


Figure 4.13: Coomassie stained SDS-PAGE gel comparing two purifications with 150 mM or 500 mM NaCl in the binding buffer.
SDS-PAGE was performed on a 4-20% gradient acrylamide gel. Red boxes indicate area where rNTR1 would run as a monomer and a dimer.

Postis *et al* discovered that high ionic strength reduced the proportion of inter-disc dimers of purified SMA-solubilised AcrB. Electron microscopy (EM) showed that SMA-AcrB associates into pairs in different orientations that are not associated with protein-protein interactions (Postis *et al*., 2015). These 'doublets' may reduce His tag affinity for IMAC resin by steric hindrance. It is theorised that the use of high salt reduces these SMALP pair formations and may increase the exposure of His tags to Nickel ions. This could improve the affinity of His tagged protein to the IMAC resin. It was decided that 500 mM NaCl was the ideal salt concentration during IMAC purification.

4.7.5 Reducing Agent

The previous Western blots of rNTR1 samples show bands likely to represent dimers and higher-order oligomers of rNTR1 that could not be separated by denaturing with LDS sample buffer. Reducing agents are often required in protein purifications to prevent intramolecular disulphide linkages which are common when proteins have exposed cysteines (Remans *et al*., 2022). rNTR1 has multiple cysteines in the transmembrane region (White *et al*., 2012). Dimerization of rNTR1 within a SMALP has been previously reported (Dathe *et al*., 2019). It was hypothesised that the inclusion of a reducing agent such as TCEP or DTT would prevent dimerization and possibly better expose the His tag on the C-terminus which may improve efficiency of the IMAC purification.

In this experiment, rNTR1-expressing cells were lysed with 5 mM TCEP in the lysis buffer. Membranes were harvested and solubilised with and without 5 mM TCEP or 5 mM DTT. The soluble material was incubated with IDA resin. A sample of the soluble material, unbound material (flow-through) and bound material was analysed by SDS-PAGE and Western blot analysis.

Figure 4.15A shows a single monomer band present in all lanes, suggesting that the inclusion of TCEP in the cell lysis step prevented oligomerisation of the rNTR1. The samples including a reducing agent in the solubilisation buffer have a higher concentration of rNTR1 compared to those without the reducing agent, shown by the intensity of the primary band in the soluble fraction lanes. However, after overnight binding to IDA resin, there was visible precipitation in the sample containing 5 mM TCEP. This precipitation will have likely meant a reduction in the rNTR1 concentration which may explain the reduced intensity of the rNTR1 band in the ‘bound to beads’ sample compared to when 5 mM DTT or no reducing agent was used.

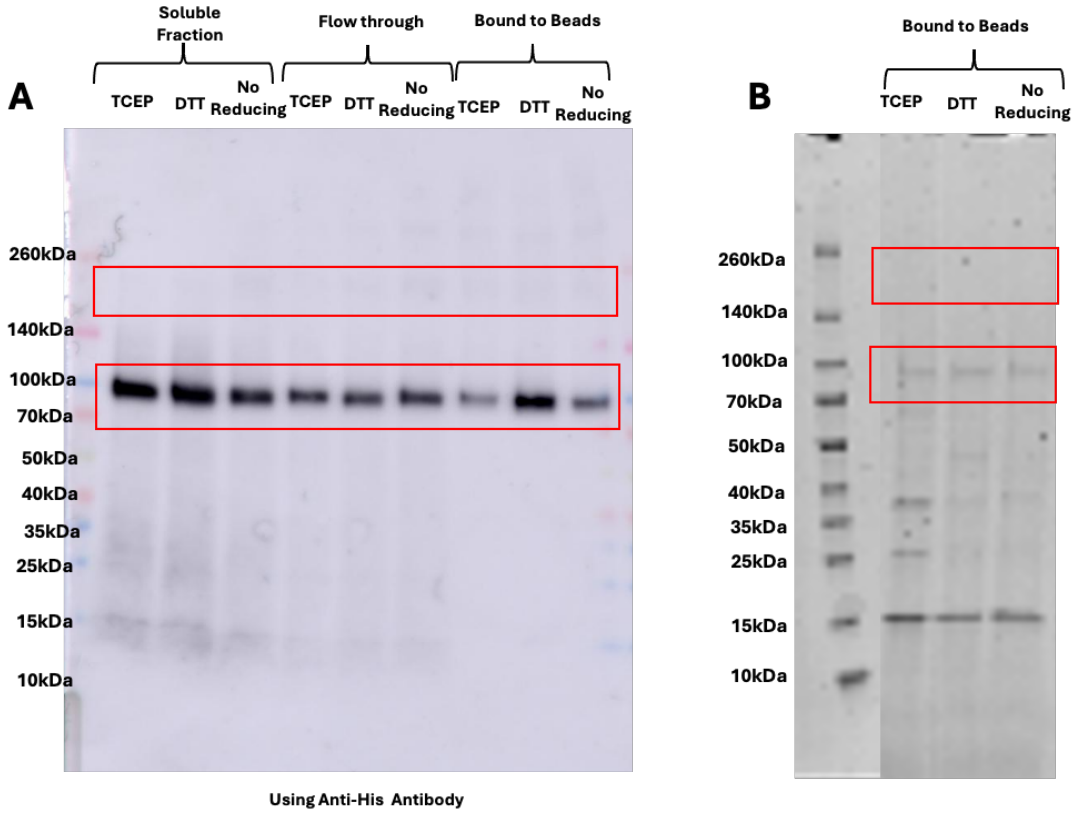


Figure 4.14: IMAC Condition Screen comparing the effect of reducing agents.
SMA-solubilised rNTR1 expressing E. coli membranes were incubated with 25 µL of IDA resin overnight in three conditions: 5 mM TCEP, 5 mM DTT and no reducing agent in the solubilisation and binding buffer
SDS-PAGE was performed on a 4-20% gradient acrylamide gel. Red boxes indicate the area where rNTR1 would run as a monomer and dimer.
(A) Western blot analysis of the soluble fraction, flow through after overnight binding to IDA resin and material bound to beads. Western blot was probed with an anti-His antibody.
(B) Coomassie-stained SDS-PAGE analysis of protein material bound to beads.

The most intense rNTR1 band in the flow-through sample was in the sample without any reducing agent. This was reflective that less rNTR1 bound to the IDA resin than in the sample with DTT and less protein was lost due to aggregation and precipitation compared to the sample with TCEP. Figure 4.15B indicated the purity of the material that bound to the IDA resin. The inclusion of TCEP resulted in two more likely contaminant bands at approximately 37 kDa and 25 kDa that appear denser than the rNTR1 band. All three samples also contained a 15 kDa protein that could be a fragment of rNTR1 without the C-terminal his tag or a contaminant.

Given that the inclusion of DTT in the binding buffer appeared to improve the binding of rNTR1 to the IDA resin. Two purifications with and without 5 mM DTT in the binding buffer were performed. The IMAC purification fractions from two comparable purifications using the IDA resin shows that the inclusion of DTT in the binding buffer improved the binding of rNTR1 (Figure 4.16). This was inferred from the higher intensity bands at the expected weight of rNTR1 (99 kDa) in the elution fractions analysed by Coomassie-stained SDS-PAGE and Western blot analysis.

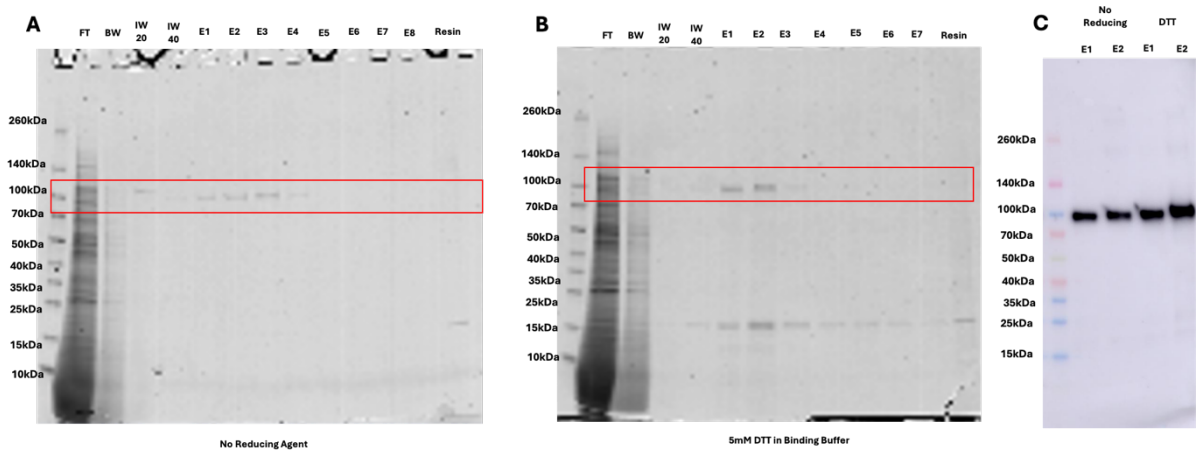


Figure 4.15: The effect of DTT on the IMAC purification of SMA-rNTR1.
(A and B) Coomassie-stained SDS-PAGE analysis of the fractions from two IMAC purifications with or without 5 mM DTT in the binding buffer. The flow through (FT), buffer wash (BW), 20 mM and 40 mM imidazole washes (IW20 and IW40), elution fractions (E1-E7/8) and material bound to the resin after elution (Resin) were separated on a 4-20% gradient acrylamide gel. Red boxes indicate the area where rNTR1 would run as a monomer.
(C) Western blot analysis of first two 500 mM imidazole elution fractions from the two purifications (labelled E1 and E2) separated on a 4-20% gradient acrylamide gel and probed with an anti-His antibody.

Despite the better yield, inclusion of DTT also reduced the purity of the elution. A band of approximately 15 kDa was visible in every elution fraction at a similar or greater intensity than the rNTR1 band. The 15 kDa band was not visible on the Western blot, which was probed with an anti-His antibody. This band could represent a fragment of rNTR1 that has lost the C-terminal His tag or another contaminant in the SMA-solubilised material. However, it appears to have a higher affinity for IDA resin with the inclusion of 5 mM DTT in the binding buffer. The increase in binding was unexpected because DTT has chelating properties which can cause leaching of cations from IMAC resins (Remans *et al*., 2022). The unpredictable

effect of a reducing agent on an IMAC resin, the protein of interest and the contamination makes it an important variable to test, particularly with low-expressing, unstable proteins.

It was decided that despite the increased concentration of rNTR1 yielded by the inclusion of DTT in the binding buffer, the efficiency of gaining purity from a single-step purification was considered more important. This was considered the final step in optimising the purification of SMA-rNTR1.

4.8 Biophysical Characterisation and Stability Analysis of rNTR1 Encapsulated in SMALP

4.8.1 Biophysical Characterisation by SEC

As discussed in Chapter 3, SEC was an ineffective method of purifying different-sized proteins solubilised with polymers. However, it can be a useful analytical tool for understanding the heterogeneity of a purified protein sample. Given that SMA-solubilised proteins were eluting closely after the void volume of a Superdex 200 increase column, it was hypothesised that a Superose 6 increase 10/300 column would be more effective at assessing the heterogeneity of the SMA-rNTR1 sample due to its improved separation of higher molecular weight species.

Figure 4.17 shows the absorbance trace for the SEC analysis as well as SDS-PAGE analysis of every other elution fraction from 11-25 mL. The volume at which the rNTR1 elutes is highlighted in blue in the absorbance trace (Figure 4.17A). The band representing rNTR1 was

only present between 15 mL and 17 mL retention volume. No other protein bands were visible on the SDS-PAGE gel (Figure 4.17B).

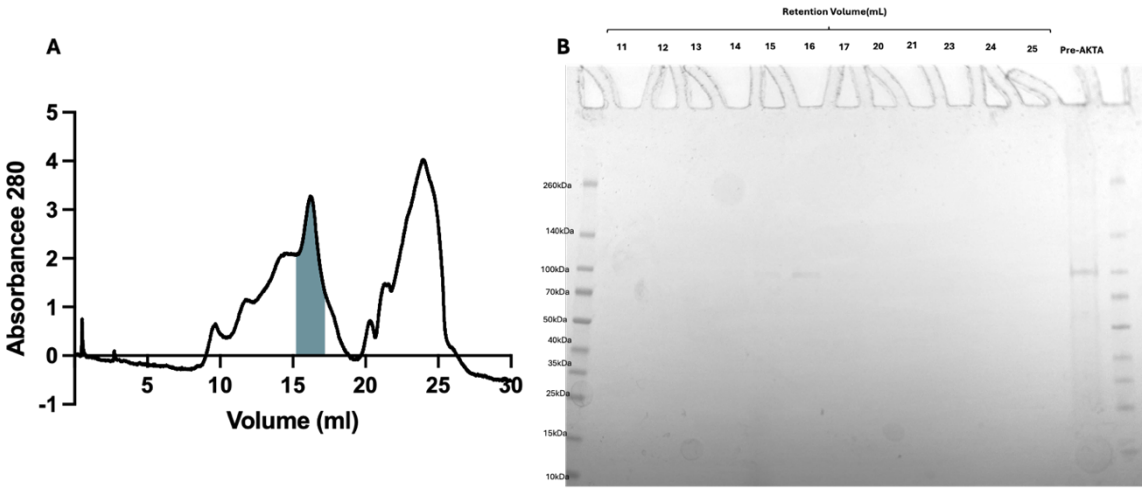


Figure 4.16 : SEC analysis of the SMA-rNTR1 using a Superose 6 increase 10/300 column.
(A) Absorbance Trace at 280 nm. The volume at which rNTR1 appears to elute (between 15-17 mL retention volume) is highlighted in blue on the absorbance trace.
(B) 30 mL Elution was collected in 0.5mL fractions. SDS -PAGE gel analysis of samples of every other elution fraction from the 11-25 mL retention volume as well as the pure rNTR1 before SEC (Pre-AKTA).

Peaks after 20 mL are most likely due to small protein fragments, SMA polymer or imidazole. Multiple peaks between 8-15 mL show that there may have been aggregation and oligomerisation of the SMALP particles. However, these peaks did not represent a large enough concentration of protein to be analysed by Coomassie-stained SDS-PAGE analysis. This suggests that the majority of the post-IMAC sample existed in a monomeric form.

The documentation for the Superose 6 Increase column used in this study showed the standard protein Ferritin (440 kDa) should elute at 16 mL (Cytiva, 2020). The SEC analysis confirms the hydrodynamic radius of SMA-rNTR1 was comparable to a globular protein with a MW 4-fold larger. This is consistent with the Superdex 200 increase SEC analysis in Chapter 3.

SEC was a useful tool for the removal of aggregates and small fragments, buffer exchange and the selection of monomeric protein within a sample. However, it was decided that since

near 100% purity was achieved by a single-step IMAC purification, the loss of protein during SEC was not worth the benefits. Instead, the imidazole and high salt from the IMAC purification were removed by dialysis and aggregates were removed by centrifugation.

4.8.2 SMA-PAGE Analysis Post-SEC

The SEC elution fractions that appeared to have rNTR1 present as identified by SDS-PAGE were analysed by SMA-PAGE. It was hypothesised that the SMA-PAGE would identify a particle that corresponded to approximately 99 kDa when comparing the band to a native marker protein.

SMA-PAGE analysis of purified SMA-rNTR1 post-IMAC purification (Figure 4.18A) shows a band visible between the 66 and 146 kDa native markers, likely representative of monomeric rNTR1. There was smearing above this band, possibly due to oligomers. The Western blot analysis of the elution fractions sampled post-SEC (Figure 4.18B) showed a band between 66 kDa and 146 kDa, with highest intensity in the 16 mL elution fraction. There was also a possible dimer band between 146 kDa and 242 kDa in the 15 mL and 15.5 mL elution fractions.

SMA-PAGE data was consistent with the absorbance trace from the SEC analysis showing that most of the rNTR1 was present as a monomer but there are also larger particles present in the sample. The band between 66-142 kDa was confirmed to represent rNTR1 by mass spectrometry analysis: 24 peptides unique to the rNTR1 sequence were identified.

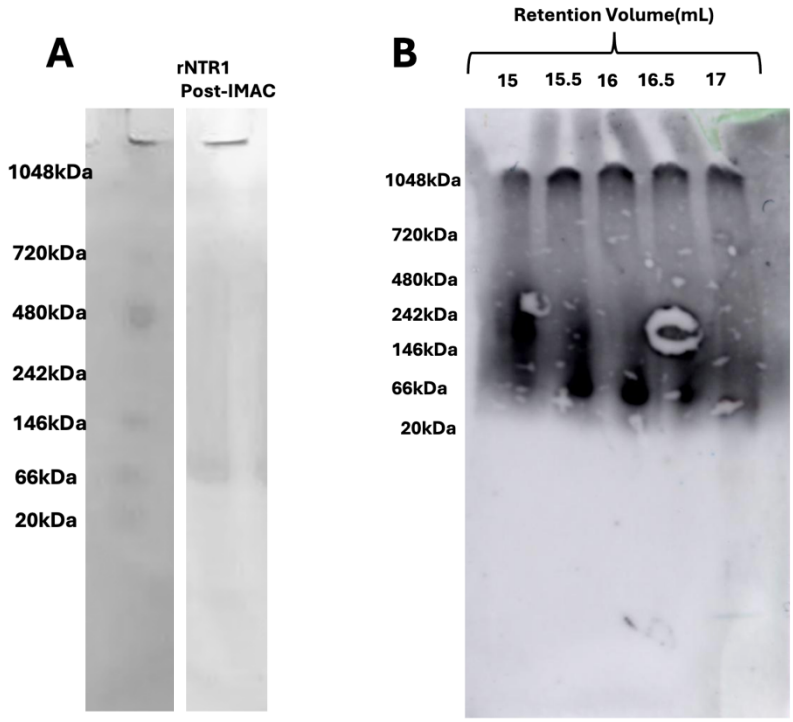


Figure 4.17: SMA-PAGE analysis of SMA-rNTR1.
(A) Coomassie-stained SMA-PAGE gel analysis of SMA-rNTR1 post-IMAC purification.
(B) Western blot analysis of SMA-PAGE gel showing elution fractions post-SEC analysis of purified SMA-rNTR1 probed using anti-His antibody.

4.8.3 Biophysical Characterisation by DLS and Comparison of Buffer Systems

DLS was a useful tool for understanding the hydrodynamic radius of the SMA-rNTR1 particles and identifying aggregation in a sample. DLS cannot provide accurate information about the proportion of each particle size in a sample due to the skew of the amount of scattered light depending on particle size. The purified rNTR1 sample was analysed by DLS before and after filtration through a 0.2 μm pore-sized filter to remove aggregated protein. The filtered sample was dialysed into three different buffer systems before re-analysis by DLS. It was hypothesised that one buffer system may be better at preventing aggregation in the sample than the other two.

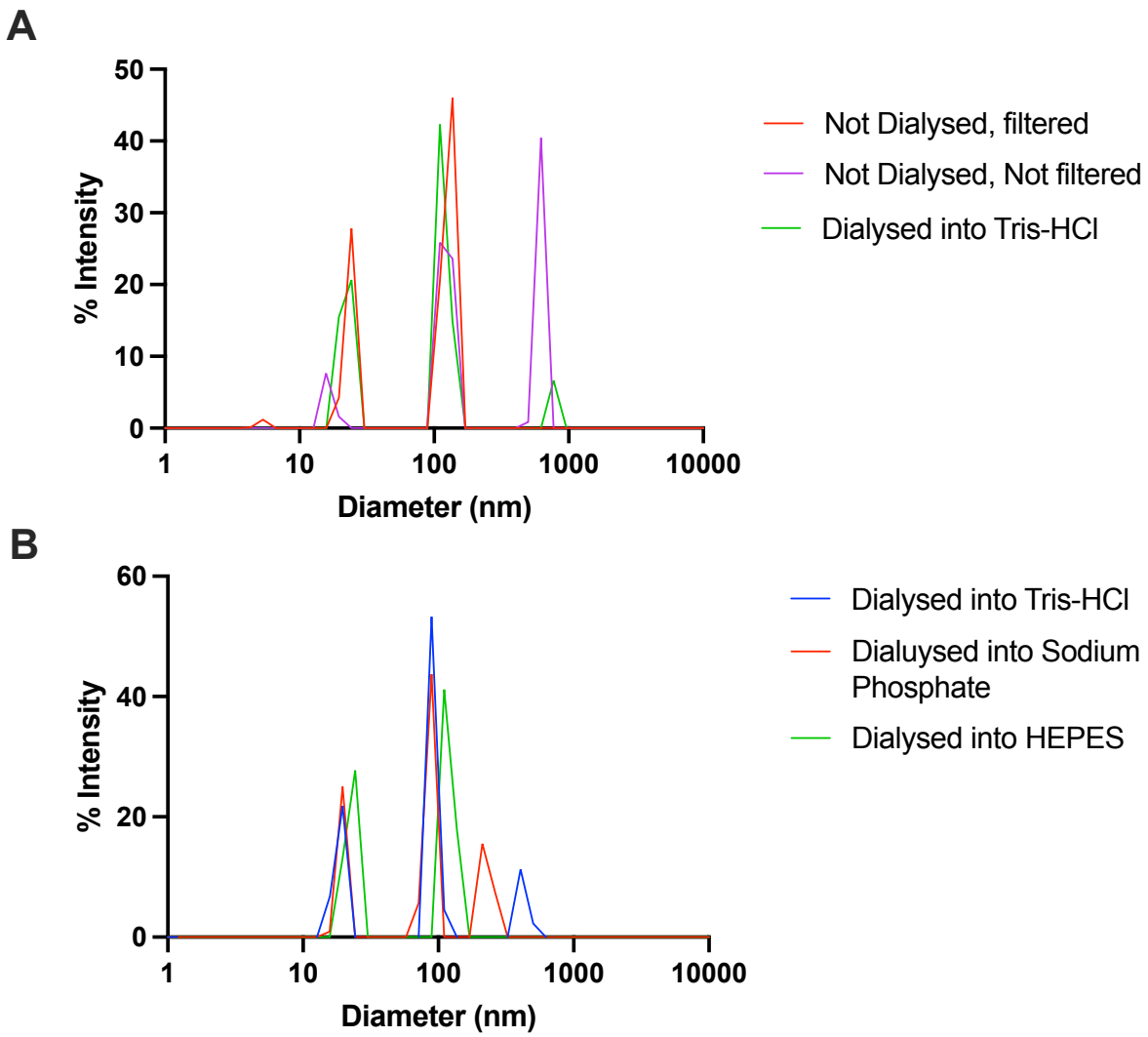


Figure 4.18: DLS analysis of purified SMA-rNTR1.
Graphs show the percentage of the scattered light that was due to a particle of a predicted diameter (% Intensity).
(A) Comparison of pure rNTR1 samples with and without filtration through a 0.2 µm pore filter as well as after overnight dialysis into the same 50mM Tris-HCl, 150 mM NaCl buffer.
(B) Comparison of pure rNTR1 samples after dialysis into three different buffer systems: 50 mM Tris, 10 mM Sodium Phosphate or 25 mM HEPES. All buffers contained 150 mM NaCl and were pH 7.8.

The percentage intensity data shown in Figure 4.19 shows how much light was scattered by particles of a specific size. The SMA-rNTR1 sample that was not filtered contained three particle sizes at approximately 20 nm, 100 nm and 1000 nm in diameter (Figure 4.19A). The diameter size close to 10 nm is as expected of an SMALP (Stroud *et al*., 2018). DLS data has estimated the diameter of SMALPs encapsulating proteins ranging from 5 – 20 nm (Ayub *et al*., 2020; Morrison *et al*., 2016; Swainsbury *et al*., 2017). The 100 nm particle size is likely due to oligomers of rNTR1 or SMALP 'doublet' formation (Postis *et al*., 2015). The 1000 nm

particle size is likely caused by aggregated protein, where the unfolding or degradation of protein causes exposed hydrophobic residues to stick together in a disordered state. Aggregated protein was successfully removed from the sample by filtering; there was no light scattering that suggested any particle larger than 150 nm in the filtered sample. The filtered sample was dialysed into the same buffer (50 mM Tris-HCl, 150 mM NaCl, pH 7.8) overnight to determine how dialysis would affect aggregation in the sample. After dialysis, a small peak likely representing aggregated protein at 1000 nm was present. This is indicative that some protein aggregation occurred during the dialysis process. The amount of aggregation was likely small as this particle size only represents 6.64% of the scattered light from the sample and larger particles scatter more light in their nature.

Figure 4.19B shows the DLS data collected from SMA-rNTR1 samples dialysed into three different buffer systems. This experiment aimed to determine if there was a preferential buffer system that prevented aggregation. Brudar and Hribar-Lee (2021) showed that buffer molecules absorb the protein surface and modulate electrostatic stability. They found that buffer did not affect the diameter of a hydrated lysozyme protein but did affect the temperature at which the protein solution started to go cloudy (Brudar and Hribar-Lee, 2021). It was not known how a buffer system may affect the stability of a protein encapsulated in an SMALP. Buffer adsorption onto the negatively charged polymer surrounding the SMALP could cause an increase or decrease in the stability of the particle.

The DLS data suggested that dialysis into the HEPES buffer appeared to have the least aggregation. There was no light scattering that suggested any particle bigger than 150 nm in the sample. The peak most likely representing the monomeric SMA-rNTR1 around 20 nm and the peak most likely representing an oligomeric rNTR1 or a clump of SMALPs both appear to increase in diameter slightly when the sample was dialysed into HEPES compared to Tris-

HCl or phosphate buffer. This could be due to the absorption of HEPES molecules onto the SMALP particle. Another factor is that HEPES has a higher solvent viscosity compared to Tris-HCl and phosphate buffer, decreasing the diffusion rate (Philo, 2023).

DLS data was able to provide valuable information on the biophysical properties of the rNTR1 including the approximate diameter under the assumption of a spherical object, which was approximately 20 nm. The DLS analysis of rNTR1 dialysed into different buffers was able to provide insight into how to best manage stability issues when working with GPCRs.

4.8.4 Determination of Optimal Storage

DLS data showed that some aggregation is likely to occur during overnight storage at 4°C whilst dialysis was occurring. This prompted an experiment to optimise how to best store SMA-rNTR1. Arginine can be preventative of aggregation (Shiraki *et al*., 2002). Clusters of arginine can form a hydrophobic surface: the interaction of arginine clusters can mask hydrophobic surfaces inhibiting protein-protein aggregation (Das *et al*., 2007). Six aliquots of SMA-rNTR1 were used to compare three different storage temperatures with and without the addition of 20 mM arginine in the buffer. After overnight storage and removal of aggregated protein by centrifugation, SDS-PAGE and Western blot analysis compared the concentration of protein in each aliquot (Figure 4.20).

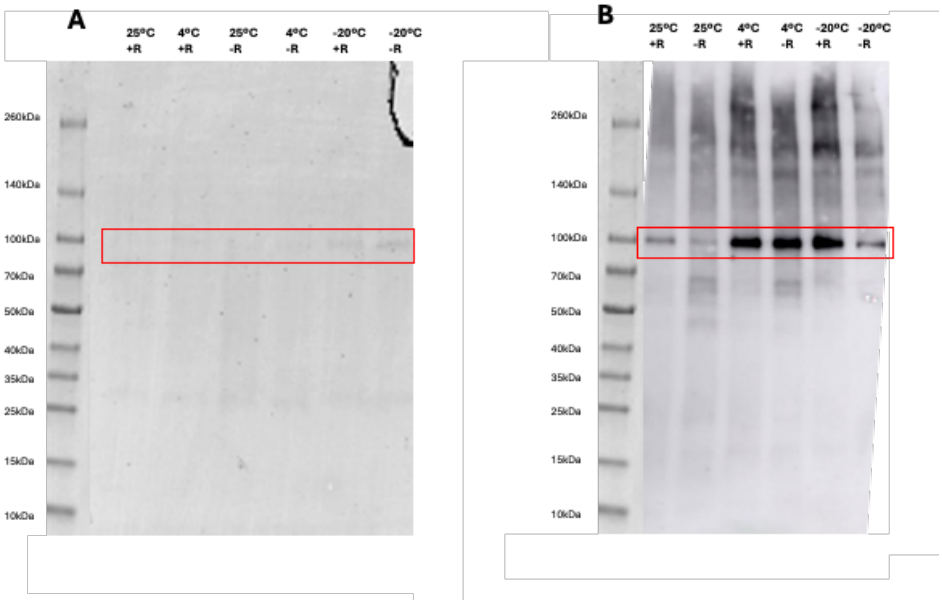


Figure 4.19: SMA-rNTR1 storage condition experiment
Aliquots of SMA-rNTR1 were stored overnight at three temperatures (25℃, 4℃ and -2℃) with (+R) and without (-R) arginine before SDS-PAGE analysis on a 4-20% gradient acrylamide gel. Red boxes indicate the area where rNTR1 would run as a monomer.
(A) Coomassie stained SDS-PAGE gel.
(B) Western blot probed with anti-His antibody.

The protein concentration was too low for a clear assessment of the best condition of Coomassie-stained SDS-PAGE (Figure 2.20A). However, there was no visible band of the expected rNTR1 size when samples were stored at 25°C. For a more sensitive detection of protein, the Western blot was used to compare rNTR1 concentration (Figure 4.20B. Intensity of the bands at approximately 99 kDa indicated the best temperature for storage of rNTR1 overnight was -20°C with the addition of 20 mM arginine. There were fragment bands close to the 70 kDa protein marker which occurred when no arginine was included in the storage buffer after storage at 25°C or -4°C. This suggests that arginine prevented fragmentation of the rNTR1. The inclusion of arginine had the largest stabilising effect after -20°C storage. This suggests arginine may have a protective effect against the degradation caused by freezing and thawing of SMA-solubilised protein.

Ice crystal formation can cause protein denaturing by several mechanisms including mechanical stress, dehydration and direct adsorption (Li *et al*., 2022). One explanation for the

protective effect of arginine is the adsorption of arginine on the polymer and protein preventing the disruption of the hydrogen bonding. The results from this experiment informed the decision that the best method for the storage of SMA-NTR1 was at -20°C with the inclusion of 20 mM arginine in the storage buffer.

4.8.5 Biophysical Characterisation by CD Spectrometry

CD spectroscopy can provide information about the secondary structure of a protein (Miles *et al*., 2021). Circularly polarized light is directed at the protein sample and chiral molecules absorb the left and right circularly polarized light to different extents depending on the structure of the protein. The difference between the left and right circularly polarized light absorption can be plotted against light wavelength to provide a CD spectrum. The near UV wavelengths (170-240 nm) can be used to interpret the secondary structure of proteins whilst the far UV wavelengths can be used to interpret information about the tertiary structure (Miles *et al*., 2021). CD spectra of membrane proteins may have wavelength shifts compared to soluble proteins causing difficulty in interpreting secondary structures when using reference databases based on soluble proteins (Wallace *et al*., 2003). Furthermore, proteins in a SMALP have been shown to have different CD spectra compared to the same protein in detergent (Ayub *et al*., 2020). The exact mechanism for this is still being investigated. It could be due to a real difference in protein structure or due to an effect of the lipids and polymer present in the sample. Therefore, the CD structure was loosely interpreted into the presence of α-helices and β-sheets.

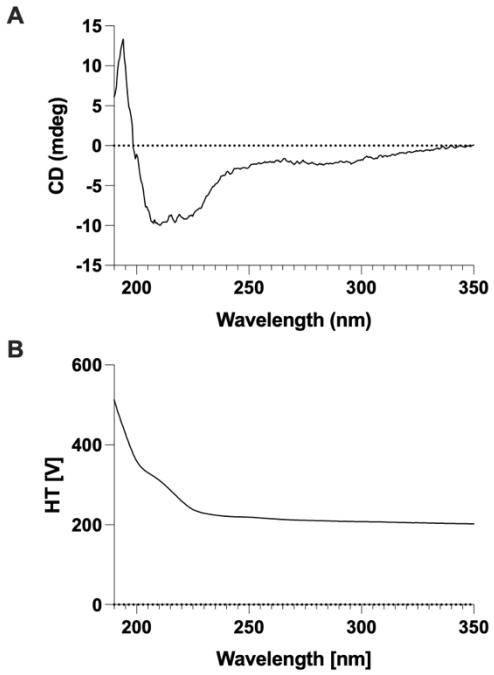


Figure 4.20: CD Spectrometry Analysis of SMA-rNTR1.
0.2 mg/mL SMA-rNTR1 concentration. Path Lenth 1 mm. 10 mM Na Phosphate Buffer, 50 mM NaF (A) CD Spectrum (B) HT[V] measurement.

The CD spectrum of SMA-rNTR1 (Figure 4.21A) revealed two negative peaks at 210 nm and 221 nm, as well as a positive peak at 194 nm. Strong negative peaks at 208 nm and 222 nm, as well as a positive band at 193 nm, are diagnostic of α-helices (Greenfield, 2006). Proteins with anti-parallel β-sheets have negative peaks at 218 nm and positive peaks at 195nm. Disordered proteins have negative peaks near 195 nm. The structure of MBP and rNTR1 contain mainly α-helices which was represented in the CD structure. Deconvolution suggested the following secondary structure: 45% helical, 16% β-sheet, 14% turns, 25% disordered. This output should be taken with caution due to the reference dataset (SMP180) consisting of mostly soluble proteins and no SMA-solubilised proteins (Abdul-Gader *et al*., 2011). However, this is strong evidence that the rNTR1 was folded correctly within a SMALP.

The HT[V] (Figure 4.21B) shows the voltage the detector in the CD spectrometer was using. If the sample is absorbing more light, less light reaches the detector which means a higher voltage is required. Buffer, water and air absorb at lower wavelengths which leads to larger

HT[V], as shown in Figure 4.21B. A HT higher than 600 V means too little light is being detected for an accurate measurement. The wavelength range 190-350 nm did not require a HT higher than 600 V; this showed that an appropriate buffer and protein concentration was used to obtain a CD spectrum.

4.8.6 Overnight Changes in Secondary Structure of rNTR1 by Interval CD Spectrometry

Although CD analysis of a protein in a SMALP cannot be used to give an exact percentage of α-helices and β-sheets, it can however be used to monitor changes in the secondary structure of a protein. Upon protein unfolding, α-helices and β-sheets unfold to a more disordered structure. To detect this, a sample of SMA-rNTR1 was left in the CD spectrometer at 25°C and a measurement was taken every hour for 17 hours. The storage experiment data and DLS data suggested that there should be some aggregation over these 17 hours.

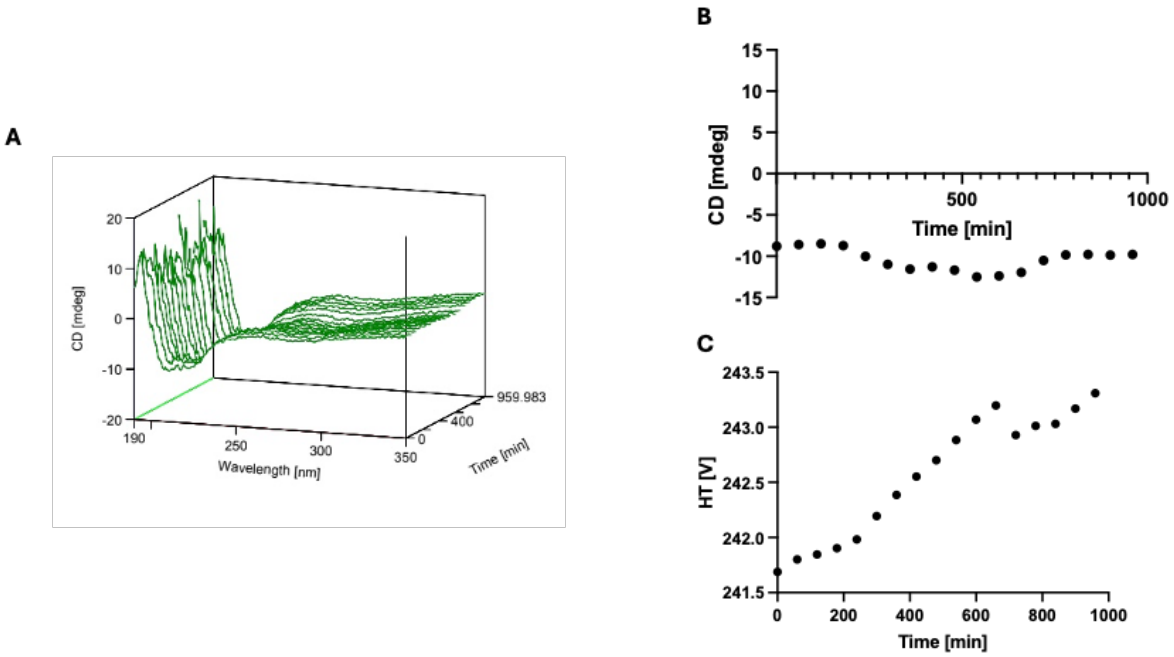


Figure 4.21: Interval CD Spectrometry Data of SMA-rNTR1 over a 960-minute timeframe
Pathlength 1mm, SMA-rNTR1 concentration was 0.2 mg/mL. in 10 mM Na Phosphate Buffer, 50 mM NaF (A) 17 CD Spectra which were collected every hour plotted against time. (B) CD measurement at the wavelength 222 nm. (C) HT[V] measurement at the wavelength 222 nm.

There was no obvious difference in the shape of CD spectra across the 17-hour timeframe (Figure 4.22A). There was no obvious trend in how the 222 nm peak measurement changed across the timeframe (Figure 4.22B). CD peak measurements can be used as a measure of protein concentration. The minimal change in the peak at 222 nm suggests the loss of folded protein across this timeframe is small. The HT[V] at 222 nm increased from 241.6V to 243.3 V across the timeframe. A small increase in absorbance in the sample causing a higher HT[V] could be an indicator of limited aggregated SMALP particles.

Overall, the consistency in the CD spectra across the interval CD measurements indicated that most of the SMA-rNTR1 in this sample remained correctly folded despite storage at 25°C for 16 hours. This is a promising finding, given the notorious instability of GPCRs. It is thought that any aggregation that occurred had minimal effect on the secondary structure of rNTR1.

4.8.7 Thermostability of rNTR1 Encapsulated in SMALP in Changes in Tryptophan Fluorescence by 350/330 Ratio

Nano differential scanning fluorimetry (nanoDSF) monitors protein unfolding and aggregation by measuring the ratio of fluorescence intensity at 350 nm and 330 nm. This indicates the environment of the tryptophan residues within rNTR1. As the temperature is increased, the protein is likely to unfold, exposing tryptophan residues to solvent. This typically causes a bathochromic shift of the emission peak, which increases the measurement of the 350/330 nm ratio. Three samples of SMA-rNTR1 were analysed by nanoDSF to understand its thermostability.

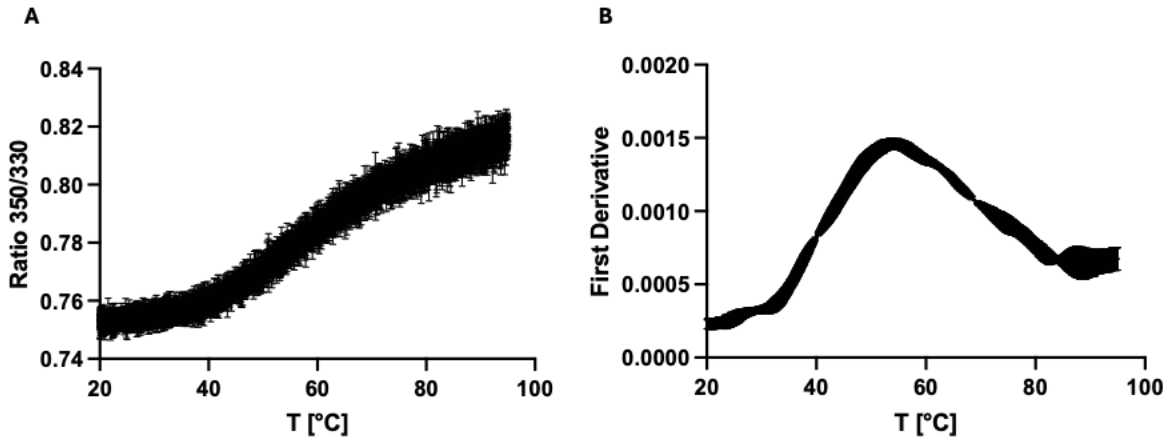


Figure 4.22: Thermostability assessment of SMA-rNTR1 by NanoDSF.
0.2 mg/mL SMA-rNTR1. (A) Mean ± SD of the ratio of 350 nm fluorescence intensity and the 330 nm fluorescence intensity. (B) The First derivative± SD of the 350/330 ratio.

Figure 4.23A shows the ratio of fluorescence intensity at 350 nm and 330 nm. There is a steeper gradient in the increase in the 350/330 ratio between 40-80°C, representative of the transition between folded and unfolded rNTR1. Plotting the first derivative of the 350/330 ratio can provide a clearer assessment of the onset of unfolding and the point of inflexion: the onset of unfolding was approximately 39°C and the point of inflexion, which provides a melting point (T_m) of SMA-rNTR1, was 57.18±0.23°C.

Klenk *et al* (2016) measured the thermostability of rNTR1 expressed in *E. coli* by radioligand binding after incubation. The T_m of DDM-NTR1 without any thermostabilising mutations was 45.2±0.1°C with the inclusion of the an agonist (neurotensin (8-13)) and 39.2±0.1°C without. (Klenk *et al*., 2016). The thermostability of SMA-rNTR1 showed a near 18°C increase in T_m compared to literature values of DDM-rNTR1 (Klenk *et al*., 2016). This is supported by other experiments that PoLiPas have a thermostabilising effect on encapsulated proteins including the GPCR $A_{2A}R$ (Jamshad *et al*., 2015a).

4.9 Summary of rNTR1

This section showed the multitude of variables which were investigated to yield a successful single-step purification method to produce pure rNTR1 encapsulated in a PoLiPa. The biophysical characterisation by DLS and CD gave evidence that rNTR1 was correctly folded in a stable state when encapsulated in an SMALP. Previous purifications of rNTR1 have required the manufacture of a neurotensin column to do ligand-specific affinity chromatography (Tucker and Grisshammer, 1996; Kumar and Plückthun, 2019). However, ligand-specific methods are not transferable to other GPCRs. Chapter 5 continues the investigation into how PoLiPa technology can improve GPCR research using a different model GPCR with different affinity tags.

CHAPTER 5: PRODUCTION AND CHARACTERISATION OF MBP-FUSED CB2 IN *E. COLI* USING POLIPA

5.1 Introduction

The rNTR1 investigations in Chapter 4 showed the production of soluble, pure, stable GPCR using PoLiPa technology. It was decided that investigating a different GPCR would be useful for the comparison of purification techniques. CB2 had the highest *E. coli* expression of the four GPCRs. This made CB2 a good choice for an in-depth investigation into the production of a second GPCR in PoLiPa.

Previous research into *E. coli* expressed CB2 has yielded moderate success. Xie *et al* described the successful expression and purification of a fragment of CB2 ($CB2_{180-233}$) (Xie *et al*., 2004). Research by the Yeliseev group has since optimised MBP-fused CB2 expression and production of detergent-solubilised CB2 by tandem affinity chromatography (Yeliseev, 2013). However, the inclusion of an anionic cholesterol derivative and a high-affinity CB2 ligand was required to stabilise CB2 in the detergent micelle (Vukoti *et al*., 2012). This research aimed to provide a new solution for the instability of CB2 outside the membrane environment using PoLiPa technology.

5.2 Expression Trials to Optimise CB2 Expression

CB2 was first expressed in *E. coli* by Calandra (1998), following the described expression protocol of how rNTR1 was expressed by Tucker and Grisshammer (1996). Expression conditions of CB2 in *E. coli* have been further optimised in the literature since the first construct was published (Berger *et al*., 2010; Krepkiy *et al*., 2006; Yeliseev, 2013). The expression trials of rNTR1 showed a significant improvement in expression caused by

changes in cell line, broth type, IPTG concentration, expression temperature and expression time. It was decided that optimisation of CB2 expression would be valuable to improve protein yield and aid downstream purification steps. Three expression trials were performed to optimise four expression variables: cell line, growth medium, IPTG concentration and expression temperature.

5.2.1 Comparison of Cell Lines and Growth Media

CB2 expression was reportedly twice as high in the use of the BL21(DE3) cell line compared to the DH5-α cell line (Yeliseev *et al*., 2005). Given the improvement in expression using the C43(DE3) strain for rNTR1 expression, it was hypothesised that C43(DE3) and C41(DE3) strains would be beneficial for CB2 expression. It was also hypothesised that the use of auto-inducing (AI) growth media may improve expression. AI growth media utilises lactose as a signal for protein expression instead of the addition of IPTG (Fox and Blommel, 2009). This method can allow a more gradual and controlled induction process, with a lower metabolic burden than that associated with IPTG induction (Fox and Blommel, 2009). Eight cultures comparing four growth mediums, and two cell lines were grown and the best expression of CB2 was determined by Western blot analysis (Figure 5.1).

The expected mass of CB2 is 85 kDa as calculated from its primary sequence. Bands at the expected MW of monomeric and dimeric (170 kDa) CB2 (highlighted in red boxes) showed that C41(DE3) and C43(DE3) cells were successfully transformed and expressed CB2. When comparing C41(DE3) and C43(DE3) cell expression between cultures grown in the same broth type, C41(DE3) cells consistently appear to express more CB2. A band between 70 kDa and 50 kDa appeared when C43(DE3) cells were grown and expressed in 2xYT or TB broth. This may be due to the proteolytic breakdown of the recombinantly expressed CB2. Given

that C41(DE3) cell expression did not have evidence of proteolytic breakdown and produced monomer and dimer bands of higher intensity, it was chosen as the better cell line.

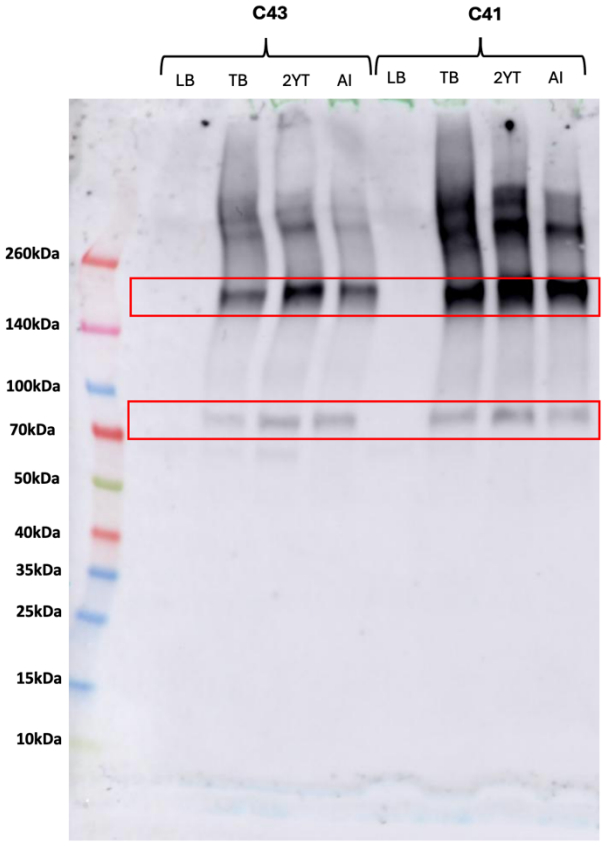


Figure 5.1: CB2 expression trial comparing four different growth media types and two different cell lines.
10 mL of Broth was inoculated with 100µL of overnight culture from transformed C43(DE3) or C41(DE3) cells. After overnight expression, cells were centrifuged and resuspended in cell lysis buffer, cells were centrifuged again. Samples of supernatant were analysed by Western blot, separated using a 4-20% polyacrylamide gel and probed using an anti-His antibody. Red boxes indicate expected MW of MBP-fused CB2 monomer and dimer.

The intensity of the monomer and dimer bands show that 2xYT Broth produced the highest expression of CB2, this was consistent between both C41(DE3) and C43(DE3) cells. This is consistent with the previously published protocol for CB2 production (Yeliseev *et al*., 2005). The use of LB Broth appeared to prevent the expression of CB2. This could be because the metabolic burden of CB2 expression required a nutrient-rich broth. Overall, the best expression of CB2 appeared to have occurred in C41(DE3) cells, in 2xYT broth.

5.2.2 Comparison of Three IPTG Concentrations

In line with previous work on rNTR1, three IPTG concentrations (0.5 mM, 0.25 mM, 0.1 mM) were compared when inducing expression. Previous expressions of CB2 in *E. coli* have used either 1 mM or 0.5 mM IPTG concentration (Berger *et al*., 2010; Krepkiy *et al*., 2006; Yeliseev, 2013). Reducing IPTG concentration can improve recombinant protein yield (Larentis *et al*., 2014). It was hypothesised that a reduction of IPTG concentration may improve CB2 expression.

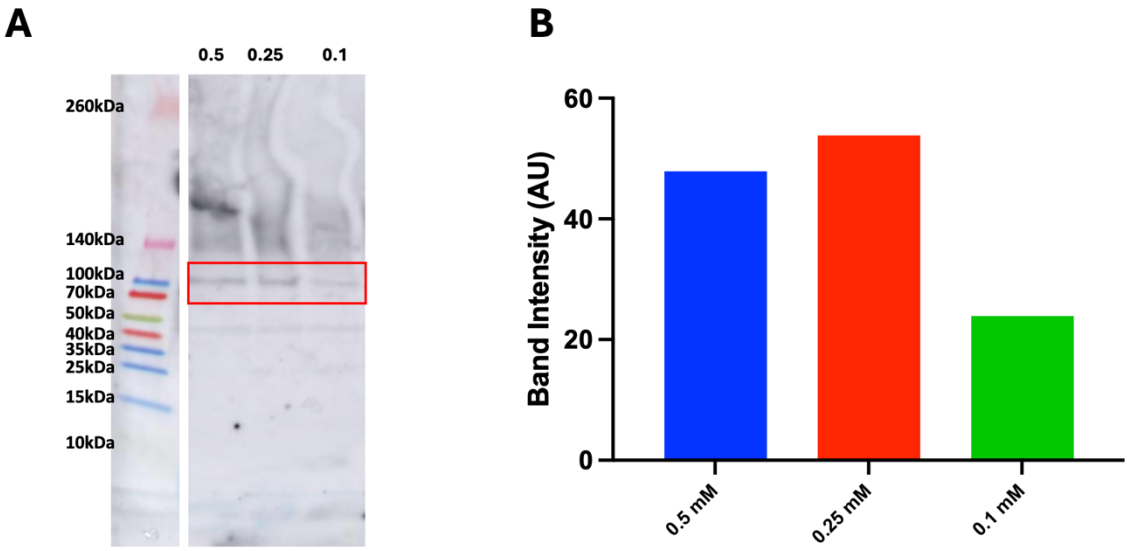


Figure 5.2: CB2 expression trial comparing three different IPTG concentrations for induction and two different cell lines.
100mL of Broth was inoculated with 1mL of overnight culture. Temperature was lowered to 18℃ and cells and induced with 0.5 mM, 0.25 mM or 0.1 mM IPTG. After overnight expression, 10 mL of cell culture were centrifuged and resuspended in cell lysis buffer, cells were centrifuged again, and sample of supernatant taken.
(A) Western blot analysis of supernatant sample separated using a 4-20% polyacrylamide gel and probed using an anti-His antibody. Red box indicates expected MW of monomeric CB2.
(B) Results of quantitative band in intensity analysis (arbitrary units (AU)) of monomeric band shown in red box using Imagelab.

Western blot analysis was used to indicate the best CB2 expression from three cultures induced with different IPTG concentrations (Figure 5.2). The intensity of the bands in the red box, representative of the concentration of monomeric CB2, showed the best CB2 expression was achieved using 0.25 mM IPTG (Figure 5.2). The band between 50-40 kDa in Figure 5.2A

could represent a fragment of CB2 that contains the His tag. This suggests proteolytic breakdown of CB2 in all three cultures. The expression trial confirmed the hypothesis that a lower IPTG concentration could improve CB2 expression; an IPTG concentration of 0.25 mM was used for subsequent expressions.

5.2.3 Comparison of Two Expression Temperatures

Expression temperature can affect the quality and quantity of recombinant protein expression. Berger *et al* compared three different expression temperatures of CB2 and found that expression at 27°C and 37°C increased expression but decreased activity of CB2 compared to expression at 20°C (Berger *et al*., 2010). This expression trial aimed to determine the most appropriate temperature for CB2 expression between 18°C and 25°C. Samples of each culture were taken 1 hour and 3 hours after induction to investigate how expression levels changed.

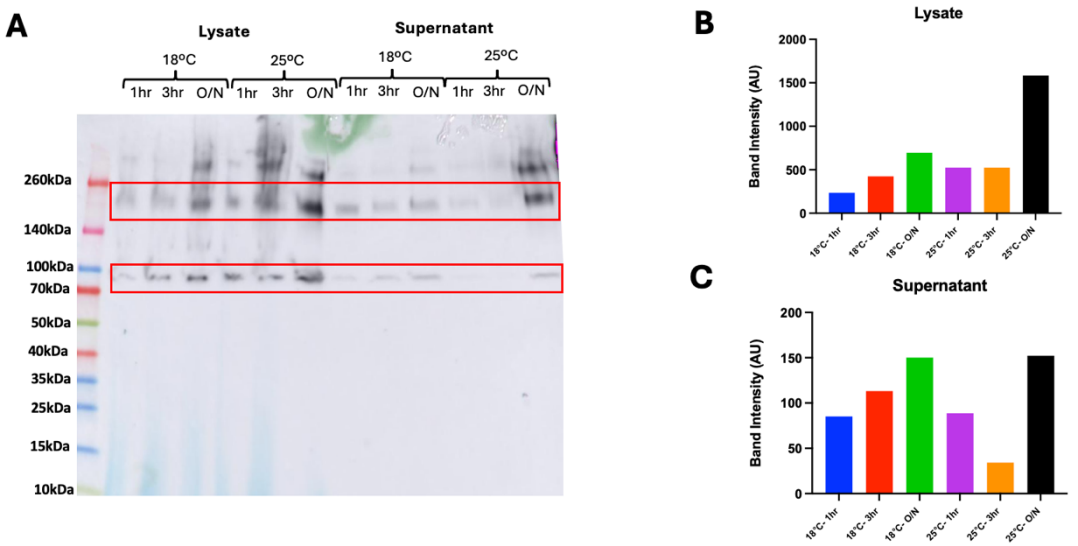


Figure 5.3: CB2 expression trial comparing two expression temperatures and three harvesting times.
100 mL of Broth was inoculated with 1mL of overnight culture. At OD 0.6-0.8, temperature was lowered to 18℃ or 25℃ and cells and induced with 0.25 mM IPTG. Cells were centrifuged and resuspended in cell lysis buffer, cells were centrifuged again, and a sample of supernatant was taken. Band Intesity analysis performed with ImageLab.
(A) Western blot analysis of supernatant sample separated using a 4-20% polyacrylamide SDS gel and probed using an anti-His antibody. The red boxes indicate the expected MW of CB2 in monomeric and dimeric forms.
(B) Results of quantitative band intensity analysis (AU) of suspected monomeric band shown in the lower red box.
(C) Results of quantitative band intensity analysis (AU) of suspected dimeric band shown in the upper red box.

The bands in the red boxes in Figure 5.3A represent the expected size of the CB2 monomer (85 kDa) and dimer (170 kDa). Intensities of the suspected monomer band were quantified and shown in Figure 5.3 (A and B). The higher band intensity in both the supernatant and lysate samples suggested that overnight expression was better than harvesting the cells one or three hours after induction.

The highest intensity of the monomer band in the lysate sample was after overnight expression at 25°C. Comparing the supernatant and lysate samples showed a large proportion of the expressed CB2 was removed by centrifugation. This is likely because aggregated or misfolded proteins in inclusion bodies were removed during centrifugation. Higher temperature and rate of expression may cause an increase in translational errors and misfolded protein (Francis and Page, 2010). The Western blot analysis suggested that the concentration of monomeric CB2 in the supernatant sample was similar whether the expression temperature was 25°C or 18°C. The band at the expected weight of dimeric CB2 was most intense in the samples expressed overnight at 25°C.

This expression trial was able to inform the decision to express CB2 at 18°C. The yield of monomeric CB2 was approximately the same as expression at 25°C whilst reducing the risk of translational errors that may reduce CB2 activity.

5.3 Assessment of Inclusion of Reducing Agent during Cell Lysis

Western blots analysed by the expression trials commonly showed a band in the expected size range of a CB2 dimer (approximately 170 kDa). CB2 has been shown to homodimerize and heterodimerise with other GPCRs including cannabinoid receptor 1 (Callén *et al*., 2012).

Dimerization events can modulate and change the signalling capabilities of the CB2 (Navarro *et al*., 2024).

Analysis of the crystal structure of CB2 shows cysteine residues in the transmembrane region that could form a disulphide bond with another cysteine residue from a second CB2 molecule within the membrane (Li *et al*., 2019). This could lead to a dimerization event that is resistant to degradation by the LDS sample buffer. This would explain the visible bands at the expected MW of a CB2 dimer when investigating CB2 expression by Western blot analysis. To investigate this theory further, a reducing agent (25 mM DTT or 5 mM TCEP) was included in the cell lysis step to prevent the formation of disulphide bonds at this stage. It was hypothesised that the inclusion of a reducing agent would decrease the concentration of dimerised CB2 and increase the concentration of monomeric CB2.

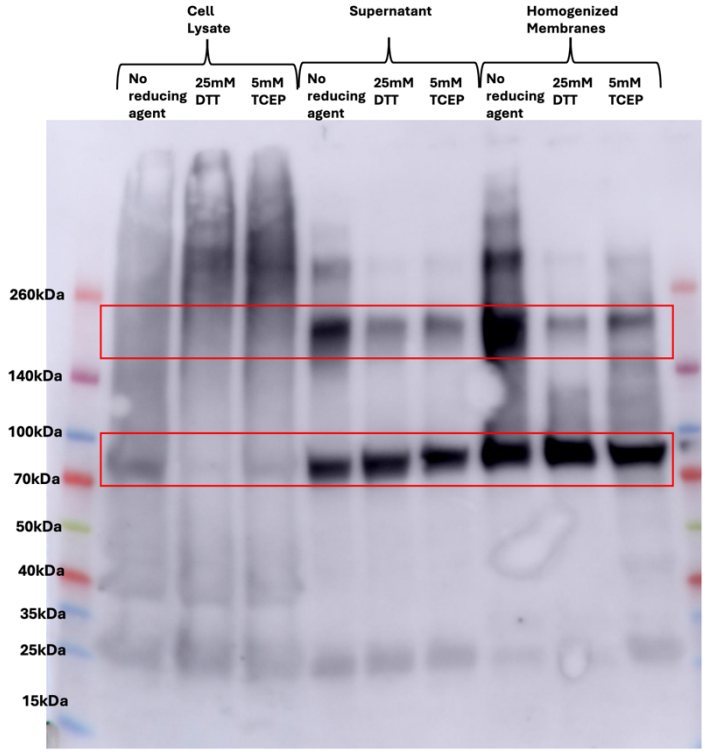


Figure 5.4: Comparing the effect of no reducing agent, 25 mM or 5 mM TCEP in the cell lysis buffer.
Western blot analysis of cell lysate, supernatant of cell lysate after centrifugation and homogenised membranes from E. coli expressing CB2. Red boxes show expected position of monomeric and dimeric CB2. SDS-PAGE was performed on a 4-20% gradient acrylamide gel and Western blot probed with anti-His antibody.

Samples of the cell lysate, supernatant after centrifugation and homogenized membranes following a membrane preparation were analysed by Western blot (Figure 5.4). The cell lysate material was difficult to compare due to smearing across the lane. Bands at the expected MW of monomeric (85 kDa) and dimeric (170 kDa) CB2 were visible after analysis of the supernatant and homogenised membrane samples. Higher-order bands, visible above the 260 kDa marker, likely represent higher oligomers of CB2. There was an increase in intensity of dimer and higher-order oligomer bands in the membrane sample compared to the supernatant sample when no reducing agent was included. It could be interpreted that oligomerisation events occurred during the process of the membrane preparation when no reducing agent was included in the buffer.

The intensity of the band expected to be a dimer of CB2 is considerably less in the supernatant and membrane samples when a reducing agent is used. The intensity of the monomer bands was relatively similar between the samples with and without a reducing agent. This implies that, despite the large reduction in dimer concentration, there was minimal increase in monomer concentration caused by the inclusion of DTT or TCEP in the lysis buffer.

This result gives evidence that expression of CB2 in *E. coli* produces monomers, dimers and higher-order oligomers of CB2 which are disulphide linked. The Western blot indicated the proportion of CB2 in each oligomeric state can be manipulated by the inclusion of reducing agents. This is important because GPCR oligomerisation is an important functional aspect; dimerization can affect GPCR binding, downstream signalling and processing within a cell (Terrillon and Bouvier, 2003). The results in this section also prove that the optimised expression protocol allowed the production of suitable starting material for PoLiPa investigation.

5.4 Solubilisation Trials on CB2 Expressed in E. coli

The expression trials determined the optimal expression conditions of CB2 in *E. coli,* and the Western blot in section 5.3 (Figure 5.4) showed a suitable level of CB2 was present in the membranes.

This allowed the progression to the next stage of production: extraction. Solubilisation trials were performed to determine which solubilisation agents yielded the best CB2 extraction. Three solubilisation trials were performed comparing different polymers to the detergent DDM, as well as testing polymer hydrophobicity and polymer concentrations.

5.4.1 Efficiency of Different Polymers

A comparison of different amphipathic polymers and DDM was performed to understand which solubilisation agents have the most efficient extraction and stabilisation of CB2. Polymers have not been used to solubilise CB2 previously, therefore it was considered important to test how well different polymers extracted CB2 from the *E. coli* compared to the detergent DDM. A detergent screen for the extraction of CB2 reported that a mixture of 3-[(3-cholamidopropyl)dimethylammonio]-1-propanesulfonate (CHAPS) and DDM yielded the most efficient extraction but additional stabilising agents including cannabinoid ligands and cholesteryl hemisuccinate (CHS) were required (Vukoti *et al*., 2012). It was hypothesised that SMA may extract CB2 more efficiently than DDM without CHS or ligands.

Figure 5.5 shows the soluble and insoluble material after the solubilisation of CB2-expressing *E. coli* membranes analysed by Western blot. The intensity of the bands at approximately 85 kDa and 170 kDa indicated the concentration of monomeric and dimeric CB2, as highlighted by the red boxes. When comparing the intensity of the monomeric CB2 in the soluble

fraction, the highest intensity bands were present when SMA, DDM and 0.25 BzAM were used as a solubilisation agent.

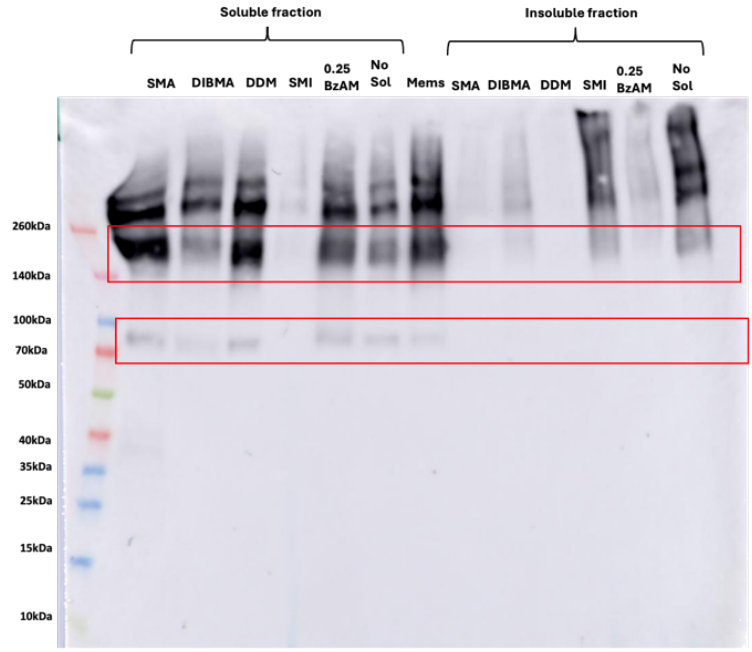


Figure 5.5: CB2 solubilisation trial comparing of four polymers and DDM.
Western blot showing soluble and insoluble fraction of CB2 expressing membranes solubilised with 2.5% (w/v) SMA, 2.5% (w/v) DIBMA, 1.5% (w/v) DDM, 2.5% (w/v) SMI, 2.5% (w/v) 0.25 BzAM or no solubilisation agent (No sol). Diluted raw membrane sample was also analysed (Mems). SDS-PAGE was performed on a 4-20% gradient acrylamide gel. Western blot was probed with anti-His antibody. Red boxes indicate area where CB2 would run as a monomer or dimer.

When comparing the bands representing dimeric CB2, the intensity suggested the BzAM polymer was not as efficient at solubilising the dimeric CB2 compared to SMA or DDM. Analysis of the SMA and DDM soluble fraction samples produced a similar band intensity to the membrane sample. This implied that nearly 100% of the CB2 was solubilised with SMA and DDM and was consistent with the observation that there were no visible bands in the insoluble fraction when SMA and DDM are used as a solubilisation agent. The intensity of the monomer and dimer bands suggested the following order of the solubilisation agents from best to worst: DDM = SMA > 0.25 BzAM > DIBMA > SMI. The intensity of the bands present after analysis of the insoluble fraction agreed with the analysis of the optimal solubilisation agent.

5.4.2 Effect of Polymer Hydrophobicity on CB2 Extraction from E. coli Membranes

To optimise CB2 extraction by polymers, this project investigated how polymer characteristics can be altered to change solubilisation efficiency. The BzAM series allowed tuneable hydrophobicity whilst retaining the same polymer length. To assess how the hydrophobicity of the polymer affected the efficiency of CB2 extraction from *E. coli* membranes, a second solubilisation trial was performed comparing the BzAM polymers, SMA 1:1 produced by RAFT, SMA 2:1 and DIBMA.

Figure 5.6 compares the soluble material obtained after the CB2 extraction from *E. coli* membranes. The intensity of the bands at approximately 85 kDa and 170 kDa indicate the concentration of monomeric and dimeric CB2 in the soluble fraction, as highlighted by the red boxes. When the BzAM polymer had less than 20% of its hydrophilic moieties converted to styrene-like moieties, there was a decrease in CB2 solubilisation efficiency. The intensity of the bands showed that all five polymers in the BzAM series from 0.2-0.4 solubilised CB2 as efficiently as SMA. The trend for how hydrophobicity of the polymer affects GPCR solubilisation was the same when comparing rNTR1 and CB2, however, the percentage of converted moieties required to reach optimal solubilisation is less when solubilising CB2. A lower concentration of CB2 was visible in the soluble fraction when using DIBMA, RAFT SMA (1:1) or 0.05 BzAM as a solubilisation agent. It was logical that RAFT SMA would have similar solubilisation efficiency to the 0.05 BzAM series since the RAFT SMA polymer was the backbone for the BzAM series and only 5% of the hydrophilic moieties were converted.

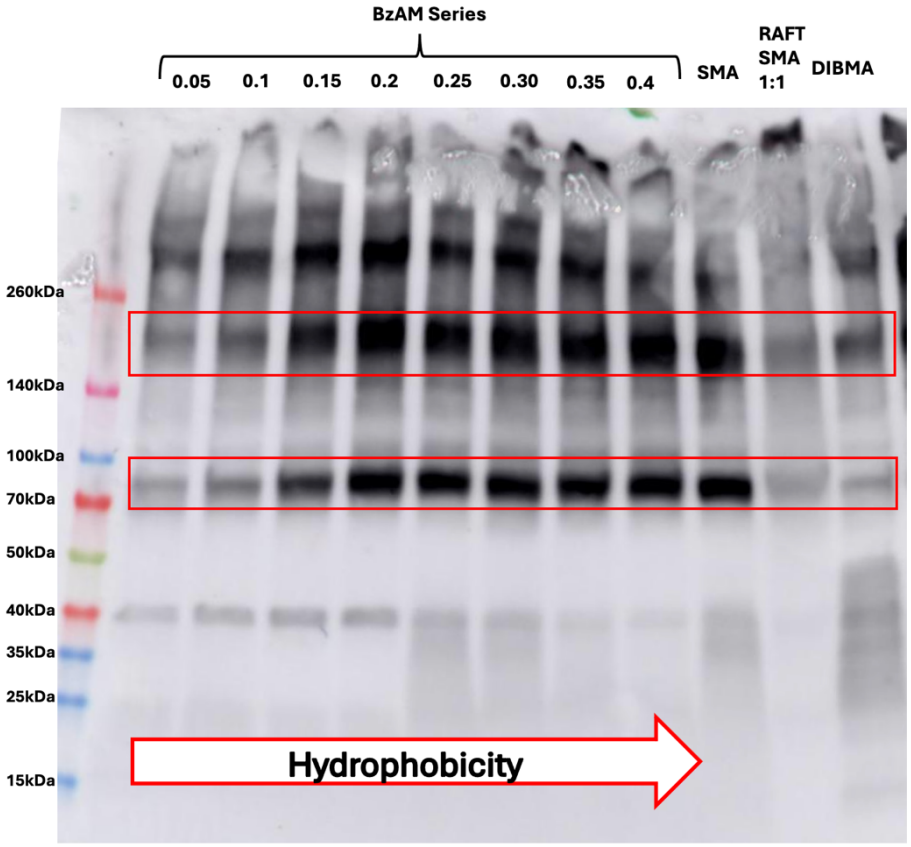


Figure 5.6: CB2 solubilisation trial comparing the BzAM polymer series to SMA, RAFT SMA 1:1 and DIBMA. *Western blot showing soluble fraction of CB2 expressing membranes solubilised with 2.5% (w/v) polymer. SDS-PAGE was performed on a 4-20% gradient acrylamide gel. WB probed with anti-His antibody. Arrow shows the increase in hydrophobicity of the BzAM series polymer. Red boxes indicate area where CB2 would run as a monomer or dimer.*

Overall, the BzAM solubilisation trial of CB2 was able to elucidate more information about how the hydrophobicity of a polymer is a factor in GPCR solubilisation. This data agrees with the previous BzAM solubilisation trial on rNTR1: as hydrophobicity increases to be more like SMA 2:1, solubilisation efficiency increases. However, there is an interesting discrepancy between CB2 and rNTR1 in the level of hydrophobicity required to reach optimal solubilisation. This protein-specific finding provides evidence that the encapsulated protein and the surrounding native lipids create a specific biophysical environment that can affect the solubilisation efficiency of less hydrophobic polymers. SMA was chosen as an optimal polymer for downstream purifications due to its high solubilisation efficiency, wide availability and low cost.

5.4.3 Optimal SMA Concentration for CB2 Homogenisation

In Chapter 4, 0.5% (w/v) SMA achieved a similar solubilisation efficiency as 2.5% (w/v) SMA when extracting rNTR1 from *E. coli* membranes. It was also found that dilution of solubilised material before binding to Ni-NTA resin improved the yield of the IMAC purification. It was suggested that the excess SMA in solution was inhibitory to the binding of the His tagged protein. For this reason, it was decided to perform a solubilisation trial to determine if a lower concentration of SMA improved CB2 solubilisation.

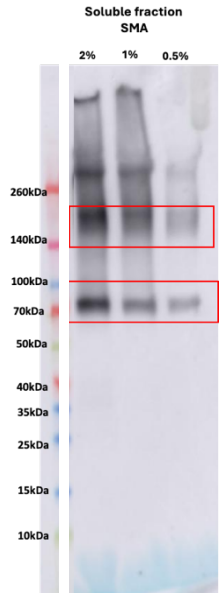


Figure 5.7: CB2 solubilisation trial comparing three SMA concentration.
Western blot showing soluble fraction of CB2 expressing membranes solubilised with 2%, 1% or 0.5% SMA. SDS-PAGE was performed on a 4-20% gradient acrylamide gel. WB probed with anti-His antibody. Red boxes indicate area where CB2 would run as a monomer or dimer.

Figure 5.7 shows a Western blot comparing the soluble material obtained after solubilisation of CB2 expressing *E. coli* membranes with 0.5-2% (w/v) SMA. The intensity of the bands at approximately 85 kDa and 170 kDa indicate the concentration of monomeric and dimeric CB2 in the soluble fraction. The Western blot showed the solubilisation efficiency was improved by the higher concentration of SMA. The higher expression of CB2 compared to rNTR1 or the increased dimerization of CB2 could be the reason for the larger SMA concentration required for optimal solubilisation. 2% (w/v) SMA was chosen as the ideal concentration for future solubilisations.

5.5 MBP Trap Purification of CB2

After the solubilisation of CB2 expressed in *E. coli* membranes, attempts to purify CB2 via its MBP-fusion protein were performed. Unfortunately, little SMA-solubilised material was able to bind to the MBP-Trap, despite attempts to bind SMA-CB2 to the MBPTrap after a Ni-NTA-based IMAC purification (Appendix 1.5). It was decided that this method was not appropriate for the purification of SMA-CB2.

5.6 FLAG Purifications Comparing CB2 Solubilised with Different Polymers or DDM

The CB2 construct contained a 6x His tag as well as a FLAG tag. The FLAG peptide sequence adjoined to the end of the C-terminus of the protein provided a tool for affinity chromatography using anti-FLAG resin. The anti-FLAG resin should have a more specific, higher affinity interaction with the FLAG-tag compared to IMAC resin with a His tag. Drawbacks of anti-FLAG include the lower protein capacity and higher cost (Lichty *et al*., 2005). Utilising anti-FLAG for the purification of proteins encapsulated in PoLiPas been previously successful (Rehan *et al*., 2017; Ekundayo *et al*., 2024). However, GPCR FLAG purification with different polymers has not been investigated. It was hypothesised that the PoLiPa or excess polymer in solution may interfere with the binding of CB2 to the resin. To test this, CB2 solubilised with DDM was used for a comparative purification.

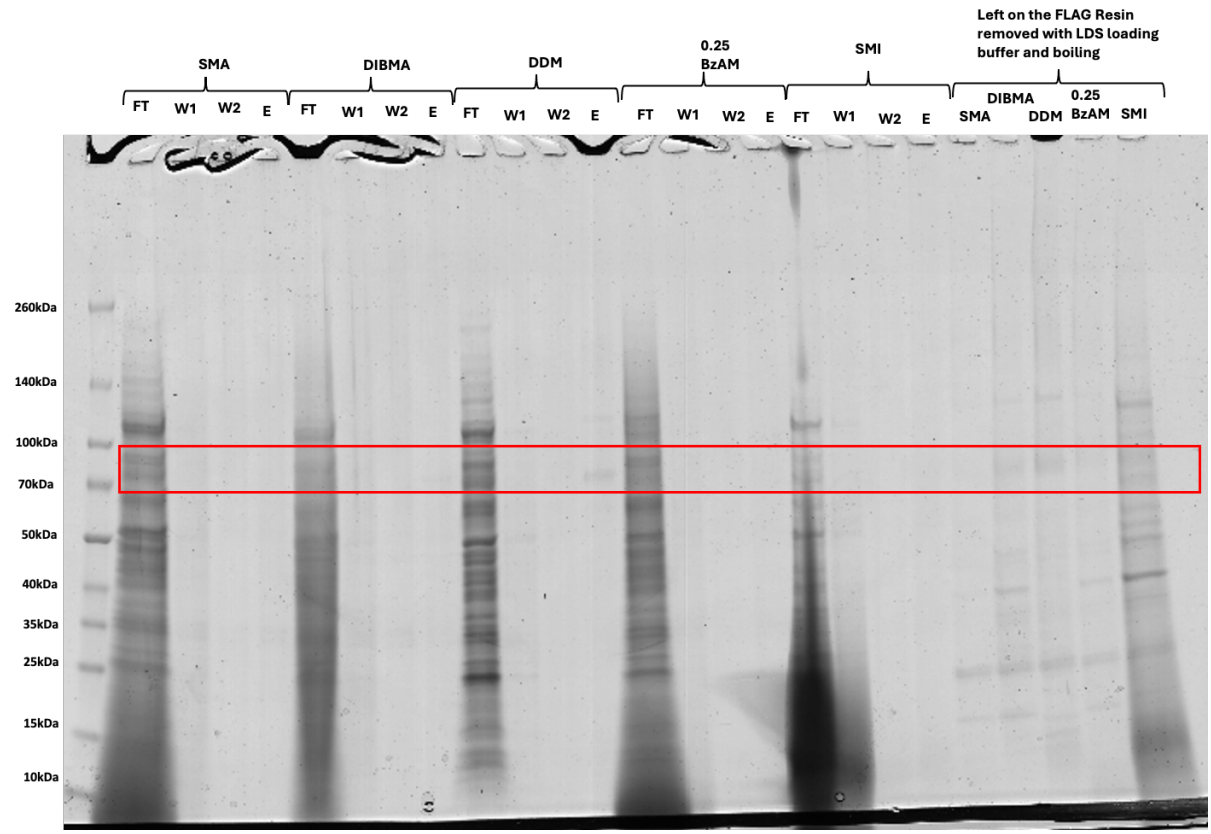


Figure 5.8: SDS-PAGE analysis of five FLAG affinity purifications of CB2 solubilised with polymers or DDM.
CB2 expressing membranes were solubilised with 2% (w/v) polymer (SMA, DIBMA, 0.25 BzAM or SMI) or 1.5% (w/v) DDM. The soluble material was incubated with anti-FLAG resin for 2 hours, resin was washed twice (W1 and W2) before elution with 0.1mg/mL FLAG peptide (E). Following elution, the resin was incubated with LDS loading buffer and boiled for 10 minutes to denature and elute protein remaining on the resin. SDS-PAGE was performed on a 4-20% gradient acrylamide gel. The red box indicates where a band may appear if at the expected MW of monomeric CB2.

Figure 5.8 shows the fractions of the 5 attempted FLAG purifications of CB2 extracted by different solubilisation agents. The elution (E) showed any protein that was bound to the anti-FLAG resin and was removed from the anti-FLAG binding sites by displacement with FLAG peptide. There were two bands at the expected size of dimeric and monomeric CB2 when DDM was used as a solubilisation agent. There is a faint possible monomeric band in the elution fraction when CB2 was solubilised with DIBMA. There were proteins bound to the resin after elution no matter the solubilisation agent, shown by the many bands at different MWs. This suggested non-specific binding that was not displaced by the FLAG peptide.

The intensity of the bands suggested that SMI-solubilised material had the largest amount of non-specific binding. This may be because SMI was the least effective at solubilising CB2 or

because of the biophysical properties of the SMILPs. Analysing the protein eluted by LDS and boiling showed bands at the expected MW of monomeric and dimeric CB2 when DDM or DIBMA was the solubilisation agent. This suggested that there was DIBMA-solubilised or DDM-solubilised CB2 bound to the resin that was not eluted using 0.1 mg/mL FLAG peptide. The intensity of the bands suggested DDM was the solubilisation agent that warranted the largest concentration of the CB2 that bound to the anti-FLAG resin.

The FLAG purifications confirmed the hypothesis that the use of PoLiPa can cause difficulties with FLAG-tag affinity purifications. A small amount of DDM-CB2 was purified by this method without prior optimisation. There was no evidence that CB2 encapsulated in a PoLiPa was able to bind to the anti-FLAG resin when testing three out of the four polymers: SMA, 0.25 BzAm and SMI. It is suspected the FLAG tag may be occluded by the lipids and polymer in the PoLiPa or that the polymer in solution is interfering with the binding. DIBMA-CB2 showed some evidence of binding to the resin. The different biophysical properties of a DIBMALP compared to a SMALP or a SMILP could allow greater flexibility which allowed the FLAG tag to bind to the resin.

The results led to the decision that FLAG purifications were not a viable option for CB2 purification when performed directly after polymer solubilisation. Although DIBMA-CB2 showed some evidence of resin binding it was inefficient for the downstream use of CB2. It was therefore decided that IMAC purifications would be a more appropriate first purification step after polymer solubilisation.

5.7 Optimising IMAC Purification of CB2 Expressed in E. coli using PoLiPa Technology

Given the successful purification of SMA-rNTR1 after IMAC optimisation, a series of experiments were performed to optimise CB2 IMAC purifications. It was suspected that CB2 may have a weaker binding affinity for the IMAC resin than rNTR1 due to the smaller number of histidine residues (6 vs 10). In this project, multiple variables (including solubilisation agent, arginine concentration, salt concentration, reducing agent inclusion and imidazole concentration) were tested to determine the protocol that would generate optimal yield and purity of CB2.

5.7.1 IMAC purification of CB2 Solubilised with DDM

Since the DDM-CB2 generated the highest yield during FLAG purification compared to the other four polymer-solubilised CB2 purifications, it was decided to also include DDM-CB2 as part of IMAC purification optimisation. This would determine if the use of detergent was beneficial for both types of CB2 purification over the use of polymers.

Figure 5.9 shows the fractions from the IMAC purification attempting to purify DDM-CB2. The soluble and insoluble fraction sample shows most of the protein material was solubilised with DDM. However, there was no band at the expected weight of CB2 (85 kDa) in the wash or the elution fractions. Characteristic contaminant bands previously identified in Chapter 3, at approximately 110 kDa, 45 kDa and 35 kDa, were visible. In the FT, there was a slightly more intense band likely representing DDM-CB2 (red arrow) that did not bind to Ni-NTA resin.

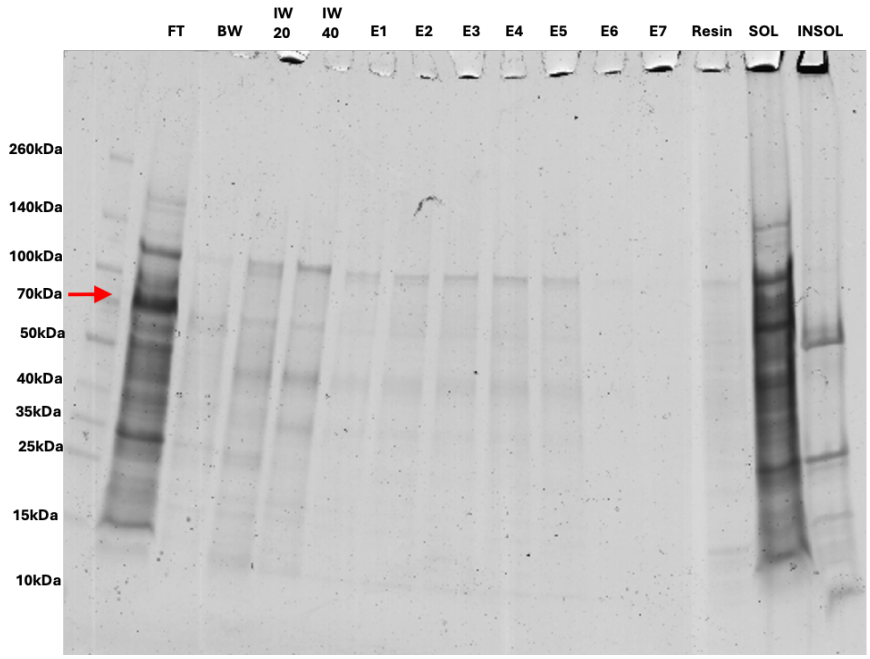


Figure 5.9: IMAC purification of DDM-CB2.
CB2 expressing membranes were solubilised with 1.5% (w/v) DDM and soluble material was incubated with Ni-NTA resin overnight at 4 ℃, resin was washed with buffer (BW), 20 mM imidazole (IW20) and 40 mM imidazole (IW40) before elution with 500 mM imidazole (E1-E7). Following elution, a sample of the resin was incubated with LDS loading buffer and boiled for 10 minutes. SDS-PAGE was performed on a 4-20% gradient acrylamide gel. Red arrow indicates where a band may appear if at the expected MW of monomeric CB2 (Box did not accommodate the curvature of the gel).

The DDM-CB2 purification demonstrated that contamination issues are not solely due to interference of PoLiPa but was likely due to the low affinity of the CB2 for the IMAC resin. It was thought that the shorter His tag and the position of the His tag before the FLAG tag may have reduced the affinity of the CB2 to the IMAC resin compared to rNTR1.

5.7.2 Resin Type, Salt Concentration and Addition of 20 mM Arginine as Variables

Following the poor binding of PoLiPa-encapsulated CB2 to anti-FLAG resin, an experiment to test the binding to IMAC resins was performed. A resin binding trial was performed in which CB2-expressing *E. coli* membranes were solubilised with SMA, DIBMA or 0.25 BzAM and then incubated Ni-NTA, IDA or TALON resin overnight. The importance of salt and arginine concentration was also assessed to generate a screen which included sixteen conditions for each polymer.

Figure 5.10 shows the SDS-PAGE analysis of the binding trial which indicated the best IMAC conditions for each polymer tested. A single band at the expected weight of the monomeric CB2 (85 kDa) would indicate successful purification in one of the conditions. When assessing the binding of SMA-CB2, initial analysis of the experiment showed that, independent of salt or arginine concentration, the best resin type for SMA-CB2 was Ni-NTA (Figure 5.10A). The inclusion of 20 mM arginine in the binding buffer appeared to improve CB2 binding and purity, particularly when 500 mM salt was included in the binding buffer. There was a persistent band at approximately 30 kDa which is expected to be a contaminant that co-elutes with CB2. The amount of the 30 kDa contaminant protein reduced when the impure sample was bound to the IDA resin as compared to Ni-NTA. Despite this improvement in purity. Ni-NTA resin was chosen to be optimal due to the overall higher yield of CB2 upon elution. Overall, the SDS-PAGE gel showed that the best purification of SMA-CB2 utilised Ni-NTA resin when 20 mM arginine and 500 mM salt were in the binding buffer.

When analysing the binding of 0.35 BzAM-solubilised CB2, the monomer band (85 kDa) was visible in every condition except when using the IDA resin with low salt and no arginine (Figure 5.10B). A band at approximately 110 kDa, suspected to be the common contaminant AcrB, was visible after Ni-NTA or TALON were used and had an increased intensity in low salt concentrations. A possible dimer band of CB2 (170 kDa) was visible when using Ni-NTA resin. This could indicate that 0.35 BzAM allowed more dimerization or better binding of CB2 dimers to Ni-NTA resin compared to SMA. Overall, when comparing monomer band intensity and purity, the best purification of 0.35 BzAM-solubilised CB2 was using Ni-NTA resin with 20 mM arginine and 500 mM salt in the binding buffer.

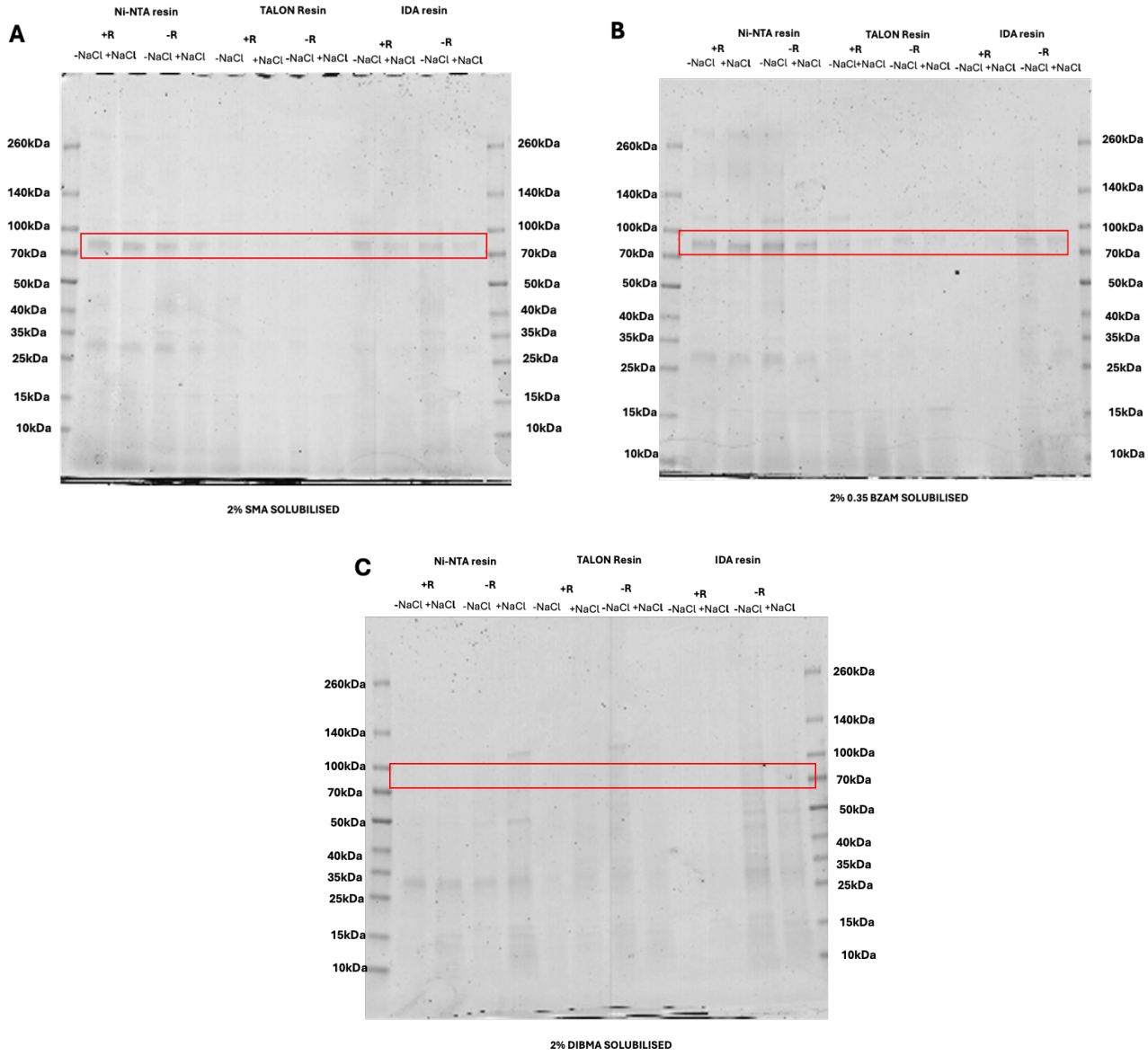


Figure 5.10: SMA-CB2-, 0.35 BzAM-CB2 and DIBMA-CB2 binding trial comparing the effect of resin-type, arginine and salt.
Polymer-solubilised material was incubated with one of three types of resin overnight (Ni-NTA, TALON and IDA) at either 150 mM NaCl concentration (-NaCl) or 500 mM NaCl concentration (+NaCl), with or without the addition of 20 mM arginine (+R or -R). The resin from each condition was washed and the bound protein eluted by addition of LDS buffer and boiling at 100 ℃ for 10 minutes.
(A) The elution for each of the 16 conditions tested in the binding screen when CB2 expressing membranes were solubilised with 2% SMA.
(B) The elution for each of the 16 conditions tested in the binding screen when CB2 expressing membranes were solubilised with 2% 0.35 BzAM
(C) The elution for each of the 16 conditions tested in the binding screen when CB2 expressing membranes were solubilised with 2% DIBMA.

DIBMA solubilised CB2 had the poorest binding trial results of the three polymers tested. The expected monomer band was not visible in any of the conditions tested (Figure 5.10C). This may be because of the low CB2 solubilisation efficiency of DIBMA compared to SMA or

0.35 BzAM. This would have caused lower concentration of DIBMA-CB2 in the soluble material and higher binding of contaminant proteins. The contaminant bands had variable intensity dependent on resin, salt and arginine conditions. Overall, it was decided that IMAC chromatography was not appropriate for the purification of DIBMA-CB2.

The binding trial was able to successfully identify the best conditions out of the tested variables. Interestingly, the effect of salt and arginine had different effects on the protein concentration and purity of the elution dependent on each resin and solubilisation polymer. This demonstrated the need for resin and polymer screening when utilising PoLiPa technology. A resin screen methodology tested on a wider range of proteins and polymers has recently been investigated to find patterns in PoLiPa purification efficiency (Unpublished).

5.7.3 Addition of 200 mM Arginine

Since SMA was one of the polymers with the best solubilisation efficiency and initial IMAC screen, it was decided to focus on the purification of SMA-CB2. The results of the binding trial showed that the inclusion of 20 mM arginine in the binding buffer improved the binding of CB2 and reduced the binding of impurities to Ni-NTA. However, the elution from the binding trial generated a sample of CB2 which was less than 50% pure. It was decided to test whether a higher concentration of arginine would increase sample purity. Two purifications using the same SMA-solubilised material were performed with and without 200 mM arginine in the binding buffer. Concentrations above 200 mM reported interfered with protein binding to Ni-columns (Abe *et al*., 2009). Fractions of each purification were analysed by SDS-PAGE and Western blot (Figure 5.11).

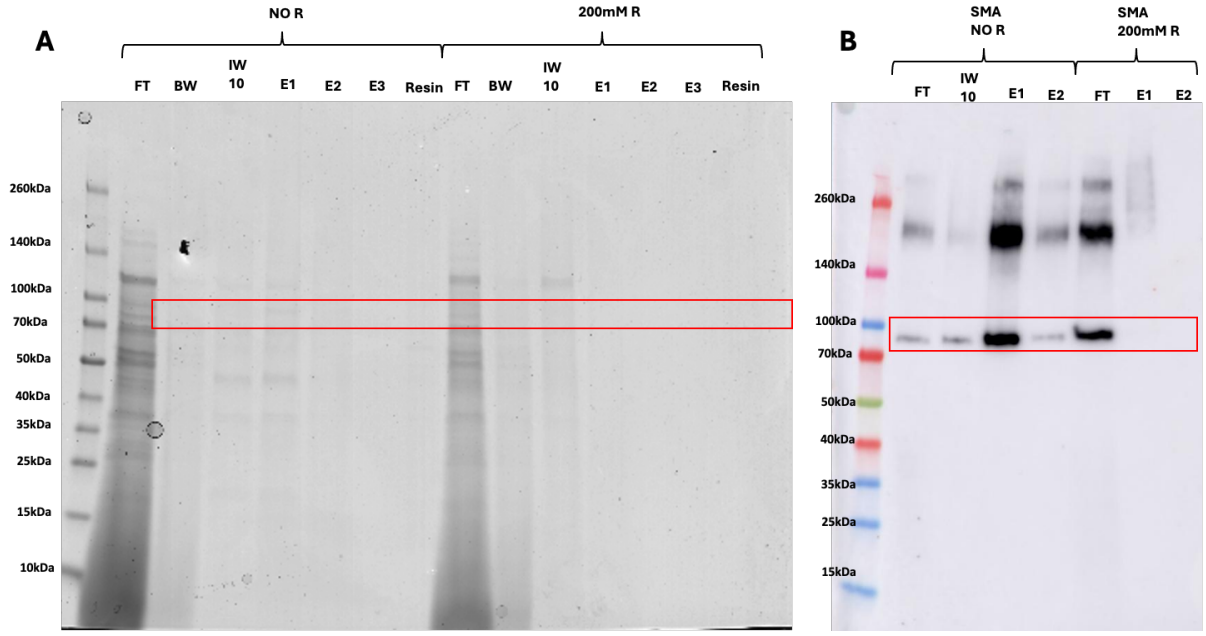


Figure 5.11: Two comparative SMA-CB2 IMAC purifications with and without 200 mM arginine in the binding buffer. *CB2 expressing membranes were solubilised with 2% SMA and soluble material was incubated with Ni-NTA resin overnight a 4℃, resin was washed with buffer (BW) and 10 mM imidazole (IW10) elution with three 2 mL fractions of 500 mM imidazole (E1, E2, E3). Following elution, a sample of the resin was incubated with LDS loading buffer and boiled for 10 minutes. Samples of each wash and elution fraction including the flow through (FT) were analysed by SDS-PAGE using a 4-20% gradient acrylamide gel. The red boxes indicate where a band may appear if at the expected MW of monomeric CB2. (A) Coomassie stained SDS-PAGE gel. (B) Western blot analysis using anti-His antibody.*

A comparison of the first elution fraction of each purification on the Coomassie-stained SDS-PAGE gel shows a ladder of multiple bands in the purification with no arginine versus no visible bands with 200 mM arginine Figure 5.11A. This shows the purification with no arginine yielded a low purity protein product whereas the purification with 200 mM arginine yielded no protein. Figure 5.11B gives a clearer comparison of how much SMA-CB2 remained in the flow through and hence did not bind to the Ni-NTA resin. The intensity of the monomer and dimer bands was lower in the flow through (FT) when no arginine was used in the binding buffer. There is no visible monomer band in the elution fractions analysed by Western blot when 200 mM arginine was used. The most intense bands on the Western blot are in the first elution from the purification without arginine. This provided evidence that arginine inhibits the binding of SMA-CB2 to IMAC resin when added to the binding buffer at a high concentration. The arginine also inhibited the binding of the contaminant proteins.

Abe *et al* showed that arginine interferes with protein binding to Ni-columns but this effect was greatly reduced below 200 mM (Abe *et al*., 2009). The PoLiPa may have made CB2 binding extra sensitive to interference with arginine. It was decided that 20 mM concentration was appropriate in the binding buffer to retain the highest yield of CB2 possible. The band at 85 kDa was confirmed to represent CB2 by mass spectrometry analysis: 13 peptides unique to the CB2 sequence were identified.

5.7.4 Effect of Reducing Agent addition to IMAC binding buffers: 25 mM DTT

The inclusion of 25 mM DTT during the lysis of CB2-expressing *E. coli* decreased the dimerization of CB2. It was hypothesised that the inclusion of a reducing agent when binding to IMAC resin may improve purification yield of SMA-CB2. The two purifications with and without 25 mM DTT in the binding buffer are shown by the SDS-PAGE gels in Figure 5.12.

DTT can reduce a proportion of Ni^{2+} ions on the resin to Ni^{1+} or uncharged Ni causing the brown colour and also strip the nickel from the resin, reducing binding capacity (Getz *et al*., 1999). The SDS-PAGE analysis showed that the inclusion of DTT improved the purity of SMA-CB2 in the elution fraction. The highest intensity band in the elution fractions is one at the expected MW of the CB2 monomer (85 kDa). In the purification with no reducing agent, there is also a band in the elution fractions which is suspected to be monomeric CB2. However, there are multiple other bands of similar intensity including the contaminant bands, identified in Chapter 3: 110 kDa, 45 kDa and 35 kDa.

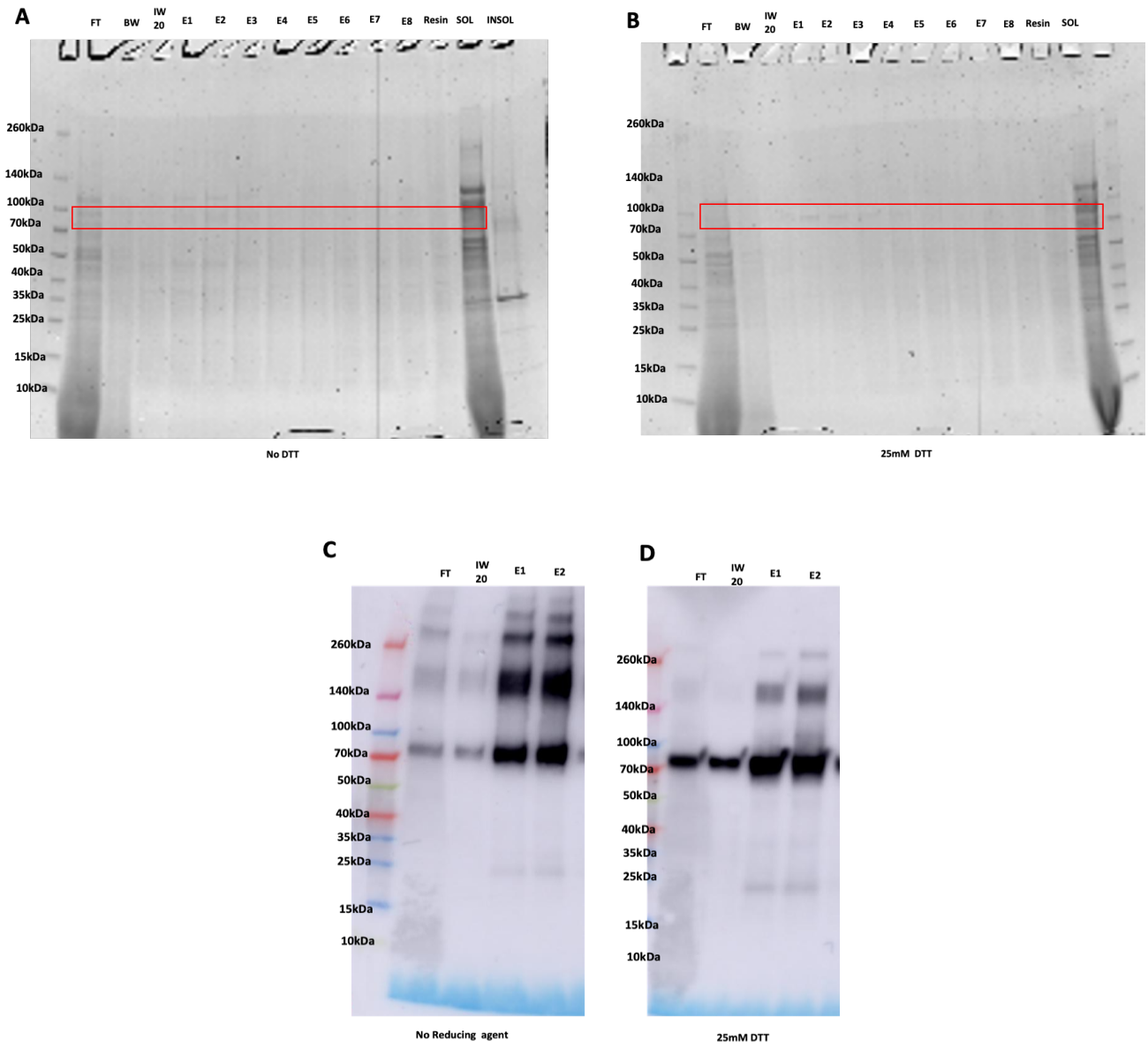


Figure 5.12: Two comparative SMA-CB2 IMAC purifications with and without 25 mM DTT in the binding buffer. *CB2 expressing membranes were solubilised with 2% SMA and soluble material was incubated with Ni-NTA resin for overnight a 4 ℃, resin was washed with buffer (BW) and 20 mM imidazole (IW20) and eluted with eight 1mL fractions of 500 mM imidazole (E1- E8). Following elution, a sample of the resin was incubated with LDS loading buffer and boiled for 10 minutes. Samples of each wash and elution fraction as well as the flow through (FT), soluble fraction (SOL) and insoluble fraction (INSOL) were analysed by SDS-PAGE using a 4-20% gradient acrylamide gel. Red box indicates where a band may appear if at the expected MW of monomeric CB2. Western blot analysis performed on specific fractions using anti-His antibody.*
(A) Coomassie stained SDS-PAGE analysis of IMAC purification with no reducing agent added.
(B) Coomassie stained SDS-PAGE analysis of IMAC purification with 25 mM DTT in the binding buffer.
(C) Western blot analysis of the flow through, imidazole wash and first two elution fractions from IMAC purification with no reducing agent added.
(D) Western blot analysis of the flow through, imidazole wash and first two elution fractions from IMAC purification with 25 mM DTT in the binding buffer.

The Western blots in Figure 5.12 (C and D) confirmed the presence of SMA-CB2 monomer and dimer. Bands at the expected MW of monomeric (85 kDa) and dimeric (170 kDa) CB2 were visible in the flow through, 20 mM imidazole wash and analysed elution fractions (E1

and E2) when analysing purifications both with and without DTT in the binding buffer. The intensity of the dimer band compared to the monomer band is lower when DTT was included in the binding buffer in the Western blot-analysed components of the IMAC purifications. This suggested DTT reduced dimerization after SMA solubilisation. The intensity of the monomer band in the flow-through (FT) represents the concentration of protein that did not bind to the resin. There was a larger proportion of the CB2 when DTT was used in the binding buffer. This is most likely due to the reduced binding capacity of the resin caused by DTT.

The results of this experiment show that the inclusion of a reducing agent had a large effect on the purity of the product yielded from an IMAC purification. It is theorised that CB2 has a greater affinity for the Ni-NTA resin as a monomer compared to a dimer. This may be because the His tag is more exposed to the resin in the monomeric form. Dimerization could occlude the tag in some way preventing binding by steric hindrance. The choice to add a reducing agent also led to the loss of binding capacity. However, a lower protein concentration was sacrificed for a significant improvement in protein purity.

5.7.5 Effect of Reducing Agent addition to IMAC binding buffer: 1 mM TCEP

TCEP is often the preferred reducing agent to DTT because it is more stable at pH values above 7.5 and a more powerful reducing agent below pH 8 (Getz *et al*., 1999). Getz *et al* found that DTT caused a higher Ni^{2+} concentration in the elution after IMAC purification compared to TCEP. It was hypothesised that using a low concentration of TCEP would avoid protein precipitation and retain the integrity of the Ni-NTA resin. An IMAC purification of SMA-CB2 was performed with 1 mM TCEP in the binding buffer. After overnight binding to the Ni-NTA resin, elution fractions were collected using a stepwise increase in imidazole concentrations to determine the optimal elution concentration. The elution fractions were

combined (total IMAC elution) and divided into four. After overnight dialysis into buffers without TCEP, the protein was re-analysed by SDS-PAGE to assess evidence of post-purification oligomerization.

Figure 5.13 shows the SDS-PAGE analysis of the IMAC purification fractions when 1 mM TCEP was included in the binding buffer. There is a band at the expected MW of CB2 in the elution fractions using 40-500 mM imidazole. The elution with the highest target protein concentration was when 100 mM imidazole was used. In this fraction, there are four other bands suspected to be contaminant proteins which have co-eluted with CB2. The band at 110 kDa is suspected to be AcrB, as identified in Chapter 3. The intensity of the bands indicates that CB2 is present at a higher concentration than the contaminant proteins. Some protein remained on the resin after the stepwise imidazole concentration elution fractions however most of the protein was eluted after the 250 mM imidazole elution.

The four lanes on the far right-hand side of the gel show the post-IMAC CB2 sample after dialysis into four slightly different buffers, all without TCEP. Comparing the post-dialysis and centrifugation samples to the total IMAC elution shows the appearance of higher-order bands above the 140 kDa marker. It is suspected that the band near the top of the gel is representative of a CB2 dimer or oligomer. This suggested that without a reducing agent, oligomerization of CB2 can occur post-solubilisation. This may indicate that proteins can move between SMALPs or two SMALP-encapsulated CB2 particles and fuse to allow a dimerization event.

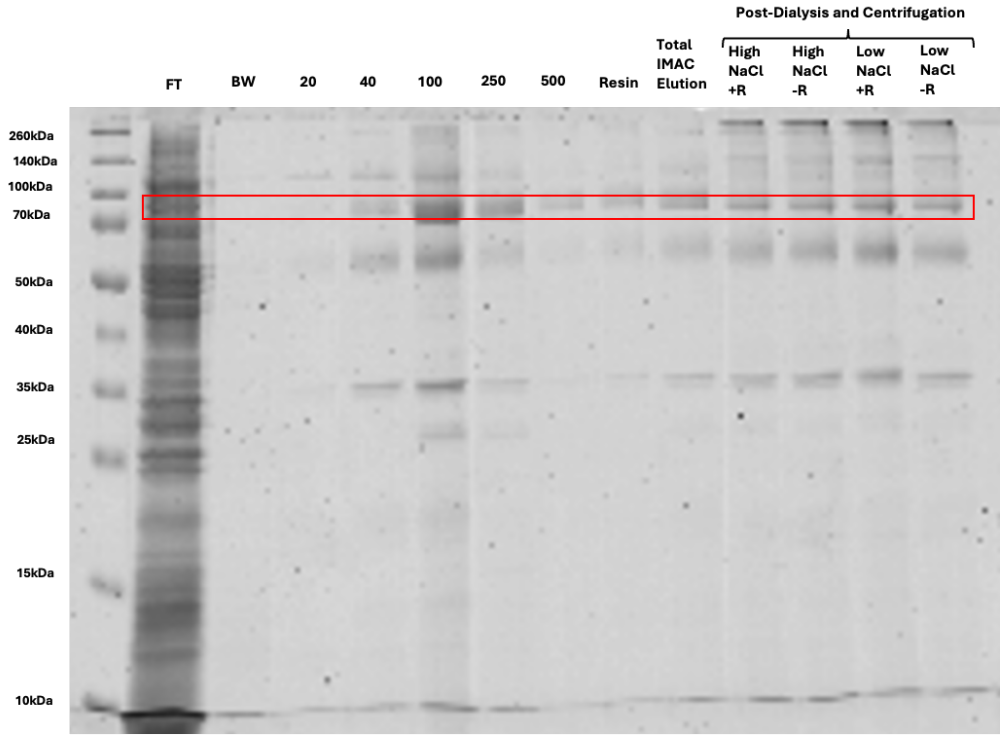


Figure 5.13: SMA-CB2 IMAC purification with 1 mM TCEP in the binding buffer.
CB2 expressing membranes were solubilised with 2% SMA and soluble material was incubated with Ni-NTA resin for overnight a 4 ℃, resin was washed with buffer (BW) and then five 5mL elution fractions with a stepwise increase in imidazole concentration (20, 40 100, 250, 500). Following elution, a sample of the resin was incubated with LDS loading buffer and boiled for 10 minutes. Elution fractions were combined (Total IMAC Elution), split into four and dialysed into four different buffers with either 500 mM NaCl or 150 mM salt, with and without 20 mM arginine. After overnight dialysis, samples were centrifuged before SDS-PAGE analysis (post-dialysis and centrifugation). Each wash and elution fraction as well as the flow through (FT) were analysed by SDS-PAGE using a 4-20% gradient acrylamide gel and visualised with Coomassie stain. Red box indicates where a band may appear if at the expected MW of monomeric CB2.

This experiment demonstrated that 1 mM TCEP could be used to prevent dimerization whilst retaining the integrity of Ni-NTA resin, yielding a condition that generated the highest concentration of CB2 from an IMAC purification. Despite reduced dimerization and suspected higher affinity for the resin, four major contaminate proteins were co-eluted with CB2. It could be that these were also co-eluted when DTT was included, but the overall concentration was too low to visualise the contaminants with Coomassie stain. Alternatively, it could be that the oxidation and leaching of the nickel ions caused by DTT reduced the affinity for contaminant proteins more selectively. The result of this experiment led to the decision that a high yield of pure polymer solubilised CB2 would not likely be achieved by a single-step purification.

5.8 FLAG Purification of CB2 Post-IMAC Purification

SMA-CB2 was not able to be purified by FLAG peptide affinity purification immediately after solubilisation. To test whether the removal of excess SMA and other solubilised proteins would improve binding, it was decided to perform a FLAG purification after an IMAC purification. The elution from the IMAC purifications in sections 5.7.4 and 5.7.5, were used to compare post-IMAC FLAG purifications using different conditions. These included testing the inclusion of reducing agents as well as different arginine and salt concentrations.

5.8.1 Addition of 25 mM DTT in Binding Buffers

The elution from the IMAC purification with 25 mM DTT was incubated with anti-FLAG resin with continued use of DTT up until elution with 2.5 mg/mL FLAG peptide. This was compared to a second FLAG purification with no reducing agent. Since previous FLAG purifications highlighted issues with removing CB2 from the resin, a higher flag peptide concentration was trialled, and the anti-FLAG resin was agitated for 2 hours at RT to promote elution. A second elution was collected after incubation with FLAG peptide without agitation before analysis of what remained on the resin by the addition of LDS buffer and boiling for 10 minutes.

Figure 5.15 shows the SDS-PAGE and Western blot analysis of the post-IMAC FLAG purifications. The post-IMAC FLAG purification with 25 mM DTT in the binding buffers showed a band at the expected MW of the CB2 monomer in the two FLAG elution fractions as well as on the anti-FLAG resin post-elution (Figure 5.15A).

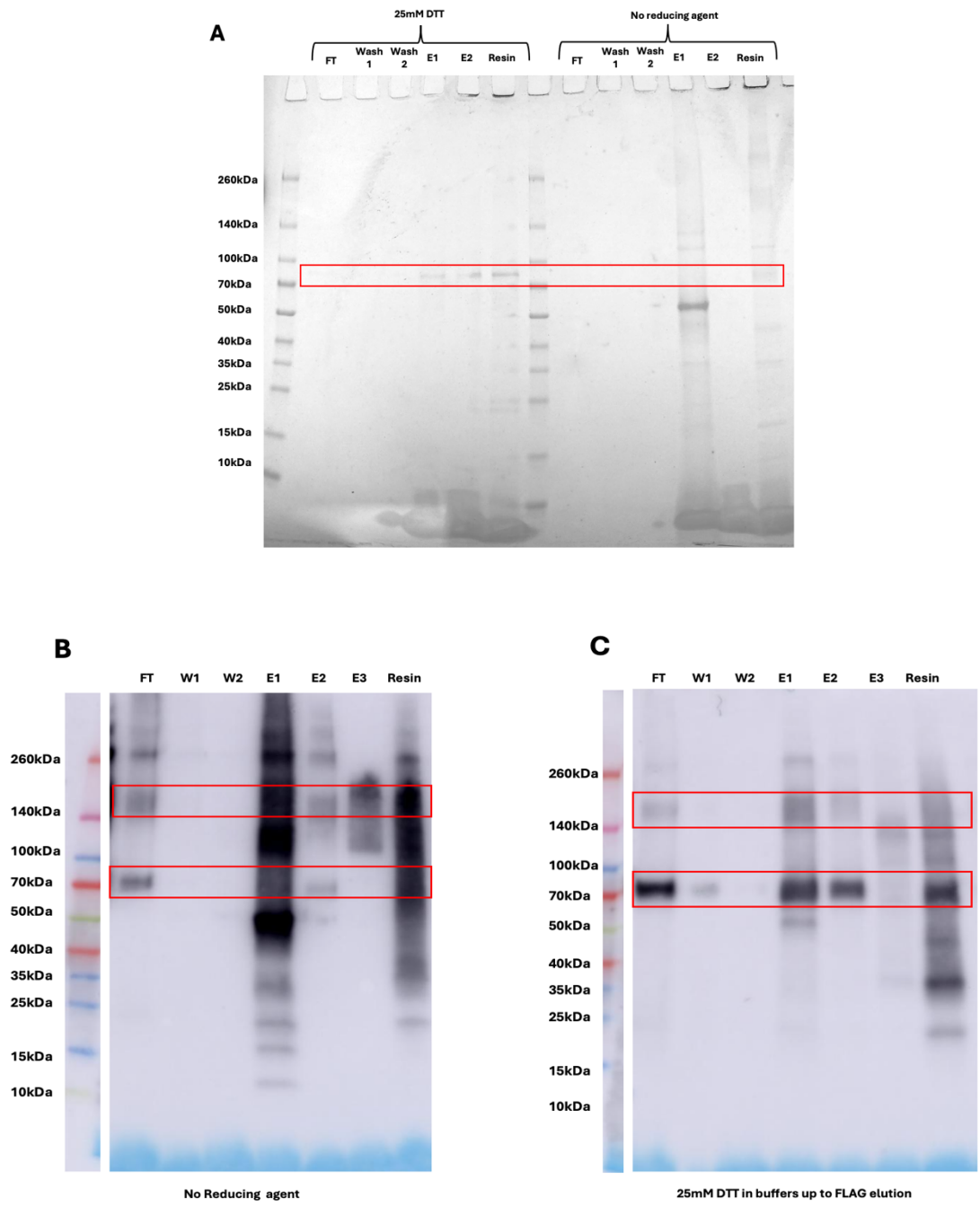


Figure 5.14: Two comparative post-IMAC FLAG purifications with and without 25 mM DTT in the binding buffers.
Elution from the IMAC purifications with and without 25 mM in the binding buffer were incubated with anti-FLAG magnetic resin for 2 hours. The resin was washed with 2x 1mL buffer wash (W1 and W2) and then incubated with 2.5mg/mL FLAG peptide for 2 hours at RT whilst being agitated. This elution was collected (E1) and the resin was incubated with 2.5mg/mL peptide for 2 hours without agitation (W2). The resin was then washed with buffer (E3) before a sample of the resin was incubated with LDS loading buffer and boiled for 10 minutes (Resin). Samples of each wash and elution fraction as well as the flow through (FT) were analysed by SDS-PAGE using a 4-20% gradient acrylamide gel. Western blot analysis performed on specific fractions using anti-His antibody.
(A) Coomassie stained SDS-PAGE gel of IMAC purification fractions with (left) or without (right) 25 mM DTT. Red box indicates where a band may appear if at the expected MW of monomeric CB2.
(B) Western blot analysis FLAG purification fractions when no reducing agent was added to the binding buffer.
(C) Western blot analysis FLAG purification fractions when 25 mM DTT added to the binding buffer.

Despite the excessively high concentration of FLAG peptide and RT agitated elution, some SMA-CB2 was not able to be eluted from the resin in both conditions, suggesting an issue of non-specific binding. Previous contaminants from the IMAC purification appeared to also bind non-specifically to the resin and were not eluted with FLAG peptide, as shown by the analysis of the resin after elution. When post-IMAC FLAG purification with no reducing agents was analysed, the common previously identified IMAC contaminant bands (110 kDa, 45 kDa and 35 kDa) were bound to the resin post-elution (Figure 5.14A, right). There was a band at approximately 50 kDa in the first elution fraction of the post-IMAC FLAG purification with no reducing agent. This is likely to be a C-terminal fragment of CB2 that included the tags as confirmed by the Western blot analysis with an anti-His antibody (Figure 5.14C.

Western blot analysis of the fractions of the post-IMAC FLAG purification with 25 mM DTT, confirmed the presence of SMA-CB2 (Figure 5.14B). There was a large proportion of SMA-CB2 left in the flow through when DTT was included in the binding buffer despite, no visible band on the Coomassie-stained SDS-PAGE gel. The primary band on the Western blot in the elution of the FLAG purification with 25 mM DTT was the approximately 85 kDa band expected to be the CB2 monomer. There was also a lower intensity band at 50 kDa suspected to be a fragment of the CB2.

Western blot analysis shown in Figure 5.14C elucidated which bands were likely CB2 or CB2 fragments from the SDS-PAGE gel in Figure 5.14A. As well as a high intensity band at approximately 50 kDa, there are many bands at a range of MWs in the first elution fraction. In the second elution, the 85 kDa monomer band and higher oligomer bands can be identified as well as a faint band at 50 kDa. This suggested that the agitation of the first elution fraction at RT caused fragmentation of the SMA-CB2. This was especially detrimental to the purification

when no reducing agent was included in the binding buffer. This could suggest that the reduced oligomerization caused by 25 mM DTT had a stabilising effect. This experiment showed that a two-step purification with addition of a reducing agent could produce a pure SMA-CB2 product.

5.8.2 Arginine and Salt Concentration

The post-IMAC FLAG purifications showed promising results defining an appropriate methodology for producing pure SMA-CB2 expressing in *E. coli*. The main drawback of this methodology was the efficiency of purification. A large proportion of the CB2 produced was lost in the flow-through of the IMAC purification or could not be removed from the anti-FLAG resin. An experiment was performed to optimise the yield of the FLAG purification step. The elution of the most efficient IMAC purification, performed with 1 mM TCEP in the IMAC binding buffer, was divided into four and dialysed into different buffers with either 500 mM or 150 mM NaCl; 0 mM or 20 mM arginine. It was hypothesised that the addition of arginine or NaCl may prevent non-specific binding of the SMA-CB2 which could not be displaced by FLAG peptide.

The SDS-PAGE gels in Figure 5.15 (A and B) compare the flow-through, wash, two elution fractions and resin of FLAG purifications in the four different conditions. There was a band at the expected weight of the CB2 monomer (85 kDa) in flow through and in the first elution for all four conditions. This suggested the amount of resin was too low to capture all the SMA-CB2 available. There were bands likely representing the IMAC contaminant proteins in the flow-through, including bands at approximately 100 kDa, 45 kDa and 35 kDa. These three bands are also present in the first elution of all four purifications. This shows a small proportion of contaminating protein can be co-eluted through a two-step purification method. It may be that these proteins are present in the same SMALP as the CB2.

The intensity of the expected CB2 monomer band in the elution fractions provided an indication of the concentration of purified SMA-CB2. The purification with low salt and no arginine in the buffers had the most intense band in both the elution fractions. There was no clear band in the second elution when using high salt and arginine. The analysis of the resin showed a faint monomeric CB2 band when arginine was added to the binding buffer. The low salt, no arginine purification resin analysis showed a ladder of different bands which included the common contaminant banding pattern as well as a higher intensity monomeric CB2 band. This suggests that a high salt concentration and 20 mM arginine can reduce the binding capacity of the anti-FLAG resin.

Figure 5.15C gave reassurance that the 85 kDa band in the first elution fraction was the CB2 monomer and suggested that the band near the top of the gel represented dimeric CB2.
The intensity of the bands on the Western blot confirmed that arginine and salt reduced the efficiency of the FLAG purification, yielding a lower concentration of CB2 in the elution.

The results did not confirm the hypothesis that arginine or a high salt concentration would improve the efficiency of the FLAG purification. This experiment successfully used the elution from a previous IMAC purification, in which the purity was less than 50% to produce a product that was over 90% pure, excluding the FLAG peptide used for elution.

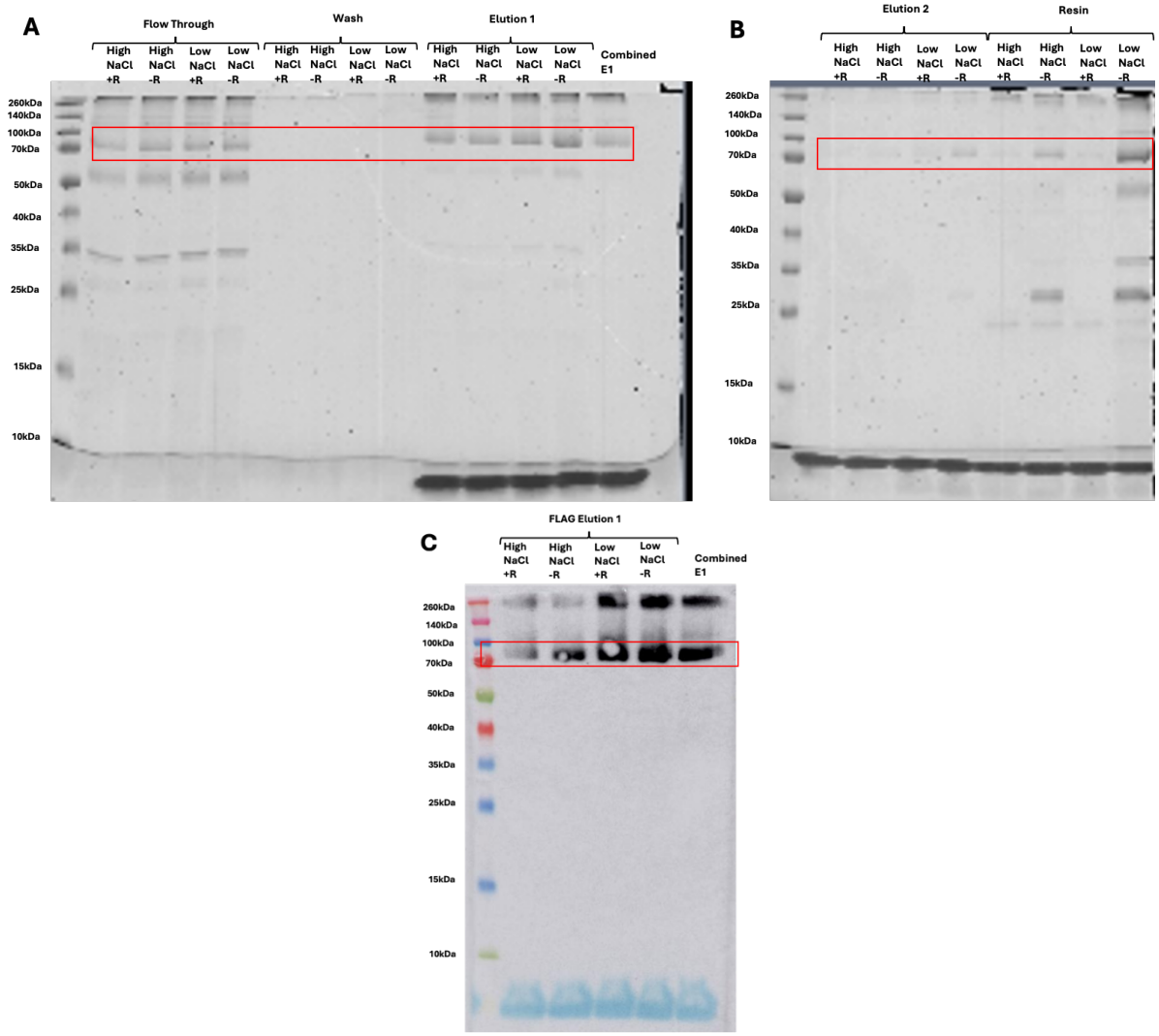


Figure 5.15: Four comparative post-IMAC FLAG purifications at low and high salt concentrations, with and without 20 mM arginine.

Elution from the IMAC purifications with 1 mM TCEP in the binding buffer were separated into four and dialysed into the four different buffer compositions with either 150 mM or 500 mM NaCl, 0 mM or 20 mM arginine.
After centrifugation, the protein was incubated with anti-FLAG magnetic resin for 2 hours. The resin was washed with 5mL buffer wash (Wash) and then incubated with 1mg/mL FLAG peptide overnight at 4℃. This elution was collected (Elution 1) and the resin was incubated with 2.5 mg/mL peptide for 2 hours at RT (Elution 2). The resin was then washed with buffer (E3) before a sample of the resin was incubated with LDS loading buffer and boiled for 10 minutes (Resin). Samples of each wash and elution fraction as well as the flow through (FT) were analysed by SDS-PAGE using a 4-20% gradient acrylamide gel. Red box indicates where a band may appear if at the expected MW of monomeric CB2. Western blot analysis performed on specific fractions using anti-His antibody. Columns are labelled to show the composition of the buffer in which the FLAG purification was performed (High Salt 20 mM arginine (+R), High Salt no arginine (-R), Low Salt 20 mM arginine (+R), Low Salt no arginine (-R)).
(A) Coomassie-stained SDS-PAGE gel showing the flow through, wash and first elution from the four FLAG purifications performed in different buffer compositions as well as a sample of all four first elution fractions combined.
(B) Coomassie-stained SDS-PAGE gel showing the second elution and resin sample from the four FLAG purifications performed in buffer compositions.
(C) Western blot analysis of the first elution fractions the four FLAG purifications performed in buffer compositions as well as a sample of all four first elution fractions combined.

5.9 Optimal Storage of SMA-CB2

Having developed a protocol for the purification of SMA-CB2 expressed in *E. coli*, the optimal overnight storage temperature of the purified protein was determined. Typically, proteins are stored at -80°C after flash-freezing aliquots in liquid nitrogen. The submersion of a protein into a -196°C temperature rapidly transitions through temperatures were proteins and prone to aggregation and degradation. Slower ice crystal formation, can increase the concentration of the solutes including the protein concentration, typically encouraging aggregation (Franks, 1993). Another method of flash-freezing involves holding the aliquot in ethanol containing dry ice, which will be approximately -78°C.

Five aliquots of SMA-CB2 were used to compare different storage methods overnight: 25°C; 4°C; -20°C; -80°C after flash freezing with liquid nitrogen or with dry ice and ethanol. To determine the best storage method, stored aliquots were centrifuged to remove aggregation before DLS analysis. A pre-centrifugation and post-centrifugation sample was taken for SDS-PAGE analysis (Figure 5.16A).

In all lanes there was a band at the expected size of monomer CB2 (85 kDa) as well as at the expected size of dimeric CB2 (170 kDa). The bands at the bottom of the gel represent the FLAG peptide that was used to elute the CB2 during purification. The most intense band representing the CB2 monomer was visible from the sample that was denatured by LDS buffer the day before the other aliquots were stored. This suggested that every storage condition caused some loss of CB2 protein. Before centrifugation, the most intense bands appeared from the aliquots which were flash-frozen. After centrifugation, the flash-frozen aliquots have the lowest intensity monomer bands compared to the aliquots stored at 24°C, 4°C or -20°C. The decrease in intensity caused by the centrifugation is likely due to

removal of aggregated CB2. After centrifugation, the highest intensity of the band at the expected MW of monomeric CB2 was from the aliquots stored at 4°C or -20°C.

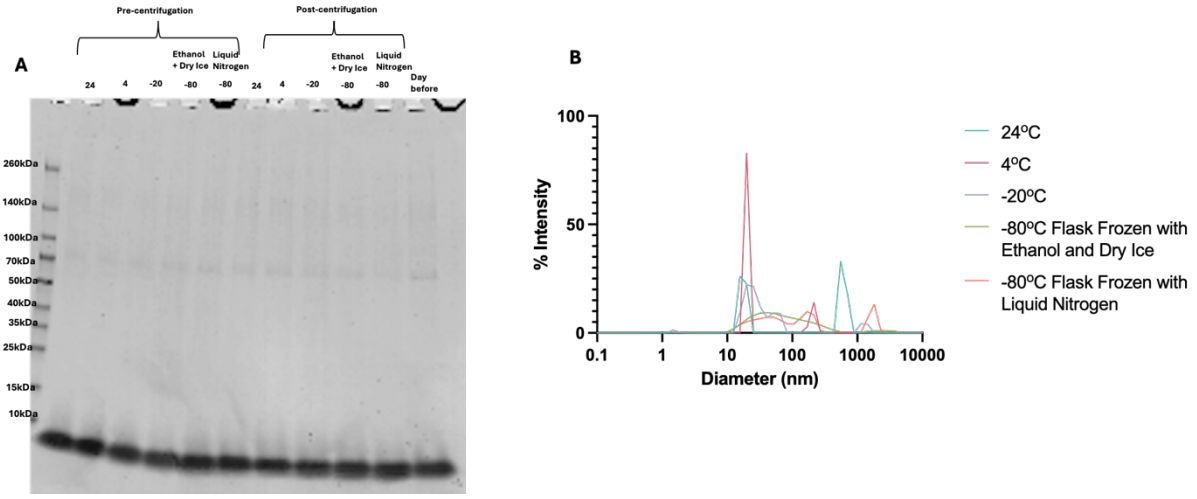


Figure 5.16: SMA-CB2 optimal storage trial.
Five aliquots of SMA-CB2 were used to test different storage methods overnight: in a cupboard at 25 ℃; in a fridge at 4 ℃; in a freezer -20 ℃; a freezer at -80 ℃ after flash freezing with liquid nitrogen or in a freezer at -80 ℃ after flash freezing with dry ice and ethanol.
(A) SDS-PAGE analysis of five of aliquots before and after centrifugation at 130,000 x g for 10 minutes and a sample of the SMA-CB2 before storage (Day before).
(B) Dynamic Light Scattering data showing the percentage of the light scattering intensity caused by particles of calculated size.

DLS analysis of the aliquots in Figure 5.16B was complementary to the SDS-PAGE analysis. It was expected that the CB2-encapsulated SMALP would be approximately 10-30 nm in diameter (Craig *et al*., 2016). When the 4°C aliquot was analysed, 83% of the light scattering was caused by particles of approximately 20 nm in diameter. Both the aliquots stored at 25°C and -20°C had similar peaks at 20 nm representing a smaller percentage of the total light scattering intensity. Considering that larger particles create a bigger signal; it can be assumed most of the particles in the aliquots stored at -20°C and 4°C are likely CB2 encapsulated in a SMALP. The flash-frozen aliquots did not appear to have a discrete peak close to 20 nm and instead suggested a range of larger particle sizes, suggestive of aggregation.

Overall, the storage condition experiment confirmed the best condition from overnight storage to be 4°C and longer-term storage may be more appropriate at -20°C. Flash-freezing storage methods were shown to be the least appropriate.

5.10 Thermostability Analysis of SMA-CB2 of NanoDSF

The stability test and DLS analysis showed aggregation and loss of CB2 protein after overnight storage. NanoDSF was used to monitor temperature-induced protein unfolding on the three samples of SMA-CB2. The ratio of fluorescence intensity at 350 nm and 330 nm is indicative of the environment of the tryptophan residues within the SMA-CB2. As temperature increases, proteins are likely to unfold and aggregate, exposing tryptophan residues to water. This causes a bathochromic shift of the emission peak, which increases the 350/330 ratio. It was hypothesised that the melting temperature (T_m) of CB2 would be increased by its encapsulation in a SMALP (Gulamhussein *et al*., 2019).

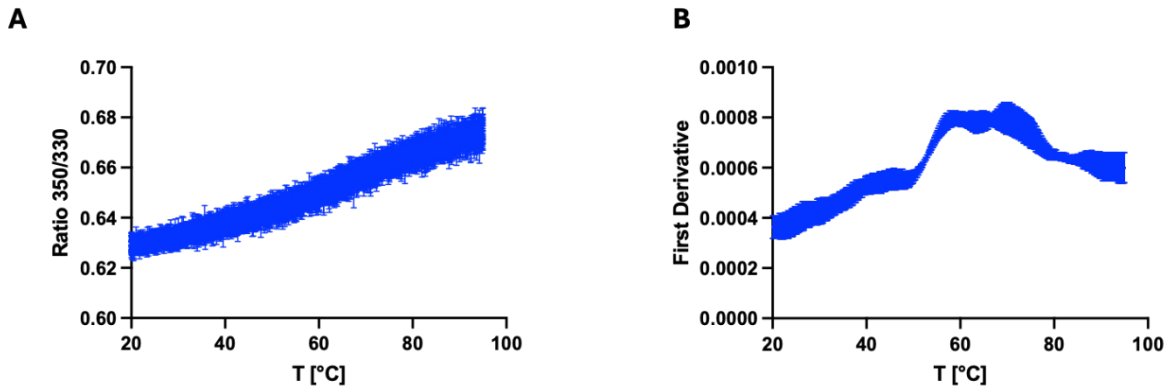


Figure 5.17: Thermostability assessment of SMA-CB2 by NanoDSF.
SMA-CB2 concentration was 0.39 mg/mL.
(A) Mean ± SD of the ratio of 350nm fluorescence intensity and the 330 nm fluorescence intensity.
(B) The first derivative of 350/330 Ratio±SD.

The 350/330 fluorescence ratio showed an increase upon an increase in temperature (Figure 5.17). The increase in 350/330 was relatively shallow and analysis of the first derivative was not able to reveal a clear onset point for unfolding below 50°C. It may be that below 50°C,

unfolding of CB2 did not occur but temperature increase caused a change in environment of the tryptophan residues in CB2 that warranted small bathochromic shift. This may have been caused by an increase in flexibility of PoLiPa and solvent exposure of CB2. The first inflexion point when the first derivative stopped increasing is at 61.05±3.4°C. This estimation of melting temperature was higher than that of SMA-rNTR1, as described in Chapter 4.

The melting temperature of detergent solubilised CB2 in a complex with Gi, stabilised by an antibody fragment, is 60.58°C (Xing *et al*., 2020). The NanoDSF analysis was able to provide a melting temperature of CB2 that was similar to CB2 stabilised with a Gi and antibody fragment interactions. The increased thermostability provided by the SMALP is consistent with other SMA-solubilised proteins including rNTR1. It was suspected that the PoLiPa caused the increase in the 350/330 ratio to be more gradual. It is thought SMA-solubilised protein may be more likely lost from solution by aggregation without complete unfolding. Due to the structural integrity of the polymer ring, temperatures higher than 50°C may be required to change the secondary structure of the encapsulated protein. This explanation is supported by the CD analysis of SMA-rNTR1 (Chapter 4), and other data recently collected by the Dafforn lab (unpublished).

5.11 Summary of CB2 Production and Characterisation using PoLiPa Technology

CB2 was successfully expressed in *E. coli,* solubilised with several polymers and purified via a two-step purification process. The concentration of salt and arginine for optimal protein yield was different for each purification step. This investigation showed that the best purification method of polymer solubilised-GPCRs was protein- and tag-dependent. Buffer component comparisons and resin binding screens are useful for optimising GPCR production, which can circumvent low expression and poor stability issues.

CHAPTER 6: EXPRESSION, SOLUBILISATION AND PURIFICATION OF GPCRS EXPRESSED IN MAMMALIAN CELLS USING POLIPA

6.1 Introduction

SMA has been used to solubilise GPCRs from several expression systems including *E. coli*, HEK293 cells, *Pichia pastoris* and Cos cells (Wiseman *et al*., 2020). *E. coli* is an efficient and cost-effective method of producing protein. However, GPCR expression in *E. coli* presents several disadvantages (Wiseman *et al*., 2020). As GPCRs are mammalian proteins, using a mammalian expression system can better simulate how GPCRs are expressed and function in the body. *E. coli* lipids co-extracted with GPCRs in PoLiPa might cause changes in the structure or function of the GPCR. Furthermore, prokaryotes do not possess the machinery for post-translational modifications such as glycosylation. Glycosylation sites on mammalian proteins can influence the way GPCRs are folded, trafficked and possibly the way they signal (Goth *et al*., 2020).

HEK293 cells are a well-established eukaryotic cell line used for producing protein. Lentiviral transduction is an attractive alternative to traditional transient transfection of mammalian cells due to its lack of large-scale plasmid production and reduced plastic and biological waste (Elegheert *et al*., 2018). Transient transfections are reported to be 65-75% efficient whereas lentiviral transductions have the capacity to transfect every HEK293 cell with one or two lentiviruses (Elegheert *et al*., 2018). This even and consistent transduction across the cells can solve problems such as toxic overexpression of protein in some cells and low yield of protein in others.

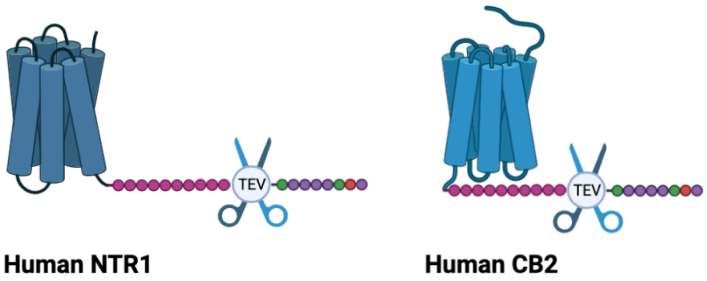


Figure 6.1: Cartoon representation of GPCRs expressed in HEK293 cells.
Wild-type Human NTR1 and Human CB2 sequences have seven transmembrane alpha helices and no fusion proteins. Both GPCRs contain a FLAG tag and 10x His tag at the C-terminus, separated by a Tabacco Etch Virus (TEV) protease cleavage site.

Figure 6.1 shows the two GPCRs expressed by lentiviral transfected HEK293 cells. The constructs included a His tag and a FLAG tag on the C-terminus with a TEV site in-between so that the FLAG tag could be cleaved off the construct. The production of human NTR1 and CB2 in mammalian cells allowed an interesting comparison to the NTR1 and CB2 expressed in *E. coli*.

Libanje *et al* (2023) discovered that hNTR1 exists in mammalian cells in three forms, visible by Western blot analysis: the less-processed hNTR1 form (hNTR1-LP) was identified at the predicted MW based on the amino acid sequence (49 kDa); a glycosylated form of hNTR1 was identified at approximately 70 kDa (hNTR1-high) and a cleaved, de-glycosylated form of hNTR1 was identified at 40 kDa (hNTR1-low) (Libanje *et al*., 2023). This finding revealed the importance of GPCR processing after translation for modulating purposes. HEK293 expressed hNTR1 has been encapsulated in a PoLiPa once before to understand oligomerisation (Dathe *et al*., 2019). However, hNTR1 has not been purified in a PoLiPa and the different identified glycosylation forms have not been extracted from mammalian cells.

Previous expression and purification of CB2 has been successful in multiple expression systems. An antagonist-bound crystal structure was achieved through insect cell expression

(Li *et al*., 2019). A protocol for producing DDM-solubilised CB2 expressed in the mammalian cell line Expi293 has also been published (Yeliseev, 2021). Both expression systems led to a product that included CB2 monomers, dimers and higher oligomers. Yeliseev *et al* (2020) compared CB2 expressed in *E. coli* and mammalian cells and found that mammalian CB2 was more active and stable at 42°C. This stabilising effect was reversed by the inclusion of Peptide: N-glycosidase, showing glycosylation helps stabilise CB2 solubilised in detergent (Yeliseev *et al*., 2020). CB2, in any version, had not been encapsulated into a PoLiPa before this project.

The resources and protocols from Dr Michael Tomlinson were utilised to produce HEK293 cell lines able to express hNTR1 or CB2. This chapter aimed to determine how PoLiPa could aid the solubilisation and purification of GPCRs expressed in mammalian tissue.

6.2 Solubilisation Screens to Understand how Efficiently Polymers Extract hNTR1 from HEK293 Cell Membranes

Membranes were harvested and solubilisation screens performed to provide comparisons of solubilisation agents and techniques. This section aimed to understand how polymer type, hydrophobicity and concentration could affect hNTR1 extraction from HEK293 cell membranes.

6.2.1 Solubilisation screen of hNTR1 Expressed in HEK293 Cells

A solubilisation screen was performed to compare solubilisation efficiency of different polymers and the detergent DDM. BzAM series polymers were included to understand how polymer hydrophobicity affected hNTR1 extraction from HEK293 membranes.

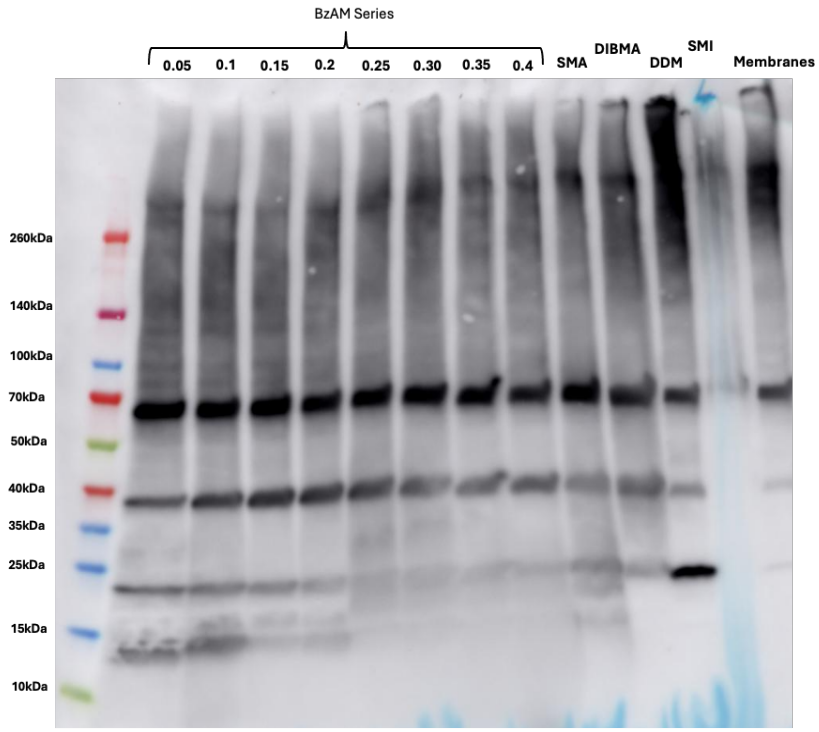


Figure 6.2: Mammalian expressed hNTR1 solubilisation trial comparing BzAM series (0.05-0.4), SMA, DIBMA, DDM and SMI

Western blot analysis of the soluble fractions after hNTR1 expressing HEK293 cell membranes were incubated with 2.5% (w/v) polymer or 1.5% (w/v) DDM. The insoluble fractions were removed by centrifugation. The soluble fractions and a sample of the membranes diluted 2-fold were analysed by SDS-PAGE on a 4-20% acrylamide gel. Western blot was probed with anti-His antibody.

Figure 6.2 shows the Western blot analysis of the soluble fraction obtained after HEK293 membranes were incubated with different solubilising agents. A sample of HEK cell membranes before solubilisation identified the size of His tagged proteins present. Three bands were visible at approximately 70 kDa, 40 kDa, and 20 kDa. A band at the expected MW based on the primary sequence of hNTR1 (46 kDa) was not visible. The 70 kDa and 40 kDa size bands were consistent with the size of the glycosylated version of hNTR1 (hNTR1-high) and the de-glycosylated cleaved version of hNTR1 (hNTR1-low) identified by Libanje *et al* (2023). The 20 kDa band was suspected to be a C-terminal fragment of hNTR1 degradation product.

BzAM series investigation showed no correlation between hydrophobicity of the polymer and solubilisation efficiency of hNTR1-high. This was inferred from the intensity of the bands at approximately 70 kDa. Extraction efficacy was comparable to SMA and DIBMA. There was a decrease in the solubilisation efficiency of hNTR1-low when using the least hydrophobic polymers in the BzAM series: 0.05 and 0.10. This trend reflected the *E. coli*-expressed GPCRs in this project.

It is noteworthy that the intensity of hNTR1-high and hNTR1-low bands from DDM extraction were less intense compared to solubilisation with SMA, DIBMA or any polymer in the BzAM series. There was more smearing at the top of the lane and a more intense 20 kDa band when DDM was the solubilisation agent. The smearing could be caused by aggregated material that could not migrate easily through the gel. The more intense 20 kDa band could suggest increased fragmentation of hNTR1. These results support the use of polymer solubilisation over DDM. The worst solubilisation agent identified by this solubilisation trial was SMI. There was a faint band at approximately 70 kDa, representing hNTR1-high suggesting SMI was not an appropriate solubilising agent from hNTR1 at the tested pH.

This solubilisation trial identified that SMA, DIBMA or any of the tested BzAM polymers were ideal solubilisation agents for hNTR1 expressed in HEK293 cells; seemingly all hNTR1-high was extracted from the HEK293 cell membranes at the concentrations tested. It is theorised that mammalian membranes are more easily solubilised with the polymer than *E. coli* membranes. This may be due to more obstacles such as peptidoglycan or the biophysical properties of the lipids themselves in bacterial membranes. The most hydrophobic polymers appeared to solubilise hNTR1-low less efficiently. This finding could be used to selectively extract glycosylated GPCRs.

6.2.2 SMA, DIBMA and Novel Polymer Series: AASTY

A solubilisation trial investigating different concentrations of SMA and DIBMA was performed to determine the minimal concentration of SMA and DIBMA for efficient solubilisation. Three polymers from the AASTY polymers series were also compared (Table 6.1). These are amphipathic polymers which utilise acrylic acid instead of maleic acid as the hydrophilic moiety in the polymer chain (Smith *et al*., 2020). To achieve a robust comparison, SMA solubilisations were performed in both HEPES and Tris-HCl buffer, as AASTY polymers were only commercially available in HEPES.

Table 6.1: Summary of AASTY Polymers in Solubilisation Trial

AASTY Polymer	**MW range (kDa)**	**Acrylic Acid (%)**	**Styrene (%)**
AASTY 11-45	10 -11	45	55
AASTY 11-55	10 -11	55	45
AASTY 6-45	5-6	45	55

Figure 6.3 shows the Western blot analysis of the soluble fractions from the solubilisation screen and a sample of hNTR1-expressing HEK293 cell membranes homogenised into HEPES buffer. All the soluble fractions and the membranes showed a band at approximately 70 kDa, consistent with the size of hNTR1-high. The membrane sample also showed bands at approximately 140 kDa, 40 kDa and 20 kDa. The 140 kDa band may represent a dimer of hNTR1-high and the band at 40kDa may represent NTR1-low. The 20 kDa band may be a C-terminal fragment of hNTR1 degradation product. The comparison of solubilisation with SMA in the two different buffer systems yielded a nearly identical result on the Western blot. This suggested that the buffer system did not have a noticeable impact on polymer solubilisation. This supported the comparison of the AASTY polymers, which were premixed with HEPES buffer, to SMA.

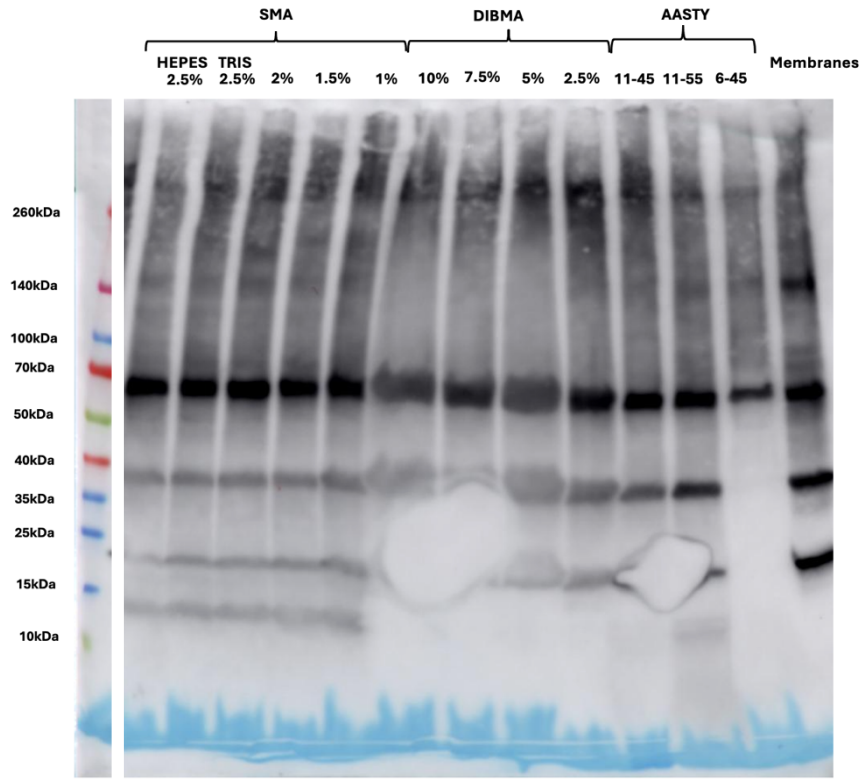


Figure 6.2: Mammalian expressed hNTR1 solubilisation trial comparing different SMA and DIBMA concentrations and the AASTY polymer series.
Western blot analysis of the soluble fractions after NTR1 expressing HEK293 cell membranes were incubated with SMA (2.5%-1% (w/v)), DIBMA (10%-2.5% (w/v)) or AASTY (2.5% (w/v)) polymers of different concentrations. 2.5% (w/v) SMA solubilisation was tested in HEPES and Tris-HCl buffer systems. The insoluble fractions were removed by centrifugation. The soluble fractions and a sample of the membranes diluted 2-fold were analysed by SDS-PAGE on a 4-20% acrylamide gel. Western blot was probed with anti-His antibody.

The higher MW AASTY polymers (AASTY 11-45 and 11-55) successfully extracted hNTR1-high and hNTR1-low. The intensity of the bands suggested a slightly lower concentration of hNTR1-high was solubilised with the AASTY polymers than SMA or DIBMA. However, AASTY 11-55 solubilised a higher concentration of the hNTR1-low than any SMA or DIBMA concentration investigated. Interestingly, the lower MW AASTY polymer (AASTY 6-45), exclusively solubilised hNTR1-high. This could be a useful tool for investigating the different hNTR1 glycosylation forms.

Of all the SMA or DIBMA concentrations tested, there was comparable extraction of hNTR1. When a DIBMA concentration of 5-10% (w/v) was used, the bands showed an increased volume but lower intensity, which was suspected to be a side effect of the excessive DIBMA

in the sample. Increasing the concentration of polymer above 2.5% (w/v) DIBMA did not improve the yield of soluble hNTR1, in contrast to the *E. coli*-expressed hNTR1 (Appendix 1.1). This suggested that mammalian membranes are more efficiently solubilised with DIBMA than bacterial membranes. This experiment also showed that a change in the buffer system between Tris-HCl and HEPES did not affect the solubilisation efficiency of SMA. Finally, this experiment tested whether the solubilisation efficiency of three AASTY polymers and discovered the MW of the polymer can influence the selectivity of protein extracted, providing a toolkit to extract differently processed GPCRs.

6.3 Binding Trials of HEK293-expressed hNTR1 Purification

The solubilisation trials confirmed that SMA was a suitable solubilisation agent for hNTR1-expressed in HEK293 cells. IMAC purification has been a common first step in the purification process for SMA-solubilised proteins (Lee *et al*., 2016). A binding trial was performed to investigate the concentration of hNTR1 bound to IMAC resin under different conditions: resin type, arginine concentration and inclusion of a reducing agent in the binding buffer. The aim was to determine the optimal conditions for IMAC purification of SMA-hNTR1 expressed in HEK293. The concentration of consecutive histidine-rich proteins that are expressed in mammalian cells is reportedly higher than those in *E. coli* cells (Bornhorst and Falke, 2000). Therefore, the GPCRs expressed in HEK293 cells may have IMAC contamination issues. Post-translational modifications such as glycosylation can also be obstructive of affinity tags (Krachmarova *et al*., 2017). It was hypothesised that varying resin types, arginine concentration or reducing agents may help circumvent these issues.

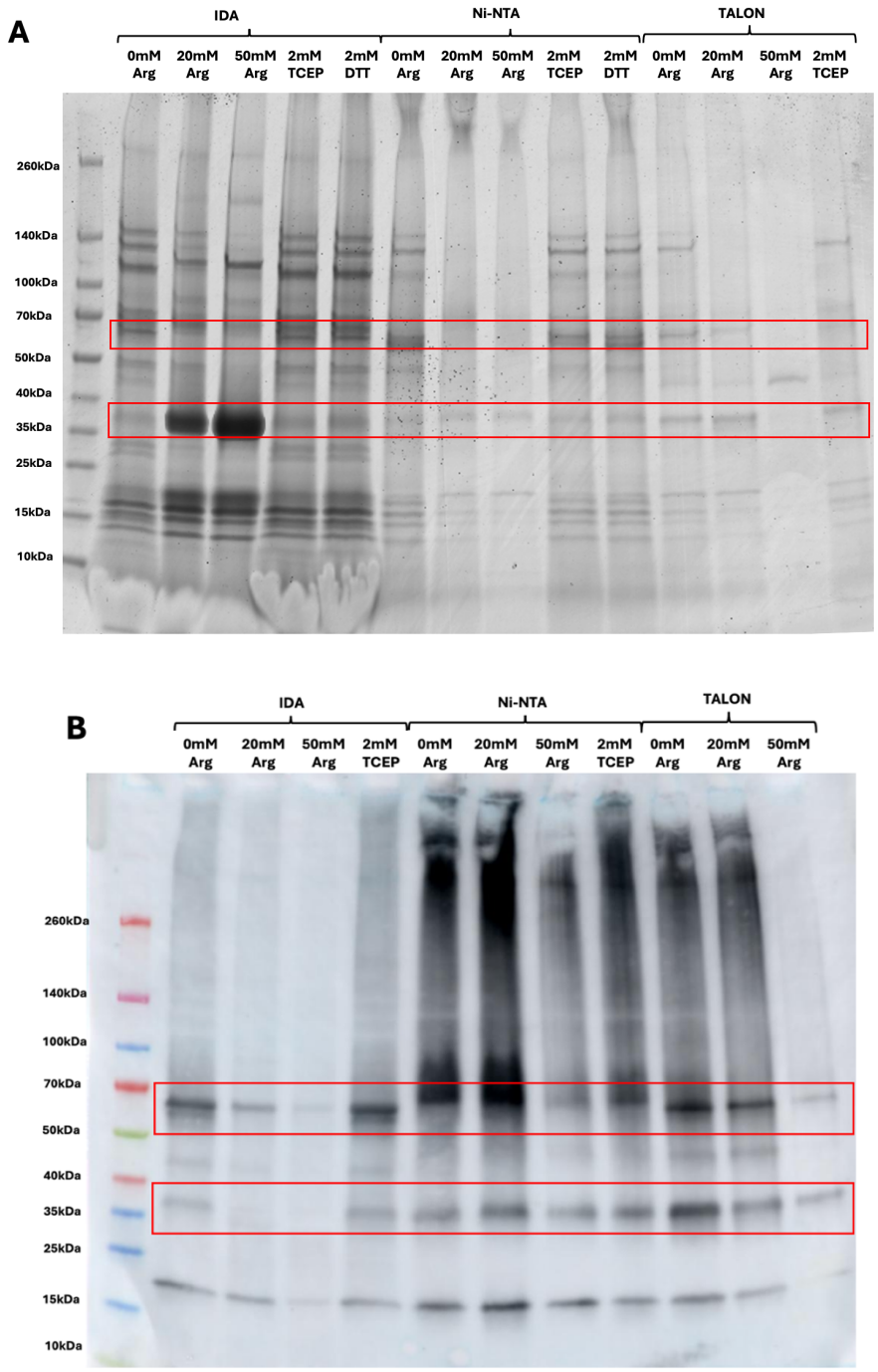


Figure 6.3: IMAC binding screen of HEK293 expressed hNTR1 on different resins (IDA, Ni-NTA, TALON), different arginine concentrations (0 mM, 20 mM, 50 mM) and with a reducing agent (2 mM TCEP or 2 mM DTT).
SDS-PAGE analysis was performed on a 4-20% acrylamide gel. The red boxes show where a representing hNTR1-high and hNTR1-low are expected to appear.
(A) Coomassie-stained SDS-PAGE analysing the protein bound to IMAC resin after overnight incubation with SMA-solubilised membranes expressing hNTR1. 14 different conditions were compared.
(B) SDS-PAGE and Western blot analysis of the protein bound to IMAC resin after overnight incubation with SMA-solubilised membranes expressing NTR. 11 conditions compared.

Figure 6.4 shows the SDS-PAGE and Western blot analysis of the material bound to IMAC resin following SMA extraction. The red boxes represent the area in which bands representing hNTR1-high (70 kDa) and hNTR1-low (40 kDa) are expected. When IDA resin was used, many contaminants were bound to the resin, as shown by the many bands on the Coomassie-stained SDS-PAGE gel (Figure 6.5A). The inclusion of arginine or a reducing agent did not cause an improvement in purity when using IDA resin. The arginine concentration correlated with increased binding of a 40 kDa contaminant, which was confirmed not to be hNTR1-low by the Western blot analysis. These results suggest IDA resin is not appropriate for IMAC purifications of proteins expressed in HEK293 cells. The intensity of the 70 kDa bands and 40 kDa on the Western blot in Figure 6.4B showed the best binding capacity was achieved by Ni-NTA resin, followed by TALON resin, followed by IDA resin. The concentration of hNTR1 bound to the TALON resin decreased with the concentration of arginine. However, samples with no arginine had the largest amount of contamination.

Interestingly, protein bound to TALON resin and IDA resin included a band at approximately 46 kDa; the less processed weight of hNTR1 based on the primary amino acid sequence. One explanation is that higher binding to hNTR1-high to Ni-NTA resin prevented the less processed hNTR1 binding. This suggests that the type of IMAC resin can have different affinities for a GPCRs in different glycosylation forms.

When using Ni-NTA-resin, hNTR1 binding was improved by the addition of 20 mM arginine but inhibited by the addition of 50 mM arginine. Figure 6.4A showed a decrease in contamination caused by the addition of arginine with the Ni-NTA binding. The inclusion of TCEP reduced the binding of hNTR1 to Ni-NTA and did not reduce contamination.

Overall, these results revealed the effect of arginine concentration between 0 mM and 50 mM can be the key to a higher yield and purity of the final product. The Western blots do not show evidence of dimers in the SMA-solubilised material. Therefore, it is consistent that reducing agents have minimal effect on hNTR1 binding affinity. After this binding screen, it was decided to proceed with an IMAC purification with Ni-NTA resin, no reducing agent and 20 mM arginine in the binding buffer.

6.4 IMAC Purification with Optimised Conditions for hNTR1

An IMAC purification of SMA-solubilised material was performed. The protein bound to the Ni-NTA resin was eluted using a stepwise increase in imidazole concentration. It was hypothesised that improved purity may be obtained by washing the resin with lower imidazole concentrations to elute low-affinity binding contaminants before elution of hNTR1.

Figure 6.5 shows the SDS-PAGE analysis of the fractions of hNTR1 IMAC purification. The FT showed what did not bind to the column: SMA-solubilised membrane proteins native to HEK293 cells, lipids and excess SMA from the solubilised material. After washing the resin with buffer (BW), the protein bound to the resin started to elute at 20 mM imidazole concentration, but most of the protein eluted with 100 mM imidazole. There were bands at the expected size of hNTR1-high but also several other protein bands in the elution fractions and bound to the Ni-NTA resin after elution.

IMAC purification was able to remove a large proportion of contaminant protein and excess polymer. However, the purity of the elution was not improved by washing with imidazole. This led to the conclusion that to remove contaminants, a second purification step would be required.

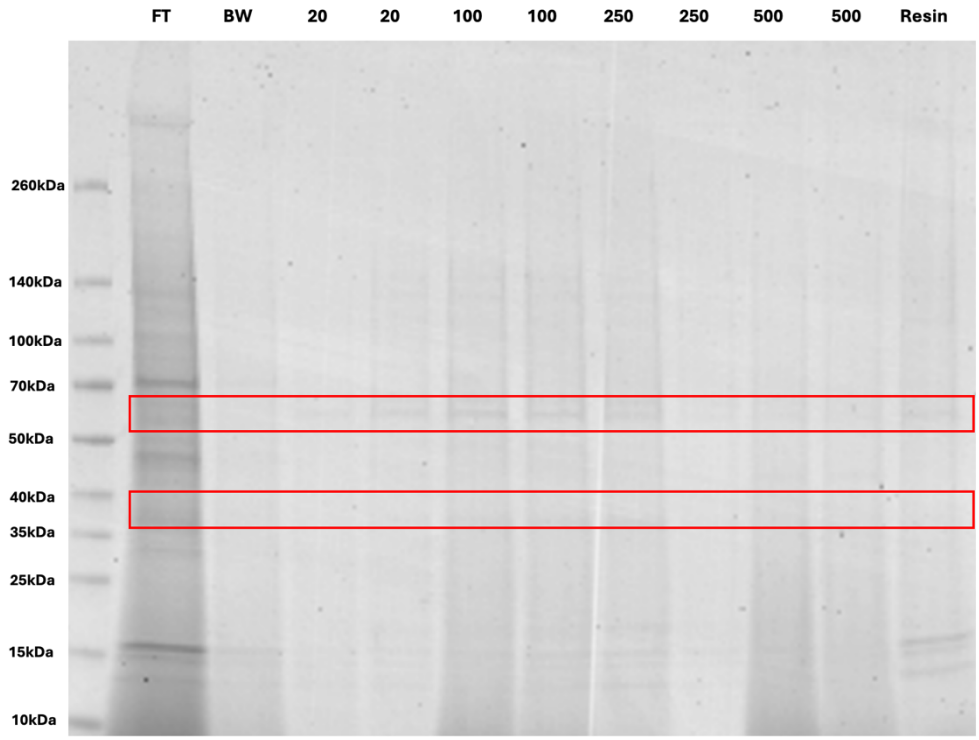


Figure 6.4: SDS-PAGE analysis of a IMAC purification of SMA-solubilised HEK293 membranes expressing hNTR1. *Flow through from the resin (FT), buffer wash (BW) and elution fractions using stepwise increases in imidazole concentration (20,20,100,100,250,250,500,500), as well as the resin after elution, were analysed by SDS-PAGE on a 4-20% acrylamide gel. Red boxes indicate expected area for NTR1-high and NTR1-low to appear.*

6.5 HEK-Expressed hNTR1 Post-IMAC FLAG Purification

To improve purity of hNTR1, a post-IMAC FLAG purification was performed. Two purifications were performed with and without 20 mM arginine in the buffers. For both purifications, the flow through, washes, elution fractions and material bound to the anti-FLAG resin after elution, were analysed by SDS-PAGE (Figure 6.6).

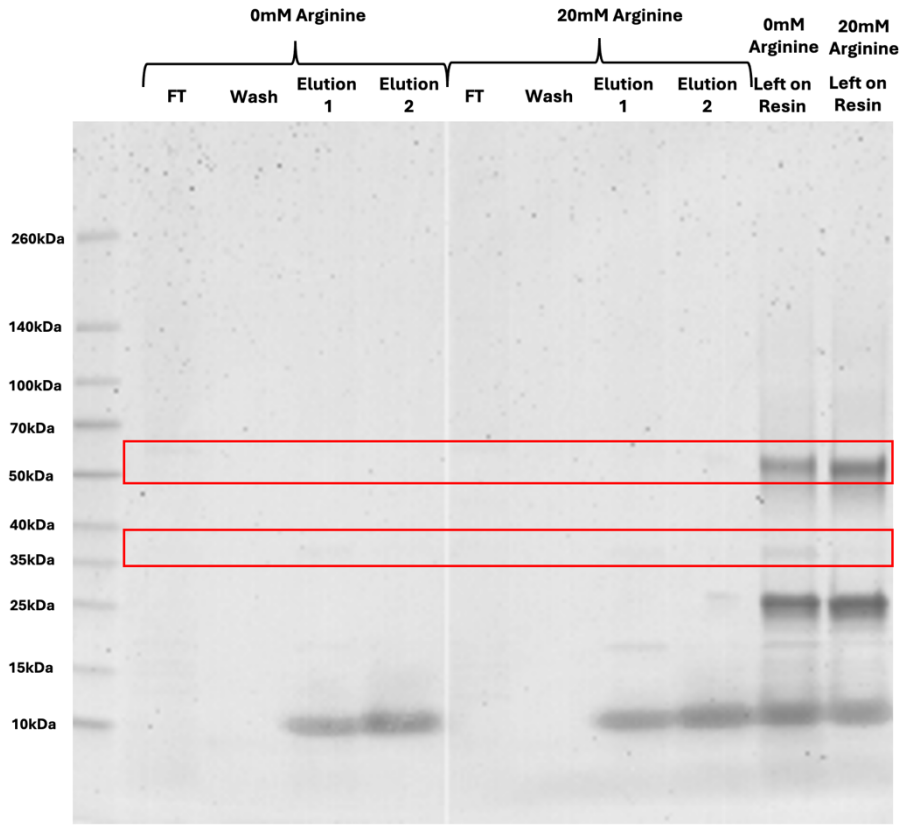


Figure 6.5: SDS-PAGE analysis of two FLAG purification of SMA-solubilised HEK293 membranes expressing NTR1.
Flow through from the resin (FT), buffer wash (BW) and two elution fractions using FLAG peptide, as well as the resin after elution, were analysed by SDS-PAGE on a 4-20% acrylamide gel. The red boxes show where a representing NTR1-high and NTR1-low are expected to appear.

The anti-FLAG resin was able to separate hNTR1 from the HEK293 cell contaminants that were present in the flow-through. In both purifications, a faint band representing hNTR1-low was present in the first elution as well as a band at approximately 20 kDa, possibly a C-terminal fragment of hNTR1. The bands at 10 kDa represent 3XFLAG peptide used to elute the hNTR1 by competing for the binding sites. A band representing hNTR1-high was not present in the elution fractions. Two intense bands are present when analysing the protein bound to the anti-FLAG resin after elution. The band at approximately 70 kDa suggested hNTR1-high was not eluted with FLAG peptide. The second band at approximately 25 kDa was possibly a fragment of hNTR1. Arginine had minimal benefit to the yield of the purification.

It is suspected that the glycosylated hNTR1-high had an issue with non-specific binding to the anti-FLAG resin that prevented its elution via competition with the FLAG peptide. There was also evidence of rNTR1 degradation after binding to the resin. The accessibility of a FLAG tag can be related to glycosylation (Müller *et al*., 2002). Glycosylation may prevent specific and promote non-specific binding to the anti-FLAG resin. This drawback could be useful for the selection and characterisation of the de-glycosylated cleaved version of hNTR1. Unfortunately, the time restraints of this project prevented further investigation into the use of PoLiPa to investigate hNTR1 expressed in HEK293 cells.

6.6 Solubilisation screens of CB2 expressed from HEK293 cells

Membranes were harvested and solubilisation screens performed to provide comparisons of solubilisation agents and techniques. This section aimed to understand how polymer type, hydrophobicity and concentration could affect CB2 extraction from HEK293 cell membranes.

6.6.1 Amphipathic Polymers and DDM

The MW of the CB2 construct based on primary sequence is 43 kDa. In insect cells, SDS-PAGE and Western blot analysis of purified CB2 bands at expected MW and a band 5 kDa higher expected to be a glycosylated version of CB2, as well as higher order bands above 87 kDa expected to be dimers and oligomers of CB2 (Filppula *et al*., 2004). A published protocol for the purification of detergent solubilised CB2 from mammalian cells identified monomers, dimers and oligomers by Western blot analysis (Yeliseev, 2021). However, there has been no previous solubilisation of CB2 with amphipathic polymers. This experiment aimed to determine whether encapsulating HEK293-expressed CB2 into a PoLiPa was an ideal extraction method. CB2-expressing HEK293 membranes were solubilised with either 2.5%

(w/v) polymer or 1.5% (w/v) DDM. Solubilisation efficiency of SMA was compared in HEPES and Tris-HCl.

Two primary bands were visible when analysing the CB2-expressing HEK293 membranes by Western blot (Figure 6.7). The band at approximately 40 kDa was suspected to be the monomeric CB2. The band at approximately 65 kDa was suspected to be dimeric CB2; this was below the expected dimer size (86 kDa) but consistent with SDS-PAGE analysis of previously expressed CB2 in mammalian cells (Yeliseev, 2019). The smeary bands at approximately 120 kDa and above 260 kDa are suspected to represent higher-order oligomers of CB2. There were multiple, less intense bands below the 35 kDa marker, suspected to be C-terminal fragments of CB2 which include the His tag. The intensity of the two bands representative of monomeric and dimeric CB2, in the red boxes, were used to compare concentration of solubilised CB2.

SMA was the most efficient solubilisation agent for dimeric CB2 extraction. The buffer system did not appear to affect the solubilisation efficiency of SMA. The intensity of the band representing monomeric CB2 was less intense in the SMA-solubilised material compared to the membrane sample. This suggested that there was a bias for the extraction of dimeric CB2 or that SMA solubilisation encouraged dimerization. On the contrary, the material solubilised with the detergent DDM appeared to have a higher proportion of monomeric CB2 than dimeric CB2. DIBMA solubilised the least CB2 in both dimeric and monomeric form.

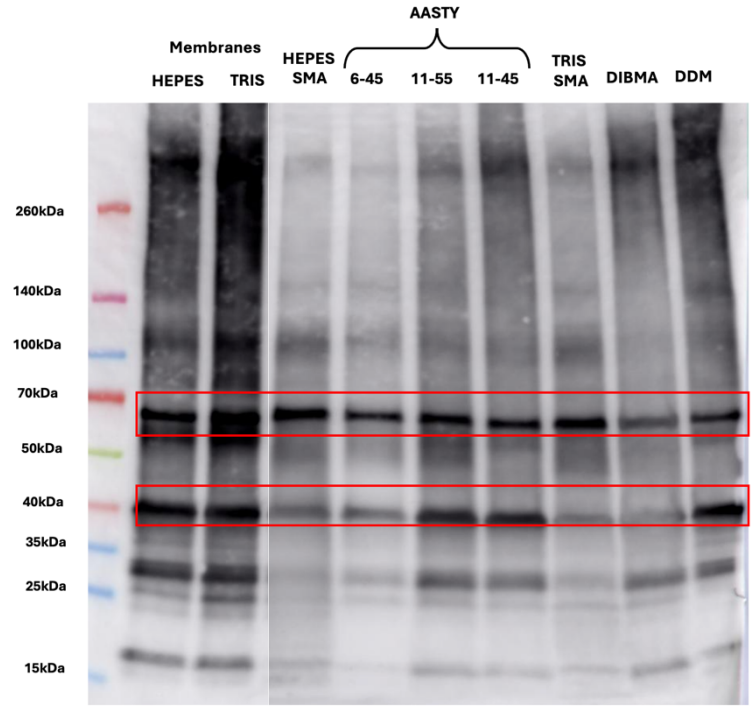


Figure 6.6: Mammalian expressed CB2 solubilisation trial comparing different SMA, DIBMA, the AASTY polymer series and DDM.
Western blot analysis of the soluble fractions after CB2-expressing HEK293 cell membranes were incubated with 2.5% (w/v) polymer and 1.5% (w/v) DDM. Tested polymers included SMA, DIBMA, AASTY 6-35, AASTY 11-55 and AASTY 11-45. Membranes were homogenised into HEPES and Tris-HCl buffer. SMA was used to compare both buffer systems. The insoluble fractions were removed by centrifugation. The soluble fractions and samples of the membranes diluted 2-fold were analysed by SDS-PAGE on a 4-20% acrylamide gel. Western blot was probed with anti-His antibody.

The AASTY series showed interesting solubilisation effects dependent on the MW and acrylic acid: styrene ratio. The smaller-length polymer (AASTY 6-45) caused a similar proportion of dimeric CB2 in the soluble fraction as SMA. However, the intensity of the bands suggested less CB2 was solubilised compared to SMA. The higher-length polymers (AASTY 11-45 and AASTY 11-55) caused a higher ratio of monomeric to dimeric CB2. Solubilisation efficiency of the AASTY polymer was improved by the smaller ratio of acrylic acid to styrene; the intensity of the bands after AASTY 11-45 solubilisation was higher than after AASTY 11-55 solubilisation.

This solubilisation trial showed that SMA and the higher MW AASTY polymers are appropriate solubilisation agents for HEK293-expressed CB2. The use of PoLiPa technology revealed a new approach to investigating oligomeric states as different polymer types or MWs were selective of the dimeric CB2.

6.6.2 Polymers with Different Hydrophobicities Compared to SMA and DIBMA

The previous solubilisation screen showed that the less hydrophobic AASTY polymer solubilised less CB2 than the AASTY polymer with more hydrophobic moieties. A solubilisation screen was performed to understand further how polymer hydrophobicity affected CB2 extraction from HEK293 membranes using the BzAM polymer series.

Figure 6.8 shows the Western blot analysis of soluble fractions after solubilisation with the BzAM polymer series, SMA or DIBMA. In the membrane sample, there was a higher proportion of monomeric CB2 than dimeric CB2. The intensity of band representative of dimeric CB2 was similar between all the polymers in the BzAM series and SMA. This suggested the concentration of dimeric CB2 in the soluble fraction was unaffected by the hydrophobicity of the BzAM polymer. DIBMA had the lowest solubilisation efficiency, as demonstrated by the lowest intensity of both bands.

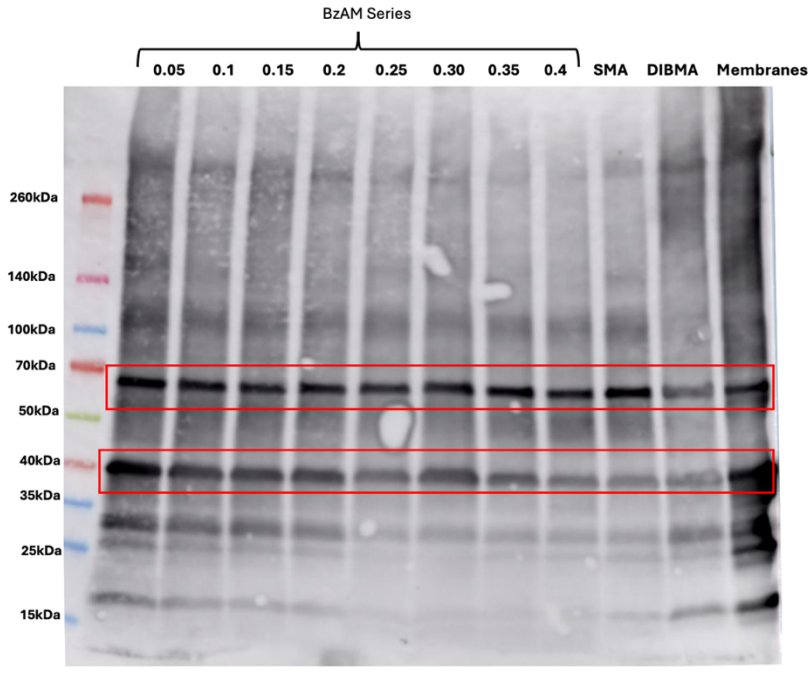


Figure 6.7: Mammalian expressed CB2 solubilisation trial comparing SMA, DIBMA and the BzAm polymer series
Western blot analysis of the soluble fractions after CB2 -expressing HEK293 cell membranes were incubated with 2.5% (w/v) polymer. Tested polymers included SMA, DIBMA and eight BzAM series polymers (0.05-0.4). The insoluble fractions were removed by centrifugation. The soluble fractions and a sample of the membranes diluted 2-fold were analysed by SDS-PAGE on a 4-20% acrylamide gel. Western blot was probed with anti-His antibody.

There was a trend in solubilisation efficiency of monomeric CB2 as polymer hydrophobicity increased: intensity of the band in the soluble fraction decreased when using a more hydrophobic polymer while the material solubilised with 0.05 BzAM showed the highest intensity monomer band. This trend was not in alignment with the previous hydrophobicity tests in this project, which have shown a decreased solubilisation efficiency when polymer hydrophobicity was in this range. This testifies to the variability caused by the protein and lipid-environment. One explanation is the influence on protein size. The lower MW bands, suspected to represent C-terminal fragments of CB2, showed a decrease in band intensity with polymer hydrophobicity. Higher MW bands above the 50 kDa marker did not show this trend.

Understanding the nuances of how polymer characteristics can be manipulated to solubilise specific proteins could be useful to GPCR investigations. The results of these experiments show that polymers could provide a new toolkit for understanding different oligomeric states of GPCRs when surrounded by native lipids.

6.6.3 SMA and DIBMA Concentration Compared to SMI and DDM

A solubilisation trial investigating different concentrations of SMA and DIBMA was performed to determine the minimal concentration of SMA and DIBMA for optimal solubilisation efficiency. It was hypothesised that a decrease in SMA concentration would maintain solubilisation efficiency whilst reducing the concentration of excess SMA in the solution. It was also hypothesised that increasing DIBMA concentration may improve solubilisation efficiency.

Figure 6.9 shows the Western blot analysis of the soluble fraction after CB2-expressing HEK293 cells were solubilised with either SMA (1-2.5% (w/v)), DIBMA (2.55-10% (w/v)), SMI or DDM. The intensity of the bands at approximately 40 kDa and 70 kDa represented the concentration of monomeric CB2 and dimeric CB2, respectively. The SMA-solubilised material also showed 120 kDa and 160 kDa bands, suspected to represent higher-order oligomers of CB2. At a concentration of 1% (w/v) SMA, the intensity of the bands was less than when using a higher concentration of SMA. This showed the minimum concentration tested for optimal solubilisation with SMA was 1.5% (w/v).

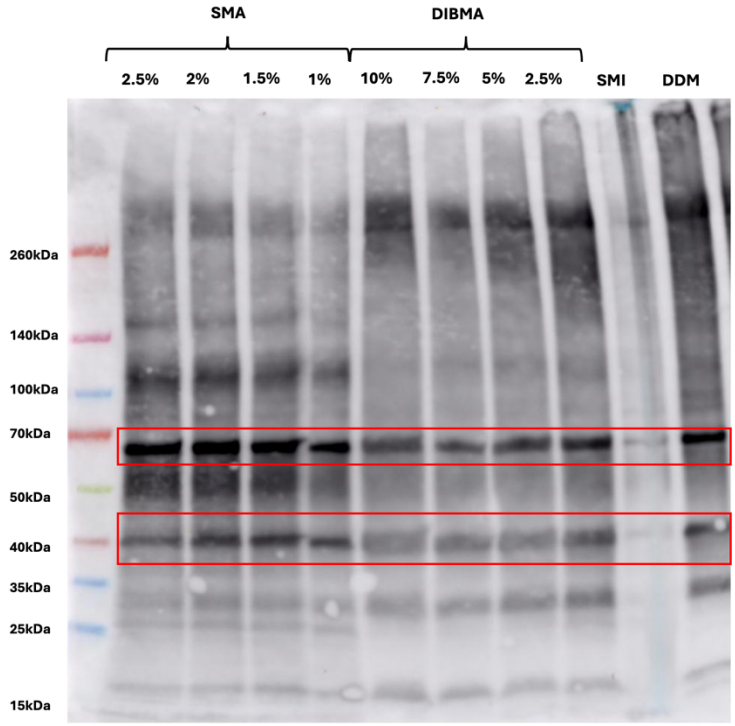


Figure 6.8: Mammalian expressed CB2 solubilisation trial comparing different SMA and DIBMA concentrations to SMI and DDM.
Western blot analysis of the soluble fractions after CB2 expressing HEK293 cell membranes were incubated with SMA (2.5%-1% (w/v)), DIBMA (10%-2.5% (w/v)), SMI (2.5% (w/v)) or DDM (1.5% (w/v)). The insoluble fractions were removed by centrifugation. The soluble fractions were analysed by SDS-PAGE on a 4-20% acrylamide gel. Western blot was probed with anti-His antibody. The red boxes represent the MW of monomeric and dimeric CB2.

An increase in DIBMA concentration above 2.5% (w/v) did not increase the extraction of CB2 from the HEK293 membranes. The intensity of the bands representing CB2 had a similar intensity no matter the concentration of DIBMA. The widening of the lanes, when a

concentration of 5-10% (w/v) DIBMA was used, was suspected to be caused by excess DIBMA in the soluble fraction. The order of the solubilisation agents tested from highest to lowest solubilisation efficiency was found to be SMA > DDM > DIBMA > SMI. There was significant precipitation of SMI-solubilised material suggesting SMI was not an appropriate polymer for the pH at which the solubilisation screen was tested.

The solubilisation screen confirmed the hypothesis that a lower concentration of SMA could provide a similar extraction for CB2 from HEK293 cell membranes as 2.5% (w/v). A concentration of 1.5% (w/v) SMA was taken as the ideal solubilisation agent. This decision led to an investigation into the purification of SMA-CB2 expressed in HEK293 cells.

6.7 Binding Trial of HEK293-expressed CB2 Purification

A binding trial was performed to investigate the concentration of CB2 bound to IMAC resin under different conditions: resin type, arginine concentration and inclusion of 2 mM TCEP in the binding buffer. The aim was to determine the optimal conditions for IMAC purification of SMA-CB2 expressed in HEK293. As previously discovered, GPCRs expressed in HEK293 cells are likely to have IMAC contamination issues and glycosylation can interfere with affinity tag binding. It was hypothesised that varying resin types, arginine concentration or reducing agents may help circumvent these issues. The high proportion of dimeric CB2 visualised by Western blot analysis of SMA-solubilised material suggested that TCEP may be beneficial. TCEP was shown to reduce oligomerisation of *E. coli*-expressed CB2 in Chapter 5. This was likely due to the reduction of cysteines and prevention of disulphide bonds between GPCRs (Nguyen *et al*., 2021).

Figure 6.10 (A and B) shows the SDS-PAGE analysis of the protein bound to IMAC resin after overnight incubation with CB2-expressing HEK293 membranes solubilised with SMA. The Coomassie-stained SDS-PAGE in Figure 6.10A showed the SMA-CB2 or host protein contaminants that bound to the IMAC resin. The Western blots in Figure 6.10 (B and C) highlighted CB2 or C-terminal fragments of CB2, which included the His tag. In Figure 6.10B, the primary band is likely to represent dimeric CB2 that bound to the IMAC resin. Bands present in Figure 6.10A and not in Figure 6.10B, are likely contaminant proteins, native to HEK293 cells, with some affinity for the IMAC resin.

IDA resin bound the largest concentration of contaminating protein, as shown by the number and intensity of protein bands present on the Coomassie-stained SDS-PAGE gel (Figure 6.10A) but not on the Western blot (Figure 6.10B). The inclusion of arginine increased the affinity of contaminant proteins to IDA resin. A large concentration of a 35 kDa protein was bound to IDA resin when 50 mM arginine was included in the binding buffer. This was consistent with the binding screen for hNTR1-expressing HEK293 membranes. The inclusion of 2 mM TCEP also appeared to increase binding of contaminants to IDA resin. These data suggest IDA resin is not suitable in purification of HEK-expressing GPCRs.

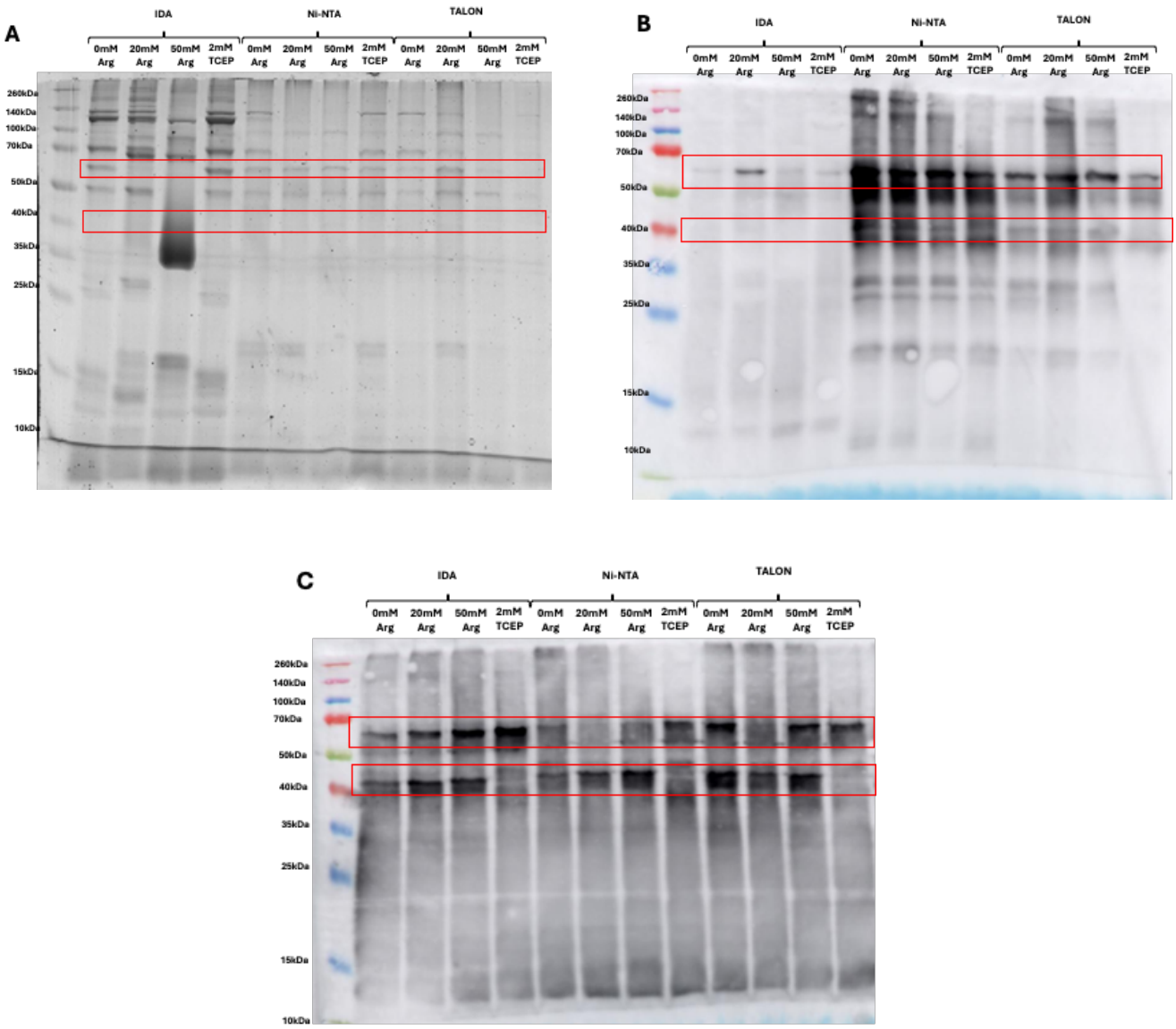


Figure 6.9: IMAC binding screen of HEK293 expressed CB2 on different resins (IDA, Ni-NTA, TALON), different arginine concentrations (0mM, 20mM,50mM) and with 1mM TCEP.
SDS-PAGE analysis was performed on a 4-20% acrylamide gel. The red boxes show where a band representing monomeric or dimeric CB2 are expected to appear. Western blots were probed with anti-His antibody.
(A) Coomassie-stained SDS-PAGE analysing the protein bound to IMAC resin after overnight incubation with SMA-solubilised membranes expressing CB2, comparing the 12 different conditions.
(B) Western blot analysis of the protein bound to IMAC resin after overnight incubation with SMA-solubilised membranes expressing CB2, comparing the 12 different conditions.
(C) Western blot analysis of protein that did not bind to IMAC resin after overnight incubation with SMA-solubilised membranes expressing CB2, comparing the 12 different conditions (flow-through sample).

TALON resin had a higher affinity for SMA-CB2 than IDA resin, but a lower affinity compared to Ni-NTA resin (Figure 6.10B). The highest concentration of CB2 was bound to TALON when 20 mM arginine was included in the binding buffer. The inclusion of 50 mM arginine or 2 mM TCEP in the binding buffer appeared to reduce the affinity of both SMA-CB2 and contaminant proteins for TALON resin. Having no arginine in the binding buffer

compared to 20 mM arginine reduced the concentration of some contaminant proteins but increased the concentration of other contaminant proteins.

Ni-NTA bound the highest concentration of SMA-CB2. This is likely because of the higher binding capacity of the resin. The amount of contaminant proteins that bound to the Ni-NTA resin was reduced by the addition of arginine but was not affected by the addition of TCEP. The addition of arginine or TCEP to the binding buffers reduced the concentration of CB2 bound to Ni-NTA resin as shown by the intensity of the bands on the Western blot (Figure 6.10B). TCEP did prevent the formation of trimers and higher-order oligomers as shown by the lack of bands above 70 kDa on the Western blot. However, this did not improve the yield or purity of the IMAC purifications.

The Western blot in Figure 6.10C analysed the flow through from the IMAC resin, providing information about the concentration of CB2 which did not bind to the IMAC resins. In all three samples with TCEP, the band representing dimeric CB2 was visible at a high intensity but the band representing monomeric CB2 was not visible. One explanation is that TCEP reverses glutathionylation of cysteine residues, restoring dimerization. Complete conversion of a protein from its monomeric to dimeric form by TCEP has been shown previously by this mechanism (Davis *et al*., 2021). The flow-through samples provided extra confidence to the results interpreted from the resin samples and provided a new understanding of the ratio of monomeric:dimeric CB2 that did not bind. Arginine decreased the binding of CB2 to IDA. The 20 mM arginine concentration increased the binding of dimeric CB2 to both TALON and Ni-NTA resin.

The results showed that the effects of arginine and TCEP on IMAC purifications were both resin- and protein-specific. The binding of SMA-solubilised monomeric and dimeric CB2 was

shown to be different. It was speculated that dimeric CB2, which represented most of the protein in the solubilised material, had a higher affinity to the IMAC resins when 20 mM arginine was included in the buffer. This effect was not consistent with the monomeric CB2. One explanation is that the low concentration of positively charged arginine reduced the charge repulsion between the negatively charged polymer and the IMAC resin. SMALPs encapsulating dimeric CB2 may have a closer interaction between the polymer and the His tag, meaning the arginine had a greater effect.

The Western blots suggested that TCEP may have encouraged CB2 dimerization whilst reducing the formation of higher-order oligomers. Unfortunately, there was no improvement in IMAC purification efficiency. Overall, the best conditions for IMAC purification were the use of Ni-NTA resin, with 20 mM arginine in the binding buffer but no TCEP.

6.8 IMAC Purification with Optimised Conditions for CB2

An IMAC purification was performed on SMA-solubilised material. It was hypothesised that washing the Ni-NTA resin multiple times with 20 mM and 40 mM imidazole may remove contaminant proteins with a lower affinity for the Ni-NTA resin than the His tagged CB2.

Figure 6.11 shows the SDS-PAGE analysis of the fractions of SMA-CB2 purification. The flow through and buffer wash sample analysis showed what did not bind to the Ni-NTA resin: SMA-solubilised membrane proteins native to HEK293 cells, lipids and excess SMA from the solubilised material. In the elution fractions which utilised 100 mM imidazole, there was a primary band suspected to represent dimeric CB2.

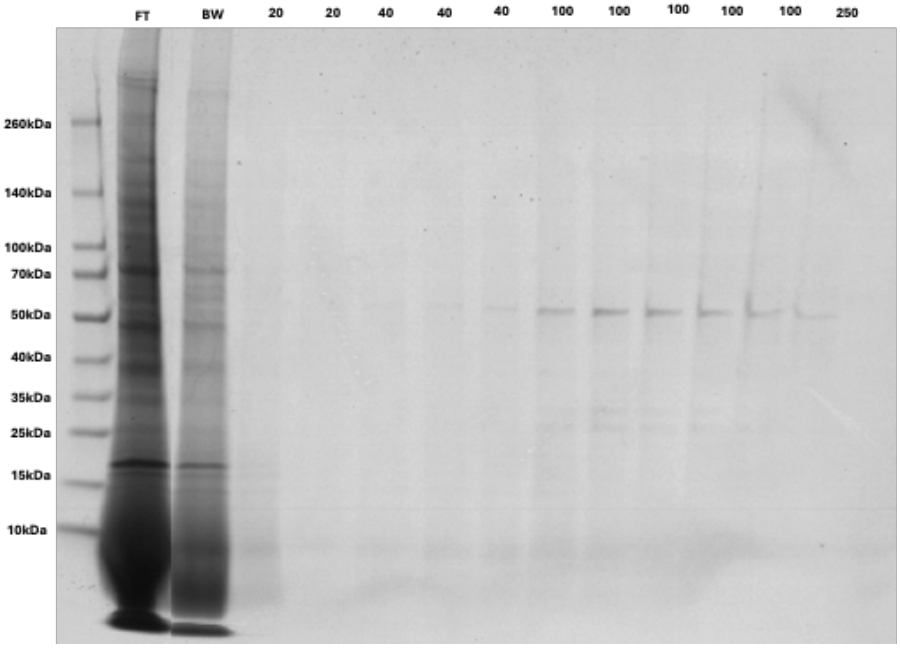


Figure 6.10: SDS-PAGE analysis of an IMAC purification of SMA-solubilised HEK293 membranes expressing CB2. *Flow through from the resin (FT), buffer wash (BW) and elution fractions using stepwise increases in imidazole concentration (20,20,40,40,40,100,100,100,100,100,250) were analysed by on a 4-20% acrylamide gel.*

There were less intense bands at approximately 30 kDa and 27 kDa, expected to be C-terminal fragments of CB2. These were previously visible on Western blot analysis of the binding screen when using Ni-NTA resin. No clear band of the size of monomeric CB2 (43 kDa) was visible. The protein bound to the resin started to elute at 40 mM imidazole concentration, but most protein eluted at 100 mM imidazole concentration. There was no difference in the purity of the elution fractions based on imidazole concentration.

These results suggested that a single IMAC purification allowed the purification of SMA-CB2. One issue identified was the possible presence of C-terminal fragments of CB2, which include both affinity tags. More stringent use of protease inhibitor tablets and ice-cold conditions may prevent CB2 degradation that leads to the presence of fragments.

6.9 Conclusions

The use of a mammalian expression system was able to elucidate new factors which influence how GPCRs can be solubilised and purified by PoLiPa technology. Different polymers and purification techniques can be manipulated to obtain different versions of the same GPCR, which could be useful for glycosylation and oligomerization investigations. GPCRs were expressed without fusion proteins or stabilising mutations. The successful purification of SMA-CB2 showed that amphipathic polymers are appropriate solubilisation agents for typically unstable proteins. However, low yields of purified SMA-GPCR were likely due to the expression restrictions. It was decided that functional analysis of the GPCRs in SMALPs would focus on the *E. coli*-produced GPCRs, due to their less expensive, higher-yielding production.

CHAPTER 7: FUNCTIONAL ASSESSMENT OF SMA-SOLUBILISED GPCRs BY LIGAND BINDING AND MINI-G PROTEIN BINDING

7.1 Introduction

This project aimed to assess whether the GPCRs investigated remained functional within a SMALP. The purpose of a GPCR is to detect a ligand and cause a downstream cell signalling effect through its protein binding partners, most notably, the activation of a G protein. Suspected ligand-binding data was obtained from TFS, FCS and spectral shift assays. Although a more thorough investigation is required to specify affinity constants confidently, this chapter elucidated the benefits and drawbacks of PoLiPa technology for different ligand binding techniques.

Engineered mini-G proteins are versions of the G protein alpha subunit, do not require the beta or gamma subunits to couple to a GPCR (Nehmé *et al*., 2017). Mini-G proteins were used to determine whether the effect of G-protein binding to SMA-solubilised GPCRs. Theoretically, G-protein binding should affect the activation state of a GPCR, typically increasing the affinity between the GPCR and agonist (Yao *et al*., 2009). This chapter began investigations to assess how mini-G proteins affected SMA-solubilised GPCR ligand binding. SMALPs have previously been shown to restrict conformational changes of the GPCR rhodopsin (Grime *et al*., 2021). This chapter aimed to decipher whether SMA-rNTR1 and SMA-CB2 retained functionality. The Mini-G proteins produced and used in this project (Table 7.1) were purified by IMAC (Appendix 1.6). Gsq is an engineered chimera of Gs and Gq which conserves the domains of Gq which interact with GPCRs (Nehmé *et al*., 2017).

Table 7.1: List of Mini-G Proteins used in this Project

Mini-G protein	Size (kDa)	Tags (N-Terminus)
Gs	28.3	-TEV- 6x His tag
Gs-GFP	55.4	-GFP-TEV- 6x His tag
Gs/q chimera	30.6	-TEV- 6x His tag

E. coli expressed SMA-rNTR1 and SMA-CB2 were produced to a high enough yield and purity to functionally characterise. Fluorescent and non-fluorescent agonists and antagonists of NTR1 and CB2 were obtained to assess ligand binding (Table 7.2)

Table 7.2: List of GPCR Ligands used in this Project

Name	GPCR Agonist / Antagonist	Molecular Weight (kDa)	Expected/Quoted Kd/Ki (nM)	Fluorescence	Reference
MK337	NTR1 agonist	1886.3	8.8	Cyanine 5 (Cy5) -like (Ex: 650 nm, Em: 670 nm)	(Keller *et al*., 2020)
MK350	NTR1 agonist	1745.72	~8	Tetramethylrhodamine (TAMRA) (Ex: 552 nm, Em: 578 nm)	(Keller *et al*., 2020)
Neurotensin 8-13	NTR1 agonist	817.0	< 2	N/A	(Schindler *et al*., 2019)
SR 48692	NTR1 antagonist	587.07	2.6	N/A	(Labbé-Jullié *et al*., 1994)
SM15 or Compound 28	CB2 agonist	594.74	130	Dimethylaminopyridine (DMAP) (Ex:420 nm, Em:520 nm)	(Spinelli *et al*., 2020)
VM7	CB2 agonist	570.65	209.4	Nitrobenzofurazan (NBD) (Ex: 488 nm, Em: 530 nm)	(Intranuovo *et al*., 2024)
4Q3CF	CB2 agonist	488.6	8.1	N/A	(Pasquini *et al*., 2011)

FTS analysis of the impure SMA-hNTR1 protein product, pure SMA-rNTR1 and SMA-CB2 were performed to characterise agonist binding. FCS analysis focused on the binding of MK337 to SMA-rNTR1 and the effect of Mini-G inclusion. Spectral shift assays were performed to demonstrate the binding of MK350 and the inhibition of MK350 binding by SR 48692 to SMA-rNTR1. SMA-PAGE was then performed to demonstrate Mini-G protein binding to SMA-rNTR1 and SMA-CB2. These techniques in conjunction were used to determine whether functionality of the SMALP encapsulated GPCRs. One comment to be noted is that most of the experiments in this chapter were only performed once due to the time restraints of the project. This limitation means that the interpretations of the data should be

caveated by the low number of repeats. Despite this, these experiments provided key starting points for the development of ligand binding assays for GPCRs encapsulated in PoLiPas.

7.2 Tryptophan Fluorescence Changes and Ligand Binding to SMA-hNTR1

Tryptophan residues have an intrinsic fluorescence that is excited by light that peaks at approximately 295 nm and emits light that peaks at approximately 340 nm. Tryptophan Fluorescence Spectroscopy (TFS) is a simple sensitive and reliable method of measuring ligand binding interactions, capable of detecting interactions undetected by isothermal titration calorimetry (Sindrewicz *et al*., 2019). The fluorescent properties of tryptophan are sensitive to the polarity of the local environment, ligand interactions and conformational changes. For example, a measurement of tryptophan fluorescence intensity typically decreases upon a decrease in hydrophobicity surrounding the tryptophan residues. This is typically coupled with an increase in peak emission wavelength (bathochromic shift) (Ghisaidoobe and Chung, 2014). Quenching of the fluorescent signal can be due to energy transfer from the aromatic side chain to a quencher, which can be amides in the protein backbone or solvent moieties (Osysko and Muíño, 2011). In this project, TFS was used to demonstrate ligand binding to SMA-solubilised GPCRs.

The hNTR1 primary sequence contains has 6 tryptophan residues. The active structure of hNTR1 (Figure 7.1). has been obtained in a complex with Gi, bound to a pseudo-peptide analogue of neurotensin (Kato *et al*., 2019). Binding of an agonist and subsequent conformational changes should have an effect to the local environments of the tryptophan residues. Three agonists which should bind to in the neurotensin binding pocket were investigated (Figure 7.1).

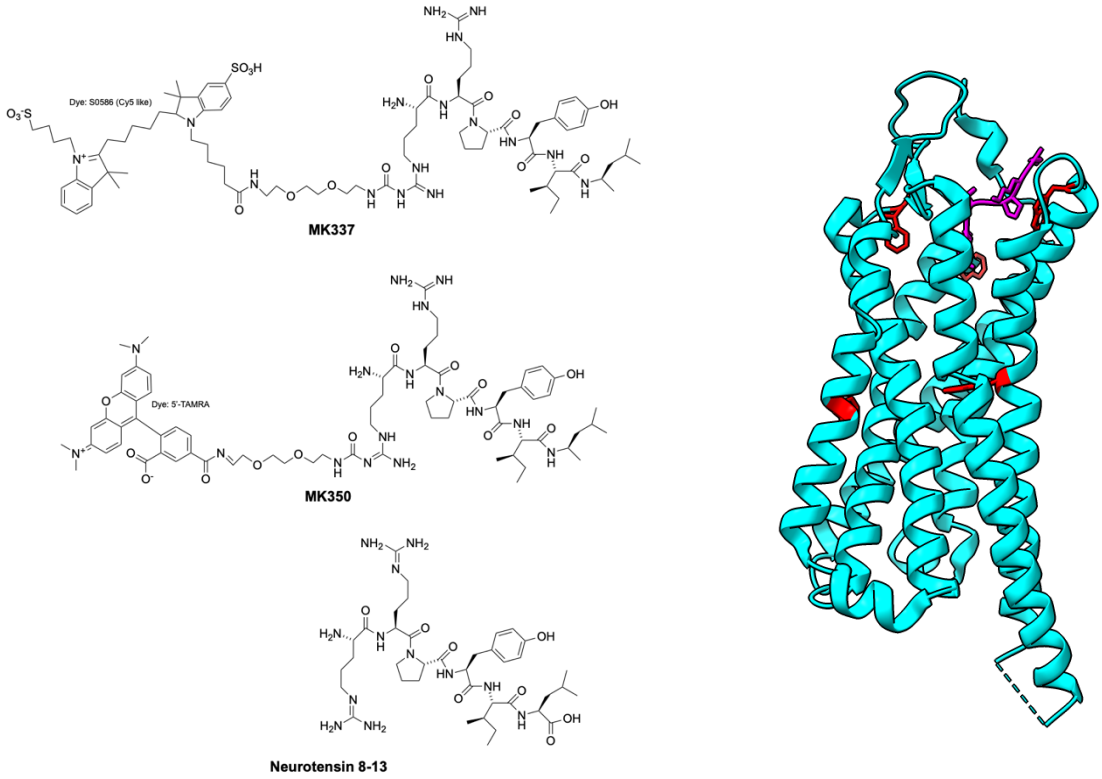


Figure 7.1: Chemical Structure of Neurotensin Receptor 1 agonists used in this project and crystal Structure of agonist-bound hNTR1 with highlighted tryptophan residues in red.
hNTR1 structure (PDB:6os9) solved in complex with Gi1, bound to JMV449 (pink); 6th Tryptophan on C-terminal domain was not modelled in the crystal structure (Kato et al., 2019). Fluorescent NTR1 ligands, MK337 and MK350, were produced and gifted by Max Keller (Keller et al., 2020).

7.2.1 SMA-hNTR1 Protein Titrated Against Fluorescent NTR1 Ligands

It was hypothesised that the fluorescent NTR1 agonists, MK337 and MK350, would bind to SMA-hNTR1. A binding event of the fluorescent ligands are expected to cause increase or decrease in hydrophobicity of the environment tryptophan residues in the binding site. FTS intensity measurements of impure SMA-hNTR1 protein product were taken after the stepwise addition and incubation of fluorescent ligand (MK337 or MK350) (Figure 7.2).

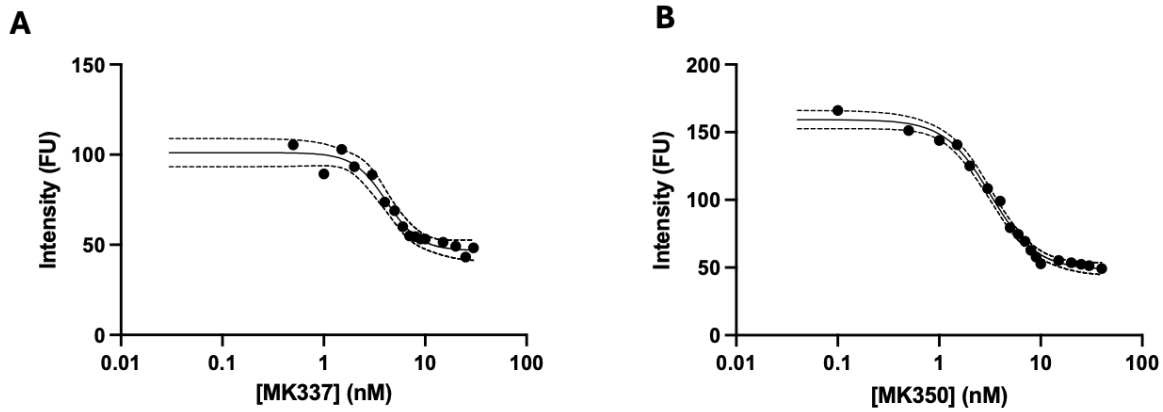


Figure 7.2: Peak intensity from FTS analysis of SMA-hNTR1, expressed in E. coli, titrated with fluorescent agonists.
SMA-hNTR1 sample was measured concentration of 0.2 mg/mL.
(A) Intensity of fluorescence at 340 nm after stepwise titration of MK337 and plotted binding curve with 95% confidence (dotted lines).
(B) Intensity of fluorescence at 340 nm after stepwise titration of MK350 and plotted binding curve with 95% confidence (dotted lines).

Sigmoidal curves characterised the decrease in fluorescence intensity as MK337 or MK350 were added, when plotted against a logarithmic scale (Figure 7.1). These data suggest fluorescent ligand binding and saturation of the binding sites at concentrations higher than 10 nM. The apparent K_d was 4.16 nM for MK337 and 3.20 nM for MK350. This was close to the expected K_d of MK337 (8.8 nM), determined by competitive radioligand binding with Chinese hamster ovary cells expressing hNTR1 (Keller *et al*., 2020). The fluorescent signal after binding saturation was 46% and 30% of the signal before MK337 or MK350 binding, respectively. This suggests a decrease in quantum yield of the tryptophan fluorescence, possibly greater when the ligand included the fluorescent dye TAMRA instead of Cy5.

A decrease in intensity is associated with a decrease in hydrophobicity. The excited state of tryptophan residues is more likely to be quenched by polar molecules. A tryptophan residue in a hydrophobic environment within a protein, will have a higher quantum yield than a tryptophan exposed to a polar solvent (Ghisaidoobe and Chung, 2014). These data suggest that the conformation changes upon binding increase the exposure of the tryptophan residues to a more polar environment. FTS analysis of SMA-A2AR found the opposite effect; partial

agonist binding increased tryptophan fluorescence suggesting a conformation change that produced a less polar local environment to the tryptophan residues (Routledge *et al*., 2020). This illustrates that the position of the tryptophan residues and the conformational changes that occur are ligand and GPCR specific.

The sigmoidal trend and close-to-expected K_d gave strong evidence that the fluorescent NTR1 ligands were binding to the SMA-NTR1 within the impure protein product. The clear sigmoidal trend was suggestive that most of the receptors in the solution bound to the ligands with a similar affinity. This is surprising because uncoupled GPCRs are typically more flexible and can show different binding affinities reflective of 'active' and 'inactive' states; G protein coupling can stabilise a GPCR in a specific conformation (DeVree *et al*., 2016). One explanation for the data is that the SMALP is stabilising hNTR1 in a specific conformation, like a G protein.

Despite the low yield and purity of hNTR1 produced without any fusion proteins or mutations, ligand binding data was collected using this sensitive technique. This advocates for PoLiPa technology for WT GPCRs investigations which are not typically produced for solution-based assays.

7.2.2 Fluorescent NTR1 Ligand Controls

Although the titrating experiment gave strong evidence of binding, control experiments were performed to confirm that the SMA-solubilised contaminants did not cause the reduction of the tryptophan fluorescent signal upon fluorescent ligand addition. An IMAC purification of SMA-solubilised *E. coli* membranes with no recombinant expression was performed to obtain the SMA-solubilised contaminant proteins. The fluorescent ligands were also titrated into

buffer to check that the fluorescent properties of the ligands were not impacting the tryptophan fluorescence measurements, such as causing an inner filter effect (Figure 7.3).

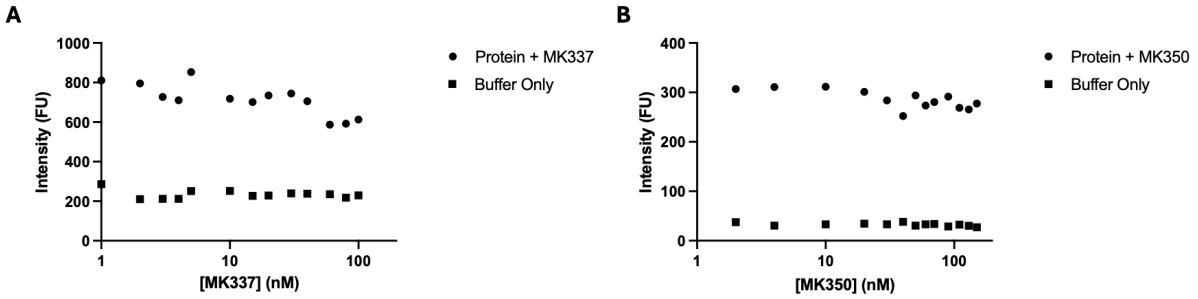


Figure 7.3: Intensity from FTS analysis of SMA-solubilised common IMAC contaminant proteins expressed in E. coli.
SMA-rNTR1 concentration was 0.2 mg/mL.
(A) Intensity of fluorescence at 340 nm after stepwise titration of MK337
(B) Intensity of fluorescence at 340 nm after stepwise titration of MK350.

There was no obvious binding curve in the fluorescent signal that correlated to the addition of the fluorescent ligands to SMA-solubilised *E. coli* proteins (Figure 7.3). This validated previous results and justified that fluorescent ligands were not independently affecting tryptophan fluorescence by inaction with lipids, protein or polymer non-specifically. There was a small decrease in tryptophan fluorescence signal when MK337 was added, however, the intensity remained within 75% of the intensity with no MK337 in the solution. When the buffer was analysed, the intensities were low due to the lack of tryptophans in the cuvette, this showed minimal fluctuation upon the addition of MK337 or MK350. This is expected because the excitation and emission wavelengths of MK337 and MK350 are over 200 nm longer than tryptophan fluorescence excitation or emission wavelengths.

These controls provided confidence that a large decrease in tryptophan fluorescence intensity that plateaus is likely due to binding events.

7.2.3 Anisotropy Changes of Tryptophan Fluorescence in SMA-Solubilised hNTR1 Protein Titrated Against NTR1 Agonists

To further validate the suspected binding of MK337 and MK350 to the hNTR1, anisotropy measurements were taken to assess how the rotational freedom of the tryptophan residues were altered by the NTR1 agonists. It was hypothesised that the binding of an NTR1 agonist to hNTR1 would restrict the rotation of the tryptophan residues, causing a polarisation of the fluorescence emission and an increase in anisotropy.

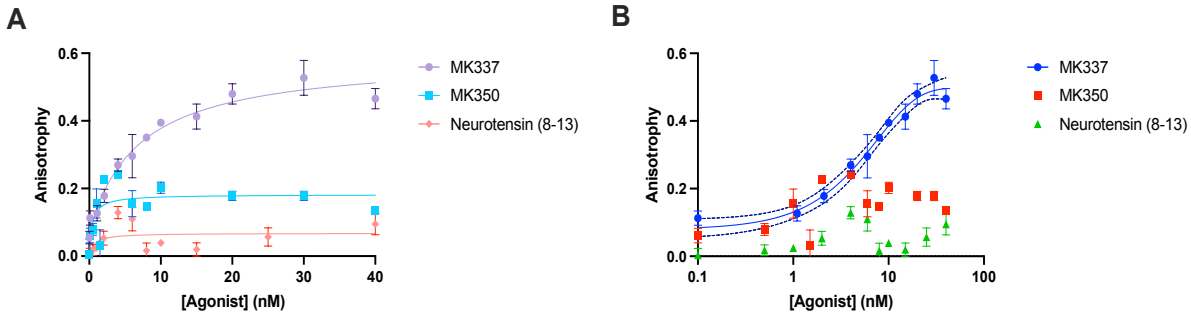


Figure 7.4: Fluorescence Anisotropy measurements taken from FTS analysis of SMA-hNTR1, expressed in E. coli after titration of NTR1 agonists (MK337, MK350 or Neurotensin 8-13).
SMA-hNTR1 sample was measured concentration of 0.2 mg/mL. Measurements were taken three times on the same sample and error bars show standard deviation between measurements
(A) Linear Scale.
(B) Logarithmic Scale- dotted lines show 95% confidence level of plotted binding curve.

Figure 7.4 shows the relationship between anisotropy the concentration of NTR1 agonist: MK337 caused a large increase in anisotropy that plateaued, likely due to saturation of the neurotensin binding sites. The sigmoidal curve in Figure 7.4B showed an apparent K_d of 5.87 nM: close to the apparent K_d derived from the FTS intensity decrease. The titration of MK350 also increased the anisotropy but less than MK337. This suggests that the TAMRA fluorophore in MK350 had a different interaction with hNTR1, reducing the rotational freedom of the tryptophan residues less than Cy5-like fluorophore in MK337.

The titration of neurotensin (8-13) caused a small change in anisotropy that could not be used to confirm or deny binding. One explanation is that the fluorophores within MK337 and MK350 had a larger influence on the rotational freedom of the tryptophan residues upon binding compared to the binding event itself. Routledge *et al* (2020) also demonstrated an anisotropy increase upon ligand binding to SMA-A2AR. They suggested that this was more likely due to reduced steric freedom of the tryptophan residues within A2AR upon binding instead of overall tumbling of the SMA-A2AR.

Overall, this data provided more confidence in the FTS results due to the consistency of binding affinity between the two measurements. Due to the expression purification issues of hNTR1, further ligand binding experiments were focused on the purified rNTR1 and CB2 (Chapters 4 and 5).

7.3 Tryptophan Fluorescence Changes and Ligand Binding to SMA-rNTR1

In this project, rNTR1 contained 16 tryptophan residues: 6 within the GPCR, 2 within Thioredoxin A and 8 within MBP. Within rNTR1, the tryptophan residue W339 is directly involved in agonist binding and the mutation W321A increases neurotensin binding affinity (Deluigi *et al*., 2021). Analysis of the structures of neurotensin-bound and antagonist-bound rNTR1 (Figure 7.5) suggested conformational changes that are likely to change the environment of the tryptophan residues (Deluigi *et al*., 2021; White *et al*., 2012).

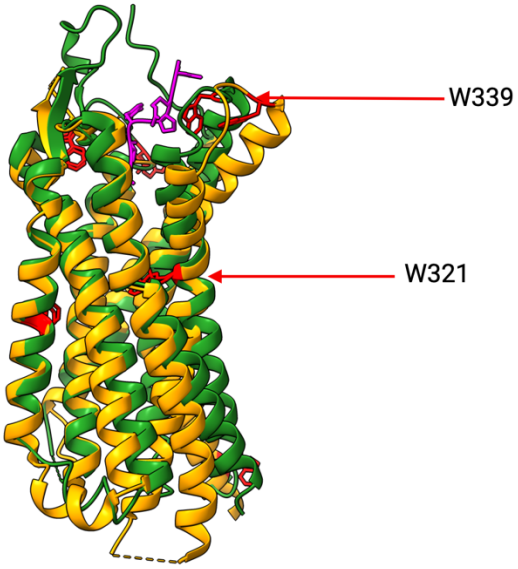


Figure 7.5: Crystal Structures of agonist and antagonist bound rNTR1 variants.
Agonist (Neurotensin 8-13-shown in pink) bound rNTR1 variant incorporated lysozyme into its structure for stability (Orange, PDB: 4grv). (White et al., 2012) Antagonist (SR 48692) bound variant incorporated H4bmx into its structure for stability (Green, PDB:6z4S) (Deluigi et al., 2021). These stabilising additions were hidden for this comparison. Red residues show position of tryptophan residues. Arrows point out two tryptophan residues that may interact with Neurotensin 8-13 (shown in pink).

7.3.3 SMA-rNTR1 Titrated Against Fluorescent MK337 Ligand and Effect of Gsq Incubation

Mini-Gsq has been shown to bind to rNTR1, increasing its thermostability (Nehmé *et al*., 2017). To understand how binding capabilities of SMA-rNTR1 are influenced by the formation of a complex with Gsq, spectra measuring the intrinsic tryptophan fluorescence emission were taken after rNTR1 was incubated with Gsq for four hours. MK337 was titrated into a cuvette with purified SMA-rNTR1 with and without Gsq. It should be noted that Gsq has three tryptophan residues. MK337 should bind to rNTR1, causing a conformational change that may also affect Gsq; changes in environment of Gsq tryptophan residues would also contribute to changes in FTS spectra. A decrease in tryptophan fluorescence intensity was expected to reflect the data collected from SMA-hNTR1.

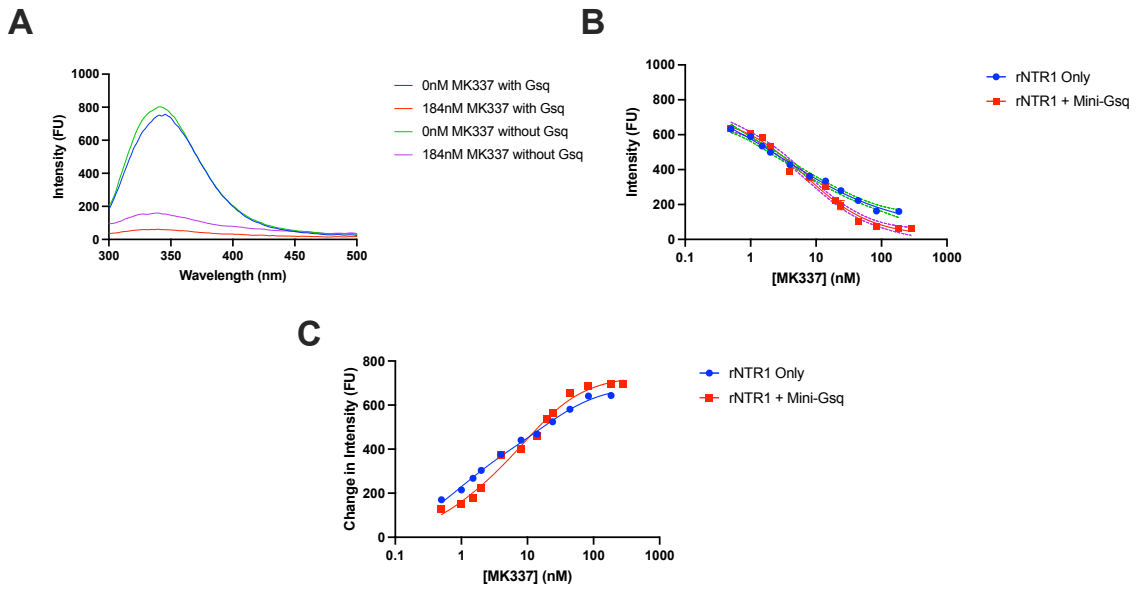


Figure 7.6: FTS analysis of SMA-rNTR1 expressed in E. coli with and without incubation with Gsq for 4 hours.
SMA-rNTR1 and Gsq concentration was 0.2 mg/mL.
(A) Fluorescence emission Spectra after excitations at a 295 nm wavelength before any addition of MK337 and after the addition of 184 nM MK337.
(B) MK337 Binding curves derived from the peak fluorescence intensity after stepwise titration of MK337. Dotted lines represent 95% confidence of the plotted binding curve. SMA-rNTR1 (R^2=0.9882) and SMA-rNTR1 incubated with Gsq (R^2=0.9870).
(C) MK337 Binding curves derived from the change peak fluorescence intensity using two affinity site model. SMA-rNTR1 (R^2=0.9971) and SMA-rNTR1 incubated with Gsq (R^2=0.9906).

Firstly, intrinsic fluorescence spectra of rNTR1 alone and rNTR1 plus Gsq were compared. (Figure 7.6A). A bathochromic shift in maximum wavelength was observed suggesting either the tryptophan residues in Gsq have a different maximum fluorescence wavelength that influences the spectrum of the complex or the formation of the complex alters the spectra of tryptophan residues in Gsq and/or rNTR1. Next the fluorescent changes that occur upon ligand binding to the complex or the GPCR alone were explored. As expected, fluorescence intensity decreased significantly upon binding of ligand to GPCR alone (80%). When Gsq was present, this change increased further (92%) possible due to the contribution of the tryptophan residues within Gsq or an altered rNTR1 response to ligand caused by Gsq. The binding curves in Figure 7.6B gave an apparent K_d of 3.2 nM without Gsq and 6.7 nM with Gsq, which were deemed acceptably close to the expected K_d of MK337 (8 nM) to validate binding.

The small decrease in affinity after Gsq incubation was unexpected as G proteins typically increase a GPCRs affinity for an agonist (Yao *et al*., 2009). Radioactive neurotensin binding data on crude *E. coli* membranes containing MBP-fused rNTR1 reported possible low- and high- affinity states of the receptor (Grisshammer and Hermans, 2001). A two-site competitive binding curve was also fitted to the FTS data and provided a better goodness of fit (Figure 7.6C). Possible low- and high- affinity states were defined (Table 7.3). Mini-Gsq seemingly caused a 2-fold decrease of the low affinity state $K_{d.}$ There was also a possible percentage decrease in fraction of receptors in the high-affinity state after Gsq incubation. This opposed the Grisshammer and Hermans (2001) data showed the fusion of Gq to the c-terminus of the rNTR1 appeared to increase the number percentage of receptors in this proposed higher affinity state and increase the affinity of the higher affinity state. The difference could be associated with the fusion of Gq directly to the receptor or effect of the SMALP.

Table 7.3: Values Derived from two-site Competitive Binding Curve fitted to MK337 SMA-rNTR1 FTS Intensity data

	SMA-hNTR1 only	**SMA-rNTR1 + Gsq**
Kd- Low affinity State (nM)	22.5	11.6
Kd- High affinity State (nM)	0.78	0.93
High affinity State proportion (%)	55.80	32.17

Both binding curves fitted the data well with and without G protein (R^2 >0.987). Triplicate repeats would validate the two binding affinity state model and determine if the effects of Mini-Gq to SMA-rNTR1 binding were significant.

7.4 Tryptophan Fluorescence Changes and Ligand Binding to SMA-CB2

Three agonists were used to investigate SMA-CB2 binding by FTS (Figure 7.7). The *E. coli*-expressed CB2 has 16 tryptophan residues: 8 within the GPCR and 8 within the MBP fusion. The crystal structures of CB2 in an active (bound to an agonist and Gi) and an inactive state (bound to an antagonist) show movement of tryptophan residues: two residues (W194, W258) appear to have direct interaction with the agonist, WIN 55212-2 (Figure 7.7) (Xing *et al*., 2020; Li *et al*., 2019). Changes in FTS spectroscopy data were used to demonstrate conformational changes within CB2 upon ligand binding.

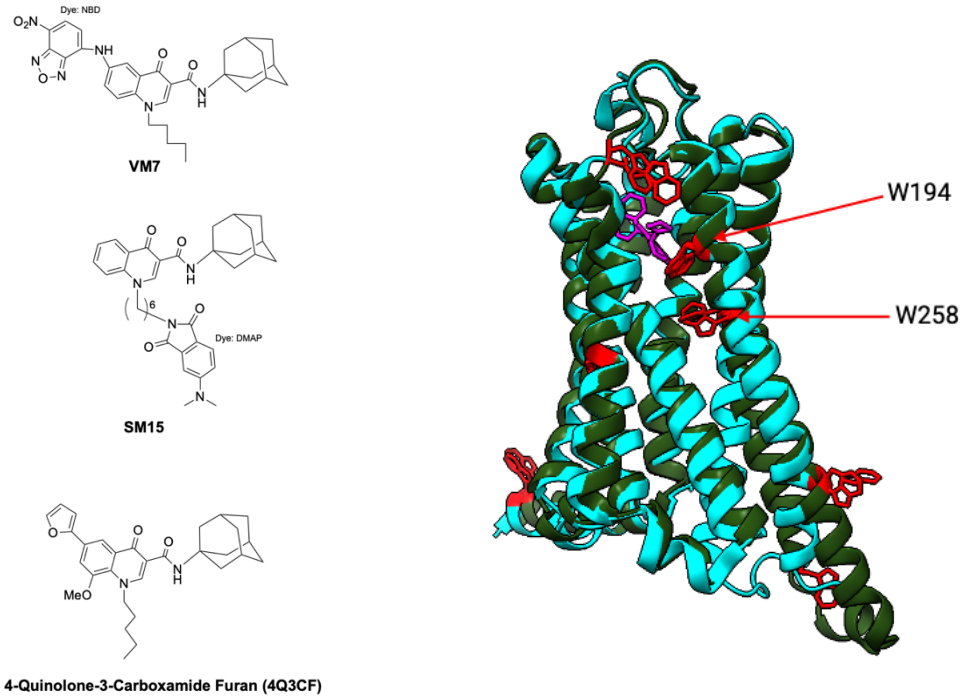


Figure 7.7: Chemical Structures of Fluorescent CB2 agonists used in this project and Crystal Structures of agonist and antagonist bound CB2 variants.
Fluorescent Ligands (left) were produced and gifted from Marialessandra Cortino's Lab (Intranuovo et al., 2024; Spinelli et al., 2020).
Agonist (WIN 55212-2) bound CB2 variant in complex with Gi (CB2 in green, PDB:6pt0) (Xing et al., 2020). Antagonist (AM10257) bound CB2 variant incorporated lysozyme into the sequence for stability (CB2 in light blue, PDB: 5zty) (Li et al., 2019). Tryptophan residues in red. Arrows point out two tryptophan residues (W194, W258) that have a direct interaction with agonist WIN 55212-2 (shown in pink) in the active structure.

7.4.4 FTS Analysis of SMA-CB2 Titrated Against SM15

The fluorescent CB2 agonist SM15 is displaced from CB2 by WIN 55212-2, suggesting SM15 binds in the same pocket, which was validated by molecular docking simulations (Spinelli *et al*., 2020). The molecular docking simulation suggested a direct interaction and movement of a tryptophan residue (W258). It was therefore hypothesised that SM15 would have a large effect on the environment of the tryptophan residues within SMA-CB2.

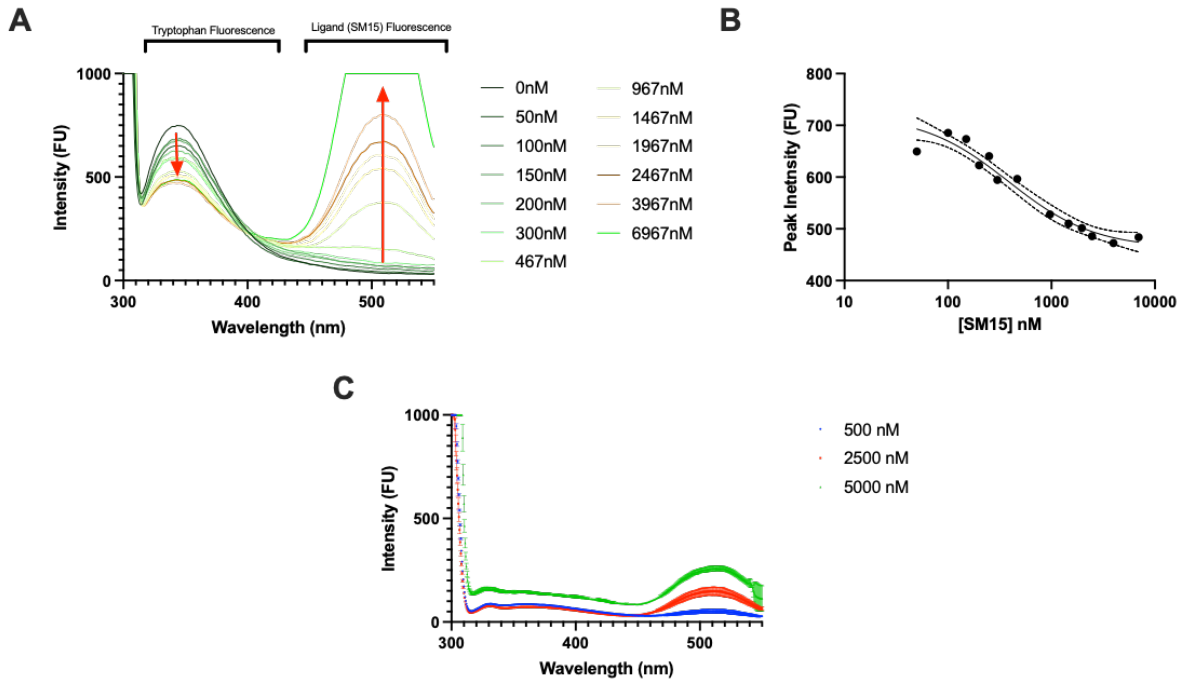


Figure 7.7: FTS analysis of SMA-CB2 expressed in E. coli. SMA-CB2 concentration was 0.2 mg/mL.
(A) Fluorescence emission spectra after excitations at a 295 nm wavelength after stepwise titration of SM15. Red arrows indicate the direction of peaks moved as SM15 was titrated.
(B) Binding curves derived from the peak fluorescence intensity between 300-400 nm after stepwise titration of SM15. Dotted lines show 95% confidence bands.
(C) FTS analysis of SM15 alone at three different concentrations. Measurements were taken three times on the same sample. Error Bars show SD between measurements.

SM15 has a fluorescence with emission that peaks at 520 nm. It should also be noted that excitation of SM15 below optimal excitation wavelength can lead to fluorescence emission (particularly at high concentrations of SM15). Hence, excitation of tryptophan residues at 295 nm can generate ligand emission. This occurred to a smaller extent when SM15 was excited at 295 nm without protein (Figure 7.8C). One explanation is Fluorescence resonance energy transfer (FRET) between tryptophan fluorescence emission and SM15 excitation: the transfer

of energy from an excited electron in the tryptophan residue could have enabled the excitation of an electron in the DMAP dye within SM15. Validation of FRET would confirm that the SM15 and CB2 are within 10-100 Å (Wu and Brand, 1994).

There was a 36% decrease in the peak intensity of the tryptophan fluorescence as SM15 was titrated into the SMA-CB2 sample. This may be due to changes in the tryptophan environment or transfer of the energy to SM15 due to FRET. Plotting the fluorescence intensity produced a sigmoidal curve; the apparent K_d was 385.5 nM. This was over 200 nM larger that than the K_i quoted from competitive radioligand binding assays on HEK293 cells expressing CB2 (Spinelli *et al*., 2020). Possible explanations include possible adsorption and degradation of SM15, differences between the binding assays and differences in the lipid environment of the CB2. The calculated K_d was deemed close enough to the expected K_d to suggest that these changes in tryptophan fluorescence were likely due to ligand binding.

7.4.5 FTS Analysis of SMA-CB2 Titrated Against VM7 and Effect of Gs Incubation

The CB2 ligand VM7 was also titrated into SMA-CB2. VM7 has a similar base structure to SM15, but a different fluorophore is linked to a different site on the molecule. Molecular docking simulations did not suggest a direct interaction with a tryptophan residue in the top score docking pose (Intranuovo *et al*., 2024). It was expected that ligand binding would cause a conformation change that would have a large effect on the environment of the tryptophan residues.

A sample of SMA-CB2 was incubated with Gs for 4 hours to understand if VM7 would have a different effect on the tryptophan residues in the SMA-CB2: Gs complex. CB2 has been most reported to activate the Gi/o class of G protein, however, Saroz *et al* reported coupling to

Gs in leukocytes (Saroz *et al*., 2019). There is also some evidence that CB2 can couple to Gq when ligands were administered intracellularly suggesting Gsq coupled CB2 was in endolysosomes (Brailoiu *et al*., 2014). It was decided to test if Gs would affect the ligand binding characteristics of VM7 by FTS analysis of SMA-CB2 (Figure 7.9).

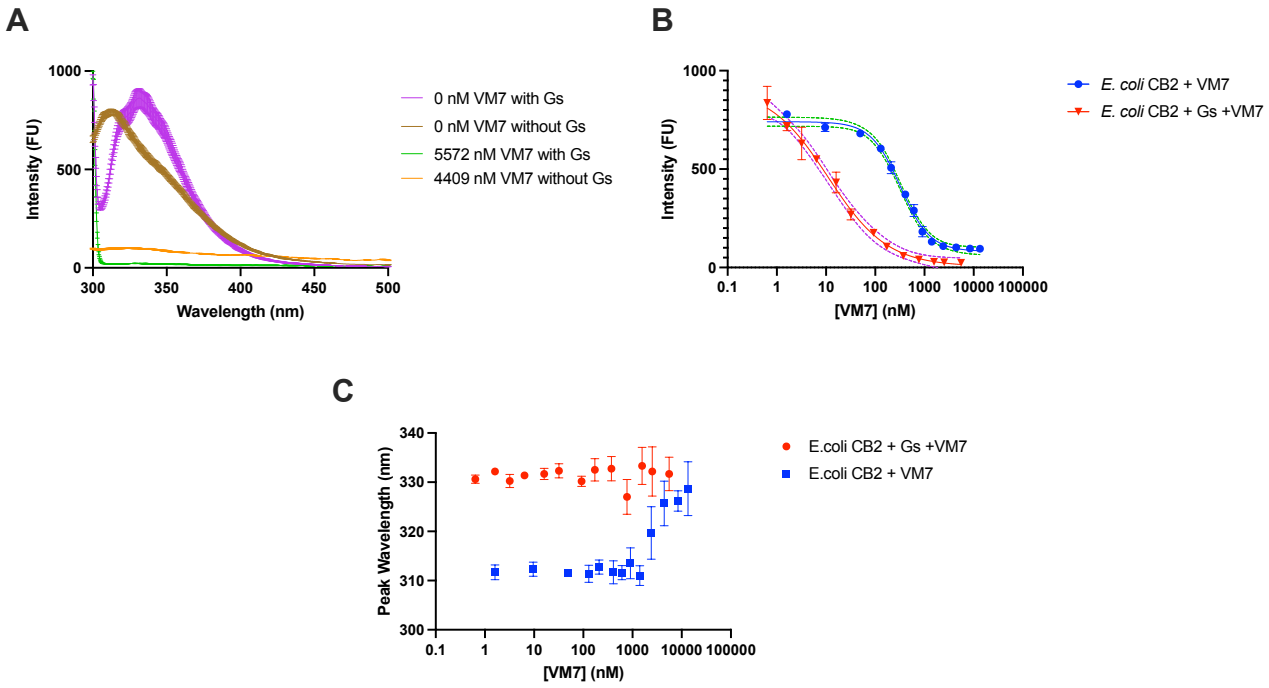


Figure 7.9: FTS analysis of SMA-CB2 expressed in E. coli. with and without incubation with Gs for 4 hours.
SMA-CB2 and Gs concentration was 0.2 mg/mL. Measurements were taken three times on the same sample and error bars show standard deviation between measurements.
(A) Fluorescence emission Spectra after excitations at a 295 nm wavelength before any addition of VM7 and after the addition of over 4000 nM VM7.
(B) Binding curves derived from the peak fluorescence intensity after stepwise titration of VM7
(C) Wavelength at which emission spectra was at its peak intensity (peak wavelength) after stepwise titration of VM7. Dotted lines show 95% confidence bands.

Before VM7 was added, there was a notable difference in peak emission wavelength when comparing the SMA-CB2 with and without Gs. Peak wavelength without Gs is 20 nm lower than SMA-CB2 only. This shift could be due to the more hydrophobic environment associated with coupling of CB2 to Gs or due to the contribution of tryptophan residues within the Gs protein, which may have a less hydrophobic environment than the tryptophan residues in SMA-CB2. Alternatively, the conformational state of the CB2 could be different when coupled to Gs, causing a more hydrophobic environment for the tryptophan residues. Figure

7.9C shows concentrations of VM7 greater than 1000 nM caused a bathochromic shift. This suggests evidence of a conformational change to a state more like Gs-coupled CB2.

The binding of VM7 caused a larger decrease in tryptophan fluorescent intensity than SM15: an 88% decrease without Gs and a 97% decrease with Gs. Tryptophan residues within the Gs protein may have accounted for the higher intensity before VM7 was added and the lower intensity after the VM7 titration. This may be caused by a conformational change in the Gs protein. Without Gs, plotting peak intensity produced a binding curve with an apparent K_d of 324.5 nM. This is over 100 nM higher than the K_i calculated from a radioligand competition assay performed on CB2 expressing HEK293 membranes (Intranuovo *et al*., 2024). This was deemed to be within a suitable range. The binding curve of VM7 titrated against SMA-CB2 with Gs showed different characteristics and a calculated K_d of 11.04 nM. This suggested the interaction between VM7 and a SMA-CB2: Gs complex had a higher affinity than the interaction between VM7 and SMA-CB2. This suggested Gs changed the conformation of CB2, which made it more sensitive to VM7 binding.

These data provided strong evidence that CB2 maintained functionality within an SMALP. The TFS experiment suggested conformational changes caused by both Gs and VM7. There was evidence of VM7 binding affecting Gs-coupled CB2 and evidence of Gs affecting VM7 binding.

7.4.6 FTS Analysis of SMA-CB2 Expressed in E. coli Titrated Against 4Q3CF

The fluorescent CB2 ligands are relatively novel. To validate the FTS experiments, a non-fluorescent CB2 agonist was titrated into SMA-CB2. 4Q3CF is an agonist of CB2, found to have a K_i of 8.5 nM calculated from competitive binding assays on CB2-expressing HEK293 membranes (Pasquini *et al*., 2011).

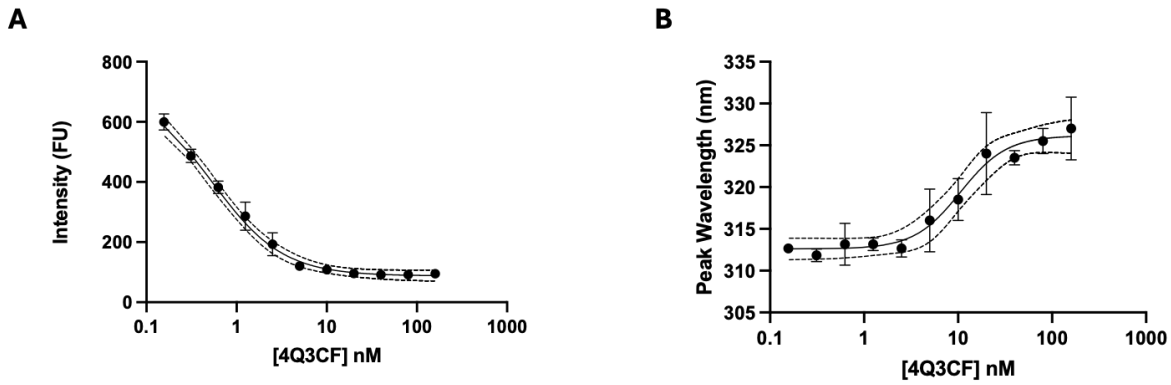


Figure 7.8: FTS analysis of SMA-CB2 expressed in E. coli, titrated with CB2 agonist 4Q3CF.
SMA-CB2 concentration was 0.2 mg/mL. Measurements were taken three times on the same sample and error bars show standard deviation between measurements.
(A) Binding curve derived from the peak fluorescence intensity after stepwise titration of 4Q3CF
(B) Wavelength at which emission spectra was at its peak intensity (peak wavelength) after stepwise titration of 4Q3CF. Dotted lines show 95% confidence bands.

Plotting the peak intensity of the tryptophan fluorescence at each 4Q3CF concentration showed a decrease in intensity, which plateaued at approximately 10 nM (Figure 7.10A). This could be indicative of conformational changes due to 4Q3CF binding. The calculated K_d of 0.53 nM suggested high affinity binding. A dose-dependent bathochromic shift may have suggested a conformational change due to 4Q3CF binding, producing a K_d of 10.58 nM (Figure 7.10B). Tryptophan fluorescence decreases and bathochromic shifts are typically due to an electronic absorption state in a more polar environment.

These data suggested high affinity binding of the non-fluorescent 4Q3CF ligand. The affinity of 4Q3CF for SMA-CB2 expressed in *E. coli* was suggested to be between 0.5-11 nM based on intensity and wavelength measurements. The expected K_d of 8.5 nM (Table 7.2) supported the demonstration of 4Q3CF binding. This non-fluorescent agonist data supported the VM7 and SM15 binding data, which was expected given the similar structure of the ligands.

7.5 Fluorescence Correlation Spectroscopy (FCS)

FCS is an exciting tool which utilises the principles of Brownian motion to decipher the diffusion rate of a fluorescent particle (Yu *et al.*, 2021). The binding of fluorescent ligands can

be characterised by FCS because the diffusion rate of a free ligand should be much faster than the diffusion rate of a bound ligand, as illustrated in Figure 7.11. The fluctuations in the fluorescent signal monitored by a confocal microscope can be used to obtain a correlation curve (Yu *et al*., 2021). This data can be used to model a situation in which one or two fluorescent particles are in solution. This can be used to determine whether the concentration of bound and free ligands. The experiments in this project utilised the fluorescent ligand MK337 to characterise binding to SMA-rNTR1. This technique has previously been used to measure binding to SMA-solubilised A2AR (Grime *et al*., 2020). This project aimed to understand the benefits and limitations of FCS for SMA-rNTR1 binding characterisation and utilised FCS to understand the effect of Mini-G protein binding.

The fluorescent ligand, MK337, has not previously been used in FCS experiments. A series of characterisation experiments were performed to determine the suitability of MK337 for FCS and to understand the appropriate buffer and laser power for binding experiments (Appendix 1.7-1.9

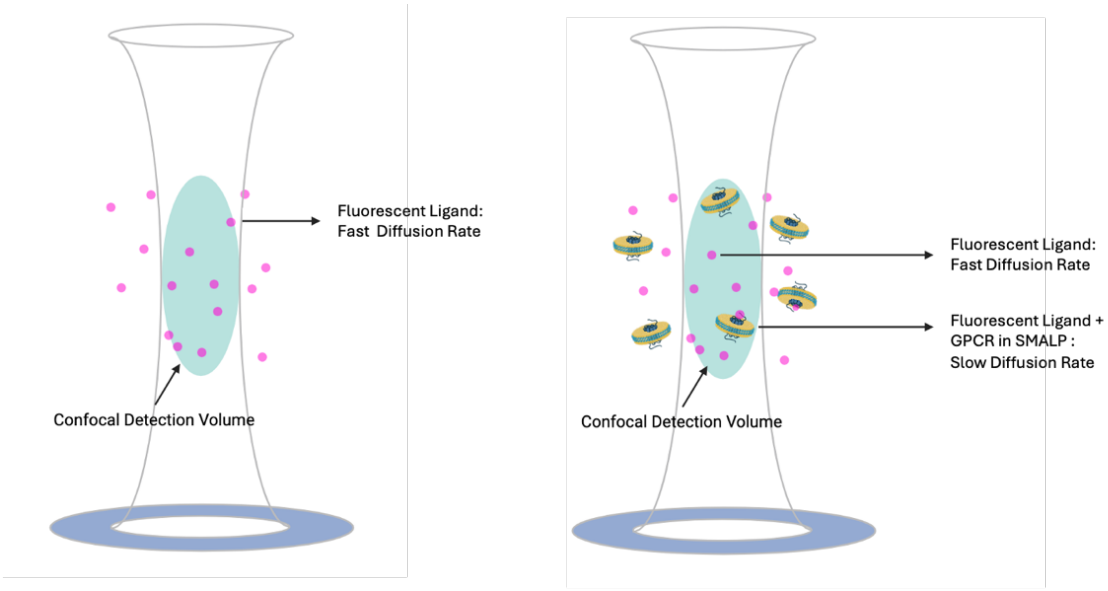


Figure 7.9: Cartoon displaying the principle of how solution-based FCS can detect ligand binding.
A confocal microscope detects fluctuations caused by the movement of fluorescent particles through the confocal detection volume. The diffusion rate of the fluorescent particle is related to its size, which is different depending on whether the fluorescent ligand is free or bound.

7.5.4 MK337 Series Binding Experiment Comparing SMA-rNTR1, SMA-CB2 and SMA-SAV With and Without SR 48692

The difference in the concentration of bound MK337 with and without the competitive antagonist SR 48692 should show specific MK337 binding. SR 48692 binds in the same binding pocket as neurotensin and therefore should prevent MK337 binding (Deluigi *et al.*, 2021). Firstly, SR 48692 was incubated with MK337 to check that the presence of the antagonist did not affect the fluorescence of the ligand. There was no significant difference in the measured concentration of MK337 with and without SR 48692 (Appendix 1.10). Then, SR 48692 was incubated with SMA-rNTR1, SMA-CB2 or SMA-SAV, followed by incubation with a series of MK337 concentrations. It was hypothesised that the concentration of MK337 bound to SMA-rNTR1 would increase with added MK337 concentration and that this increase would be less after pre-incubation with SR 48692. It was also hypothesised that SR 48692

would not affect the concentration of MK337 bound to SMA-CB2 or SMA-SAV due to the lack of a neurotensin binding pocket in these proteins.

Figure 7.12A shows how the concentration of MK337 bound to SMA-rNTR1 increased as the concentration of MK337 increased. There was a much smaller increase when the SMA-rNTR1 was pre-incubated with the antagonist. Both repeats had a larger concentration of bound MK337 when 125 nM and 67.25 nM were used compared to the antagonist pre-incubated sample.

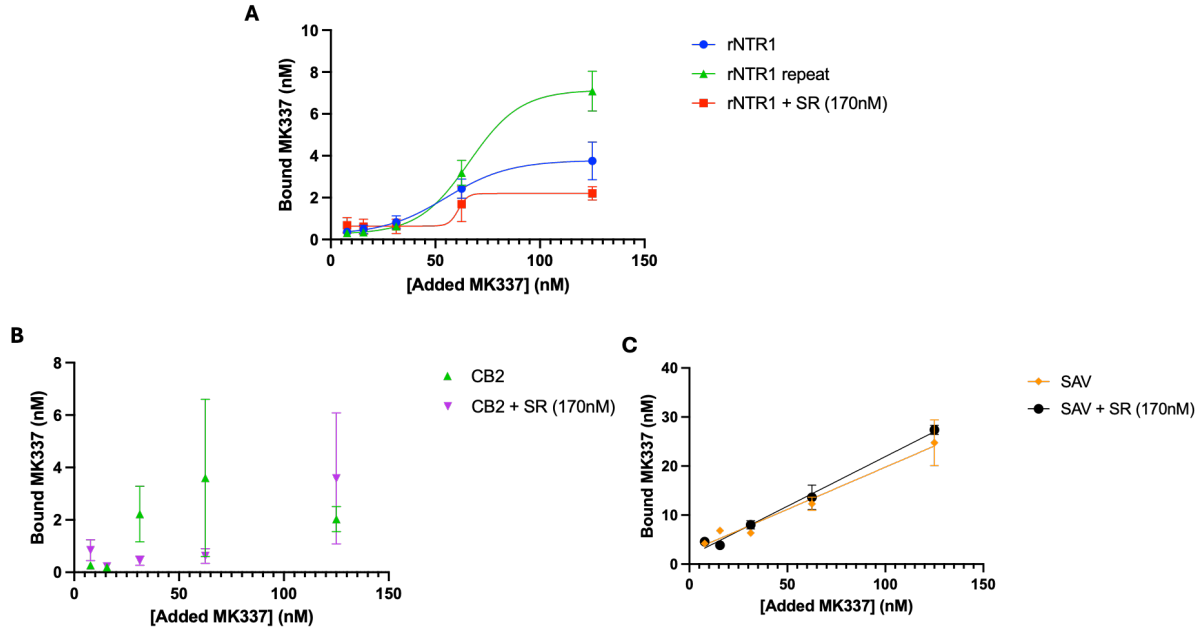


Figure 7.10: FCS analysis of MK337 binding to SMA-rNTR1, SMA-CB2 or SMA-SAV
Concentration of bound MK337 calculated from a 2-component model after solution-based FCS analysis of five different MK337 (7.8nM – 125nM) concentrations incubated with SMA-solubilised proteins, with and without pre-incubation with 170 nM SR 48692 (SR). SMA-rNTR1 concentration was 0.2 mg/mL. Measurements of the same sample were taken and input into the model three times and error bars show standard deviation between measurements.
(A) MK337 bound to SMA-rNTR1
(B) MK337 bound to SMA-CB2
(C) MK337 bound to SMA-SAV.

Two SMA-solubilised membrane proteins were used as controls. Neither CB2 nor SAV showed evidence of specific binding which increased with added MK337 concentration. Figure 7.12B shows the concentration of MK337 bound to SMA-CB2, the two-component model yielded variable concentrations of bound MK337 and the highest MK337

concentration had less bound protein than after SR 48692 incubation. Figure 7.12C shows a linear relationship between added MK337, and the concentration bound to SMA-solubilised SAV. The same linear relationship was reflected after SR 48692 incubation suggesting all the MK337 bound non-specifically. This demonstrated that the amount of non-specific binding is related to the protein: after 125 nM of MK337 was added, SAV had >8-fold more non-specific binding compared to CB2 or rNTR1.

Overall, the data provided a measure of specific binding: [bound MK337] – [bound MK337 after antagonist pre-incubation]. There was an increase in specific binding to SMA-rNTR1 that was related to the added MK337 concentration. This was able to produce binding curves that suggested the K_d was 60.6 nM (n=2). Accounting for the decrease in concentration due to adsorption, this yielded an estimated K_d of 9.7 nM. A larger number of MK337 concentrations and repeats would provide a better K_d estimation. The use of two control proteins verified SR 46892 was able to distinguish specific binding.

7.5.5 Specific MK337 binding to SMA-rNTR1 Incubated with Gs or Gsq

It was decided to investigate if the addition of a mini-G protein would influence the concentration of MK337 bound to SMA-rNTR1. Gsq has been shown to couple to NTR1 by thermostability analysis but no coupling of Gs to rNTR1 was proven by this method (Nehmé *et al*., 2017). NTR1 is a promiscuous GPCR that can couple to multiple G protein subtypes; however it is most predominately associated with Gq-coupling (Kato *et al*., 2019). This experiment aimed to understand how incubation with mini-G proteins for 4 hours influenced the specific binding of MK337 to SMA-rNTR1.

Figure 7.13 (A and B) shows the relationship between bound MK337 and added MK337 with and without pre-incubation with SR 48692. When Gsq and SMA-rNTR1 were incubated, there was a specific binding increase that correlated with the concentration of MK337 added when 125 nM of MK337 was added. This was larger than when Gsq was not included. When Gs and SMA-rNTR1 were incubated there was no evidence of specific binding. There was an increase in the amount of non-specific binding when a concentration of 125 nM MK337 was added. This could indicate an interaction between Gs and MK337.

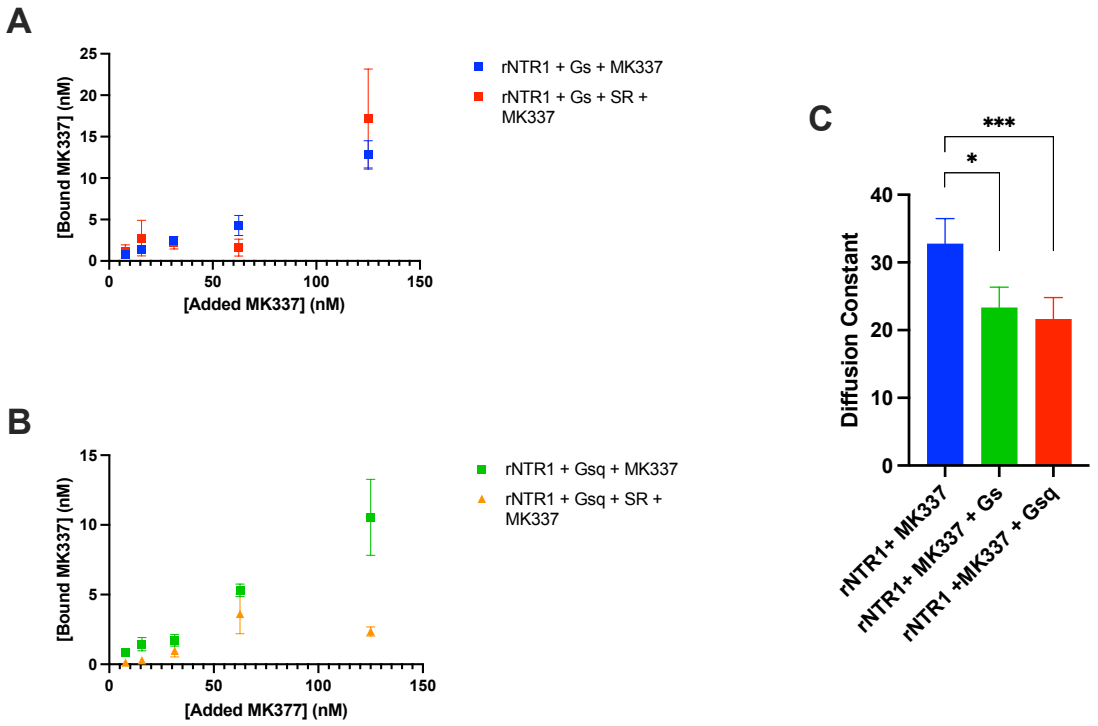


Figure 7.11: FCS analysis of MK337 binding to SMA-rNTR1 incubated with Mini-G proteins
(A and B) Concentration of bound MK337 calculated from a 2-component model after solution-based FCS analysis of five different MK337 (7.8nM – 125nM) concentrations incubated with SMA-rNTR1- Mini G, with and without pre-incubation with 170 nM SR 48692 (SR). SMA-rNTR1, Gs and Gsq concentration was 0.2 mg/mL after incubation.
(A) SMA-rNTR1 incubated with Gsq 4 hours before any ligand addition. Measurements of the same sample were taken and input into the model three times and error bars show standard deviation between measurements
(B) SMA-rNTR1 incubated with Gs 4 hours before any ligand. Measurements of the same sample were taken and input into the model three times and error bars show standard deviation between measurements
(C) Average diffusion rate of bound MK337 component from all MK337 concentrations without any antagonist. Student's t test was performed to determine significance (=p<0.05, *** =p < 0.0005). Error Bars represent SD (n=5).*

Figure 7.13C shows the average diffusion rates obtained from the two component models produced without competitive inhibition of SR 48692. The larger the diffusion rate the smaller the size of the particle. There was a significant decrease in the diffusion rate of the bound MK337 particles after Gsq incubation ($p<0.0005$). This provided evidence of SMA-rNTR1-

Gsq coupled particle binding to MK337, which is larger than uncoupled SMA-rNTR1. There was also a significant difference between the diffusion rate of MK337 bound SMA-rNTR1 and MK337 bound SMA-rNTR1 incubated with Gs ($p<0.05$). This indicated interactions occurred between both mini-G proteins and SMA-rNTR1.

7.5.6 Key findings of FCS Experiments

Overall, FCS experiments were able to confirm binding of the fluorescent ligand MK337 to SMA-rNTR1. There was an increase in binding caused by Gsq incubation and a decrease in binding caused by Gs incubation. This is consistent with the findings of the Nehma *et al* (2017).

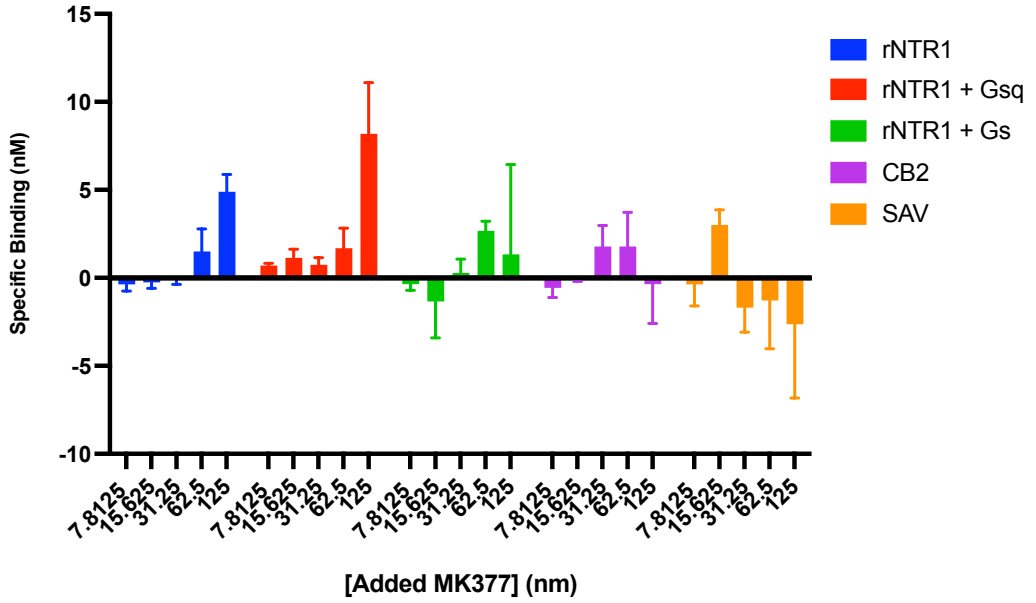


Figure 7.12: Specific binding of MK337 to a neurotensin binding site calculated from FCS analysis.
Specific Binding calculated from 2-component models after solution-based FCS analysis, with and without pre-incubation with 170 nM SR 48692 (SR). Five different MK337 (7.8nM – 125nM) concentrations incubated with SMA-solubilised proteins including SMA-rNTR1 pre-incubated with Gs or Gsq for four hours. SMA-rNTR1, Gs and Gsq concentration was 0.2 mg/mL. Measurements of the same sample were taken and input into the model three times and error bars show standard deviation between measurements. For alone rNTR1 (n=2) and graph shows mean ± SD of 6 measurements.

Figure 7.14 summarises the amount of specific binding at each added MK337 concentration. This distinguishes the difference in binding between the SMA-solubilised control proteins and SMA-rNTR1, as well as the effect of coupling mini-G proteins. More MK337 concentrations should be tested to obtain accurate K_d values. However, this project has demonstrated how FCS is a powerful tool for investigating GPCR function.

7.6 Spectral Shift Assays

A key element of this project was to assess ligand binding methods used by industrial partner Domainex, such as spectral shift assays. A spectral shift assay was performed to monitor changes in fluorescence of a dye used to label SMA-rNTR1, as a measure of ligand binding. The SMA-rNTR1 was labelled with a fluorescent Nanotemper Red-NTA dye. This dye binds non-covalently to the 6x His tag present at the N-terminus of the protein. The premise behind this technique is that ligand binding should cause a change in the chemical environment of the His tag bound dye. The change could be due to binding-induced changes in conformation, charge distribution or solvation dynamics (Langer *et al*., 2022). The experiment involves excitation of the dye at 590 nm and readout of emission at 650 and 670 nm. Changes in the ratio of fluorescent signal (670/650) vs ligand concentration were recorded: a dose response curve would indicate binding. The dye inherently induces a bathochromic spectral shift at 650 nm. This emission signal at 650 nm is mostly stable throughout the varying ligand concentrations except in cases of ligand interference with the dye fluorescence.

7.6.1 MK350 Dose-Dependent Changes in Fluorescent Properties of Labelled SMA-NTR1

It was hypothesised that binding of MK350 to dye-labelled SMA-rNTR1 would induce a conformational change in the protein and change the fluorescent properties of the dye. The 670/650 nm ratio (Figure 7.15A) and 650 nm fluorescence intensity (Figure 7.16B) were recorded after incubation of labelled SMA-rNTR1 with 12 different MK350 concentrations.

MK350 appeared to lower the 670/650 nm ratio but also impact the 650 nm fluorescence intensity in a dose-dependent manner. Figure 7.15A indicated a possible dose-response at a weaker affinity than expected since the response was not saturated. The estimated K_d was 100-fold higher than expected. A possible reason could be that the concentration of MK350 was over-estimated in the experiment. A lower concentration of soluble MK350 than expected could be due to degradation and surface adsorption of the ligand.

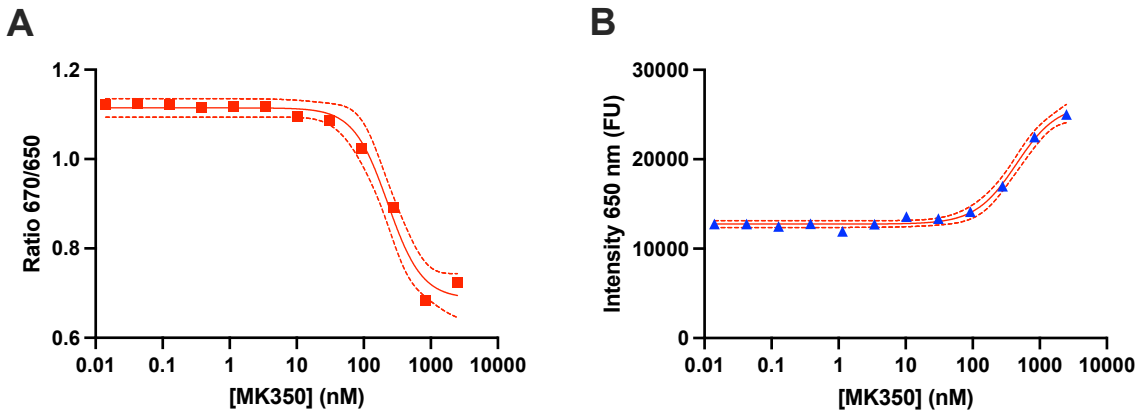


Figure 7.13: Spectral shift assay investigating the effect of MK350 concentration on fluorescently labelled SMA-rNTR1.
Red-labelled SMA-NTR1 concentration was 0.2 mg/mL. Dotted lines show 95% confidence bands.
(A) Relationship between MK350 concentration and 670/650 fluorescence ratio.
(B) Relationship between MK350 concentration and 650 fluorescence. Dotted lines show 95% confidence bands.

Figure 7.15B suggested a ligand-induced fluorescence change at 650 nm instead of an unchanged fluorescence intensity as would be expected. Another explanation was that changes in fluorescence were not due to binding of MK350 and SMA-rNTR1 but due to an independent effect of MK350 on the measured fluorescence. To test this theory, MK350 was titrated against buffer and a fluorescently labelled His tagged peptide. MK350 alone could not provide readable data due to a lack of red fluorophore in the solution. MK350 and fluorescently labelled His tagged peptide showed no change in ratio or intensity relating to MK350 concentration. This indicated that the fluorescence of MK350 was not interfering with the spectral shift measurements of the red-fluorescent label.

7.6.2 SR 48692 Prevents MK350 Dose-dependent Changes in Fluorescent Properties of Labelled SMA-NTR1

The increase in fluorescence intensity and decrease in 670/650 nm ratio was further investigated to determine the association of MK350 binding in the neurotensin binding pocket. Figure 7.16 shows that when fluorescently labelled SMA-rNTR1 was incubated with the antagonist SR 48692, there was no dose-dependent decrease in 670/650 nm ratio and no increase in fluorescent intensity.

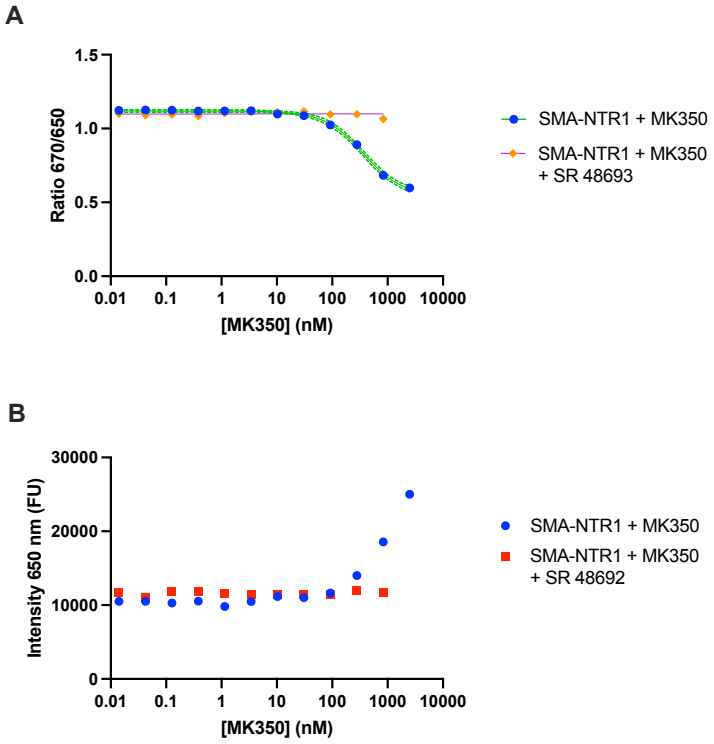


Figure 7.14: A spectral shift assay investigating the effect of MK350 concentration on fluorescently labelled SMA-rNTR1 with and without competitive inhibition with SR 48692.
Red-labelled SMA-NTR1 concentration was 0.2 mg/mL
(A) Relationship between MK350 concentration and 650/630 fluorescence ratio. Dotted lines show 95% confidence bands
(B) Relationship between MK350 concentration and 650 fluorescence.

An accurate estimation of the affinity of MK350 for SMA-rNTR1 could not be determined from the Spectral Shift data due to the lack of saturation. This may be due to the degradation/ adsorption of MK350 and hence underestimation of MK350 in solution, which could not be explored further. These data do show evidence of specific binding of MK350 to SMA-rNTR1.

7.6.3 Competitive Assay Shows SR 48692 Dose-Dependent Changes in Fluorescent Properties of Labelled SMA-NTR1 After Incubation with MK350

The MK350 concentration series showed evidence of specific binding at a measured concentration of 500 nM. It was hypothesised that SR 48692 would therefore increase the 670/650 nm ratio and decrease fluorescent intensity at 650 nm in a dose-dependent way, reversing the effects of MK350. To determine a possible K_i of SR 48692, 12 concentrations of SR 48692 were incubated with fluorescently labelled SMA-NTR1 before incubation with 500 nM MK350. This was compared to a control in which no MK350 was added.

Figure 7.17 shows the dose-dependent effect of SR 48692 with and without MK350. The shape of the curve plotted is indicative of SR 48692 binding. At higher SR 48982 concentrations, less binding sites contain MK350 causing an increase in the 670/650 ratio and a decrease in fluorescence intensity at 650 nm. The curve in Figure 7.17A was used to calculate a IC50 of 5.34 nM and Ki of 2.25 nM. The curve in Figure 7.17B calculated a IC50 of 6.25 nM and a Ki of 2.65 nM. This was close to the expected K_i of 2.6 nM.
The similar K_i values provided confidence that the changes in intensity and 670/650 ratio were caused by the same conformational changes of the SMA-rNTR1. The control showed that SR 48692 did not have an independent effect on the fluorescently labelled SMA-rNTR1.

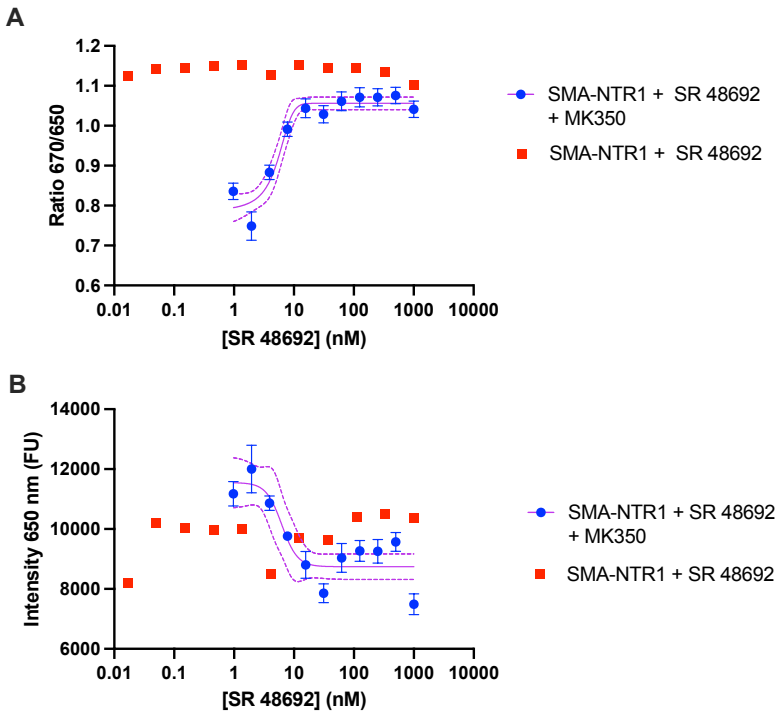


Figure 7.15: A spectral shift assay investigating the effect of SR 48692 concentration on fluorescently labelled SMA-rNTR1 with and without 500 nM MK350.
Red-labelled SMA-NTR1 concentration was 0.2 mg/mL Dotted lines show 95% confidence bands.
(A) Relationship between SR 48692 concentration and 650/630 fluorescence ratio
(B) Relationship between SR 48692 concentration and 650 nm fluorescence.

These data overall showed specific binding consistent with a fully functional rNTR1 protein encapsulated in a SMALP. This is a key starting point for the use of spectral shift assays for SMA-solubilised protein functional analysis, which has not been previously utilised.

7.7 SMA-PAGE to Assess Mini-G Protein Binding

Nehme *et al* developed a method that determined mini-G binding to GPCRs using SEC. As shown already, SMA-PAGE has the potential to be more sensitive technique than SEC, it is therefore possible that SMA-PAGE could be used to explore whether Mini-G proteins bind to GPCRs. An SMA-solubilised GPCR bound to a Mini-G protein should be 28-55 kDa larger than the SMA-solubilised GPCR alone, causing slower migration of a GPCR: Mini-G complex through an acrylamide gel.

SMA-CB2, SMA-rNTR1 and SMA-SAV (negative control) were incubated with Mini-G proteins overnight or for 4 hours and the samples were analysed by SMA-PAGE. Two samples of Gs/q were tested, with and without the His tag. The SMA-PAGE was analysed by Western blot using an anti-His antibody (Figure 7.18A). After image collection, the Western blot was re-probed with anti-CB2 antibody (Figure 7.18B). A separate incubation of SMA-solubilised hNTR1 and the mini-G proteins was investigated by SMA-PAGE and Western blot analysis using anti-NTR1 antibody (Figure 7.18C). The difference between the anti-His probed Western blots and GPCR-specific antibodies was expected to indicate a signal due to the His tagged Mini-G proteins. SMA-PAGEs are typically more smeared than SDS-PAGEs because proteins in their native state have more variable sizes and charges (Wittig and Schägger, 2005).

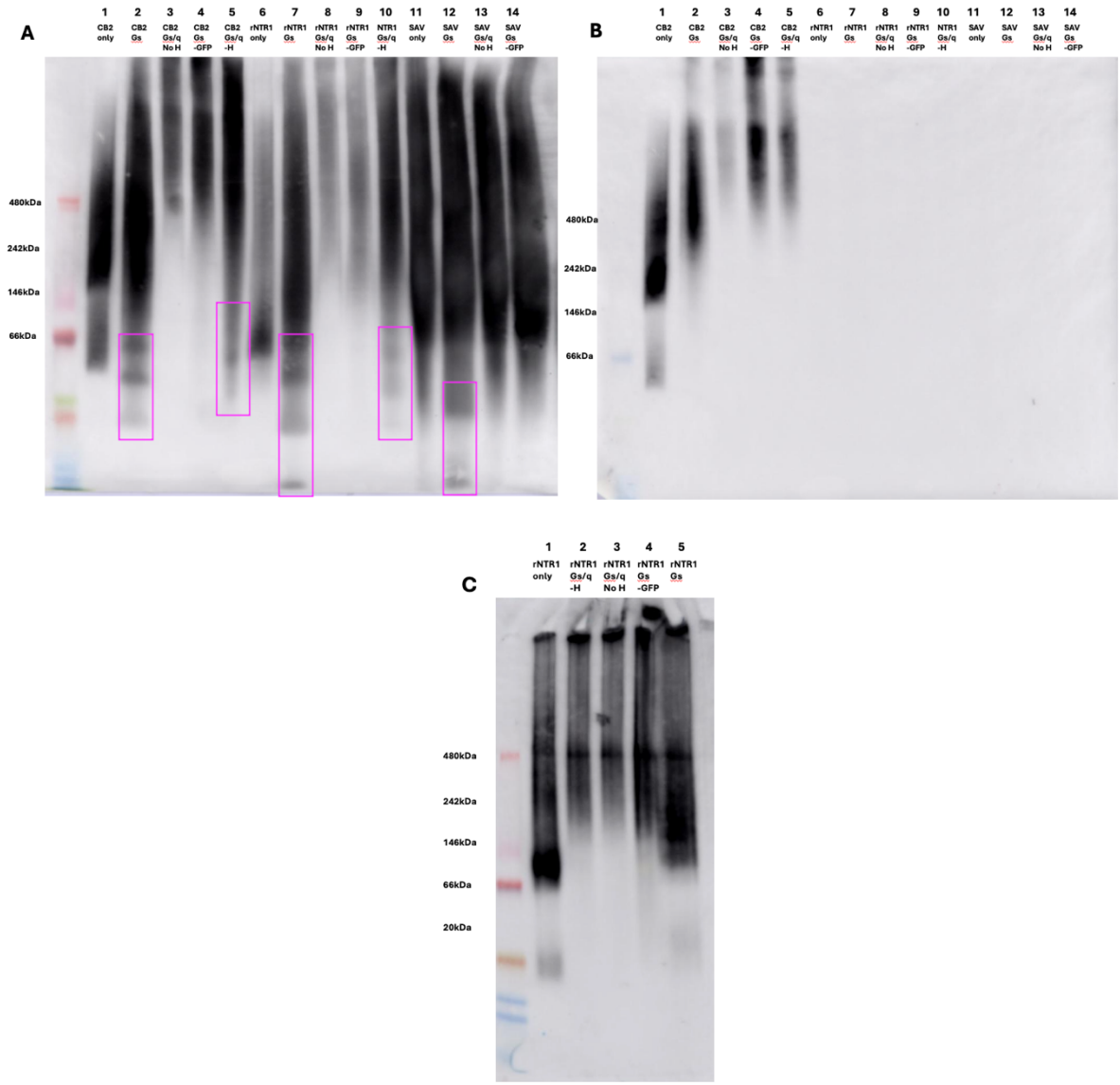


Figure 7.16: SMA-PAGE and Western blot analysis of SMA-CB2, rNTR1 and SAV after incubation with and without Mini-G proteins.
Four mini-G proteins were tested: Gs, Gs/q without His tag (Gs/q NoH), Gs/q with His tag (Gs/q-H) and Gs-GFP. All protein concentrations diluted to be 0.2 mg/mL final concentration.
(A) anti-His probed Western blot. Pink boxes represent the bands expected to represent Mini-G proteins which have migrated independently of the SMA-solubilised GPCR.
(B) Same SMA-PAGE analysis, re-probed Western blot with anti-CB2.
(C) Different rNTR1 and G protein samples analysed with anti-NTR1 antibody.

The Western blot analysis with an anti-His antibody would have detected His tagged rNTR1, CB2, SAV and Mini-G proteins. Without any Mini-G incubation the control protein SAV showed a large smear across 70% of the lane (Figure 7.18A (Lane 11)). Despite the smearing, a band was visible between 66-146 kDa, likely representative of SMA-SAV. The band

position suggested the same migration with and without the addition of Mini-G proteins (Lane 11-14). This is indicative that SMA-solubilised SAV did not interact with any of the Mini-G proteins, making it a successful negative control.

When SAV was incubated with Gs, two lower bands were visible (Figure 7.1A (Lane 12)), suggested to be Gs migrated separately from SAV. It is unlikely that Gs would have migrated faster than the SMA-SAV by itself. The slight negative charge caused by the intrinsic properties of Gs at pH 8.0 (caused by pI of 8.5) would have caused migration at a slower rate than the negatively charged SMALPs. One explanation is that the Mini-G proteins interact with SMA or SMALPs, causing their migration through the SMA-PAGE gel without interacting with the SMA-solubilised protein. These particles are expected to cause the bands highlighted in pink boxes. This theory was validated by incubation of the SMA-solubilised proteins with Gs/q with and without a His tag (Figure 7.1A (Lanes 4, 5, 9 and 10)). The additional bands caused by Gs/q-His on the anti-His probed Western blot were caused by Gs/q protein not associated with the SMA-solubilised protein.

When SMA-CB2 was analysed by SMA-PAGE (Lane 1 in Figure 4.1 (A and B)), two bands were visible using both anti-His and anti-CB2 antibodies at approximately 60 kDa and 200 kDa. The higher MW band was more intense than the lower MW band. This is consistent with findings in Chapter 5 that showed significant dimerization of CB2. The lack of signal from SMA-NTR1 or SMA-SAV samples (Lanes 6-14) provided confidence in the specific binding of anti-CB2 (Figure 4.1B). Upon the addition of all Mini-G proteins, the band representing SMA-CB2 appeared at a higher position (Lanes 2-5). This suggested an increase in the size of the SMA-CB2 particle caused by an interaction with the Mini-G protein. The smallest increase was caused by Gs, a 28 kDa protein (Lanes 2). Gs-GFP and Gs/q caused a larger increase to a similar position (Lanes 3-5). It was suggested that bands at the top of the

Western blot are likely due to protein aggregation causing no migration. After incubation with Mini-G protein, the CB2 monomer and dimer bands could not be resolved. It is theorised that Mini-G complexes could encourage dimerization or SMALP 'doublet' formation.

The analysis of SMA-solubilised rNTR1 by SMA-PAGE showed a similar result to that of SMA-CB2. When SMA-rNTR1 was ran alone, a band suspected to be monomer rNTR1 was present at approximately the expected MW of rNTR1: 99kDa (Figure 7.1 (A-Lane 5 and B-Lane 1)). The second rNTR1 SMA-PAGE analysis probed with anti-NTR1 showed more resolved bands identifying a likely fragment of rNTR1 below 20kDa and a larger particle at approximately 480kDa suspected to be an oligomer of rNTR1 (Figure 7.1B Lane 1). The anti-His Western blot (Figure 7.1A Lanes 6-10) showed the smeared bands representative of rNTR1 and Mini-G proteins were at a higher placement compared to rNTR1 only. The bands highlighted in pink in Lane 7 and Lane 10 are suspected to represent G proteins, which are not associated with rNTR1 but have interacted with SMA in some way to migrate through the gel. The anti-NTR1 Western blot (Figure 7.1C Lanes 2-5) confirmed that the band at approximately 99 kDa was absent when Mini-G proteins were added. After incubation with Gs, the band is at a higher position, indicative of an rNTR1-Gs complex (Lane 5). The bands possibly representative of oligomeric rNTR1 were not affected by the mini-G proteins (Lane 1-5). This could be because the higher order oligomeric state of the protein was not conducive to Mini-G protein binding. The signal from the well in Figure 7.1C suggest aggregation of all the rNTR1 protein samples. The intensity of the bands indicates a larger amount of aggregation upon the addition of mini-G proteins.

Overall, the SMA-PAGEs successfully identified SMA-rNTR1 and SMA-CB2 using multiple antibodies. Without Mini-G incubation, bands were visible at the expected approximate MWs

of dimeric CB2 and monomeric rNTR1. Slower migration after Mini-G incubation provided evidence of SMA-GPCR: Mini-G complex formation.

7.8 Conclusion

The results in this chapter were able to show the potential of solution-based fluorescence techniques for GPCR investigations using PoLiPas. This chapter provided evidence for the coupling of mini-G proteins to SMA-solubilised GPCRs, which has only been reported once before with a different GPCR. There was evidence that mini-G protein coupling affected the ligand binding characteristic of both SMA-rNTR1 and CB2. This confirmed production of soluble, functional GPCRs by PoLiPa technology was successful.

CHAPTER 8: DISCUSSION

8.1 Summary of Key Findings

GPCRs have a massive therapeutic potential but are difficult to extract for structural and functional analysis techniques (Laeremans *et al*., 2022). This is due to their instability, highly flexible structure and location within the plasma membrane (Weis and Kobilka, 2018). Nanodiscs have been used to gain a crystal structure of the rNTR1-Gi complex, revealing that lipids interact with the complex and anchor G proteins to the membrane (Deluigi *et al*., 2021). The use of negatively charged lipids strengthened the rNTR1-G protein interaction (Deluigi *et al*., 2021). This indicates the benefits of maintaining 'native' lipids, a capability specific to PoLiPa technology.

This project has utilised PoLiPa technology to produce soluble GPCRs and demonstrated functionality of SMA-solubilised GPCRs. This project systematically optimised SMA-solubilised GPCR purification. Preliminary investigations into the use of FTS, FCS and spectral shift successfully indicated that both rNTR1 and CB2 were capable of binding to appropriate ligands and G-proteins within a SMALP. This project supports the need for stable, functional, and soluble GPCRs in a 'native-like' environment, which can be used for potential pharmaceutical screening.

8.2 Interpretation of Results

8.2.1 Expression of GPCRs in E. coli

E. coli is a favourable expression system due to its preferred cost, speed, efficiency, scalability and ease of manipulation (Wiseman *et al*., 2020). *E. coli* expression of GPCRs has been shown to be a challenging task, with success dependent on the specific GPCR. Lundstrom *et al* found that when testing the expression of 103 GPCRs: only 50% were detected in *E. coli*

membranes or inclusion bodies, whereas 95% were detected after expression in Semliki Forest virus-infected HEK293 cells (Lundstrom *et al*., 2006). Of 50 studies on GPCR expression in *E. coli,* 37% were re-folded from inclusion bodies and 63% were harvested from membranes (Abiko *et al*., 2021).

There has been previous research into the expression of rNTR1 and CB2 in *E. coli* (Table 8.1). This project was able to validate and build upon previous expressions of these proteins to produce enough GPCR for polymer-based investigations. Yu's group showed successful expression of GPCRs in *E. coli* by the addition of an N-terminal transmembrane sequence called P9, which stabilised the protein and aided membrane insertion (Kim *et al*., 2024). This included human endothelin receptor A (Han *et al*., 2017b), lysophosphatidic acid receptors 1 and 2 (LPA1 and 2) (Han *et al*., 2017a), prostaglandin E2 receptor 4 (EP4) (Kim *et al*., 2021a) and glucagon-like peptide 1 receptor (Kang *et al*., 2021). A different fusion tag called AT10 (KYYKYYKYYK) reportedly increased expression of 18 human olfactory receptors and 7 non-olfactory GPCRs, measured by Western blot analysis (Cho *et al*., 2023).

E. coli expression of GPCRs has typically only been successful after the identification of multiple stabilising mutations within the GPCR and the addition of stabilising ligands (Rosenbaum *et al*., 2009). Sarkar *et al* (2008) described a directed evolution method using *E. coli* to find stabilising mutations. The starting protein in the directed evolution method was the same MBP-fused rNTR1-Thioredoxin A protein investigated in this project. Error prone polymerase chain reaction (PCR) was used to create a set of random mutations; fluorescently labelled neurotensin and fluorescence activated cell sorting (FACS) were used to select the highest expressing cells (Sarkar *et al*., 2008). Plasmid was collected from these cells and fresh bacteria transformed. After 4 rounds of error-prone PCR and selection, the clone with the best expression level had 10-fold higher expression than WT rNTR1 and 14 nucleotide

substitutions (Sarkar *et al*., 2008). Binding characteristics of the mutant rNTR1 were the same as WT rNTR1. This method is not transferable to many other GPCRs because of the lack of fluorescent ligands and the inability of *E. coli* to express most GPCRs. This project avoided the use of stabilising ligands or stabilising mutations aside from truncations and fusion proteins, providing a more physiologically relevant receptor construct.

Table 8.1: Summary of Expression Conditions Optimised in this Project Compared to Literature

Protein	***E. coli* Cell Line**	**IPTG Conc (mM)**	**Expression Temp (ºC)**	**Expression Time (hours)**	**Broth**	**Reference**
rNTR1	C43(DE3)	0.25 mM	18	20-24	LB Broth	This Project
rNTR1	DH5α	0.25 mM	22	40	2xYT+0.2% (w/v) glucose	White *et al* (2004)
rNTR1	DH5α	0.5 mM	20	40	2xYT+0.2% (w/v) glucose	Tucker and Grisshammer (1996)
rNTR1	BL21(DE3)	1 mM	29	Not specified	2xYT + 1% (w/v) glucose	Egloff PhD Thesis (2014)
rNTR1	BL21(DE3)	1 mM	24 or 28	20 or 16	2 x YT + 0.2% (w/v) glucose	Egloff *et al* (2014)
rNTR1	BL21(DE3)	0.25 mM Or AI	20ºC	30	2xYT + 0.2% (w/v) glucose or AI media	Attrill *et al* (2009)
CB2	C41(DE3)	0.25 mM	18	20-24	2xYT	This Project
CB2	DH5α	0.5 mM	20	40	2 x YT + 0.2% (w/v) glucose	Calandra (1996)
CB2	BL21(DE3)	1 mM	20	40	2 x YT + 0.2% (w/v) glucose	Yeliseev *et al* (2009)
CB2	BL21(DE3)	0.5 mM	20	40	2 x YT or Mineral salt medium for isotope labelling	Berger (2010)
CB2	BL21(DE3)	1 mM	20	40	2 x YT + 0.2% (w/v) glucose	Krepkiy *et al* (2006)

Abiko *et al* used the previously thermostabilised sequence of mutated turkey β1 adrenergic receptor (β1AR) and after expression optimisation produced 0.2-0.3 mg/L of culture (Abiko *et al*., 2021). β1AR was cloned into the same pRG plasmids used in this study for the MBP-fused GPCR expression in *E. coli*. Cholesterol was shown to stabilise β1AR but prevent cell

growth. The data in this project agrees with most literature about other GPCRs expressed in *E. coli* regarding optimal expression at low temperatures and low IPTG concentrations. The highest improvement in expression was achieved by varying the cell line and broth.

This project demonstrated the importance of expression level optimisation for the successful purification of a GPCR. Tesdesco *et al* reported a method utilising SMALP technology for purification of low-expressing GPCR, however, the final product had a low concentration and purity (Tedesco *et al*., 2021). In Tesdesco *et al*, positive confirmation of the GPCR after purification was achieved by dot blot analysis, a highly sensitive technique shown to detect some proteins down to 50 μg/mL (Zulkarnain *et al*., 2022). In this project, the most successful purifications (from 4 L of broth) were able to produce 400 μL of 0.9 mg/mL CB2 and 3 mL of 0.2 mg/mL rNTR1 from *E. coli* expression.

8.2.2 Expression of GPCRs in HEK293 Cells

Expression of GPCRs in a mammalian cell line can be equally as challenging as *E. coli* expression, however, it is a commonly preferred expression system for GPCR production because of post-translational modification capabilities (Goth *et al*., 2020). A stable GPCR-expressing cell line is difficult to obtain due to the metabolic stress caused by expression, post-translational modifications and trafficking of the GPCR, as well as the signalling caused by the over-expressed GPCRs (Tate and Grisshammer, 1996). Lentiviral transduction was an attractive technique because it allows the delivery of DNA constructs into the genomes of non-dividing mammalian cells (Campeau *et al*., 2009). The optimisation of the GPCR expression in HEK293 cells was not within the scope of this project however a higher expression level would likely aid downstream purification steps. A possible avenue that could be investigated is inducible GPCR expression to prevent decreasing expression over time due to toxicity. Inducible expression was previously used to produce the human olfactory receptor

(Cook *et al*., 2008) and β2 adrenergic receptor (Chelikani *et al*., 2006). Another avenue could be the use of a specialised master cell line that could aid integration of the GPCR into the genome (Schucht *et al*., 2011).

8.2.3 Polymer Solubilisation and Polymer Selection of GPCR Oligomerisation states or Glycosylation States

Of 50 studies investigating GPCRs in *E. coli*, the most used solubilisation agent was a combination of DDM, CHAPS and CHS (Abiko *et al*., 2021). PoLiPa have been used to extract the Ghrelin receptors expressed in *E. coli* and β_2-adrenergic receptors from mammalian cell membranes. rNTR1 has been previously expressed in HEK293T cells and has been previously encapsulated in an SMALP but no purification of the solubilised receptor was performed (Dathe *et al*., 2019). This project investigated the polymer solubilisation of five different GPCRs: hNTR1, rNTR1 and CB2 from *E. coli*, and hNTR1 and CB2 from HEK293 cells. There were distinct differences in the solubilisation efficiency of different polymers depending on GPCR-type and expression system. This demonstrated that many factors may influence the efficacy of polymers extraction, including oligomerisation state, glycosylation, expression level, MW and cysteine reduction. SMA extracted the GPCRs with consistently high efficiency. This was chosen for the downstream purification of most of the GPCRs because it was the most cost-effective. However, several other polymers were deemed good solubilising agents in this project and could be used to produce GPCR-encapsulating PoLiPas, with different biophysical characteristics (Table 8.2).

Table 8.2: Summary of Polymer Solubilisation Performance on Different GPCRs

	SMA	DIBMA	RAFT SMA 1:1	SMI	DDM	BzAM Series (0.05)	BzAM Series (0.1)	BzAM Series (0.15)	BzAM Series (0.25-0.4)	BzAM Series (0.25-0.4)	BzAM Series (0.25-0.4)	BzAM Series (0.25-0.4)	BzAM Series (0.25-0.4)	AASTY 6-45	AASTY 11-55	AASTY 11-45
WT-hNTR1 (*E. coli*) Monomer			-	-	-									-	-	-
WT-hNTR1 (*E. coli*) Dimer			-	-	-									-	-	-
rNTR1 (*E. coli*) Monomer			-	-	-									-	-	-
rNTR1 (E. coli) Dimer			-	-	-									-	-	-
CB2 (E. coli) Monomer														-	-	-
CB2 (E. coli) Dimer														-	-	-
NTR1-High (HEK)			-													
NTR1-Low (HEK)			-													
CB2 (HEK) Monomer			-													
CB2 (HEK) Dimer			-													

Green= Good solubilisation, Orange= Moderate solubilisation, Red= Minimal/no solubilisation

Previous solubilisation trials with different polymers showed protein-specific differences in solubilisation efficiency. The solubilisation efficiency of different SMA polymers varying in length and maleic acid content were tested on three membrane proteins of different size and shape: Brma, ZipA and LeuT. Solubilisation of the homodimer-forming Brma protein was more sensitive to decreases in polymer hydrophobicity than ZipA or LeuT but SMA 2:1 yielded the highest solubilisation consistently (Morrison *et al*., 2016). The polymers tested in this project suggested that polymers and reducing agents can be manipulated to encourage a bias toward GPCRs in a particular oligomeric state. This concept was investigated by Walker *et al* who designed an experiment to interpret the oligomerisation states within PoLiPas by single nanodisc photobleaching. Seven GFP-labelled proteins showed different oligomerisation states. Two different membrane proteins formed monomers, dimers and higher order oligomerises but there was a difference between the ratio of particles in different oligomerisation states dependent on solubilisation by SMA or by AASTY (Walker *et al*., 2023). This validates the Western blot interpretations in this project.

8.2.4 Purification Optimisation

This project systematically investigated different purification conditions and discovered key variables that should be optimised when purifying SMA-solubilised GPCRs. This study demonstrated that the primary issues with SMA-solubilised GPCR yield, and purity are due to the lack of affinity for IMAC resin, non-specific binding to the anti-FLAG resin and co-elution of contaminant proteins. Yeliseev *et al* was able to purify 1-2 mg of detergent-solubilised CB2 from *E. coli* expression with 80-90% purity from a one-step IMAC purification (Yeliseev *et al*., 2005). This demonstrates that despite the benefits of PoLiPa technology, its use can sometimes be detrimental to purification techniques. This supports the requirement for more optimisation.

Table 8.3 summarises the final optimised conditions for the SMA-solubilised GPCRs purified in this thesis. Three out of the five GPCRs produced in this project were able to be purified to over 90% purity. Key protein-specific variables for optimal GPCR production included: IMAC resin type, presence of arginine, and reducing agent concentration in IMAC binding buffers. Some consistently beneficial factors included diluting the solubilised material pre-IMAC purification and use of high (500 mM) NaCl concentration during IMAC purification. Factors that had minimal change in GPCR yield or purity included adjusting the imidazole concentration or the FLAG peptide concentration in the wash and elution fractions of an IMAC or FLAG purification.

Table 8.3: Summary of Optimised GPCR Production in this Project

GPCR	**rNTR1**	**CB2**	**hNTR1**	**CB2**
Expression System	*E. coli*	*E. coli*	HEK293	HEK293
Solubilisation	0.5% (w/v) SMA	2% (w/v) SMA	1% (w/v) SMA	1.5% (w/v) SMA
IMAC Purification Conditions	IDA Resin 2-fold dilution before resin binding. Buffer: 50 mM Tris-HCl (pH 8) 500 mM NaCl 20 mM Arginine 10% v/v Glycerol	Ni-NTA Resin 2-fold dilution before resin binding. Buffer: 50 mM Tris-HCl (pH 8) 500 mM NaCl 20 mM Arginine 1 mM TCEP 10% v/v Glycerol	Ni-NTA Resin 2-fold dilution before resin binding. Buffer: 50 mM Tris-HCl (pH 8) 500 mM NaCl 10% v/v Glycerol	Ni-NTA Resin 2-fold dilution before resin binding. Buffer: 50 mM Tris-HCl (pH 8) 500 mM NaCl 10% v/v Glycerol
Second-step FLAG Purification Conditions	-	Buffer: 50 mM Tris-HCl (pH 8) 150 mM NaCl 10% v/v Glycerol	Not appropriate, poor elution	-
Purity Achieved	High	High	Low	High
Optimised Yield from single purification	600 μg	360 μg	50 μg	100 μg

SEC was not a useful purification method for the separation of different proteins encapsulated within a SMALP or a DIBMALP. One explanation is that the large PoLiPa size, generally accepted to be approximately 10 nm, does not correlate to the MW on the encapsulated protein (Ayub *et al*., 2020; Morrison *et al*., 2016; Swainsbury *et al*., 2017). Another factor was heterogeneity between SMA-solubilised hNTR1 likely caused by oligomerisation, SMALP 'doublet' formation and the differences in the number of polymer and lipids per particle. This may have prevented distinguishable differences between SMA- or DIBMA- solubilised proteins that could allow their separation via SEC.

This project did not achieve a successful FLAG purification of polymer-solubilised CB2 directly after solubilisation. A FLAG purification has successfully purified a SMA-solubilised protein to >90% previously without an IMAC purification (Rehan *et al*., 2017). It is suspected that better expression levels, differences in the contaminating proteins and exposure of the FLAG tag in the protein contributed to the success of the FLAG purification in Rehan *et al*.

This project recommends performing an IMAC purification before a FLAG purification to remove excess polymer.

A consideration that this project did not investigate was the manipulation of the size and position of the affinity tags. It was suggested in this project that some purification improvements were due to the flexibility and exposure of the His tags. Adding a linker region before the affinity tags may cause the tags to be further away from the PoLiPa, aiding purification. Damian *et al* extended the 6x His tag to a double 10x His tag to optimize SMA-GPCR binding to an IMAC resin (Damian *et al*., 2018). In this project, it was observed that 6x His tagged CB2 was more difficult to purify than 10x His tagged rNTR1. Extension of the affinity tags could be a solution to purification problems associated with PoLiPas.

This project investigated multiple purification methods: IMAC, FLAG purification, MBP purification and SEC. However, the literature reports methods specifically for the purification of GPCRs, given the known challenges in their production. Production of a column that contains an appropriate GPCR ligand has been used to successfully purify NTR1 (Egloff *et al*., 2015), A2AR (Weiss and Grisshammer, 2002), BLT2 receptor (Arcemisbéhère *et al*., 2010) and GHS-R1a (Damian *et al*., 2012). This method allows the selection of active GPCRs which functionally bind to the ligand. However, it requires the immobilisation of a specific ligand which requires knowledge of the ligand binding characteristics of the GPCR being investigated.

Attachment of a 9-residue bovine rhodopsin affinity tag has been used for immunoaffinity purifications of multiple GPCRs (Chelikani *et al*., 2006; Cook *et al*., 2008). A mammalian expressed human olfactory receptor was purified this way after solubilisation with fos-

choline-14 (Chelikani *et al*., 2006). This may induce less non-specific binding than the FLAG immunoaffinity purifications investigated in this project.

Some studies report the purification of proteins in amphipols or detergents before utilising PoLiPas (Dalal *et al*., 2024; Damian *et al*., 2018). IMAC purifications of GPCRs have also been performed in denaturing conditions before refolding (Arcemisbéhère *et al*., 2010; Damian *et al*., 2012). This agrees with the findings of this project that suggest the interference of PoLiPas and other solubilising agents in resin binding and elution. This project provides new insight into an optimised purification protocol whilst retaining the 'native' surrounding lipids of a GPCR.

8.2.5 Biophysical Analysis Techniques

DLS, SEC and SMA-PAGE data suggested that purified polymer solubilised GPCRs are likely to be heterogeneous because of oligomers, 'doublets' and aggregates. Previously, SMALPs containing AcrB have been shown to form 'doublet' particles which can be visualised by negative stain (Postis *et al*., 2015). The biophysical analysis methods were also able to guide purification and storage protocols. DLS and CD data suggested that the loss of SMA-solubilised NTR1 was due to aggregation instead of unfolding. Steps were taken to prevent aggregation including the use of reverse concentrators at a low speed, storage at 4°C for less than a day or -20°C for the long term, minimal freeze-thawing and consistent removal of aggregation by centrifugation.

There was some evidence for the fluidity of oligomerisation after solubilisation. To achieve a pure monomeric GPCR, manipulation of polymer type and reducing agents could be investigated. However, for this project heterogeneity in the sample was deemed acceptable.

8.2.6 Stabilising Effect of PoLiPa Compared to Other Methods

CD and nanoDSF analysis of SMA-solubilised GPCRs in this project suggested a stabilising effect of SMA. Yeliseev's group have produced several publications about the production and use of CB2 using detergent (Yeliseev *et al*., 2005). They found the use of CHS was an important addition for stabilising CB2 (Vukoti *et al*., 2012). CHS has also been needed to stabilise three other GPCRs in detergent: GHS-R1a (Damian *et al*., 2012), β2-adrengeric receptor (Rosenbaum *et al*., 2007) and μ-opioid receptor (Kuszak *et al*., 2009). CHS also has a stabilising effect on SMA-solubilised A2AR (Charlton., 2016). Despite this optimisation of CB2 stability by detergent selection and CHS, the nanoDSF analysis was able to provide a melting temperature larger than the detergent-solubilised CB2 (Yeliseev *et al*., 2020). This is consistent with the increased thermostability of SMA-A2AR compared to DDM-A2AR (Jamshad *et al*., 2015a).

The stabilising effect of PoLiPas could be a major benefit in GPCR investigations. Previously, specialised methods for the directed evolution of GPCRs stable in detergent have been investigated (Scott and Plückthun, 2013). This has been called cellular high-throughput encapsulation, solubilisation and screening (CHESS). Scott and Plückthun were able to produce three rNTR1 mutants stable in harsh detergents in which the precursor mutant was unstable. A structure of a stable NTR1 was obtained using this method (Egloff *et al*., 2014). This project provides an alternative stabilising method that requires minimal alteration of the GPCR primary sequence.

Other stabilising tools include the addition of ligands and the production of stabilising nanobodies (Laeremans *et al*., 2022). Both typically must be designed specifically for each

GPCR. PoLiPa provide a non-specific stabilising tool which could be used in conjunction with ligands, CHS, amino acids such as arginine and possibly nanobodies to improve stability further.

8.2.7 Functional Analysis

The use of PoLiPas as opposed to detergent as a solubilisation agent provides different benefits and hindrances to different ligand binding techniques. One of the major drawbacks associated with detergent is the need for a concentration of detergent over the CMC in the buffer system. Detergent screens are often required to determine which detergents do not interfere with ligand binding. Beckner *et al* found concentrations above 0.25 mM of Façade-TEG interfered with CB2 binding due to non-specific partitioning of the hydrophobic ligands (Beckner *et al*., 2020).

The use of PoLiPas allows for minimal buffer additions that could interfere with ligand binding. However, PoLiPas can cause other issues. SMA has been shown to cause the 'conformational trapping' of an encapsulated protein because of the rigidity of the lipids (Pollock *et al*., 2022). One of the aims of this project was to confirm that the GPCRs were functional whilst encapsulated inside a SMALP by their capacity to bind to known ligands and Mini-G proteins. SMA-PAGE, FTS, FCS and spectral shift assays provided promising data that the GPCRs maintain functionality.

The FTS and FCS data provided evidence of ligand binding, influenced by Mini-G proteins. The spectral shift assays showed the expected inhibitory effect of SR 48693. SMA-PAGE provided evidence of SMA-GPCR complex formation with Mini-G proteins.

8.2.7.1 FTS

FTS has been used to demonstrate ligand binding to a SMALP-encapsulated GPCR previously (Routledge *et al*., 2020). FTS is especially useful as it can monitor conformational changes within a GPCR. The FTS data on hNTR1 demonstrated the sensitivity of FTS as a technique. The large quenching effect associated with the binding of fluorescent NTR1 ligands was measurable despite the impurity and low concentration of the SMA-hNTR1. This demonstrates that PoLiPa technology and FTS can be used to yield binding data of a WT GPCR in solution. The SMA-solubilised *E. coli* protein control supported that the NTR1 binding was specific. FTS assessment of specific binding makes this technique relevant to large-scale compound screening of potential GPCR binding partners. PoLiPa technology could prevent the detection of false positives that may bind to detergent-solubilised GPCR but not to the protein in its native environment. This may produce a more accurate screening technology for potential pharmaceuticals.

Another fluorescent signal that appeared to change upon binding was anisotropy. Rotational freedom of a fluorophore typically decreases upon binding, increasing the anisotropy (Rinken *et al*., 2018). This was demonstrated in this project from the FTS signal, with the binding to ligands. Routledge *et al* (2020) also demonstrated an anisotropy increase upon ligand binding to SMA-A2AR. They suggested that this was more likely due to reduced steric freedom of the tryptophan residues within A2AR upon binding instead of overall tumbling of the SMA-A2AR. In this project, the level of anisotropy increase was variable between the three NTR1 agonist, despite all three containing the same functional groups expected to bind to the neurotensin binding pocket of hNTR1. This suggested an effect of the fluorophores in the fluorescent ligands causing a larger reduction in the steric freedom of the tryptophan residues in hNTR1. The ligand that caused the largest anisotropy change was used to characterise

binding, and this data was supportive of the changes in the FTS intensity and the expected K_d of the ligand.

A fluorescence anisotropy assay with a fluorescent ligand has been suggested as a suitable tool for screening of new active compounds that bind to GPCRs (Veiksina *et al*., 2021). The drawbacks of this method are the requirement of bright fluorophores and low non-specific binding (Rinken *et al*., 2018). This project suggests this method could be feasible using PoLiPa-encapsulated GPCRs.

8.2.7.2 FCS

The project presents the first FCS experiments used to measure GPCR ligand binding when coupled to a G protein. This proves that solution-based FCS on PoLiPa encapsulated GPCRs is a useful tool for GPCR ligand binding characterisation and possibly GPCR: G protein complex characterisation. The use of FCS for GPCR ligand binding has been validated once before in which A2AR was used to define the K_i of the A2AR antagonist by measuring specific binding in a similar methodology used in this project (Grime *et al*., 2020). Grime *et al* reported the potential of FCS to investigate allosteric modulation of GPCRs. This project continues this research and shows the allosteric modulation of two Mini-G proteins. The diffusion rate data suggested that both Gs and Gsq form complexes with SMA-rNTR1. This is consistent with the capability of NTR1 to activate Gs, Gq and Gi dependent on the host cell (Pelaprat, 2006). The effect of the Mini-G protein on ligand binding was different: Gsq appeared to increase ligand binding whereas Gs appeared to reduce binding. Removal of the C-terminal domain of NTR1 reduced Gs activation but not Gq activation (Najimi *et al*., 2002). It is suggested that Gq interaction involves the third intracellular loop and the Gs

interaction involves the C-terminal domain (Pelaprat, 2006). This different binding site is likely to mediate a different effect on the affinity of a ligand.

G protein complex formation with a GPCR encapsulated in a PoLiPa has only been reported once before (Damian *et al*., 2018). This was done by a FRET-based assay of a GPCR heteromer encapsulated in a SMALP (GHSR and D2R). It was reported that excess SMA reduced the mobility and reduced the ability of the GPCR to activate G proteins. G protein activation was measured by the changes in the tryptophan emission of Gi which had been labelled with 5-hydroxytryptophan. The paper reported the use of multiple fluorophores to elucidate the binding characteristics of different G proteins. This supports the functional assays in this project which demonstrate the usefulness of fluorescence in monitoring protein interactions and conformational changes of polymer-solubilised GPCRs

8.2.7.3 SMA-PAGE for GPCR: Mini-G protein complex detection

This project demonstrated SMA-PAGE to be a useful tool for the assessment of GPCR: G protein complex formation. The technique only required 15 µl of material and was sensitive to concentrations less than 0.1 mg/mL. This was chosen as a tool for complex characterisation over SEC due to its sensitivity and time efficiency. This technique overall validated the FTS and FCS data that suggested Mini-G proteins interacted with the GPCRs, causing a change in the GPCR binding characteristics. Others tool useful for understanding complex formations include analytical ultracentrifugation (Edwards *et al*., 2020), pull-down assays (Perry *et al*., 2019) and FRET-based assays (Zhou *et al*., 2021). A wider-scale investigation into the protein-binding partners of GPCRs could be more easily accessible after polymer-solubilisation.

8.3 Implications of the findings and contribution to the field of drug discovery

8.3.1 PoLiPa Technology Implications

PoLiPa technology has become increasingly useful for investigating membrane proteins. This section discusses other uses and compatible techniques of PoLiPas. This project has produced SMA-solubilised NTR1 and CB2, which could also be investigated further by new oligomerisation and complex formation studies, other ligand binding assays, structural tools, antibody development or reconstitution. This suggests the potential of this work to yield exciting outcomes for investigating GPCRs.

One promising aspect of PoLiPa technology is the possibility of investigating complexes. Wang *et al* recently published the purification and biophysical characterisation of a Collagen/Fibrinogen glycoprotein VI and Fc receptor γ complex in a SMALP. Proteins were proven functional by collagen binding; SEC and SMA-PAGE results suggested multiple oligomerization states (Wang *et al*., 2024). Identification of possible oligomers was common across all the GPCRs in this study, and this appears to be common in several other PoLiPa investigations (Han *et al*., 2023; Ullrich *et al*., 2024; Wang *et al*., 2024). Hetero-oligomers of GPCRs have been shown to form with a SMALP and regulate G protein conformations (Damian *et al*., 2018). This shows the potential for PoLiPas to encapsulate multiple membrane proteins and characterise protein-protein interactions that may not be stable in detergent.

Recent advances in cryo-EM have led to the more common use of PoLiPas for protein structure determination. The structure of the transient receptor potential melastatin 4 (TRPM4) was solved in SMALP and found to be identical to previously identified structures of TRPM4 in detergent micelles (Ekundayo *et al*., 2024). However, SMA caused poorer resolution of cytosolic regions. Another example used an SMA amide derivative to extract

full-length integrin αIIbβ3 directly from platelet membranes (Adair *et al*., 2023). The allowed structure determination of the transmembrane domain bound to native lipids. An atomic structure of a GPCR bound to native lipids could demonstrate new conformations and lipid interactions. This project could aid the production of polymer-solubilised GPCRs for structural determination.

PoLiPa have been utilised to reconstitute proteins from the cells in proteo-liposomes. For example, SMA and SMA-amide derivatives have been used to reconstitute ion channels from proteo-liposomes, which were used in patch clamp studies (Yang *et al*., 2021). There is potential for this method to be used to move proteins from the cells they were expressed into other membranes, liposomes or cells.

8.3.2 GPCR Implications

Given the importance of GPCRs as drug targets, many other approaches have been investigated to produce stable soluble GPCRs. This section will discuss other strategies in comparison to PoLiPa technology.

One exciting strategy is the use of immunoglobulin single variable domains to stabilise a GPCR in a distinct conformation (Laeremans *et al*., 2022). These have been called nanobodies or sdAbs. Three GPCR structures in their inactive states were solved with the same nanobody that recognised a grafted intracellular loop (Robertson *et al*., 2022). Sachdev *et al.* found tethering of a GPCR peptide agonist of the type 1 parathyroid hormone receptor to a nanobody allowed the selection of a specific pathway. The Gs activation remained comparable to the peptide agonist alone but the β-arrestin 2 recruitment and Gq activation did not occur (Sachdev *et al*., 2024). Schlimgen *et al* characterised an antagonistic nanobody for

atypical chemokine receptor 3 by an in-cell assay and analysis of AlphaFold models (Schlimgen *et al*., 2024). Despite the success of computational methods, the experimental data of GPCR investigations is often limited to in-cell assays. This project has aided the production of stable soluble GPCRs for *in vitro* assays. PoLiPa could be used in conjunction with nanobodies to further manipulate GPCR conformation. Polymer-solubilised GPCRs could also be useful for developing new nanobodies and antibodies that specifically target the GPCR extracellular or intercellular regions of the protein.

Amphipathic polymers have also been produced to be stabilising agents for GPCRs, without the formation of PoLiPas. Han *et al* used amphiphilic-γ-glutamate (APG) as an addition to detergent solubilisation and to reduce the CMC required to allow reconstitution into liposomes (Han *et al*., 2014). The use of this polymer does not produce a lipid particle but was found to change the encapsulated GPCR to an active conformation. This demonstrates the potential benefits of alternative stabilising and solubilising agents. This production of stable, soluble GPCRs in this study offers a detergent-free method that could be more suitable for reconstitution and less impactful on GPCR conformation.

As discussed, producing GPCRs in an expression system like the ‘native’ environment has many challenges. Kim *et al* used APG to reconstitute *E. coli*-expressed mammalian membrane proteins (including the GPCRs EP4 and GLP1R) into the plasma membranes of live mammalian cells. This was only possible with the polymer APG because using higher detergent concentrations reduced cell viability (Kim *et al*., 2024). Kim *et al* credited the use of the polymer APG and the addition of the phage membrane protein (P9) N-terminal sequence in keeping the GPCRs in a ‘native’ conformation. Yu’s group used APG and the P9 additional sequence for antibody discovery against low-expressing GPCRs (Kim *et al*., 2023), G protein preference determination (Han *et al*., 2017a) and allosteric modulator identification

(Kang *et al*., 2021). This project adds to the continuous research on how to best express, solubilise and purify GPCRs. The primary benefit of PoLiPa for GPCR investigations is the inclusion of a local lipid environment that can be included in solution-based assays. The PoLiPa not only has a stabilising effect but allows a more 'native' environment that other techniques often sacrifice in pursuit of a more stable GPCR.

8.4 Limitations of the study

8.4.1 Low yield

One of the largest limitations of the project was the low yield of the GPCR despite optimisation. This meant minimal optimisation of the tested functional assays and a low number of measurements. An increased protein concentration would allow more data points when establishing a binding curve and a higher number of repeats. Further investigation into higher-yielding GPCR production could have been achieved by using a different expression system, different polymers, or different affinity tags.

8.4.2 GPCRs in this Project may not be Representative of GPCRs in a 'Native' Environment

Fusion proteins, affinity tags and stabilising truncations utilised in this project to express and purify GPCRs may cause changes to the structure and function of the GPCR that change the binding characteristics. Less stabilising mutations were utilised in this project compared to other GPCR studies (Egloff *et al*., 2014). *E. coli* expression prevents post-translational modifications of GPCRs which may be important to its function (Wiseman *et al*., 2020). This may have aided its purification but prevents an understanding of how glycosylation can impact GPCR function.

Another difference between GPCRs expressed in *E. coli* or HEK293 cells and native GPCRs, is the difference in local environment. The surrounding lipids have also been proven to affect

the structure and function of a GPCR. *E. coli* lipids are vastly different to mammalian lipids and therefore the lipids in a SMALP encapsulating a GPCR could be interfering with its structure and function (Deluigi *et al*., 2021). HEK293 cells provide a more native lipid environment and appropriate post-translational modification because it is a mammalian expression system. However, no expression system is perfect; over-expressing HEK293 cells are likely to produce different post-translational modifications and different lipids to differentiated cells *in vivo*. Over-expression itself has been proven to influence oligomerisation which affects the binding characteristics of a GPCR (Dijkman *et al*., 2018).

Natively, GPCRs are highly regulated by their environment: interacting with many proteins, lipids and ligands, as well as being systemically trafficked in and out of this plasma membrane (Leysen *et al*., 2021). This is impossible to replicate extracellularly, however, the tools in this project produce a more 'native' environment than other solubilisation methods.

8.4.3 GPCRs investigated are not representative of the whole class

The GPCRs investigated in this project are well-studied type A GPCRs, with various crystal structures of the stabilised GPCR variants bound to various ligands and/or proteins (Deluigi *et al*., 2021; White *et al*., 2012; Li *et al*., 2019). This project provided generalised rules for optimising the production of a polymer-solubilised GPCR on a basis of the GPCRs investigated. However, there were several protein-specific variables during the expression, solubilisation and purification process. To fully elucidate the potential of PoLiPa technology, GPCRs from different classes and with different G protein biases should be tested. The GPCRs investigated also have previously been solubilised and purified in detergent. To fully display the stabilising ability of PoLiPa technology, a GPCR that has not been successfully purified previously should be investigated.

8.5 Recommendations for Future Research

8.5.1 New Polymers

After solubilisation trials, this project focused predominantly on the use of SMA as a solubilisation agent, primarily due to the low cost and wide availability of the polymer. Since the discovery of SMALPs, an increasing number of polymers have become available offering the possibility of increased solubilisation efficiency or different PoLiPa characteristics (Workman *et al*., 2023). SMA has been shown to cause conformational trapping of an ATPase-binding cassette transporter and has been shown to change the structure of ligand-gated ion channels, including the size of the ligand binding pocket compared to the use of membrane scaffold proteins (Dalal *et al*., 2024; Pollock *et al*., 2022). An investigation into GPCR production using a larger number of polymers might reveal a higher yield of GPCR or may reveal different binding characteristics.

One pitfall in the use of SMALPs are the sensitivity of divalent cations, inducing aggregation (Gulamhussein *et al*., 2019). Cations are involved in the functioning of many proteins including GPCRs. For example, Mg^{2+} and Ca^{2+} are allosteric modulators of A2AR: shifting the equilibrium of A2AR towards more active states (Ye *et al*., 2018). Some polymers, such as DIBMA, have been shown to have less cation sensitivity and, therefore could be a more appropriate solubilising agent for investigation of cation regulation of GPCRs (Gulamhussein *et al*., 2020).

Research into functionalised polymers such as fluorescent polymers or biotinylated polymers is ongoing. Fluorescence polymers would be highly useful for tracking polymer concentration and could provide another tool for ligand binding techniques including FCS and FRET-based assays (Neville *et al*., 2022). Biotinylated polymers could be used to adsorb GPCRs onto a

surface, which could be useful of SPR and other surface-based detection systems (Lindhoud *et al*., 2016).

8.5.2 New GPCRs

NTR1 and CB2 are validated as potential therapeutic targets (Dhopeshwarkar and Mackie, 2014; More *et al*., 2024). These GPCRs were chosen as 'model' GPCRs with known ligands and structures. 94% of approved drugs or drugs in clinical trials that target GPCRs, target Class A receptors (Hauser *et al*., 2017). A bottleneck for the investigation of many understudied GPCRs, with unknown endogenous ligands, is a lack of chemical tools for binding characterisation (Wacker *et al*., 2017). Utilising PoLiPa technology could provide a new platform for ligand screening for understudied GPCRs. Future research into new GPCRs could therefore be highly impactful.

8.5.3 Oligomerisation Studies

GPCR dimerization has recently become more widely accepted and shown to have a large effect on the downstream signalling caused by a GPCR. NTR1 and NTR2 have been proven to form heterodimers (Hwang *et al*., 2010). PoLiPa technology allows the investigation of the effect of dimerization in solution. GHRa and Dopamine receptors modulate each other's G protein activation in a SMALP (Damian *et al*., 2018). The use of PoLiPas removes the indirect effects from the co-expression of two receptors.

The oligomerisation of GPCRs may be possible across SMALPs. Fluorescent assays, SEC and SMA-PAGE may be used to further investigate this concept. NTR1 oligomerisation can be induced by ligand binding in HEK293T cells (Westphal *et al*., 2019). PoLiPa technology could be used to detect this effect extracellularly.

8.5.4 Solution-based Assessment of GPCR Interactions - Utilising Fluorescent Assays and Validation of Binding Experiments.

The preliminary functional assays performed in this project provide a key starting point for other polymer-solubilised GPCR investigations, however, this work requires further validation. An n of 3 for all binding curves and enough data points to achieve saturation would be required to confidently quote a K_d value. After this, there are many possibilities for how this project could have continued to investigate GPCRs encapsulated in a PoLiPa.

FTS could be used to monitor conformational changes of the PoLiPas in different conditions. For example, with various polymers, buffer components or oligomeric states. Mutations to the tryptophan residues could further elucidate the contribution to the FTS signal and allow interpretation of the conformational changes within the GPCR. For example, the exchange of the tryptophan residues within the ligand binding site could confirm that the emission spectra changes were due to conformational changes to the GPCR instead of changes in the local environment caused by the ligand directly. Biosynthetically incorporating 5-hydroxytryptophan (5-HW) could aid the selection of specific tryptophan residues in a GPCR-Mini-G protein complex. The hydroxy group causes a specific red shift causing 5-HW to absorb light at a wavelength of 310-320 nm, making the fluorescence distinguishable from other tryptophan residues (Petrović *et al*., 2013). FTS is a method proven to be appropriate for SMALP-encapsulated GPCRs (Routledge *et al*., 2020). Future experiments to utilise this technique for potential new ligand discovery could be highly impactful.

FCS could be used to track fluorescently labelled proteins and ligands simultaneously. The construct for GFP-tagged Mini-G proteins could be used to monitor the diffusion rate of the SMA-GPCR:G protein complex to validate the MK337 data collected in this project.

FCS has less potential than FTS at being a high-throughput technique due to the restrictions of the well chamber plates for the use of the confocal microscope. However, information about diffusion rate, binding characteristics and ligand concentration from FCS could still be highly useful for drug discovery processes.

One of the major benefits of PoLiPa technology is the inclusion of 'native' lipids in solution-based techniques. GPCRs are modulated by the surrounding lipids (Table 8.4). Exchanging the lipids within the SMALP has been proven by FRET and small-angle neutron scattering experiments (Cuevas Arenas *et al*., 2017). The addition of different lipids to a SMALP-encapsulated GPCR could affect its ligand binding characteristics due to allosteric modulation. Approximately, 44% of Class A GPCRs are expected to have a cholesterol-binding site (Hanson *et al*., 2008). Despite this, the effect of the stabilising agent CHS on ligand binding is not well-defined.

Table 8.4: Non-exhaustive List of Known Lipids Capable of GPCR Allosteric Modulation

Lipid Allosteric Modulator	**GPCR**	**Effect**	**Reference**
Phosphatidylethanolamine	β2-Adrenoreceptor	Increased agonist binding, facilitated activation	(Dawaliby *et al*., 2016)
Phosphatidylglycerol	β2-Adrenoreceptor	Increased antagonist binding and stabilised inactive states	(Dawaliby *et al*., 2016)
Cholesterol	Several GPCRs including Oxytocin Receptor	Increase in affinity for oxytocin	(Gimpl *et al*., 1995)
Phosphatidylinositol 4,5 bisphosphate (PIP2)	β1-Adrenoreceptor	Increase Gs preference over other G proteins	(Yen *et al*., 2018)
PIP2 and glycosphingolipid	Ghrelin Receptor	Shifts equilibrium towards active states – increases G protein binding	(Damian *et al*., 2021)
Docosahexaenoic Acid	A2AR	Shifts equilibrium towards active states- increases G protein binding	(Mizumura *et al*., 2020)

The solution-based ligand binding experiments in this project could be used to investigate the concept of allosteric modulation further. This is particularly exciting for drug discovery as it could lead to the discovery of compounds which can 'fine-tune' the response of a GPCR. Currently (September 2024), there are 530 GPCR targeting drugs in clincal trials and 14 are allosteric modulators (GPCRdb: Accessed September 2024)) (Pándy-Szekeres *et al*., 2022).

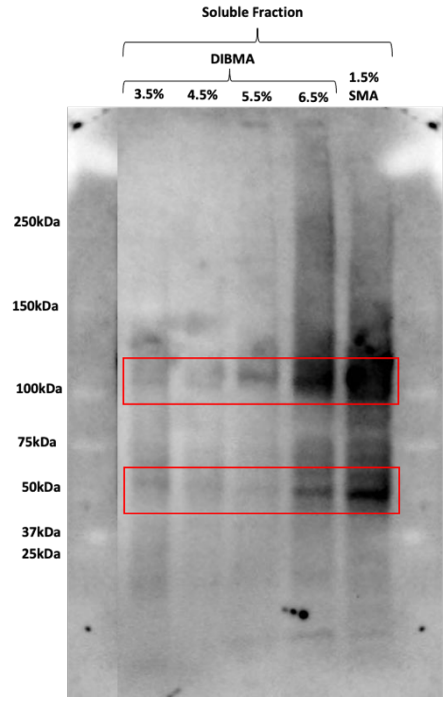
This project showed the binding of two GPCRs encapsulated in a PoLiPa to multiple ligands and G proteins. This demonstrated the potential of fluorescence-based assays to elucidate the complex binding characteristics of GPCRs. There is a wealth of interest in GPCR binding to aptamers (Takahashi, 2022), nanobodies (Laeremans *et al*., 2022) and natural products from bacteria, algae, fungi and plants (Serrano-Marín *et al*., 2020). The methodology developed in this project could be used to assess the binding of new therapeutic agents and investigate GPCR interactions with their many binding partners.

8.6 Final Remarks

This project aimed to determine the optimal expression, solubilisation and purification of GPCRs using PoLiPa technology and to determine if polymer-solubilised GPCRs were capable of ligand binding. This project optimised the production of two GPCRs expressed in *E. coli* and one GPCR expressed in HEK293 cells. There was preliminary evidence of two of these GPCRs having functional activity in a SMALP. This project contributed to the development of PoLiPa technology by discovering new ways to overcome purification issues associated with PoLiPas and low-expressing, unstable proteins, such as GPCRs. Continued research into the functionality of polymer-solubilised GPCRs could be highly beneficial to drug discovery.

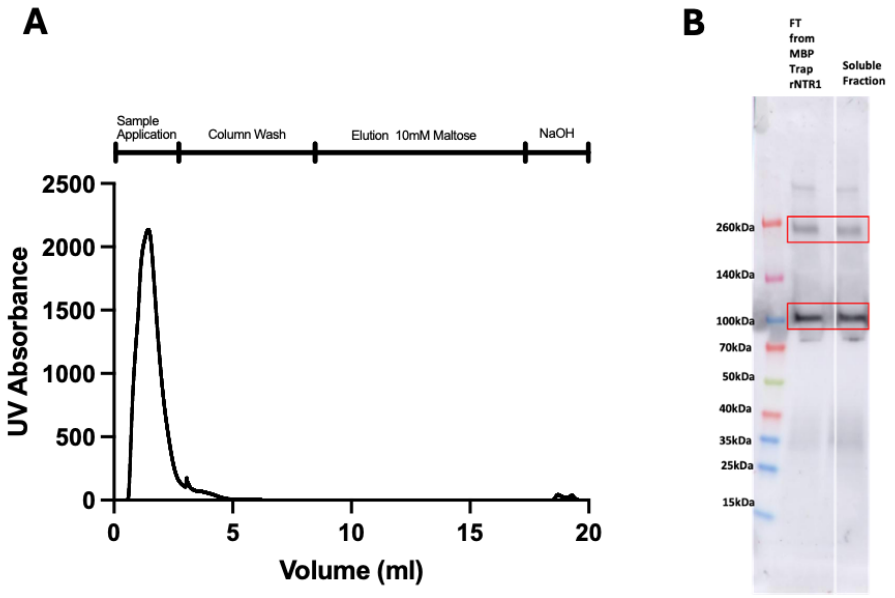
APPENDIX

Appendix 1.1 – E. coli expressed hNTR1 extraction with different DIBMA concentrations.



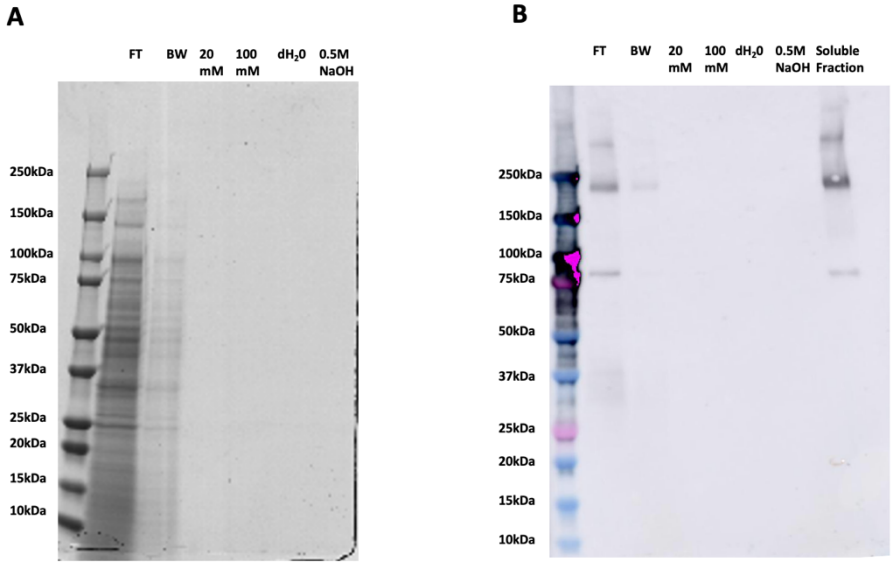
Appendix 1.1: E. coli expressed hNTR1 solubilisation trial comparing 4 concentrations of DIBMA (3.5%, 4.5%, 5.5%, 6.5%) and 1.5% w/v SMA.
Soluble fraction of hNTR1 expressing E. coli membranes were sampled and analysed by SDS-PAGE and Western blot using a 4-20% gradient acrylamide gel and using Anti-His antibody. Red boxes indicate area where hNTR1 would run as a monomer (46kDa) or a dimer (92kDa).

Appendix 1.2 Use of MBP fusion protein as a means of purification of MBP-fused rNTR1 Expressed in E. coli



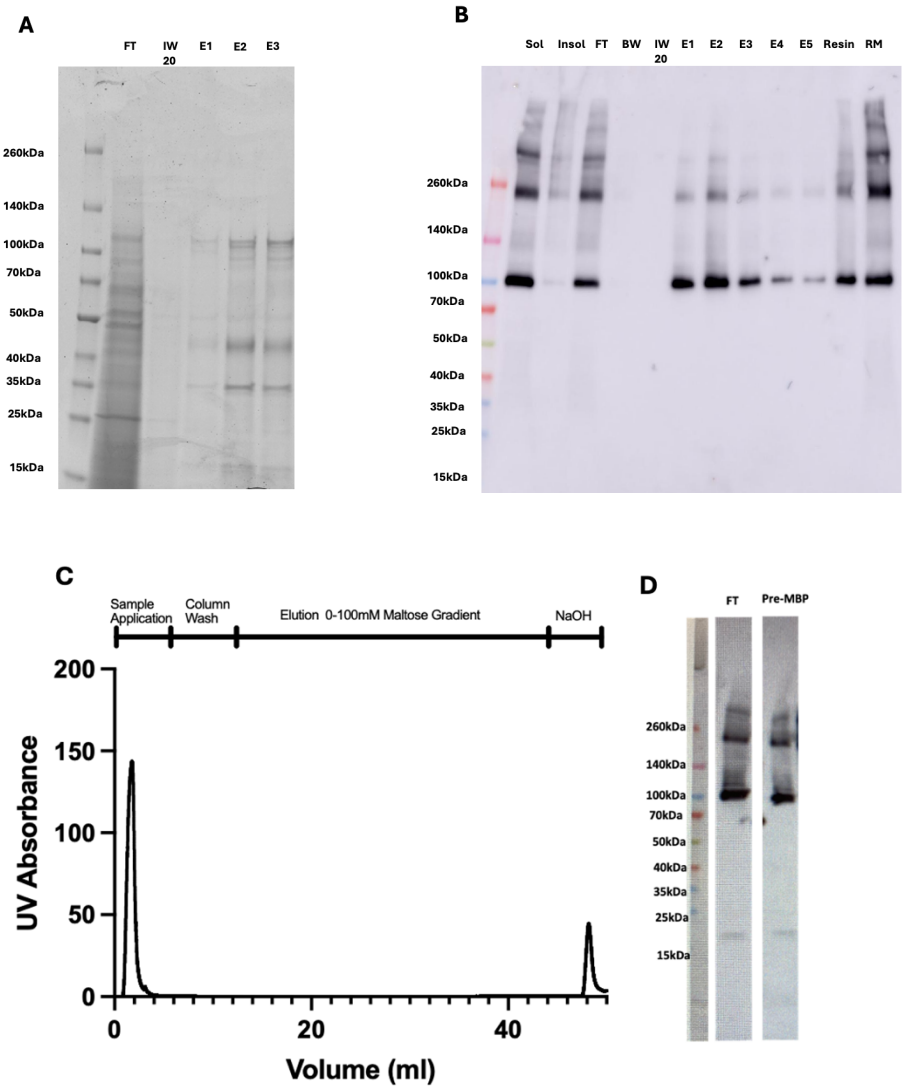
Appendix 1.2: Result of attempted MBPTRap Purification of SMA-rNTR1 expressing E. coli membranes.
(A) Absorbance E Trace measuring 280nm wavelength absorbance as SMA-rNTR1 expressing E. coli membranes sample were applied to an MBPTrap column and elution attempted by a 0-100mM Maltose gradient, followed by a 0.6M NaOH column wash.
(B)Western blot using an anti-His antibody to show the soluble fraction sample before application to the MBPTrap Column (Soluble fraction) and the flow through from the MBP-Trap Column collected during the sample application to the column. Red boxes indicate area where rNTR1 would run as a monomer and dimer. Analysis performed on a 4-20% gradient acrylamide gel.

Appendix 1.3 – Overnight binding to MBPTrap column to improve the use of MBP fusion protein as a means of purification of rNTR1 Expressed in E. coli, overnight binding to column



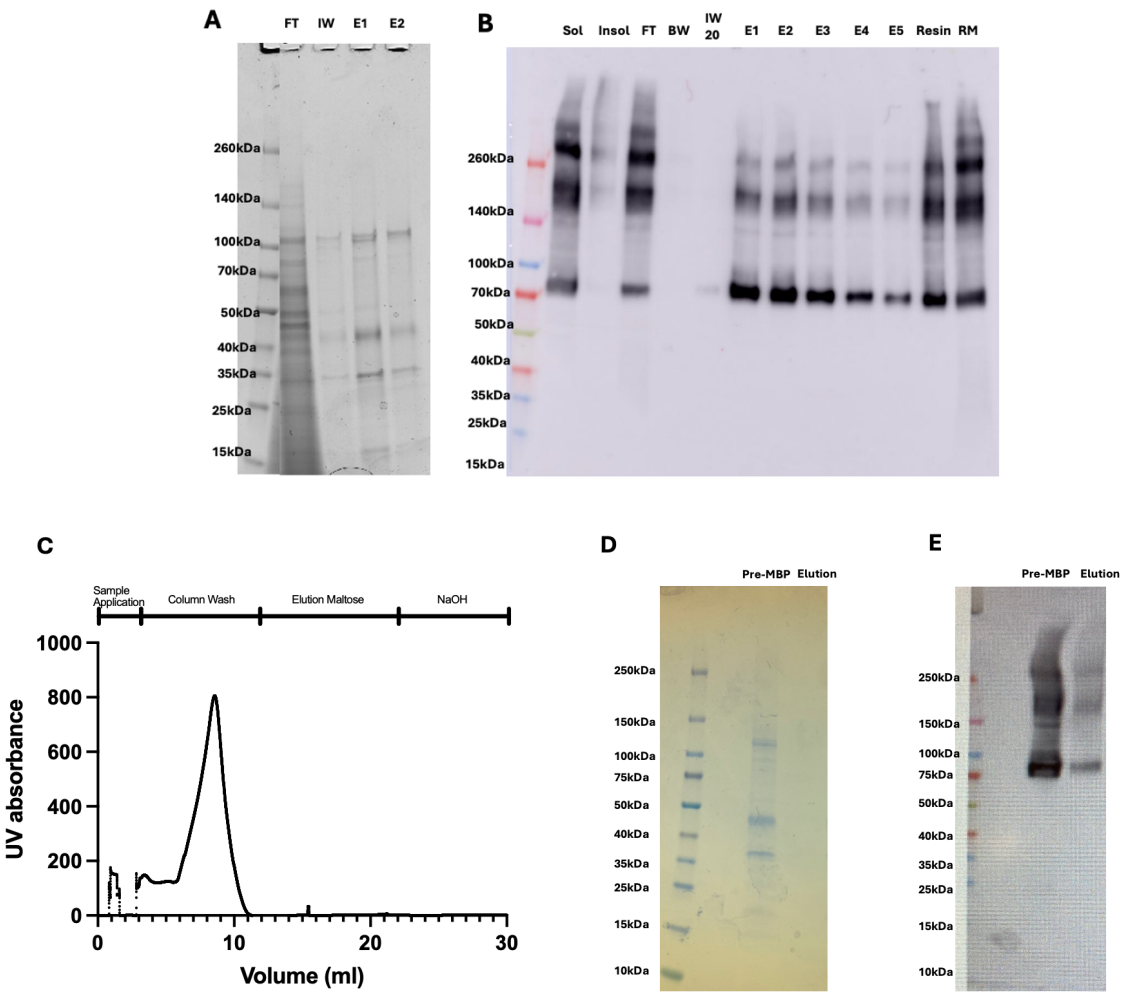
Appendix 1.3: SDS-PAGE and Western blot analysis of the MBPTrap purification method when SMA-rNTR1 expressing membranes were continuously applied to the MBPTrap column overnight.
(A) Coomassie stained SDS-PAGE gel showing the flow through (FT), Buffer Wash (BW), 20mM Maltose and 100mM Maltose elution fractions, column wash with water (dH_20) and 0.5M NaOH Wash Analysis performed on a 4-20% gradient acrylamide gel..
(B) Western blot of MBPTrap purification fractions plus a sample of the soluble material before application of the MBPTrap Column. Analysis performed on a 4-20% gradient acrylamide gel.

Appendix 1.4 –IMAC purification followed by MBPTrap purification to determine the possible benefit of MBPTrap Binding of SMA-rNTR1 expressed in E. coli



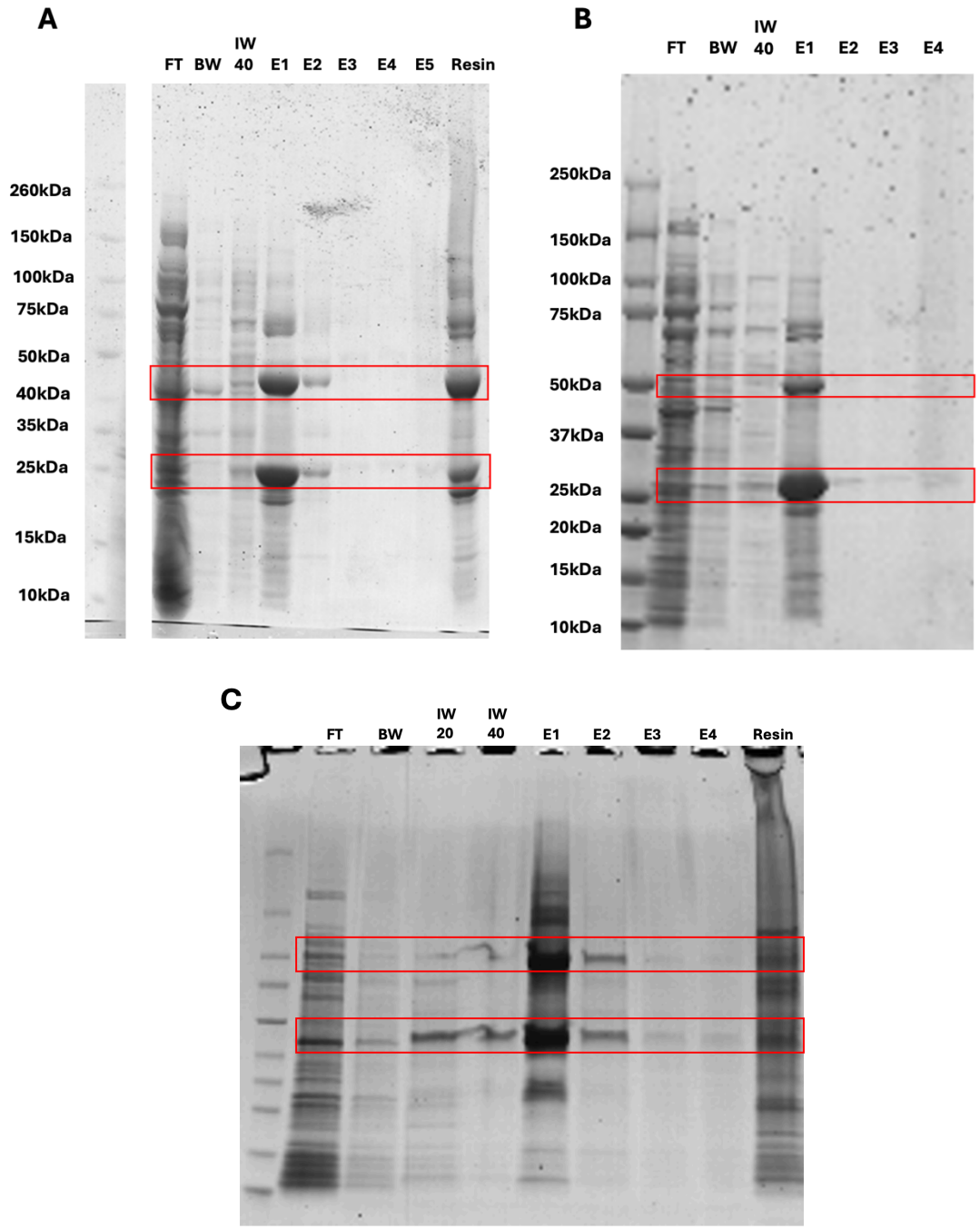
Appendix 1.4: Results of IMAC purification followed by MBP purification of MBP-fused rNTR1 expressed in E. coli.
All SDS-PAGE analysis was performed on a 4-20% gradient acrylamide gel.
(A) Coomassie-stained SDS-PAGE gel shows the flow through (FT), 20mM imidazole wash fraction (IW) and three of the five 500mM imidazole elution fractions (E1, E2, E3) after binding SMA-rNTR1-expressing E. coli membranes to Ni-NTA resin.
(B) Western blot using an anti-His antibody to detect theHistagged rNTR1 in the fractions of the IMAC purification. Columns show the soluble (SOL) and insoluble (INSOL) fractions after the addition of 2.5% (w/v) SMA; the flow through (FT); imidazole wash (IW20); the five elution fractions (E1, E2, E3, E4, E5); a sample of the Ni-NTA resin after the imidazole elution (Nickel Resin) and the raw membranes (RM) before solubilisation.
(C) Absorbance Trace measuring 280nm wavelength absorbance as post- IMAC sample was applied to an MBPTrap column and elution attempted by a 0-100 mM Maltose gradient, followed by a 0.6M NaOH column wash.
(D) Western blot analysis ofPost-IMAC Pre-MBP purification sample (Pre-MBP) and flow through (FT) from the MBPTrap.

Appendix 1.5 – SMA-solubilised E. coli membranes expressing rNTR1 IMAC purification followed by MBPTrap purification



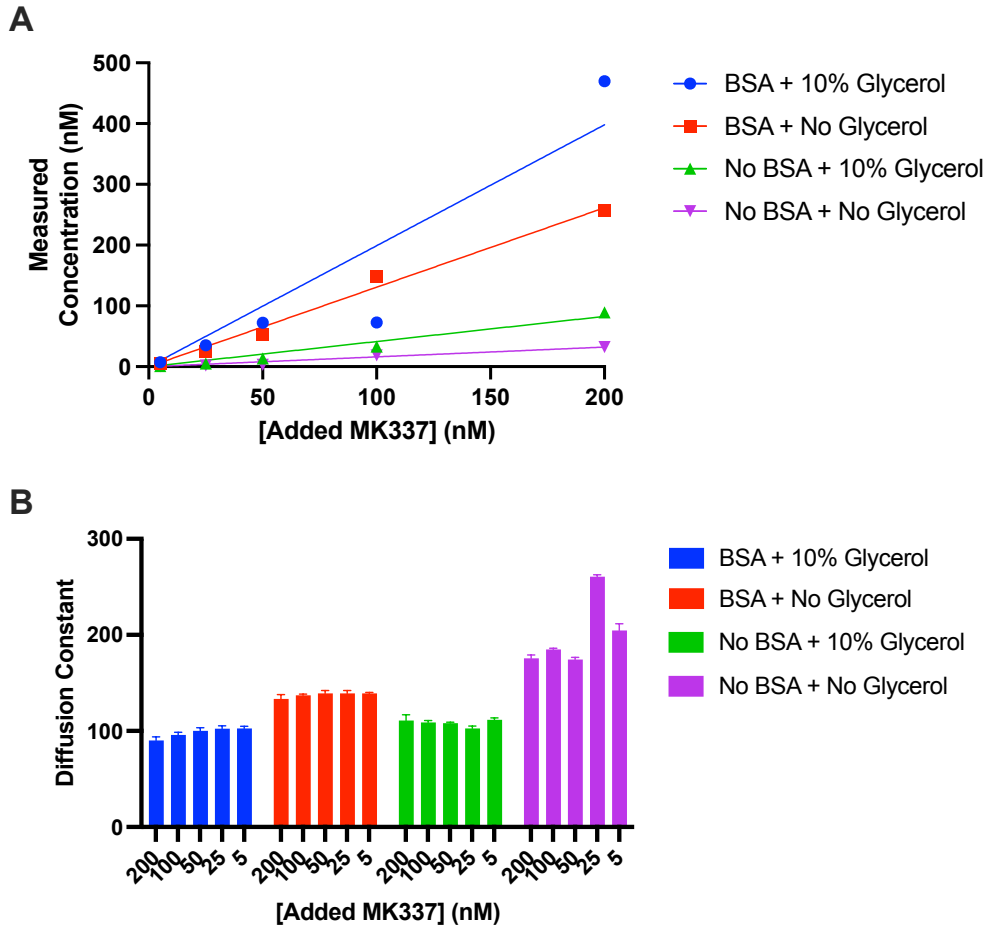
Appendix 1.5: Results of IMAC purification followed by MBP purification of MBP-fused CB2 -expressed in E. coli.
All SDS-PAGE analysis was performed on a 4-20% gradient acrylamide gel.
(A) Coomassie-stained SDS-PAGE gel shows the flow through (FT), 20mM imidazole wash fraction (IW) and three of the five 500mM imidazole elution fractions (E1, E2) after binding SMA-rNTR1-expressing E. coli membranes to Ni-NTA resin.
(B) Western blot analysis to detect theHistagged rNTR1 in the fractions of the IMAC purification. Columns show the soluble (SOL) and insoluble (INSOL) fractions after the addition of 2.5% SMA; the flow through (FT); imidazole wash (IW20); the five elution fractions (E1, E2, E3, E4, E5); a sample of the Ni-NTA resin after imidazole elution (Nickel Resin) and the raw membranes (RM) before solubilisation. Probed using anti-His antibody.
(C) Absorbance Trace measuring 280nm wavelength absorbance as post- IMAC sample was applied to an MBPTrap column and elution attempted by a 0-100 mM Maltose gradient, followed by a 0.6M NaOH column wash.
(D) SDS-PAGE analysis of Post-IMAC Pre-MBP purification sample (Pre-MBP) and Elution fraction collected at 15ml.
(E) Western blot analysis of Post-IMAC Pre-MBP purification sample (Pre-MBP) and Elution fraction at 15ml. Probed using anti-His antibody.

Appendix 1.6 – IMAC Purifications of E. coli Expressed Mini-G proteins



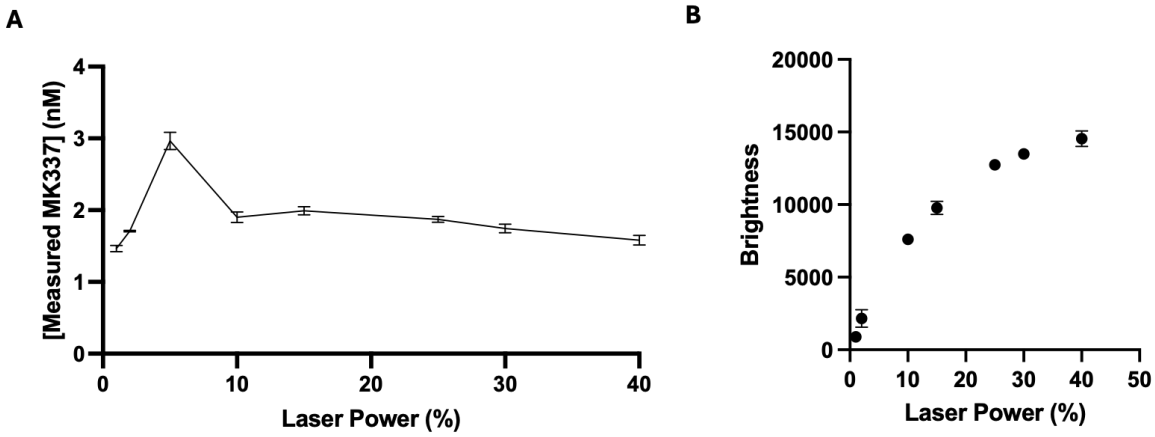
Appendix 1.6: SDS-PAGE analysis of fractions from Mini-G protein IMAC Purifications.
Analysis of the flow through (FT); imidazole washes (IW20/IW40); elution fractions (E1-E4/5); a sample of the Ni-NTA resin after imidazole elution (Resin) were performed on a 4-20% gradient acrylamide gel.
(A) Gs Purification. Red boxes indicate suspected monomer and dimer bands.
(B) Gsq Purification. Red boxes indicate suspected monomer and dimer bands.
(C) Gs-GFP Purification.

Appendix 1.7 – MK337 Characterisation for FCS: Testing the inclusion of BSA and glycerol in the buffer on the measured concentration of MK337 and the calculated diffusion rate



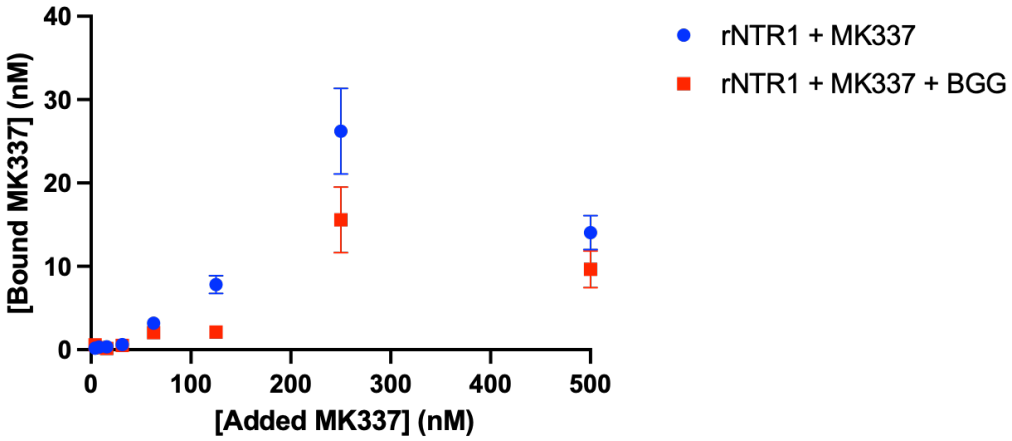
Appendix 1.7: MK337 characterisation in four different buffer systems: with and without 5 mg/mL BSA and 10% (v/v) glycerol.
Five different MK337 concentrations (12.5 nM, 25 nM, 50 nM, 100 nM, 250 nM) were analysed by solution-based FCS. (A) Measured concentration of MK337 calculated from a 1-component model after FCS analysis and plotted linear relationship (B) Average Diffusion Rate of MK337 calculated from a 1-component model after FCS analysis. Measurements of the same sample were taken and input into the model three times and error bars show standard deviation between measurements.

Appendix 1.8 – MK337 Characterisation for FCS: Testing the effect of laser power of MK337 measured concentration and brightness



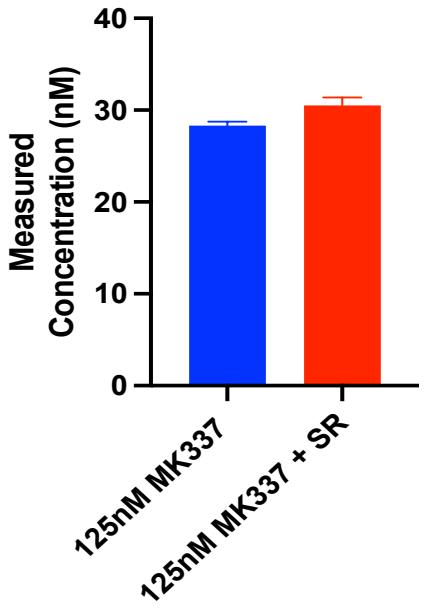
Appendix 1.8: MK337 characterisation using eight different laser power strengths (1- 40%).
Measurements of the same sample were taken and input into the model three times and error bars show standard deviation between measurements.
(A) Measured concentration of MK337 calculated from a 1-component model after solution-based FCS analysis of 50nM MK337 using different laser powers
(B) Brightness of MK337 measured after solution-based FCS analysis of 50nM MK337 using different laser powers.

Appendix 1.9 – MK337 Characterisation for FCS: MK337 series to determine the possible increase in bound MK337 to SMA-solubilised NTR1 with and without Bovine Gamma Globulin (BGG)



Appendix 1.9: Concentration of bound MK337 calculated from a 2-component model after solution-based FCS analysis of seven different MK337 (7.8 nM – 500 nM) concentrations incubated with SMA-rNTR1, with and without bovine gamma globulin (BGG).
SMA-rNTR1 concentration was 0.2 mg/mL. Measurements of the same sample were taken and input into the model three times and error bars show standard deviation between measurements.

Appendix 1.10 – MK337 Characterisation for FCS: The effect of antagonist SR 48692.



Appendix 1.9: MK337 characterisation with and without 170 nM SR 48692.
Measured concentration of MK337 calculated from a 1-component model after FCS analysis and plotted linear relationship.

REFERENCES

Abdul-Gader A, Miles AJ and Wallace BA (2011) A reference dataset for the analyses of membrane protein secondary structures and transmembrane residues using circular dichroism spectroscopy. *Bioinformatics* 27(12): 1630-1636.

Abe R, Kudou M, Tanaka Y, *et al*. (2009) Immobilized metal affinity chromatography in the presence of arginine. *Biochemical and Biophysical Research Communications* 381(3): 306-310.

Abiko LA, Rogowski M, Gautier A, *et al*. (2021) Efficient production of a functional G protein-coupled receptor in *E. coli* for structural studies. *J Biomol NMR* 75(1): 25-38.

Adair BD, Xiong J-P, Yeager M, *et al*. (2023) Cryo-EM structures of full-length integrin αIIbβ3 in native lipids. *Nature Communications* 14(1): 4168.

Allen JA, Halverson-Tamboli RA and Rasenick MM (2007) Lipid raft microdomains and neurotransmitter signalling. *Nature Reviews Neuroscience* 8(2): 128-140.

Arakawa J, Uegaki M and Ishimizu T (2011) Effects of l-arginine on solubilization and purification of plant membrane proteins. *Protein Expression and Purification* 80(1): 91-96.

Arakawa T, Ejima D, Tsumoto K, *et al*. (2007) Suppression of protein interactions by arginine: A proposed mechanism of the arginine effects. *Biophysical Chemistry* 127(1): 1-8.

Arcemisbéhère L, Sen T, Boudier L, *et al*. (2010) Leukotriene BLT2 receptor monomers activate the G(i2) GTP-binding protein more efficiently than dimers. *J Biol Chem* 285(9): 6337-6347.

Attrill H, Harding PJ, Smith E, *et al*. (2009) Improved yield of a ligand-binding GPCR expressed in *E. coli* for structural studies. *Protein Expression and Purification* 64(1): 32-38.

Ayub H, Clare M, Milic I, *et al*. (2020) CD81 extracted in SMALP nanodiscs comprises two distinct protein populations within a lipid environment enriched with negatively charged headgroups. *Biochim Biophys Acta Biomembr* 1862(11): 183419.

Baccouch R, Rascol E, Stoklosa K, *et al*. (2022) The role of the lipid environment in the activity of G protein coupled receptors. *Biophysical Chemistry* 285: 106794.

Bada Juarez JF, Muñoz-García JC, Inácio dos Reis R, *et al*. (2020) Detergent-free extraction of a functional low-expressing GPCR from a human cell line. *Biochimica et Biophysica Acta (BBA) - Biomembranes* 1862(3): 183152.

Bartlow P, Uechi GT, Cardamone JJ, *et al*. (2011) Identification of native Escherichia coli BL21 (DE3) proteins that bind to immobilized metal affinity chromatography under high imidazole conditions and use of 2D-DIGE to evaluate contamination pools with respect to recombinant protein expression level. *Protein Expression and Purification* 78(2): 216-224.

Bartoschik T, Galinec S, Kleusch C, *et al*. (2018) Near-native, site-specific and purification-free protein labeling for quantitative protein interaction analysis by MicroScale Thermophoresis. *Scientific reports* 8(1): 4977.

Beckner RL, Zoubak L, Hines KG, *et al*. (2020) Probing thermostability of detergent-solubilized CB(2) receptor by parallel G protein-activation and ligand-binding assays. *J Biol Chem* 295(1): 181-190.

Berger C, Ho JTC, Kimura T, *et al*. (2010) Preparation of stable isotope-labeled peripheral cannabinoid receptor CB2 by bacterial fermentation. *Protein Expression and Purification* 70(2): 236-247.

Besserer-Offroy É, Brouillette RL, Lavenus S, *et al*. (2017) The signaling signature of the neurotensin type 1 receptor with endogenous ligands. *Eur J Pharmacol* 805: 1-13.

Boivin S, Kozak S and Meijers R (2013) Optimization of protein purification and characterization using Thermofluor screens. *Protein Expr Purif* 91(2): 192-206.
Bokhove M, Sadat Al Hosseini H, Saito T, *et al*. (2016) Easy mammalian expression and crystallography of maltose-binding protein-fused human proteins. *Journal of Structural Biology* 194(1): 1-7.
Bolanos-Garcia VM and Davies OR (2006) Structural analysis and classification of native proteins from *E. coli* commonly co-purified by immobilised metal affinity chromatography. *Biochimica et Biophysica Acta (BBA) - General Subjects* 1760(9): 1304-1313.
Bornhorst JA and Falke JJ (2000) Purification of proteins using polyhistidine affinity tags. *Methods Enzymol* 326: 245-254.
Brailoiu GC, Deliu E, Marcu J, *et al*. (2014) Differential activation of intracellular versus plasmalemmal CB2 cannabinoid receptors. *Biochemistry* 53(30): 4990-4999.
Briddon SJ, Kellam B and Hill SJ (2011) Design and use of fluorescent ligands to study ligand-receptor interactions in single living cells. *Methods Mol Biol* 746: 211-236.
Bumbak F, Thomas T, Noonan-Williams BJ, *et al*. (2020) Conformational Changes in Tyrosine 11 of Neurotensin Are Required to Activate the Neurotensin Receptor 1. *ACS Pharmacology & Translational Science* 3(4): 690-705.
Callén L, Moreno E, Barroso-Chinea P, *et al*. (2012) Cannabinoid receptors CB1 and CB2 form functional heteromers in brain. *J Biol Chem* 287(25): 20851-20865.
Campeau E, Ruhl VE, Rodier F, *et al*. (2009) A Versatile Viral System for Expression and Depletion of Proteins in Mammalian Cells. *PLoS One* 4(8): e6529.
Carpenter B and Tate CG (2017) Active state structures of G protein-coupled receptors highlight the similarities and differences in the G protein and arrestin coupling interfaces. *Current Opinion in Structural Biology* 45: 124-132.
Cavasotto CN and Palomba D (2015) Expanding the horizons of G protein-coupled receptor structure-based ligand discovery and optimization using homology models. *Chemical Communications* 51(71): 13576-13594.
Chelikani P, Reeves PJ, Rajbhandary UL, *et al*. (2006) The synthesis and high-level expression of a β2-adrenergic receptor gene in a tetracycline-inducible stable mammalian cell line. *Protein Science* 15(6): 1433-1440.
Cho S, Lee H, Han YH, *et al*. (2023) Design of an effective small expression tag to enhance GPCR production in *E. coli*-based cell-free and whole cell expression systems. *Protein Science* 32(12): e4839.
Chu C, Vargas C, Barbosa MC, *et al*. (2024) Capturing G protein-coupled receptors into native lipid-bilayer nanodiscs using new diisobutylene/maleic acid (DIBMA) copolymers. *bioRxiv*. DOI: 10.1101/2024.01.20.576420. 2024.2001.2020.576420.
Cook BL, Ernberg KE, Chung H, *et al*. (2008) Study of a synthetic human olfactory receptor 17-4: expression and purification from an inducible mammalian cell line. *PLoS One* 3(8): e2920.
Corin K, Baaske P, Geissler S, *et al*. (2011) Structure and function analyses of the purified GPCR human vomeronasal type 1 receptor 1. *Scientific Reports* 1(1): 172.
Craig AF, Clark EE, Sahu ID, *et al*. (2016) Tuning the size of styrene-maleic acid copolymer-lipid nanoparticles (SMALPs) using RAFT polymerization for biophysical studies. *Biochimica et Biophysica Acta (BBA) - Biomembranes* 1858(11): 2931-2939.
Cuevas Arenas R, Danielczak B, Martel A, *et al*. (2017) Fast Collisional Lipid Transfer Among Polymer-Bounded Nanodiscs. *Scientific Reports* 7(1): 45875.
Cunningham RD, Kopf AH, Elenbaas BOW, *et al*. (2020) Iterative RAFT-Mediated Copolymerization of Styrene and Maleic Anhydride toward Sequence- and Length-Controlled Copolymers and Their Applications for Solubilizing Lipid Membranes. *Biomacromolecules* 21(8): 3287-3300.
Cytiva (2020) Size Exclusion Chromatography Principles and Methods.

Dalal V, Arcario MJ, Petroff JT, *et al*. (2024) Lipid nanodisc scaffold and size alter the structure of a pentameric ligand-gated ion channel. *Nature Communications* 15(1): 25.
Damian M, Louet M, Gomes AAS, *et al*. (2021) Allosteric modulation of ghrelin receptor signaling by lipids. *Nature Communications* 12(1): 3938.
Damian M, Marie J, Leyris JP, *et al*. (2012) High constitutive activity is an intrinsic feature of ghrelin receptor protein: a study with a functional monomeric GHS-R1a receptor reconstituted in lipid discs. *J Biol Chem* 287(6): 3630-3641.
Damian M, Pons V, Renault P, *et al*. (2018) GHSR-D2R heteromerization modulates dopamine signaling through an effect on G protein conformation. *Proc Natl Acad Sci U S A* 115(17): 4501-4506.
Das U, Hariprasad G, Ethayathulla AS, *et al*. (2007) Inhibition of protein aggregation: supramolecular assemblies of arginine hold the key. *PLoS One* 2(11): e1176.
Dathe A, Heitkamp T, Pérez I, *et al*. (2019) *Observing monomer - dimer transitions of neurotensin receptors 1 in single SMALPs by homoFRET and in an ABELtrap.*
Davis DA, Bulut H, Shrestha P, *et al*. (2021) Regulation of the Dimerization and Activity of SARS-CoV-2 Main Protease through Reversible Glutathionylation of Cysteine 300. *bioRxiv*. Epub ahead of print 20210412. DOI: 10.1101/2021.04.09.439169.
Dawaliby R, Trubbia C, Delporte C, *et al*. (2016) Allosteric regulation of G protein–coupled receptor activity by phospholipids. *Nature Chemical Biology* 12(1): 35-39.
Deluigi M, Klipp A, Klenk C, *et al*. (2021) Complexes of the neurotensin receptor 1 with small-molecule ligands reveal structural determinants of full, partial, and inverse agonism. *Sci Adv* 7(5).
DeVree BT, Mahoney JP, Vélez-Ruiz GA, *et al*. (2016) Allosteric coupling from G protein to the agonist-binding pocket in GPCRs. *Nature* 535(7610): 182-186.
Dhopeshwarkar A and Mackie K (2014) CB2 Cannabinoid receptors as a therapeutic target-what does the future hold? *Mol Pharmacol* 86(4): 430-437.
Dijkman PM, Castell OK, Goddard AD, *et al*. (2018) Dynamic tuneable G protein-coupled receptor monomer-dimer populations. *Nature Communications* 9(1): 1710.
Dumon-Seignovert L, Cariot G and Vuillard L (2004) The toxicity of recombinant proteins in Escherichia coli: a comparison of overexpression in BL21(DE3), C41(DE3), and C43(DE3). *Protein Expr Purif* 37(1): 203-206.
Duong-Ly KC and Gabelli SB (2015) Affinity Purification of a Recombinant Protein Expressed as a Fusion with the Maltose-Binding Protein (MBP) Tag. *Methods Enzymol* 559: 17-26.
Edwards GB, Muthurajan UM, Bowerman S, *et al*. (2020) Analytical Ultracentrifugation (AUC): An Overview of the Application of Fluorescence and Absorbance AUC to the Study of Biological Macromolecules. *Curr Protoc Mol Biol* 133(1): e131.
Egloff P, Deluigi M, Heine P, *et al*. (2015) A cleavable ligand column for the rapid isolation of large quantities of homogeneous and functional neurotensin receptor 1 variants from *E. coli*. *Protein Expr Purif* 108: 106-114.
Egloff P, Hillenbrand M, Klenk C, *et al*. (2014) Structure of signaling-competent neurotensin receptor 1 obtained by directed evolution in Escherichia coli. *Proc Natl Acad Sci U S A* 111(6): E655-662.
Ejima D, Yumioka R, Arakawa T, *et al*. (2005a) Arginine as an effective additive in gel permeation chromatography. *J Chromatogr A* 1094(1-2): 49-55.
Ejima D, Yumioka R, Tsumoto K, *et al*. (2005b) Effective elution of antibodies by arginine and arginine derivatives in affinity column chromatography. *Anal Biochem* 345(2): 250-257.
Ekundayo B, Arullampalam P, Gerber CE, *et al*. (2024) Identification of a Binding Site for Small Molecule Inhibitors Targeting Human TRPM4. *bioRxiv*. DOI: 10.1101/2024.01.22.576650. 2024.2001.2022.576650.

Elegheert J, Behiels E, Bishop B, *et al*. (2018) Lentiviral transduction of mammalian cells for fast, scalable and high-level production of soluble and membrane proteins. *Nature Protocols* 13(12): 2991-3017.
Eroglu Ç, Cronet P, Panneels V, *et al*. (2002) Functional reconstitution of purified metabotropic glutamate receptor expressed in the fly eye. *EMBO reports* 3(5): 491-496.
Filppula S, Yaddanapudi S, Mercier R, *et al*. (2004) Purification and mass spectroscopic analysis of human CB2 cannabinoid receptor expressed in the baculovirus system. *The Journal of Peptide Research* 64(6): 225-236.
Fiori MC, Jiang Y, Altenberg GA, *et al*. (2017) Polymer-encased nanodiscs with improved buffer compatibility. *Scientific reports* 7(1): 7432.
Fotiadis D and Harder D (2012) *Preparation of detergent-solubilized membranes from Escherichia coli.*
Fox BG and Blommel PG (2009) Autoinduction of protein expression. *Curr Protoc Protein Sci* Chapter 5: 5.23.21-25.23.18.
Francis DM and Page R (2010) Strategies to optimize protein expression in *E. coli*. *Curr Protoc Protein Sci* Chapter 5(1): 5.24.21-25.24.29.
Franks F (1993) Storage Stabilization of Proteins. In: Franks F (ed) *Protein Biotechnology: Isolation, Characterization, and Stabilization*. Totowa, NJ: Humana Press, pp.489-531.
Getz EB, Xiao M, Chakrabarty T, *et al*. (1999) A comparison between the sulfhydryl reductants tris(2- carboxyethyl)phosphine and dithiothreitol for use in protein biochemistry. *Analytical Biochemistry* 273(1): 73-80.
Ghisaidoobe AB and Chung SJ (2014) Intrinsic tryptophan fluorescence in the detection and analysis of proteins: a focus on Förster resonance energy transfer techniques. *Int J Mol Sci* 15(12): 22518-22538.
Gimpl G, Klein U, Reilaender H, *et al*. (1995) Expression of the human oxytocin receptor in baculovirus-infected insect cells: high-affinity binding is induced by a cholesterol-cyclodextrin complex. *Biochemistry* 34(42): 13794-13801.
Gomes L, Monteiro G and Mergulhão F (2020) The Impact of IPTG Induction on Plasmid Stability and Heterologous Protein Expression by Escherichia coli Biofilms. *Int J Mol Sci* 21(2).
Goth CK, Petäjä-Repo UE and Rosenkilde MM (2020) G Protein-Coupled Receptors in the Sweet Spot: Glycosylation and other Post-translational Modifications. *ACS Pharmacology & Translational Science* 3(2): 237-245.
Gray D (2001) Overview of protein expression by mammalian cells. *Curr Protoc Protein Sci* Chapter 5(1): Unit5.9.
Greenfield NJ (2006) Using circular dichroism collected as a function of temperature to determine the thermodynamics of protein unfolding and binding interactions. *Nat Protoc* 1(6): 2527-2535.
Grime RL, Goulding J, Uddin R, *et al*. (2020) Single molecule binding of a ligand to a G-protein-coupled receptor in real time using fluorescence correlation spectroscopy, rendered possible by nano-encapsulation in styrene maleic acid lipid particles. *Nanoscale* 12(21): 11518-11525.
Grime RL, Logan RT, Nestorow SA, *et al*. (2021) Differences in SMA-like polymer architecture dictate the conformational changes exhibited by the membrane protein rhodopsin encapsulated in lipid nano-particles. *Nanoscale* 13(31): 13519-13528.
Grisshammer R (2009) Purification of recombinant G-protein-coupled receptors. *Methods in enzymology* 463: 631-645.
Grisshammer R and Hermans E (2001) Functional coupling with Gαq and Gαi1 protein subunits promotes high-affinity agonist binding to the neurotensin receptor NTS-1 expressed in Escherichia coli. *FEBS Letters* 493(2): 101-105.

Gulamhussein AA, Meah D, Soja DD, *et al*. (2019) Examining the stability of membrane proteins within SMALPs. *European Polymer Journal* 112: 120-125.
Gulamhussein AA, Uddin R, Tighe BJ, *et al*. (2020) A comparison of SMA (styrene maleic acid) and DIBMA (di-isobutylene maleic acid) for membrane protein purification. *Biochimica et Biophysica Acta (BBA) - Biomembranes* 1862(7): 183281.
Hall SCL, Tognoloni C, Charlton J, *et al*. (2018) An acid-compatible co-polymer for the solubilization of membranes and proteins into lipid bilayer-containing nanoparticles. *Nanoscale* 10(22): 10609-10619.
Hamm HE (1998) The many faces of G protein signaling. *Journal of Biological Chemistry* 273(2): 669-672.
Han C-T, Nguyen KDQ, Berkow MW, *et al*. (2023) Lipid membrane mimetics and oligomerization tune functional properties of proteorhodopsin. *Biophysical journal* 122(1): 168-179.
Han S-G, Baek S-I, Son TJ, *et al*. (2017a) Preparation of functional human lysophosphatidic acid receptor 2 using a P9∗ expression system and an amphipathic polymer and investigation of its in vitro binding preference to Gα proteins. *Biochemical and Biophysical Research Communications* 487(1): 103-108.
Han S-G, Ko S, Lee W-K, *et al*. (2017b) Determination of the endothelin-1 recognition sites of endothelin receptor type A by the directed-degeneration method. *Scientific Reports* 7(1): 7577.
Han S-G, Na J-H, Lee W-K, *et al*. (2014) An amphipathic polypeptide derived from poly-γ-glutamic acid for the stabilization of membrane proteins. *Protein Science* 23(12): 1800-1807.
Hanson MA, Cherezov V, Griffith MT, *et al*. (2008) A specific cholesterol binding site is established by the 2.8 A structure of the human beta2-adrenergic receptor. *Structure* 16(6): 897-905.
Harwood CR, Sykes DA, Hoare BL, *et al*. (2021) Functional solubilization of the β(2)-adrenoceptor using diisobutylene maleic acid. *iScience* 24(12): 103362.
Hauser AS, Attwood MM, Rask-Andersen M, *et al*. (2017) Trends in GPCR drug discovery: new agents, targets and indications. *Nature Reviews Drug Discovery* 16(12): 829-842.
Hong P, Koza S and Bouvier ES (2012) Size-Exclusion Chromatography for the Analysis of Protein Biotherapeutics and their Aggregates. *J Liq Chromatogr Relat Technol* 35(20): 2923-2950.
Hu J, Feng Z, Ma S, *et al*. (2016) Difference and Influence of Inactive and Active States of Cannabinoid Receptor Subtype CB2: From Conformation to Drug Discovery. *J Chem Inf Model* 56(6): 1152-1163.
Huang W, Masureel M, Qu Q, *et al*. (2020) Structure of the neurotensin receptor 1 in complex with β-arrestin 1. *Nature* 579(7798): 303-308.
Hughes JP, Rees S, Kalindjian SB, *et al*. (2011) Principles of early drug discovery. *Br J Pharmacol* 162(6): 1239-1249.
Hulme EC and Trevethick MA (2010) Ligand binding assays at equilibrium: validation and interpretation. *British journal of pharmacology* 161(6): 1219-1237.
Hwang JR, Baek MW, Sim J, *et al*. (2010) Intermolecular cross-talk between NTR1 and NTR2 neurotensin receptor promotes intracellular sequestration and functional inhibition of NTR1 receptors. *Biochemical and Biophysical Research Communications* 391(1): 1007-1013.
Inagaki S, Ghirlando R, White JF, *et al*. (2012) Modulation of the interaction between neurotensin receptor NTS1 and Gq protein by lipid. *Journal of Molecular Biology* 417(1-2): 95-111.
Insel PA, Sriram K, Gorr MW, *et al*. (2019) GPCRomics: An Approach to Discover GPCR Drug Targets. *Trends in pharmacological sciences* 40(6): 378-387.

Intranuovo F, Majellaro M, Mastropasqua F, *et al*. (2024) N-Adamantyl-1-alkyl-4-oxo-1,4-dihydroquinoline-3-carboxamide Derivatives as Fluorescent Probes to Detect Microglia Activation through the Imaging of Cannabinoid Receptor Subtype 2 (CB2R). *J Med Chem* 67(13): 11003-11023.

Jamshad M, Charlton J, Lin Y-P, *et al*. (2015a) G-protein coupled receptor solubilization and purification for biophysical analysis and functional studies, in the total absence of detergent. *Bioscience Reports* 35(2): e00188.

Jamshad M, Grimard V, Idini I, *et al*. (2015b) Structural analysis of a nanoparticle containing a lipid bilayer used for detergent-free extraction of membrane proteins. *Nano Res* 8(3): 774-789.

Kang S, Kim NH and Yu YG (2021) Identification of novel positive allosteric modulators of GLP1R that stimulate its interaction with ligands and Gα subunits. *Biochemical and Biophysical Research Communications* 583: 162-168.

Kato HE, Zhang Y, Hu H, *et al*. (2019) Conformational transitions of a neurotensin receptor 1-G(i1) complex. *Nature* 572(7767): 80-85.

Keller M, Mahuroof SA, Hong Yee V, *et al*. (2020) Fluorescence Labeling of Neurotensin(8–13) via Arginine Residues Gives Molecular Tools with High Receptor Affinity. *ACS Medicinal Chemistry Letters* 11(1): 16-22.

Kenakin T (2019) Biased Receptor Signaling in Drug Discovery. *Pharmacol Rev* 71(2): 267-315.

Kim NH, Kang S, Park GH, *et al*. (2023) A robust antibody discovery platform for difficult-to-express G protein-coupled receptors. *Protein Science* 32(1): e4520.

Kim NH, Kim K-S, Shin SC, *et al*. (2021a) Functional expression of human prostaglandin E2 receptor 4 (EP4) in *E. coli* and characterization of the binding property of EP4 with Gα proteins. *Biochemistry and Biophysics Reports* 25: 100871.

Kim NH, Shim G, Park GH, *et al*. (2024) A nondestructive membrane engineering method using an amphiphilic polymer. *Protein Science* 33(9): e5143.

Kim SH, Yoo HJ, Park EJ, *et al*. (2021b) Nano Differential Scanning Fluorimetry-Based Thermal Stability Screening and Optimal Buffer Selection for Immunoglobulin G. *Pharmaceuticals (Basel)* 15(1).

Klenk C, Ehrenmann J, Schütz M, *et al*. (2016) A generic selection system for improved expression and thermostability of G protein-coupled receptors by directed evolution. *Sci Rep* 6: 21294.

Klumperman B and Heuts JPA (2020) The solution copolymerization of styrene and maleic anhydride in a continuous stirred tank reactor and its theoretical modelling. *Polymer* 202: 122730.

Knowles TJ, Finka R, Smith C, *et al*. (2009) Membrane Proteins Solubilized Intact in Lipid Containing Nanoparticles Bounded by Styrene Maleic Acid Copolymer. *Journal of the American Chemical Society* 131(22): 7484-7485.

Kobilka BK (2007) G protein coupled receptor structure and activation. *Biochimica et Biophysica Acta (BBA) - Biomembranes* 1768(4): 794-807.

Kotov V, Bartels K, Veith K, *et al*. (2019) High-throughput stability screening for detergent-solubilized membrane proteins. *Scientific Reports* 9(1): 10379.

Krachmarova E, Tileva M, Lilkova E, *et al*. (2017) His-FLAG Tag as a Fusion Partner of Glycosylated Human Interferon-Gamma and Its Mutant: Gain or Loss? *Biomed Res Int* 2017: 3018608.

Kram KE and Finkel SE (2015) Rich Medium Composition Affects Escherichia coli Survival, Glycation, and Mutation Frequency during Long-Term Batch Culture. *Appl Environ Microbiol* 81(13): 4442-4450.

Krepkiy D, Wong K, Gawrisch K, *et al*. (2006) Bacterial expression of functional, biotinylated peripheral cannabinoid receptor CB2. *Protein Expr Purif* 49(1): 60-70.

Kristiansen K (2004) Molecular mechanisms of ligand binding, signaling, and regulation within the superfamily of G-protein-coupled receptors: molecular modeling and mutagenesis approaches to receptor structure and function. *Pharmacol Ther* 103(1): 21-80.

Kumar A and Plückthun A (2019) In vivo assembly and large-scale purification of a GPCR - Gα fusion with Gβγ, and characterization of the active complex. *PLoS One* 14(1): e0210131.

Kuszak AJ, Pitchiaya S, Anand JP, *et al*. (2009) Purification and Functional Reconstitution of Monomeric μ-Opioid Receptors: allosteric modulation of agonist binding by Gi2*. *Journal of Biological Chemistry* 284(39): 26732-26741.

Labbé-Jullié C, Deschaintres S, Gully D, *et al*. (1994) Effect of the nonpeptide neurotensin antagonist, SR 48692, and two enantiomeric analogs, SR 48527 and SR 49711, on neurotensin binding and contractile responses in guinea pig ileum and colon. *J Pharmacol Exp Ther* 271(1): 267-276.

Laeremans T, Sands Z, Claes P, *et al*. (2022) Accelerating GPCR Drug Discovery With Conformation-Stabilizing VHHs. *Frontiers in Molecular Biosciences* 9.

Lakowicz J (2006) *Principles of Fluorescence Spectroscopy.*

Langer A, Bartoschik T, Cehlar O, *et al*. (2022) A New Spectral Shift-Based Method to Characterize Molecular Interactions. *Assay Drug Dev Technol* 20(2): 83-94.

Larentis AL, Nicolau JF, Esteves Gdos S, *et al*. (2014) Evaluation of pre-induction temperature, cell growth at induction and IPTG concentration on the expression of a leptospiral protein in *E. coli* using shaking flasks and microbioreactor. *BMC Res Notes* 7: 671.

Lebendiker M and Danieli T (2011) Purification of Proteins Fused to Maltose-Binding Protein. In: Walls D and Loughran ST (eds) *Protein Chromatography: Methods and Protocols*. Totowa, NJ: Humana Press, pp.281-293.

Lee S, Ghosh S, Jana S, *et al*. (2020) How Do Branched Detergents Stabilize GPCRs in Micelles? *Biochemistry* 59(23): 2125-2134.

Lee SC, Collins R, Lin Y-p, *et al*. (2019) Nano-encapsulated Escherichia coli Divisome Anchor ZipA, and in Complex with FtsZ. *Scientific Reports* 9(1): 18712.

Lee SC, Knowles TJ, Postis VL, *et al*. (2016) A method for detergent-free isolation of membrane proteins in their local lipid environment. *Nat Protoc* 11(7): 1149-1162.

Leysen H, Walter D, Christiaenssen B, *et al*. (2021) GPCRs Are Optimal Regulators of Complex Biological Systems and Orchestrate the Interface between Health and Disease. *Int J Mol Sci* 22(24).

Li X, Hua T, Vemuri K, *et al*. (2019) Crystal Structure of the Human Cannabinoid Receptor CB2. *Cell* 176(3): 459-467.e413.

Li X, Qian S, Song Y, *et al*. (2022) New insights into the mechanism of freeze-induced damage based on ice crystal morphology and exudate proteomics. *Food Research International* 161: 111757.

Libanje F, Delille R, Young PA, *et al*. (2023) NTSR1 glycosylation and MMP dependent cleavage generate three distinct forms of the protein. *Scientific Reports* 13(1): 4663.

Lichty JJ, Malecki JL, Agnew HD, *et al*. (2005) Comparison of affinity tags for protein purification. *Protein Expression and Purification* 41(1): 98-105.

Lindhoud S, Carvalho V, Pronk JW, *et al*. (2016) SMA-SH: Modified Styrene–Maleic Acid Copolymer for Functionalization of Lipid Nanodiscs. *Biomacromolecules* 17(4): 1516-1522.

Logez C, Damian M, Legros C, *et al*. (2016) Detergent-free Isolation of Functional G Protein-Coupled Receptors into Nanometric Lipid Particles. *Biochemistry* 55(1): 38-48.

Lundstrom K, Wagner R, Reinhart C, *et al*. (2006) Structural genomics on membrane proteins: comparison of more than 100 GPCRs in 3 expression systems. *Journal of Structural and Functional Genomics* 7(2): 77-91.

Magnusdottir A, Johansson I, Dahlgren L-G, *et al*. (2009) Enabling IMAC purification of low abundance recombinant proteins from *E. coli* lysates. *Nature Methods* 6(7): 477-478.
Mahmood N and Xie J (2015) An endogenous 'non-specific' protein detected by a His-tag antibody is human transcription regulator YY1. *Data in Brief* 2: 52-55.
Mahmood T and Yang PC (2012) Western blot: technique, theory, and trouble shooting. *N Am J Med Sci* 4(9): 429-434.
Mellacheruvu D, Wright Z, Couzens AL, *et al*. (2013) The CRAPome: a contaminant repository for affinity purification–mass spectrometry data. *Nature Methods* 10(8): 730-736.
Miles AJ, Janes RW and Wallace BA (2021) Tools and methods for circular dichroism spectroscopy of proteins: a tutorial review. *Chem Soc Rev* 50(15): 8400-8413.
Mizumura T, Kondo K, Kurita M, *et al*. (2020) Activation of adenosine A(2A) receptor by lipids from docosahexaenoic acid revealed by NMR. *Sci Adv* 6(12): eaay8544.
Mizuno N and Itoh H (2009) Functions and regulatory mechanisms of Gq-signaling pathways. *Neurosignals* 17(1): 42-54.
More SA, Deore RS, Pawar HD, *et al*. (2024) CB2 Cannabinoid Receptor as a Potential Target in Myocardial Infarction: Exploration of Molecular Pathogenesis and Therapeutic Strategies. *International Journal of Molecular Sciences* 25(3): 1683.
Morrison KA, Akram A, Mathews A, *et al*. (2016) Membrane protein extraction and purification using styrene–maleic acid (SMA) copolymer: effect of variations in polymer structure. *Biochemical Journal* 473(23): 4349-4360.
Müller KM, Arndt KM, Bauer K, *et al*. (1998) Tandem Immobilized Metal-Ion Affinity Chromatography/Immunoaffinity Purification of His-tagged Proteins— Evaluation of Two Anti-His-Tag Monoclonal Antibodies. *Analytical Biochemistry* 259(1): 54-61.
Müller M, Yong M, Peng XH, *et al*. (2002) Evidence for the role of glycosylation in accessibility of the extracellular domains of human MRP1 (ABCC1). *Biochemistry* 41(31): 10123-10132.
Najimi M, Gailly P, Maloteaux J-M, *et al*. (2002) Distinct regions of C-terminus of the high affinity neurotensin receptor mediate the functional coupling with pertussis toxin sensitive and insensitive G-proteins. *FEBS Letters* 512(1): 329-333.
Navarro G, Gómez-Autet M, Morales P, *et al*. (2024) Homodimerization of CB₂ cannabinoid receptor triggered by a bivalent ligand enhances cellular signaling. *bioRxiv*. DOI: 10.1101/2024.05.10.593612. 2024.2005.2010.593612.
Navratilova I, Besnard J and Hopkins AL (2011) Screening for GPCR Ligands Using Surface Plasmon Resonance. *ACS Medicinal Chemistry Letters* 2(7): 549-554.
Nehmé R, Carpenter B, Singhal A, *et al*. (2017) Mini-G proteins: Novel tools for studying GPCRs in their active conformation. *PLoS One* 12(4): e0175642.
Neville GM, Edler KJ and Price GJ (2022) Fluorescent styrene maleic acid copolymers to facilitate membrane protein studies in lipid nanodiscs. *Nanoscale* 14(15): 5689-5693.
Nguyen KDQ, Vigers M, Sefah E, *et al*. (2021) Homo-oligomerization of the human adenosine A(2A) receptor is driven by the intrinsically disordered C-terminus. *Elife* 10.
Osysko AP and Muíño PL (2011) Fluorescence quenching of tryptophan and tryptophanyl dipeptides in solution. *Journal of Biophysical Chemistry* Vol.02No.03: 6.
Palmer I and Wingfield PT (2004) Preparation and extraction of insoluble (inclusion-body) proteins from Escherichia coli. *Curr Protoc Protein Sci* Chapter 6: 6.3.1-6.3.18.
Pandey A, Shin K, Patterson RE, *et al*. (2016) Current strategies for protein production and purification enabling membrane protein structural biology. *Biochem Cell Biol* 94(6): 507-527.

Pándy-Szekeres G, Caroli J, Mamyrbekov A, *et al*. (2022) GPCRdb in 2023: state-specific structure models using AlphaFold2 and new ligand resources. *Nucleic Acids Research* 51(D1): D395-D402.
Pasquini S, De Rosa M, Pedani V, *et al*. (2011) Investigations on the 4-Quinolone-3-carboxylic Acid Motif. 4. Identification of New Potent and Selective Ligands for the Cannabinoid Type 2 Receptor with Diverse Substitution Patterns and Antihyperalgesic Effects in Mice. *Journal of Medicinal Chemistry* 54(15): 5444-5453.
Pelaprat D (2006) Interactions between neurotensin receptors and G proteins. *Peptides* 27(10): 2476-2487.
Perry NA, Zhan X, Gurevich EV, *et al*. (2019) Using In Vitro Pull-Down and In-Cell Overexpression Assays to Study Protein Interactions with Arrestin. *Methods Mol Biol* 1957: 107-120.
Petrović DM, Hesp BH and Broos J (2013) Emitting State of 5-Hydroxyindole, 5-Hydroxytryptophan, and 5-Hydroxytryptophan Incorporated in Proteins. *The Journal of Physical Chemistry B* 117(37): 10792-10797.
Pettersen EF, Goddard TD, Huang CC, *et al*. (2021) UCSF ChimeraX: Structure visualization for researchers, educators, and developers. *Protein Sci* 30(1): 70-82.
Philo JS (2023) SEDNTERP: a calculation and database utility to aid interpretation of analytical ultracentrifugation and light scattering data. *European Biophysics Journal* 52(4): 233-266.
Pitch SG, Yao W, Szundi I, *et al*. (2021) Functional integrity of membrane protein rhodopsin solubilized by styrene-maleic acid copolymer. *Biophysical journal* 120(16): 3508-3515.
Pollock NL, Lloyd J, Montinaro C, *et al*. (2022) Conformational trapping of an ABC transporter in polymer lipid nanoparticles. *Biochem J* 479(2): 145-159.
Pollock NL, Rai M, Simon KS, *et al*. (2019) SMA-PAGE: A new method to examine complexes of membrane proteins using SMALP nano-encapsulation and native gel electrophoresis. *Biochim Biophys Acta Biomembr* 1861(8): 1437-1445.
Postis V, Rawson S, Mitchell JK, *et al*. (2015) The use of SMALPs as a novel membrane protein scaffold for structure study by negative stain electron microscopy. *Biochim Biophys Acta* 1848(2): 496-501.
Pouresmaeil M and Azizi-Dargahlou S (2023) Factors involved in heterologous expression of proteins in *E. coli* host. *Archives of Microbiology* 205(5): 212.
Raetz CR and Dowhan W (1990) Biosynthesis and function of phospholipids in Escherichia coli. *J Biol Chem* 265(3): 1235-1238.
Raran-Kurussi S and Waugh DS (2017) Expression and Purification of Recombinant Proteins in Escherichia coli with a His(6) or Dual His(6)-MBP Tag. *Methods Mol Biol* 1607: 1-15.
Rehan S, Paavilainen VO and Jaakola V-P (2017) Functional reconstitution of human equilibrative nucleoside transporter-1 into styrene maleic acid co-polymer lipid particles. *Biochimica et Biophysica Acta (BBA) - Biomembranes* 1859(5): 1059-1065.
Remans K, Lebendiker M, Abreu C, *et al*. (2022) Protein purification strategies must consider downstream applications and individual biological characteristics. *Microb Cell Fact* 21(1): 52.
Rich RL, Miles AR, Gale BK, *et al*. (2009) Detergent screening of a G-protein-coupled receptor using serial and array biosensor technologies. *Anal Biochem* 386(1): 98-104.
Rinken A, Lavogina D and Kopanchuk S (2018) Assays with Detection of Fluorescence Anisotropy: Challenges and Possibilities for Characterizing Ligand Binding to GPCRs. *Trends Pharmacol Sci* 39(2): 187-199.
Robertson MJ, Papasergi-Scott MM, He F, *et al*. (2022) Structure determination of inactive-state GPCRs with a universal nanobody. *Nature Structural & Molecular Biology* 29(12): 1188-1195.

Rosano GL and Ceccarelli EA (2014) Recombinant protein expression in Escherichia coli: advances and challenges. *Front Microbiol* 5: 172.
Rosenbaum DM, Cherezov V, Hanson MA, *et al*. (2007) GPCR engineering Yyelds high-resolution structural insights into beta2-adrenergic receptor function. *Science* 318(5854): 1266-1273.
Rosenbaum DM, Rasmussen SG and Kobilka BK (2009) The structure and function of G-protein-coupled receptors. *Nature* 459(7245): 356-363.
Routledge S, Jamshad M, Little H, *et al*. (2020) Ligand-induced conformational changes in a SMALP-encapsulated GPCR. *Biochimica et Biophysica Acta (BBA) - Biomembranes* 1862: 183235.
Saboury AA (2006) A review on the ligand binding studies by isothermal titration calorimetry. *Journal of the Iranian Chemical Society* 3(1): 1-21.
Sachdev S, Creemer BA, Gardella TJ, *et al*. (2024) Highly biased agonism for GPCR ligands via nanobody tethering. *Nature Communications* 15(1): 4687.
San-Miguel T, Pérez-Bermúdez P and Gavidia I (2013) Production of soluble eukaryotic recombinant proteins in *E. coli* is favoured in early log-phase cultures induced at low temperature. *Springerplus* 2(1): 89.
Sarkar CA, Dodevski I, Kenig M, *et al*. (2008) Directed evolution of a G protein-coupled receptor for expression, stability, and binding selectivity. *Proc Natl Acad Sci U S A* 105(39): 14808-14813.
Saroz Y, Kho DT, Glass M, *et al*. (2019) Cannabinoid Receptor 2 (CB2) Signals via G-alpha-s and Induces IL-6 and IL-10 Cytokine Secretion in Human Primary Leukocytes. *ACS Pharmacology & Translational Science* 2(6): 414-428.
Scheidelaar S, Koorengevel MC, Pardo JD, *et al*. (2015) Molecular model for the solubilization of membranes into nanodisks by styrene maleic Acid copolymers. *Biophysical journal* 108(2): 279-290.
Schindler L, Bernhardt G and Keller M (2019) Modifications at Arg and Ile Give Neurotensin(8–13) Derivatives with High Stability and Retained NTS1 Receptor Affinity. *ACS Medicinal Chemistry Letters* 10(6): 960-965.
Schlimgen RR, Peterson FC, Heukers R, *et al*. (2024) Structural basis for selectivity and antagonism in extracellular GPCR-nanobodies. *Nature Communications* 15(1): 4611.
Schucht R, Lydford S, Andzinski L, *et al*. (2011) Rapid Establishment of G-Protein-Coupled Receptor–Expressing Cell Lines by Site-Specific Integration. *SLAS Discovery* 16(3): 323-331.
Scott DJ and Plückthun A (2013) Direct Molecular Evolution of Detergent-Stable G Protein-Coupled Receptors Using Polymer Encapsulated Cells. *Journal of Molecular Biology* 425(3): 662-677.
Sejdiu BI and Tieleman DP (2020) Lipid-Protein Interactions Are a Unique Property and Defining Feature of G Protein-Coupled Receptors. *Biophysical Journal* 118(8): 1887-1900.
Serrano-Marín J, Reyes-Resina I, Martínez-Pinilla E, *et al*. (2020) Natural Compounds as Guides for the Discovery of Drugs Targeting G-Protein-Coupled Receptors. *Molecules* 25(21).
Shiraki K, Kudou M, Fujiwara S, *et al*. (2002) Biophysical effect of amino acids on the prevention of protein aggregation. *J Biochem* 132(4): 591-595.
Sindrewicz P, Li X, Yates EA, *et al*. (2019) Intrinsic tryptophan fluorescence spectroscopy reliably determines galectin-ligand interactions. *Scientific Reports* 9(1): 11851.
Smith AAA, Autzen HE, Faust B, *et al*. (2020) Lipid Nanodiscs via Ordered Copolymers. *Chem* 6(10): 2782-2795.
Smith JS, Lefkowitz RJ and Rajagopal S (2018) Biased signalling: from simple switches to allosteric microprocessors. *Nature reviews. Drug discovery* 17(4): 243-260.

Spinelli F, Giampietro R, Stefanachi A, *et al*. (2020) Design and synthesis of fluorescent ligands for the detection of cannabinoid type 2 receptor (CB2R). *European Journal of Medicinal Chemistry* 188: 112037.
Sriram K and Insel PA (2018) G Protein-Coupled Receptors as Targets for Approved Drugs: How Many Targets and How Many Drugs? *Molecular pharmacology* 93(4): 251-258.
Stetefeld J, McKenna SA and Patel TR (2016) Dynamic light scattering: a practical guide and applications in biomedical sciences. *Biophys Rev* 8(4): 409-427.
Stetsenko A and Guskov A (2017) An Overview of the Top Ten Detergents Used for Membrane Protein Crystallization. *Crystals* 7(7): 197.
Stoddart LA, Goulding J and Briddon SJ (2022) Advances in the application of fluorescence correlation spectroscopy to study detergent purified and encapsulated membrane proteins. *The International Journal of Biochemistry & Cell Biology* 146: 106210.
Stroud Z, Hall SCL and Dafforn TR (2018) Purification of membrane proteins free from conventional detergents: SMA, new polymers, new opportunities and new insights. *Methods* 147: 106-117.
Swainsbury DJK, Scheidelaar S, Foster N, *et al*. (2017) The effectiveness of styrene-maleic acid (SMA) copolymers for solubilisation of integral membrane proteins from SMA-accessible and SMA-resistant membranes. *Biochim Biophys Acta Biomembr* 1859(10): 2133-2143.
Sykes DA, Stoddart LA, Kilpatrick LE, *et al*. (2019) Binding kinetics of ligands acting at GPCRs. *Molecular and cellular endocrinology* 485: 9-19.
Syrovatkina V, Alegre KO, Dey R, *et al*. (2016) Regulation, Signaling, and Physiological Functions of G-Proteins. *Journal of Molecular Biology* 428(19): 3850-3868.
Takahashi M (2022) Nucleic Acid Aptamers Emerging as Modulators of G-Protein-Coupled Receptors: Challenge to Difficult Cell Surface Proteins. *Cells* 11(11).
Tan E, Chin CSH, Lim ZFS, *et al*. (2021) HEK293 Cell Line as a Platform to Produce Recombinant Proteins and Viral Vectors. *Front Bioeng Biotechnol* 9: 796991.
Tate CG and Grisshammer R (1996) Heterologous expression of G-protein-coupled receptors. *Trends in biotechnology* 14(11): 426-430.
Tedesco D, Maj M, Malarczyk P, *et al*. (2021) Application of the SMALP technology to the isolation of GPCRs from low-yielding cell lines. *Biochimica et Biophysica Acta (BBA) - Biomembranes* 1863(9): 183641.
Teo ACK, Lee SC, Pollock NL, *et al*. (2019) Analysis of SMALP co-extracted phospholipids shows distinct membrane environments for three classes of bacterial membrane protein. *Scientific reports* 9(1): 1813.
Thomas JB, Navarro H, Warner KR, *et al*. (2009) The identification of nonpeptide neurotensin receptor partial agonists from the potent antagonist SR48692 using a calcium mobilization assay. *Bioorganic & medicinal chemistry letters* 19(5): 1438-1441.
Tsumoto K, Umetsu M, Kumagai I, *et al*. (2004) Role of Arginine in Protein Refolding, Solubilization, and Purification. *Biotechnology Progress* 20(5): 1301-1308.
Tucker J and Grisshammer R (1996) Purification of a rat neurotensin receptor expressed in Escherichia coli. *Biochem J* 317 (Pt 3)(Pt 3): 891-899.
Turcotte C, Blanchet MR, Laviolette M, *et al*. (2016) The CB(2) receptor and its role as a regulator of inflammation. *Cell Mol Life Sci* 73(23): 4449-4470.
Tuteja N (2009) Signaling through G protein coupled receptors. *Plant Signal Behav* 4(10): 942-947.
Ullrich J, Haueis L, Ohlhoff C, *et al*. (2024) Solubilization of Oligomeric Cell-Free Synthesized Proteins Using SMA Copolymers. *Methods Mol Biol* 2762: 293-308.
Veesler D, Blangy S, Cambillau C, *et al*. (2008) There is a baby in the bath water: AcrB contamination is a major problem in membrane-protein crystallization. *Acta Crystallogr Sect F Struct Biol Cryst Commun* 64(Pt 10): 880-885.

Veiksina S, Tahk M-J, Laasfeld T, *et al*. (2021) Fluorescence Anisotropy-Based Assay for Characterization of Ligand Binding Dynamics to GPCRs: The Case of Cy3B-Labeled Ligands Binding to MC4 Receptors in Budded Baculoviruses. In: Martins SAM and Prazeres DMF (eds) *G Protein-Coupled Receptor Screening Assays: Methods and Protocols*. New York, NY: Springer US, pp.119-136.

Velloso JPL, de Sá AGC, Pires DEV, *et al*. (2024) Engineering G protein-coupled receptors for stabilization. *Protein Science* 33(6): e5000.

Verma R, Boleti E and George AJT (1998) Antibody engineering: Comparison of bacterial, yeast, insect and mammalian expression systems. *Journal of Immunological Methods* 216(1): 165-181.

Vladislav Victorovich K, Tatyana Aleksandrovna K, Victor Vitoldovich P, *et al*. (2021) Spectra of tryptophan fluorescence are the result of co-existence of certain most abundant stabilized excited state and certain most abundant destabilized excited state. *Spectrochimica Acta Part A: Molecular and Biomolecular Spectroscopy* 257: 119784.

Vukoti K, Kimura T, Macke L, *et al*. (2012) Stabilization of Functional Recombinant Cannabinoid Receptor CB2 in Detergent Micelles and Lipid Bilayers. *PLoS One* 7(10): e46290.

Wacker D, Stevens RC and Roth BL (2017) How Ligands Illuminate GPCR Molecular Pharmacology. *Cell* 170(3): 414-427.

Walker G, Brown C, Ge X, *et al*. (2023) Determination of oligomeric organization of membrane proteins from native membranes at nanoscale-spatial and single-molecule resolution. *bioRxiv*. DOI: 10.1101/2023.02.19.529138. 2023.2002.2019.529138.

Wallace BA, Lees JG, Orry AJ, *et al*. (2003) Analyses of circular dichroism spectra of membrane proteins. *Protein Sci* 12(4): 875-884.

Wang D, Tan Y-c, Kreitzer GE, *et al*. (2006) G Proteins G12 and G13 Control the Dynamic Turnover of Growth Factor-induced Dorsal Ruffles*. *Journal of Biological Chemistry* 281(43): 32660-32667.

Wang T, Li Z, Cvijic ME, *et al*. (2004) Measurement of cAMP for G(αs)- and G(αi) Protein-Coupled Receptors (GPCRs). In: Markossian S, Grossman A, Arkin M, *et al*. (eds) *Assay Guidance Manual*. Bethesda (MD): Eli Lilly & Company and the National Center for Advancing Translational Sciences.

Wang X, Slater A, Lee SC, *et al*. (2024) Purification and characterisation of the platelet-activating GPVI/FcRγ complex in SMALPs. *Archives of Biochemistry and Biophysics* 754: 109944.

Watson H (2015) Biological membranes. *Essays Biochem* 59: 43-69.

Waugh DS (2016) Crystal structures of MBP fusion proteins. *Protein Sci* 25(3): 559-571.

Weis WI and Kobilka BK (2018) The Molecular Basis of G Protein-Coupled Receptor Activation. *Annu Rev Biochem* 87: 897-919.

Weiss HM and Grisshammer R (2002) Purification and characterization of the human adenosine A(2a) receptor functionally expressed in Escherichia coli. *Eur J Biochem* 269(1): 82-92.

Westphal A, Sielaff H, Reuter S, *et al*. (2019) *Ligand-induced oligomerization of the human GPCR neurotensin receptor 1 monitored in living HEK293T cells.*

Wheatley M, Charlton J, Jamshad M, *et al*. (2016) GPCR–styrene maleic acid lipid particles (GPCR–SMALPs): their nature and potential. *Biochemical Society Transactions* 44(2): 619-623.

White JF, Noinaj N, Shibata Y, *et al*. (2012) Structure of the agonist-bound neurotensin receptor. *Nature* 490(7421): 508-513.

Whitmore L and Wallace B (2004) DICHROWEB, an online server for protein secondary structure analyses from circular dichroism spectroscopic data. *Nucleic Acids Research* 32(suppl_2): W668-W673.

Wingler LM and Lefkowitz RJ (2020) Conformational Basis of G Protein-Coupled Receptor Signaling Versatility. *Trends Cell Biol* 30(9): 736-747.
Wiseman DN, Otchere A, Patel JH, *et al*. (2020) Expression and purification of recombinant G protein-coupled receptors: A review. *Protein Expr Purif* 167: 105524.
Wittig I and Schägger H (2005) Advantages and limitations of clear-native PAGE. *Proteomics* 5(17): 4338-4346.
Wootten D, Christopoulos A, Marti-Solano M, *et al*. (2018) Mechanisms of signalling and biased agonism in G protein-coupled receptors. *Nature Reviews Molecular Cell Biology* 19(10): 638-653.
Workman CE, Bag P, Cawthon B, *et al*. (2023) Alternatives to Styrene- and Diisobutylene-Based Copolymers for Membrane Protein Solubilization via Nanodisc Formation. *Angewandte Chemie International Edition* 62(43): e202306572.
Wu P and Brand L (1994) Resonance energy transfer: methods and applications. *Anal Biochem* 218(1): 1-13.
Xie Q, Soutto M, Xu X, *et al*. (2011) Bioluminescence resonance energy transfer (BRET) imaging in plant seedlings and mammalian cells. *Methods in molecular biology (Clifton, N.J.)* 680: 3-28.
Xie XQ, Zhao J and Zheng H (2004) Expression, purification, and isotope labeling of cannabinoid CB2 receptor fragment, CB2(180-233). *Protein Expr Purif* 38(1): 61-68.
Xing C, Zhuang Y, Xu T-H, *et al*. (2020) Cryo-EM Structure of the Human Cannabinoid Receptor CB2-Gi Signaling Complex. *Cell* 180(4): 645-654.e613.
Yang L, Catalano C, Xu Y, *et al*. (2021) A native cell membrane nanoparticles system allows for high-quality functional proteoliposome reconstitution. *BBA Advances* 1: 100011.
Yao XJ, Vélez Ruiz G, Whorton MR, *et al*. (2009) The effect of ligand efficacy on the formation and stability of a GPCR-G protein complex. *Proceedings of the National Academy of Sciences* 106(23): 9501-9506.
Yatani A, Imoto Y, Codina J, *et al*. (1988) The stimulatory G protein of adenylyl cyclase, Gs, also stimulates dihydropyridine-sensitive Ca2+ channels. Evidence for direct regulation independent of phosphorylation by cAMP-dependent protein kinase or stimulation by a dihydropyridine agonist. *J Biol Chem* 263(20): 9887-9895.
Ye L, Neale C, Sljoka A, *et al*. (2018) Mechanistic insights into allosteric regulation of the A(2A) adenosine G protein-coupled receptor by physiological cations. *Nat Commun* 9(1): 1372.
Yeliseev A (2019) Expression and Preparation of a G-Protein-Coupled Cannabinoid Receptor CB(2) for NMR Structural Studies. *Curr Protoc Protein Sci* 96(1): e83.
Yeliseev A, Berg A, Zoubak L, *et al*. (2020) Thermostability of a recombinant G protein-coupled receptor expressed at high level in mammalian cell culture. *Scientific Reports* 10.
Yeliseev AA (2013) Methods for recombinant expression and functional characterization of human cannabinoid receptor CB2. *Comput Struct Biotechnol J* 6: e201303011.
Yeliseev AA (2021) Recombinant Expression and Purification of Cannabinoid Receptor CB2, a G Protein-Coupled Receptor. In: Martins SAM and Prazeres DMF (eds) *G Protein-Coupled Receptor Screening Assays: Methods and Protocols*. New York, NY: Springer US, pp.61-76.
Yeliseev AA, Wong KK, Soubias O, *et al*. (2005) Expression of human peripheral cannabinoid receptor for structural studies. *Protein Science* 14(10): 2638-2653.
Yen HY, Hoi KK, Liko I, *et al*. (2018) PtdIns(4,5)P(2) stabilizes active states of GPCRs and enhances selectivity of G-protein coupling. *Nature* 559(7714): 423-427.
Yu L, Lei Y, Ma Y, *et al*. (2021) A Comprehensive Review of Fluorescence Correlation Spectroscopy. *Frontiers in Physics* 9: 644450.
Zhou Y, Meng J, Xu C, *et al*. (2021) Multiple GPCR Functional Assays Based on Resonance Energy Transfer Sensors. *Front Cell Dev Biol* 9: 611443.

Zhu L, Zhao H, Wang Y, *et al*. (2022) Solubilization, purification, and ligand binding characterization of G protein-coupled receptor SMO in native membrane bilayer using styrene maleic acid copolymer. *PeerJ* 10: e13381.

Zulkarnain Z, Ulhaq ZS, Sujuti H, *et al*. (2022) Comparative performance of ELISA and dot blot assay for TSH-receptor antibody detection in Graves' disease. *J Clin Lab Anal* 36(4): e24288.

